AN ADJOINT-BASED FORMALISM FOR OPTIMAL DESIGN OF TIME-DELAY SYSTEMS AND UNCERTAINTY QUANTIFICATION IN STOCHASTIC SYSTEMS

BY

ZAID AHSAN

DISSERTATION

Submitted in partial fulfillment of the requirements
for the degree of Doctor of Philosophy in Mechanical Engineering
in the Graduate College of the
University of Illinois Urbana-Champaign, 2022

Urbana, Illinois

Doctoral Committee:

Professor Harry Dankowicz, Chair
Assistant Professor Kathryn Matlack
Professor Zoi Rapti
Professor Srinivasa Salapaka

Abstract

The objectives of this dissertation are to develop computational techniques for i) tracking solutions to multi-segment, delay-coupled boundary-value problems, with particular emphasis on periodic orbits and quasiperiodic invariant tori for delay differential equations (DDEs), ii) solving single-objective optimal design problems along families of such solutions using a technique of successive continuation, and iii) characterizing the effects of noise on the asymptotic dynamics in the vicinity of transversally stable periodic and quasiperiodic solutions in deterministic limits of stochastic differential equations (SDEs). Considerable attention is placed on an algorithmic formalism and problem discretization that supports straightforward implementation in the Matlab-based software package COCO.

In the case of delay-coupled boundary-value problems, the analysis in this dissertation demonstrates how a Lagrangian formulation for constrained design optimization may be used to derive the necessary optimality conditions in terms of additional delay-coupled adjoint boundary-value problems that are linear in corresponding sets of Lagrange multipliers. Importantly, these adjoint boundary-value problems are shown to decompose into contributions associated with individual differential or algebraic constraints. As a consequence, their construction is found to conform with the staged construction paradigm of COCO, and complex problems may be constructed by gluing together instances of simpler problems. In particular, this dissertation shows how a boundary-value problem for design optimization along families of quasiperiodic invariant tori may be constructed by gluing together multiple instances of single-segment trajectory problems using all-to-all boundary conditions. Several

candidate implementations of this paradigm in a set of COCO-compatible toolbox constructors are used to demonstrate such optimization according to a previously developed sequential methodology for finding stationary points of an objective function along implicitly defined manifolds. By their generality, these constructors are also shown to be compatible with problems from optimal control, phase response analysis, and continuation of homo- and heteroclinic trajectories.

For transversally stable periodic orbits (limit cycles) and quasiperiodic invariant tori in the deterministic limit of SDEs, this dissertation proposes a novel covariance boundary-value problem to quantify the asymptotic dynamics near these objects in the presence of small amounts of Brownian noise. Here, the adjoint boundary-value problems associated with phase-response analysis are used to construct a continuous family of projections onto transversal hyperplanes that are invariant under the linearized flow near the limit cycle or quasiperiodic invariant torus. The asymptotic dynamics in the presence of noise are shown to be represented by a stationary distribution whose restriction to individual hyperplanes is Gaussian with a covariance given by the solution to the corresponding covariance boundary-value problem. In the case of limit cycles, the analysis improves upon results in the literature through the explicit use of transversal projections and modifications that ensure uniqueness of the solution despite the lack of hyperbolicity along the limit cycle. These same innovations are then generalized to the case of a two-dimensional quasiperiodic invariant torus, as a model of the formalism required for a torus of arbitrary dimension. As in the case of DDEs, using a COCO implementation of suitable toolbox constructors, the covariance analysis of a quasiperiodic invariant torus is shown to parallel the decomposition into multiple instances of single-segment trajectory problems using all-to-all boundary conditions derived for design optimization.

to my parents

Acknowledgments

This thesis would not have been possible without the love and support of many people. First of all I would like to thank my adviser, Prof. Harry Dankowicz for accepting me as a PhD student and guiding me all the way throughout this long journey. I learnt a lot from him. He is an awesome advisor and the kind of research problems that we solved during my PhD would not have been possible without his guidance. He genuinely cares about his students, their future, and is always available to answer their queries. I also had an opportunity to instruct a course with him; it was a great learning experience that helped me to understand the nuances of teaching.

In addition, I would like to thank my committee members: Profs. Matlack, Rapti, and Salapaka for their valuable feedback on my dissertation. I really enjoyed my interactions with Prof. Salapaka when I worked as a TA for him, as well as when we instructed a course together, and appreciate his guidance and help.

A special thanks to Prof. C.P. Vyasarayani, my undergraduate project and Master's thesis advisor, who has been guiding me since my undergraduate days. His encouragement during difficult times of my doctoral studies helped me to stay calm and finish my degree. I will forever be grateful to him.

Thanks to the Department of Mechanical Science and Engineering at UIUC for providing me with assistantships as well as teaching opportunities during my graduate studies. The staff in the department is super friendly, especially Kathy Smith, who helped me on numerous occasions with various administrative issues.

I would also like to thank my lab members for making this journey memorable. You guys were awesome. A special thanks to Mingwu, Yu, and Chris for always being available for discussions. I will definitely miss the time spent with my Chambana friends Sreenath, Chaitanya, Ameya, Navjot, and Mubeen.

Finally, I am very grateful to my family members for their love and support during my studies. Thank you for always supporting me. I am really lucky to have you in my life. I would also like to thank my wife Anam for being there with me and supporting me in the final stages of my degree.

Table of contents

List of Tables

List of Figures

Chapter 1

INTRODUCTION

This chapter[1] gives an overview of the research documented in this dissertation, reviews the necessary literature, and enumerates the specific objectives addressed during the study. Broadly speaking, this dissertation has a twofold objective: first, development of formulations that use adjoint variables for optimal design of dynamical systems with time-delay and uncertainty analysis of noise contaminated systems, and second, the implementation of the proposed methodologies in algorithms compatible with the software package COCO.

In the context of constrained design optimization, the dissertation first generalizes an already existing continuation-based methodology for optimization of scalar objective functions on constraint manifolds to the case of periodic and quasiperiodic orbits of time-delay systems. The methodology relies on the construction of a suitable Lagrangian in terms of auxiliary adjoint variables (Lagrange multipliers) and the subsequent derivation of a set of adjoint conditions that may be further constrained to obtain the necessary conditions for stationary points on the constraint manifold. It is demonstrated through several examples that these conditions can be solved by performing a sequence of successive continuation runs, starting with a trivial solution and ending at the sought stationary point.

Inspired by the successful application of the continuation paradigm to time-delay problems, the dissertation proposes a general algorithmic formulation that supports the analysis of

[1]The content of this chapter is reproduced from Ahsan, Dankowicz and Sieber, "Optimization along families of periodic and quasiperiodic orbits in dynamical systems with delay," *Nonlinear Dynamics*, **99**(1), 837–854, 2020 [1], and included here with permission from the publisher. The chapter also contains material reproduced from Ahsan, Dankowicz, Li and Sieber, "Methods of Continuation and their Implementation in the COCO Software Platform with Application to Delay Differential Equations," *Nonlinear Dynamics*, **107**(4), 3181–3243, 2022 [2], and included here with permission from the publisher.

arbitrary delay-coupled multi-segment boundary-value problems with a single constant delay per segment. The formulation is designed to support a staged construction paradigm, consistent with the philosophy of the COCO package. Through several examples, it is demonstrated that the formulation and its realization in a COCO toolbox template allows for continuation of solutions to boundary-value problems corresponding to periodic orbits, quasiperiodic orbits, initial-value problems, connecting orbits, and optimal control problems, including those of problems without delay.

In the next part of the dissertation, a novel boundary-value problem is proposed for capturing the effects of noise on the local behavior near limit cycles and transversally stable quasiperiodic invariant tori of dynamical systems without time delay. Here, adjoint variables are used to construct a foliation of hyperplanes, transversal to the limit cycle or invariant torus, respectively, in which the effects of noise may be uniquely analyzed. The theory assumes that there exists a stationary probability density in state space that captures the local dynamics that i) result from the competition between the stabilizing influence of the local deterministic vector field and the destabilizing effects of Brownian process noise and ii) is locally Gaussian in each hyperplane. Solutions to the proposed boundary-value problem include the covariance matrix of each such Gaussian distribution and can be continued under parameter variations for purposes of design. The text shows how the formulation may be integrated with appropriate COCO toolboxes and validates the predicted results using numerical integration of several toy problems.

1.1 Design optimization in problems with delay

The optimization of time-delay systems has been the subject of intensive research for many years. Such systems arise naturally in control applications where unmodeled actuator dynamics results in delays between input signals and actuator responses [3], car following models that account for driver reaction times [4], and machine tool dynamics due to the

regenerative effect [5]. The wide range of applications has motivated the development of novel techniques for their optimization. For example, Göllmann *et al.* [6] used a formulation based on the Pontryagin minimum principle to derive necessary optimality conditions for optimal control problems with delays in state and control variables. The obtained equations were discretized and transformed into a large-scale nonlinear programming model, which was then solved using off-the-shelf solvers. In another investigation, Yusoff and Sims [7] combined the semi-discretization method [8] for time-periodic delay equations with differential evolution to optimize a variable helix/pitch tool geometry for regenerative chatter mitigation. Their results were also validated experimentally, confirming the predicted significant improvements in chatter stability. This problem of optimal selection of parameters for subtractive manufacturing was also reported in [9]–[11]. Liao *et al.* [12] developed an optimization technique for periodic solutions of delay differential equations using the harmonic balance method and continuation techniques. They posed an amplitude optimization problem subject to the algebraic constraints obtained by substitution of a truncated Fourier representation in the governing equation along with the stability conditions. The sensitivity expressions were analytically derived, and the optimization problem was then solved for the unknown Fourier coefficients and the unknown parameters. The delayed Duffing oscillator was used to validate the methodology.

The calculus of variations serves as a useful tool for constrained optimization problems. Here, a Lagrangian functional is constructed by combining the objective function with the imposed constraints using Lagrange multipliers (adjoint variables) as coefficients. The vanishing of the variations of the Lagrangian with respect to the design variables and the Lagrange multipliers then yields the necessary optimality conditions for a stationary point. In general, these equations cannot be solved directly. Instead, nonlinear solvers may be applied to various finite-dimensional discretizations. A major challenge with this approach is the selection of a good initial guess which converges to the desired solution. A resolution built on principles of parameter continuation was originally proposed in the work of Kernévez

and Doedel [13]. There, a sequence of properly initialized stages of continuation along one-dimensional manifolds of solutions to a subset of the necessary optimality conditions was used to connect the local extremum to an initial solution guess with vanishing Lagrange multipliers. This methodology was recently revisited by Li and Dankowicz [14] and there cast in terms of partial Lagrangians relevant to the general context of constrained optimization of integro-differential boundary-value problems *without delay*. Importantly, this work showed how the Lagrangian structure was consistent with a staged construction paradigm implemented in the software package COCO.

In this work, we generalize the successive continuation approach of Kernévez and Doedel to optimization along families of periodic and quasiperiodic orbits in dynamical systems *with delay*. We derive the necessary optimality conditions from a suitably constructed Lagrangian without first discretizing the governing equations and unknowns. This approach is in contrast to other studies [15], in which the discretization of the governing equations is first carried out and then the Lagrangian is constructed based on the discretized equations. In our formulation, the Lagrange multipliers satisfy coupled, piecewise-defined, boundary-value problems with both delayed and advanced arguments. Depending on the imposed constraints, the Lagrange multipliers may be discontinuous or nonsmooth at the interval boundary points, naturally resulting in a multi-segment problem [16].

1.2 A toolbox for delay-coupled boundary-value problems

There exist several software packages for continuation and bifurcation analysis of dynamical systems. These include AUTO [17] and the wrapper XPPAUT [18], a popular choice for continuation-based analysis of ordinary differential equations (ODEs), MATCONT [19] for ODEs/maps, DDE-BIFTOOL [20], [21] and KNUT [22] for delay differential equations (DDEs), PDE2PATH [23], [24] for partial differential equations (PDEs), and HOMPACK [25] for globally-convergent homotopy analysis of arbitrary nonlinear equations.

With an emphasis on utility, these packages were designed to address specific problem classes/types, while leaving open the possibility of additional creative uses (e.g., the development of special purpose wrappers for AUTO, including MANBVP [26] for computing invariant manifolds, SLIDECONT [27] for bifurcation analysis of Filippov systems, $\widehat{\text{TC}}$ [28] for bifurcation analysis of periodic orbits in hybrid dynamical systems, and the computation of global isochrons in [29]). In contrast, an emphasis on universality was the guiding principle behind the creation of the COCO software package. Instead of building solutions, build a tool that others could use to build solutions. Define the platform, the language of discourse, and the paradigm of problem construction and analysis. Reward a tight coupling between rigorous mathematics and computational encoding.

The staged construction paradigm in COCO leveraged an object-oriented perspective, conceiving of a system of equations as decomposed into multiple object instances, describing subsets of equations and unknowns with inherent meaning, coupled together through appropriate gluing conditions (cf. the terminology used in multibody systems [30], [31]). With the recognition of common examples of mathematical objects (e.g., equilibria, trajectory segments, and periodic orbits) as constituting abstract classes of equations and unknowns, there resulted a hierarchy of problem construction whereby new abstract classes could be constructed from the composition of existing ones, and different versions of existing abstract classes could be substituted at will. As an example, problems involving the simultaneous analysis of an equilibrium (E), a periodic orbit (P), and an E-to-P connecting orbit were constructed with ease by leveraging existing abstract classes for each of these objects, glued together with a sparse set of boundary conditions [32]–[34].

Another unique feature of COCO is the support of the parallel staged construction of (a critical subset of) the adjoint necessary conditions for extrema along constraint manifolds [14], [35]. This expansion reflects the decomposition of a problem Lagrangian into a sum of individual constraints linearly paired with corresponding adjoint variables (also called dual variables or Lagrange multipliers) that measure the sensitivities of an objective function to

constraint violations at stationary points of the Lagrangian. Since the Lagrangian is linear in the adjoint variables, the contributions to the adjoint conditions from each term of the Lagrangian are also linear in the adjoint variables [1]. The complete set of adjoint conditions may therefore again be built in stages in a one-to-one mapping to the stages used to construct the full set of constraints.

In this work, we propose a COCO compatible toolbox template that can handle a broad class of multi-segment delay-coupled boundary-value problems. The template is based on the introduction of additional variables to simplify construction. Specifically we make use of additional variables to replace the original DDE with a set of ODEs coupled to each other through algebraic state variables and coupling conditions. Such a framework representation then allows one to consider initial-value problems, connecting orbits, periodic orbit problems, and multi-segment boundary-value problems describing approximations of quasiperiodic invariant tori. Furthermore, the representation also allows for the automatic construction of the adjoint contributions. We discuss the complete discretization of the framework representation and perform an implementation of the discretized equations in COCO.

1.3 Noise induced perturbations in systems without delay

Noise is intrinsic to the dynamics of systems. If not properly addressed, it can destabilize the system dynamics [36], induce chaotic behavior [37], or result in stochastic jumps [38] between equilibrium states of an underlying deterministic system. On the other hand, noise is sometimes intentionally introduced in a system to stabilize the original unstable system dynamics [39]. Also, noise may be used to enhance the energy harvesting potential of micro- and nanoelectromechanical devices [40]–[42].

When noise is introduced to the dynamics near an attractor of an underlying deterministic system, there is a competition between the stabilizing effects of the local drift and the destabilizing effects of noise. For small noise intensities, the stochastic trajectories are

expected to stay close to the underlying attractor over long time scales. Different approaches have been used to characterize the effects of noise on the local dynamics. A direct approach is to solve a Fokker-Planck PDE [43] for a corresponding probability density function. As an alternative, direct numerical integration of solution trajectories may be used to estimate such a density [44].

Of greater relevance to the work described in this dissertation, a number of authors have studied linear boundary-value problems that characterize the covariance matrix of a local Gaussian distribution of intersections of sample trajectories with hyperplanes orthogonal to limit cycles [45]–[47] or quasiperiodic invariant tori [48] in steady state. Using projections onto such hyperplanes, the cumulative effects of noise along a limit cycle or quasiperiodic invariant torus (corresponding to the neutral directions of the vector field), which result in unbounded growth of variance, may be ignored. An example of the use of such a formulation in the case of quasiperiodic oscillations is found in [49], which concerned the effects of noise in a map-based neuron model with Canard-type dynamics. In another investigation [50], similar techniques were used to analyze the effects of noise on a biochemical model.

In this work, we propose an alternative covariance boundary-value problem formulation to capture the effects of noise near limit cycles or transversally stable quasiperiodic invariant tori of autonomous dynamical systems. Rather than relying on hyperplanes perpendicular to the local tangent direction or tangent hyperplane (as in the literature cited above), the formulation uses adjoints to project the dynamics onto hyperplanes transversal (but not perpendicular) to the limit cycle or torus. This construction is particularly amenable to implementation in COCO due to its support for constructing adjoint equations.

1.4 Contributions of the dissertation

This dissertation broadly deals with the generalization and development of techniques using adjoints for the analysis of time-delay and stochastic systems. Focus has also been on the

implementation aspects of the formulation in the context of the continuation package COCO. The contributions of this dissertation may be described as follows.

Chapter 2, which contains material reproduced from [2], reviews the staged construction paradigm for extended continuation problems implemented in COCO and generalizes this to a class of augmented continuation problems that include the Karush–Kuhn–Tucker conditions of constrained optimization with inequality constraints. The generality offered by the staged style of construction is illustrated through examples of a data assimilation problem and a phase response formulation for periodic orbits. Material from [2] is reproduced in this and other chapters with permission from the publisher and the co-authors, who contributed equally to its conception and writing.

The content of Chapter 3 is reproduced from [1], and is included here with permission from the publisher and the co-authors, who contributed equally to its conception and writing. This chapter describes an original derivation of first-order necessary optimality conditions using the calculus of variations for the optimization of scalar objective functionals subjected to periodic or quasiperiodic boundary-value problems with single discrete delays. The formulation is purposely chosen to support a method of solution that relies on a paradigm of successive continuation and is shown to be compatible with the implementation of the augmented continuation problem in the software package COCO.

The content of Chapter 4 is also reproduced from [2]. Motivated by the staged construction paradigm of COCO, described in Chapter 2, and the applicability of the successive continuation paradigm for delay problems, shown in Chapter 3, this chapter proposes an original, systematic framework for analyzing a large class of delay-coupled multi-segment boundary-value problems, including the automated staged construction of the corresponding adjoint contributions. A COCO-compatible toolbox implementation is discussed in detail, with emphasis on problem discretization.

Chapter 5 contains material reproduced from [51], included here with permission from the publisher and the co-authors, who contributed equally to its conception and writing. It

proposes a novel boundary-value problem formulation for capturing the effects of noise near limit cycles. The methodology uses adjoints to construct a projection matrix which projects the dynamics onto hyperplanes transversal, but not in general perpendicular, to the orbit, as has been done in previous literature. A rigorous derivation shows the existence of a unique solution of this boundary-value problem corresponding to a family of covariance matrices that describe the steady-state distribution of intersections with such hyperplanes along the orbit. The text shows how this may again be implemented in COCO by relying on the staged construction paradigm and existing functionality for computing adjoints.

Chapter 6 generalizes the boundary-value problem formulation from Chapter 5 to stochastic trajectories near transversally stable quasiperiodic invariant two-tori. Here, a partial differential equation boundary-value problem is derived that includes the boundary-value problem describing the deterministic torus, two sets of boundary-value problems describing suitably constructed adjoints, and one boundary-value problem for a torus family of covariance matrices. As in Chapter 5, the adjoint variables are used to project the dynamics onto hyperplanes transversal, but not perpendicular, to the torus. A detailed discussion demonstrates how the problem may be discretized in terms of a Fourier series and collocation discretization along characteristics, as is then implemented in COCO.

Chapter 2

METHODS OF CONTINUATION

In this chapter[1], we discuss comprehensively the construction of problems from nonlinear dynamics and constrained optimization amenable to parameter continuation techniques. The discussion is grounded in the context of the COCO software package and its explicit support for community-driven development. The chapter formalizes the COCO construction paradigm for augmented continuation problems compatible with simultaneous analysis of implicitly defined manifolds of solutions to nonlinear equations and the corresponding adjoint variables associated with optimization of scalar objective functions along such manifolds. Using a data assimilation problem for finite time histories and a phase response analysis of periodic orbits, a universal paradigm of construction is identified that permits abstraction and generalization. Along with a systematic discussion of problem construction, the chapter includes an original derivation using Lagrangian sensitivity analysis of phase-response functionals for periodic-orbit problems in abstract Banach spaces.

2.1 Introduction

While the possibility of closed-form analysis is fortuitous and perhaps career-changing, computation is the bread and butter of applied research in nonlinear dynamics. Computational techniques derive their power from rigorous mathematical analysis, but extend far beyond the

[1]The content of this chapter is reproduced from Ahsan, Dankowicz, Li and Sieber, "Methods of Continuation and their Implementation in the COCO Software Platform with Application to Delay Differential Equations," *Nonlinear Dynamics*, **107**(4), 3181–3243, 2022 [2], and included here with permission from the publisher.

reach of theoretical tools (see, e.g., the analysis of global bifurcations of the Lorenz manifold in [52], [53]). With their aid, systematic exploration becomes possible, e.g., of the dependence of system responses on model parameters [54], the sensitivity of these responses to parameter uncertainty [55], and the determination of optimal selections of parameter values [56], [57]. Such exploration inspires further theoretical advances, including of methods for projecting the dynamics of large-scale systems onto reduced-order models [58]–[61], amenable to efficient computation and powerful visualization.

Continuation methods are a class of deterministic computational techniques for exploring smooth manifolds of solutions to nonlinear equations [32], [62]. By now classical algorithms convert common questions of interest to applied dynamicists into such nonlinear equations, enabling their analysis using continuation. Prominent among such uses are bifurcation analyses of equilibria [63], periodic orbits [64], connecting orbits [65], quasiperiodic invariant tori [66], and stable and unstable manifolds [67] for smooth and piecewise-smooth vector fields, including in problems with delay [68]–[71]. By their versatility, continuation methods are an invaluable tool in the researcher's arsenal.

In this chapter, we purposely avoid stepping over well-trodden ground dealing with the specific algorithms used to cover solution manifolds or with examples of bifurcation analysis, as these topics have been discussed in great detail in a number of key sources [72], [73]. Instead, completely new content develops a formalism for problem construction, inspired by functionality available in the COCO software platform [74] illustrates its use on problems from data assimilation and phase response analysis.

2.2 Problem formulation

It is customary in treatments of continuation methods (e.g., [75]) to begin with a discussion of the implicit function theorem, as the theoretical foundation for analyzing solutions of abstract nonlinear problems. Such a discussion naturally concerns itself with a decomposition

of the unknowns into independent and dependent variables, and establishes conditions under which such a decomposition makes (local) sense. These conditions are then leveraged to give meaning to the notion of *continuation*: the local and continuous expansion of the known universe of solutions along implicitly defined manifolds.

Here, we largely depart from such a focus on solutions and their geometry by instead emphasizing the process of problem construction. Our concern is not principally with the techniques used to *perform* continuation, but with a systematic approach to formulating problems *amenable* to continuation, without imposing any preferred decompositions among the problem unknowns. As we show in this section, such a problem-oriented focus may yield benefits also to the process of continuation, as different formulations are more or less well-conditioned. Nevertheless, our primary aim is to identify patterns and structure in the way common problems arise in the study of dynamical systems, and to build useful abstractions around such patterns.

It is instructive to begin this journey into methods of continuation and their implementations in software within the realm of problems amenable to closed-form analysis. Such analysis removes consideration of various numerical approximations, inevitable in a computational implementation, and offers an opportunity for code verification. For the particular examples considered in this section, it points to generalizations to nonlinear problems without closed-form solutions. More importantly, it illustrates principles of intuitive and flexible problem construction, partially agnostic to the final objectives of the analysis. We argue that such flexibility should take precedence in the engineering of general-purpose software for continuation problems.

2.2.1 Looking for inflection points

Many problems of interest in the analysis and control of nonlinear dynamical systems may be formulated as problems of constrained design optimization (see, e.g., the study of periodically forced bioreactors in [76] or bubble motion driven by acoustic forcing in [77], [78]). In this

section, we consider the search for optimal points along manifolds of solutions to algebraic and/or differential constraints in terms of objective functions characterizing the local manifold geometry (for an applied context, see [79] for a recent study of non-monotonic dependence of the response dynamics of premixed flames on forcing amplitude).

Specifically, along the family of steady-state periodic responses of a harmonically-excited, linear oscillator parameterized by the excitation frequency ω, at most two values of ω correspond to local extrema in the rate of change of the response amplitude with respect to ω, as shown in the left panel of Fig. 2.1. To locate these values, we write the governing equation in the normalized form

$$\ddot{x} + 2\zeta\dot{x} + x = \cos\omega t,\ \zeta, \omega > 0, \tag{2.1}$$

make the ansatz $x(t) = C\cos(\omega t - \theta)$ for $C > 0$, and obtain

$$C = \frac{1}{\sqrt{(1-\omega^2)^2 + 4\zeta^2\omega^2}}. \tag{2.2}$$

Differentiation twice with respect to ω then yields inflection points at the roots of the polynomial

$$3\omega^6 + 5(2\zeta^2 - 1)\omega^4 + (16\zeta^4 - 16\zeta^2 + 1)\omega^2 + 1 - 2\zeta^2 \tag{2.3}$$

or, equivalently, at points (ζ, ω) with

$$\zeta = \frac{1}{4\omega}\sqrt{1 + 8\omega^2 - 5\omega^4 \pm \sqrt{1 + 38\omega^4 - 23\omega^8}} \tag{2.4}$$

as illustrated in the bottom panel of Fig. 2.1. It follows that only one such root exists for $\zeta > 1/\sqrt{2}$, whereas two roots bracket the global maximum of the response amplitude at $\omega = \sqrt{1 - 2\zeta^2}$ for $\zeta \leq 1/\sqrt{2}$. At these points, the response amplitude is given by

$$\frac{2}{\sqrt{5 - \omega^4 \pm \sqrt{1 + 38\omega^4 - 23\omega^8}}} \tag{2.5}$$

and $1/\sqrt{1-\omega^4}$, respectively, as shown in Fig. 2.2.

In lieu of the analysis afforded by the explicit expression (2.2) for the response amplitude, consider the equations

$$(1-\omega^2)A + 2\zeta\omega B - 1 = 0,\ (1-\omega^2)B - 2\zeta\omega A = 0 \tag{2.6}$$

obtained by substitution of the ansatz $A\cos\omega t + B\sin\omega t$ in (2.1). To locate inflection points in the response amplitude $C = \sqrt{A^2+B^2}$, we may directly constrain a finite-difference approximation of its second derivative per the collection of polynomial constraints

$$C_1^2 - A_1^2 - B_1^2 = 0,\ C_2^2 - A_2^2 - B_2^2 = 0,\ C_3^2 - A_3^2 - B_3^2 = 0, \tag{2.7}$$

$$(1-\omega_1^2)A_1 + 2\zeta\omega_1 B_1 - 1 = 0,\ (1-\omega_1^2)B_1 - 2\zeta\omega_1 A_1 = 0, \tag{2.8}$$

$$(1-\omega_2^2)A_2 + 2\zeta\omega_2 B_2 - 1 = 0,\ (1-\omega_2^2)B_2 - 2\zeta\omega_2 A_2 = 0, \tag{2.9}$$

$$(1-\omega_3^2)A_3 + 2\zeta\omega_3 B_3 - 1 = 0,\ (1-\omega_3^2)B_3 - 2\zeta\omega_3 A_3 = 0, \tag{2.10}$$

$$\omega_1 - \omega_2 - \epsilon = 0,\ \omega_2 - \omega_3 - \epsilon = 0,\ C_1 - 2C_2 + C_3 = 0 \tag{2.11}$$

in the limit as $\epsilon \to 0$. As an alternative, consider instead *the constrained optimization* of the *objective function* $C_1 - C_2$ with respect to ω_1 in the limit as $\epsilon \to 0$, given the polynomial *constraints*

$$C_1^2 - A_1^2 - B_1^2 = 0,\ C_2^2 - A_2^2 - B_2^2 = 0,\ \omega_1 - \omega_2 - \epsilon = 0, \tag{2.12}$$

$$(1-\omega_1^2)A_1 + 2\zeta\omega_1 B_1 - 1 = 0,\ (1-\omega_1^2)B_1 - 2\zeta\omega_1 A_1 = 0, \tag{2.13}$$

$$(1-\omega_2^2)A_2 + 2\zeta\omega_2 B_2 - 1 = 0,\ (1-\omega_2^2)B_2 - 2\zeta\omega_2 A_2 = 0. \tag{2.14}$$

By the calculus of variations [80], [81], we obtain necessary conditions for such loci of optimality by considering vanishing variations of a suitably constructed constraint Lagrangian. Here,

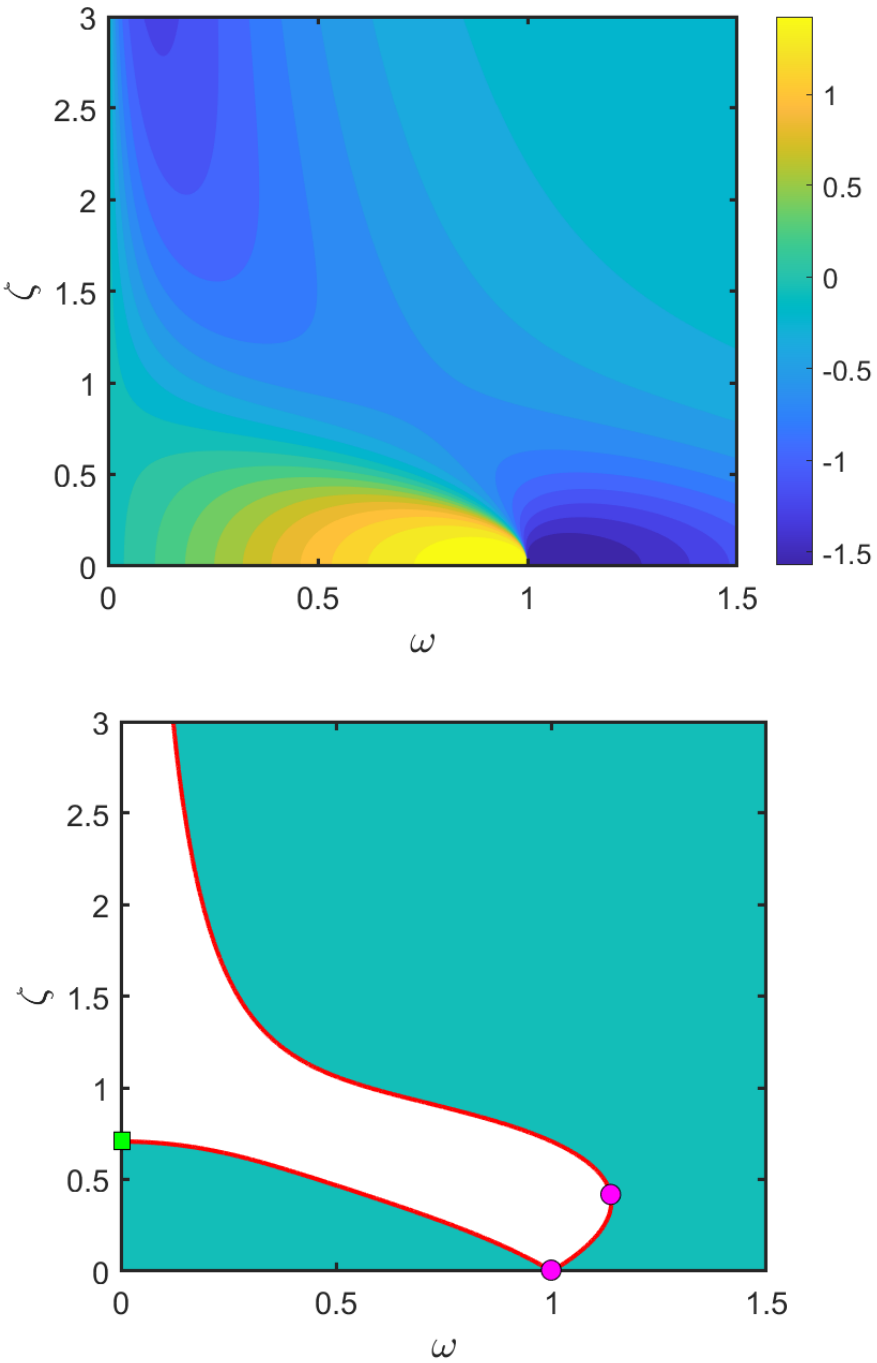

Figure 2.1: (top) Contour plot of the inverse tangent (arctan) of the partial derivative of the response amplitude C in (2.2) with respect to ω. (The inverse tangent operator is used to handle the singularity of the partial derivative when $(\zeta, \omega) \to (0, 1)$.) (bottom) The zero level sets of the polynomial in (2.3) (red lines) coincide with the zero contour of the second order partial derivative of the response amplitude C with respect to ω (bounding the dark green region). The filled circles (magenta) are singular points when the curve is parameterized by $\zeta(\omega)$, and the filled box (light green) is a singular point if the curve is parameterized by $\omega(\zeta)$.

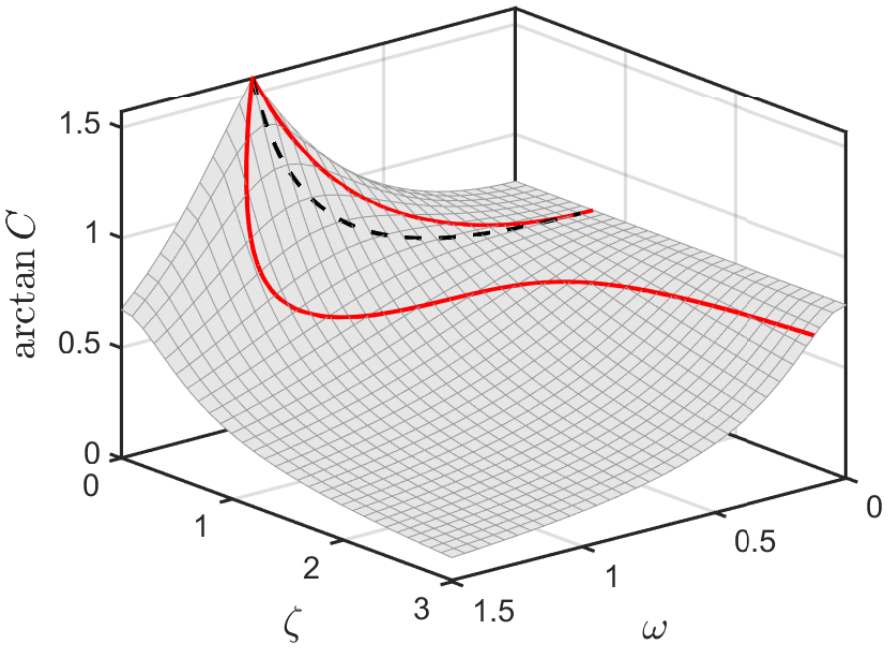

Figure 2.2: Frequency response surface of the harmonically forced linear oscillator. Here, the surface plot is based on the explicit expression for C in (2.2), the solid (red) lines are the sought extrema in the rate of change of the response amplitude C with respect to ω based on (2.3) and (2.4), and the dashed line (black) locates the global maximum of the response amplitude for $\zeta \leq 1/\sqrt{2}$.

such an analysis results in the constraints (2.12)-(2.14) coupled with the adjoint conditions

$$1 + 2C_1\lambda_1 = -1 + 2C_2\lambda_2 = 0, \tag{2.15}$$

$$-2A_1\lambda_1 + (1-\omega_1^2)\lambda_4 - 2\zeta\omega_1\lambda_5 = 0,\ -2A_2\lambda_2 + (1-\omega_2^2)\lambda_6 - 2\zeta\omega_2\lambda_7 = 0, \tag{2.16}$$

$$-2B_1\lambda_1 + 2\zeta\omega_1\lambda_4 + (1-\omega_1^2)\lambda_5 = 0,\ -2B_2\lambda_2 + 2\zeta\omega_2\lambda_6 + (1-\omega_2^2)\lambda_7 = 0, \tag{2.17}$$

$$\lambda_3 + 2(\zeta B_1 - \omega_1 A_1)\lambda_4 - 2(\zeta A_1 + \omega_1 B_1)\lambda_5 = 0, \tag{2.18}$$

$$-\lambda_3 + 2(\zeta B_2 - \omega_2 A_2)\lambda_6 - 2(\zeta A_2 + \omega_2 B_2)\lambda_7 = 0 \tag{2.19}$$

in terms of the Lagrange multipliers λ_1 through λ_7 that describe the sensitivity of the objective function at stationary points to violations of each of the constraints (2.12)-(2.14). Solutions are obtained only for ω_1 and $\omega_2 = \omega_1 - \epsilon$ that satisfy the equation

$$\frac{\omega_1(1-2\zeta^2-\omega_1^2)}{((1-\omega_1^2)^2+4\zeta^2\omega_1^2)^{3/2}} - \frac{\omega_2(1-2\zeta^2-\omega_2^2)}{((1-\omega_2^2)^2+4\zeta^2\omega_2^2)^{3/2}} = 0, \tag{2.20}$$

or, equivalently,

$$0 = \frac{3\omega_1^6 + 5(2\zeta^2-1)\omega_1^4 + (16\zeta^4 - 16\zeta^2 + 1)\omega_1^2 + 1 - 2\zeta^2}{((1-\omega_1^2)^2+4\zeta^2\omega_1^2)^{5/2}}\epsilon + \mathcal{O}(\epsilon^2), \tag{2.21}$$

again yielding the condition (2.3) on ω_1 from the previous paragraph. In this case, $C_1, C_2 > 0$ imply that

$$\lambda_1 = -\frac{\sqrt{(1-\omega_1^2)^2+4\zeta^2\omega_1^2}}{2},\ \lambda_2 = \frac{\sqrt{(1-\omega_2^2)^2+4\zeta^2\omega_2^2}}{2}, \tag{2.22}$$

$$\lambda_3 = -\frac{2\omega_1(1-2\zeta^2-\omega_1^2)}{((1-\omega_1^2)^2+4\zeta^2\omega_1^2)^{3/2}},\ \lambda_4 = -\frac{1}{\sqrt{(1-\omega_1^2)^2+4\zeta^2\omega_1^2}}, \tag{2.23}$$

$$\lambda_5 = 0,\ \lambda_6 = \frac{1}{\sqrt{(1-\omega_2^2)^2+4\zeta^2\omega_2^2}},\ \lambda_7 = 0. \tag{2.24}$$

In contrast to the discussion that led directly to (2.3) in the first part of this section, we do not presuppose an explicit expression for the response amplitude, one that can be differentiated

arbitrarily with respect to ω. Instead, we use a finite-difference approximation in terms of a fixed change ϵ in the independent variable and show that the predicted extremum converges to the desired solution when $\epsilon \to 0$.

We may take a further step back from an explicit analysis by considering the constrained optimization with respect to ω_1 of the objective function $x_1(0) - x_2(0)$ for $x_1(0), x_2(0) > 0$, given the differential constraints

$$\ddot{x}_1 + 2\zeta\dot{x}_1 + x_1 = \cos(\omega_1 t - \theta_1),\ \ddot{x}_2 + 2\zeta\dot{x}_2 + x_2 = \cos(\omega_2 t - \theta_2), \tag{2.25}$$

the boundary conditions

$$x_1(0) = x_1(T_1),\ \dot{x}_1(0) = \dot{x}_1(T_1) = 0,\ x_2(0) = x_2(T_2),\ \dot{x}_2(0) = \dot{x}_2(T_2) = 0 \tag{2.26}$$

with $T_1 = 2\pi/\omega_1$ and $T_2 = 2\pi/\omega_2$, and the algebraic constraint $\omega_1 - \omega_2 = \epsilon$ in the limit as $\epsilon \to 0$. The boundary conditions ensure that solutions are periodic with local extrema at $t = 0$. In this case, the necessary conditions for optimality append to these constraints the adjoint conditions

$$\ddot{\lambda}_1 - 2\zeta\dot{\lambda}_1 + \lambda_1 = 0,\ \ddot{\lambda}_2 - 2\zeta\dot{\lambda}_2 + \lambda_2 = 0, \tag{2.27}$$

$$1 - 2\zeta\lambda_1(0) + \dot{\lambda}_1(0) + \lambda_3 = 0,\ -1 - 2\zeta\lambda_2(0) + \dot{\lambda}_2(0) + \lambda_6 = 0, \tag{2.28}$$

$$2\zeta\lambda_1(T_1) - \dot{\lambda}_1(T_1) - \lambda_3 = 0,\ 2\zeta\lambda_2(T_2) - \dot{\lambda}_2(T_2) - \lambda_6 = 0, \tag{2.29}$$

$$-\lambda_1(0) + \lambda_4 = 0,\ \lambda_1(T_1) + \lambda_5 = 0,\ -\lambda_2(0) + \lambda_7 = 0,\ \lambda_2(T_1) + \lambda_8 = 0, \tag{2.30}$$

$$-\int_0^{T_1} \lambda_1 \sin(\omega_1 t - \theta_1)\,\mathrm{d}t = 0,\ -\int_0^{T_2} \lambda_2 \sin(\omega_2 t - \theta_2)\,\mathrm{d}t = 0, \tag{2.31}$$

$$\int_0^{T_1} \lambda_1 t \sin(\omega_1 t - \theta_1)\,\mathrm{d}t + 2\pi\lambda_3\dot{x}_1(T_1)/\omega_1^2 - 2\pi\lambda_5\ddot{x}_1(T_1)/\omega_1^2 + \lambda_9 = 0, \tag{2.32}$$

$$\int_0^{T_2} \lambda_2 t \sin(\omega_2 t - \theta_2)\,\mathrm{d}t + 2\pi\lambda_6\dot{x}_2(T_2)/\omega_2^2 - 2\pi\lambda_8\ddot{x}_2(T_2)/\omega_2^2 - \lambda_9 = 0 \tag{2.33}$$

in terms of the Lagrange multipliers λ_1 through λ_9 that describe the sensitivity of the objective

function at stationary points to violations of the differential constraints (2.25), boundary conditions (2.26), or algebraic constraint $\omega_1 - \omega_2 - \epsilon = 0$, respectively. We again find that solutions exist only for ω_1 and $\omega_2 = \omega_1 - \epsilon$ that satisfy (2.20), in which case, for example,

$$\lambda_1(t) = -\frac{1}{2\sqrt{\zeta^2-1}}\left(\frac{e^{t(\zeta-\sqrt{\zeta^2-1})}}{e^{2\pi(\zeta-\sqrt{\zeta^2-1})/\omega_1}-1} - \frac{e^{t(\zeta+\sqrt{\zeta^2-1})}}{e^{2\pi(\zeta+\sqrt{\zeta^2-1})/\omega_1}-1}\right), \tag{2.34}$$

$$\lambda_2(t) = -\frac{1}{2\sqrt{\zeta^2-1}}\left(\frac{e^{t(\zeta+\sqrt{\zeta^2-1})}}{e^{2\pi(\zeta+\sqrt{\zeta^2-1})/\omega_2}-1} - \frac{e^{t(\zeta-\sqrt{\zeta^2-1})}}{e^{2\pi(\zeta-\sqrt{\zeta^2-1})/\omega_2}-1}\right), \tag{2.35}$$

and

$$\lambda_9 = -\frac{2\omega_1(1-2\zeta^2-\omega_1^2)}{((1-\omega_1^2)^2+4\zeta^2\omega_1^2)^{3/2}}. \tag{2.36}$$

In contrast to the previous two approaches, we neither presuppose an explicit expression for the response amplitude nor for the form of the periodic response. Instead, the corresponding adjoint conditions (2.27)–(2.33) are here derived directly from the governing differential constraints and boundary conditions in a step that immediately generalizes to nonlinear problems for which closed-form solutions would not be available. As before, the finite-difference approximation in terms of a fixed change ϵ in the independent variable again approximates the loci of the inflection points to lowest order in ϵ.

The same discussion applies to the simpler search for a local extremum in the response amplitude under variations in ω, known to exist at $\omega = \sqrt{1-2\zeta^2}$ for $\zeta < 1/\sqrt{2}$. In this case, we might consider optimization of C with respect to ω given the polynomial constraints

$$C^2 - A^2 - B^2 = 0,\ 1 - A - 2B\zeta\omega + A\omega^2 = 0,\ B - 2A\zeta\omega - B\omega^2 = 0, \tag{2.37}$$

or optimization of $x(0) > 0$ with respect to ω given the boundary-value problem

$$\ddot{x} + 2\zeta\dot{x} + x = \cos(\omega t - \theta),\ x(0) = x(2\pi/\omega),\ \dot{x}(0) = \dot{x}(2\pi/\omega) = 0. \tag{2.38}$$

Alternatively, we could consider imposition of the additional constraint $C_1 = C_2$ to the

polynomial constraints (2.12)-(2.14) in the limit as $\epsilon \to 0$, or imposition of the additional constraint $x_1(0) = x_2(0)$ to the differential constraints (2.25), boundary conditions (2.26), and algebraic constraint $\omega_1 - \omega_2 = \epsilon$ in the limit as $\epsilon \to 0$. In doing so, one should reasonably ask which of these approaches generalize to nonlinear boundary-value problems and to other objective functions.

2.2.2 Lessons and inspirations

The examples in the previous section are notably concerned not with a singular excitation response in isolation, but with a property of such a response in relation to nearby responses along a continuous (and locally differentiable) family of responses. Although we held ζ fixed in our analysis, the implicit relationship in (2.3) further defines continuous families of inflection points and corresponding values of ζ. We are inevitably drawn to a methodology for charting such continuous families and for monitoring the values of one or several objective functions along such families.

As we approach this task, a count of degrees of freedom proves useful. We generically reduce the number of degrees of freedom by one for every algebraic constraint imposed on an *a priori* unknown algebraic variable. Similarly, for every *a priori* unknown solution to a differential constraint, we generically append as many degrees of freedom as the number of required initial conditions. As an example, Eq. (2.3) imposes one algebraic constraint on two *a priori* unknown algebraic variables, yielding a problem with (generically) a single degree of freedom. Similarly, the seven constraints (2.12)-(2.14) constrain the ten *a priori* unknown algebraic variables A_1, B_1, C_1, ω_1, A_2, B_2, C_2, ω_2, ζ, and ϵ to yield a problem with (generically) three degrees of freedom. The eight adjoint conditions (2.15)-(2.19) add seven more *a priori* unknown algebraic variables for a net of (generically) two degrees of freedom. Generically, the differential constraints (2.25), boundary conditions (2.26), and algebraic constraint $\omega_1 - \omega_2 = \epsilon$ on the *a priori* unknown variables $x_1(\cdot)$, ω_1, θ_1, $x_2(\cdot)$, ω_2, θ_2, ζ, and ϵ result in a problem with three degrees of freedom. The adjoint conditions (2.27)-(2.33) add

nine more *a priori* unknown variables for a net of (generically) two degrees of freedom.

The number of degrees of freedom of a differentiable continuation problem characterizes the dimension of a local manifold of solutions through any regular (in the sense of the implicit-function theorem [82]) solution point. This dimension represents a deficit of constraints relative to the number of *a priori* unknown variables, and so we often speak of the dimensional deficit of a continuation problem. For all the continuation problems of interest here, the dimensional deficit is a finite number, even as the problem domain may be infinite dimensional.

Problems with zero dimensional deficit generically have at most isolated solutions [75]. For example, by inspection of the partial derivative with respect to ζ and ω, respectively, the roots of the multivariable polynomial in (2.3) are found to be locally unique with respect to ζ for all positive $\zeta \neq 1/\sqrt{2}$ (cf. the green square at the bottom panel of Fig. 2.1) and locally unique with respect to ω for all positive $\omega \neq 1$ or $((19 + 8\sqrt{6})/23)^{1/4}$ (cf. the two magenta circles at the bottom panel of Fig. 2.1). By inspection of the Jacobian with respect to A_1, B_1, C_1, ω_1, A_2, B_2, C_2, ω_2, and λ_1 through λ_7, solutions of the polynomial constraints (2.12)-(2.14) and the corresponding adjoint conditions (2.15)-(2.19) are locally unique with respect to ζ and ϵ for all positive $\zeta \neq 1/\sqrt{2}$ and sufficiently small ϵ. Similarly, by inspection of the Jacobian with respect to A_1, B_1, C_1, A_2, B_2, C_2, ω_2, ζ, and λ_1 through λ_7, solutions are found to be locally unique with respect to ω_1 and ϵ for all positive $\omega_1 \neq 1$ or $((19 + 8\sqrt{6})/23)^{1/4}$ and sufficiently small ϵ. For solutions to the differential constraints (2.25), boundary conditions (2.26), algebraic constraint $\omega_1 - \omega_2 = \epsilon$ and the corresponding adjoint conditions (2.27)-(2.33), the same conclusions would be theoretically available by showing the invertibility of the linearization with respect to $x_1(\cdot)$, ω_1, θ_1, $x_2(\cdot)$, ω_2, θ_2, $\lambda_1(\cdot)$, $\lambda_2(\cdot)$, and λ_3 through λ_9 or $x_1(\cdot)$, θ_1, $x_2(\cdot)$, ω_2, θ_2, ζ, $\lambda_1(\cdot)$, $\lambda_2(\cdot)$, and λ_3 through λ_9, respectively.

Local uniqueness affords us confidence that an approximate algorithm to locate a solution to a problem with zero dimensional deficit will not be distracted by other nearby solutions. Provided that we initialize a search with an initial solution guess in the vicinity of the sought solution, we trust that a well-designed solver, e.g., based on Newton's or Broyden's

methods [83], will rapidly converge to this solution. For the first two formulations of the inflection point problem in Section 2.2.1, we apply such a solver directly to the system of nonlinear equations. For the formulation in terms of differential boundary-value problems, some form of discretization must first be employed.

Inspired by these observations, a general continuation methodology for a problem $\mathbf{P}$ with nonzero dimensional deficit may be obtained by iteratively

- constructing auxiliary constraints [32], [84], [85] that when appended to $\mathbf{P}$ result in a problem $\mathbf{P}_0$ with zero dimensional deficit;
- constructing an initial solution guess for $\mathbf{P}_0$ using a previously found solution to $\mathbf{P}$ [32], [63], [86]; and
- solving $\mathbf{P}_0$ using an iterative algorithm based at the initial solution guess.

By definition, a solution to $\mathbf{P}_0$ also solves $\mathbf{P}$. The success of such a methodology thus depends on its ability to ensure that solutions to $\mathbf{P}_0$ are locally unique; that the iterative solver is able to converge to such a solution; and that the succession of such solutions suitably captures the geometry of the manifold of solutions to $\mathbf{P}$ [32], [87].

Consider, for example, the problem obtained by replacing (2.15) in the necessary conditions for an extremum of $C_1 - C_2$ under the polynomial constraints (2.12)-(2.14) with

$$\eta - 2C_1\lambda_1 = -\eta - 2C_2\lambda_2 = 0. \tag{2.39}$$

For fixed ζ and ϵ, we obtain a problem $\mathbf{P}$ with nominal dimensional deficit equal to one, generically resulting in the existence of a unique one-dimensional solution curve through any regular solution point. In fact, by linearity and homogeneity of the adjoint conditions (2.15)-(2.19) with respect to η and the Lagrange multipliers, one such curve is obtained from solutions $(A_1, B_1, C_1, \omega_1, A_2, B_2, C_2, \omega_2)$ to (2.12)-(2.14) together with $\eta = \lambda_1 = \cdots = \lambda_7 = 0$. For the same reason, all solutions with nonzero η lie on a straight line with ω_1 and $\omega_2 = \omega_1 - \epsilon$

that satisfy (2.20) and Lagrange multipliers given by the right-hand sides of (2.22)-(2.24) multiplied by η. Curiously, but not accidentally [13], [35], the two curves intersect precisely at a local extremum of $C_1 - C_2$ along the first curve, at a singular point of $\mathbf{P}$, as illustrated in the top panel of Fig. 2.3.

For this problem, at each iterate of the continuation methodology we construct $\mathbf{P}_0$ by appending a single auxiliary constraint to $\mathbf{P}$. It comes as no surprise that trouble brews on a vicinity of the singular point as local uniqueness fails there for the sought solution to $\mathbf{P}_0$. With some luck, we may be able to step past the singularity along one of the curves, detect such a crossing, and then switch to the other curve. Such a branch-switching strategy [73], [86] may allow us to locate the sought inflection points starting from an arbitrary solution to (2.12)-(2.14) together with $\eta = \lambda_1 = \cdots = \lambda_7 = 0$.

As an alternative, we seek to construct an augmented continuation problem $\mathbf{P}^*$ by introducing one additional *a priori* unknown, say χ, such that the two solution curves to $\mathbf{P}$ satisfy $\mathbf{P}^*$ for $\chi = 0$. With a bit of care, all solutions of $\mathbf{P}^*$ near the singular point of $\mathbf{P}$ are regular points of $\mathbf{P}^*$. Here, we simply subtract $\epsilon\chi$ from the left-hand side of (2.19) such that solutions to $\mathbf{P}^*$ are obtained only for ω_1, $\omega_2 = \omega_1 - \epsilon$, η, and χ that satisfy the equation

$$0 = \left(\chi - 2\eta \frac{3\omega_1^6 + 5(2\zeta^2 - 1)\omega_1^4 + (16\zeta^4 - 16\zeta^2 + 1)\omega_1^2 + 1 - 2\zeta^2}{((1 - \omega_1^2)^2 + 4\zeta^2\omega_1^2)^{5/2}} \right) \epsilon + \mathcal{O}(\epsilon^2). \tag{2.40}$$

For sufficiently small ϵ, it follows that the dimensional deficit of $\mathbf{P}^*$ (two) equals the dimension of the solution manifold and all solutions near (and including) the singular point of $\mathbf{P}$ are regular points of $\mathbf{P}^*$, as demonstrated in the bottom panel of Fig. 2.3. In this case, at each iterate of the continuation methodology we construct a problem $\mathbf{P}_0^*$ with zero dimensional deficit by appending two auxiliary scalar constraints to $\mathbf{P}^*$.

It it straightforward to verify that an equivalent set of observations follows from

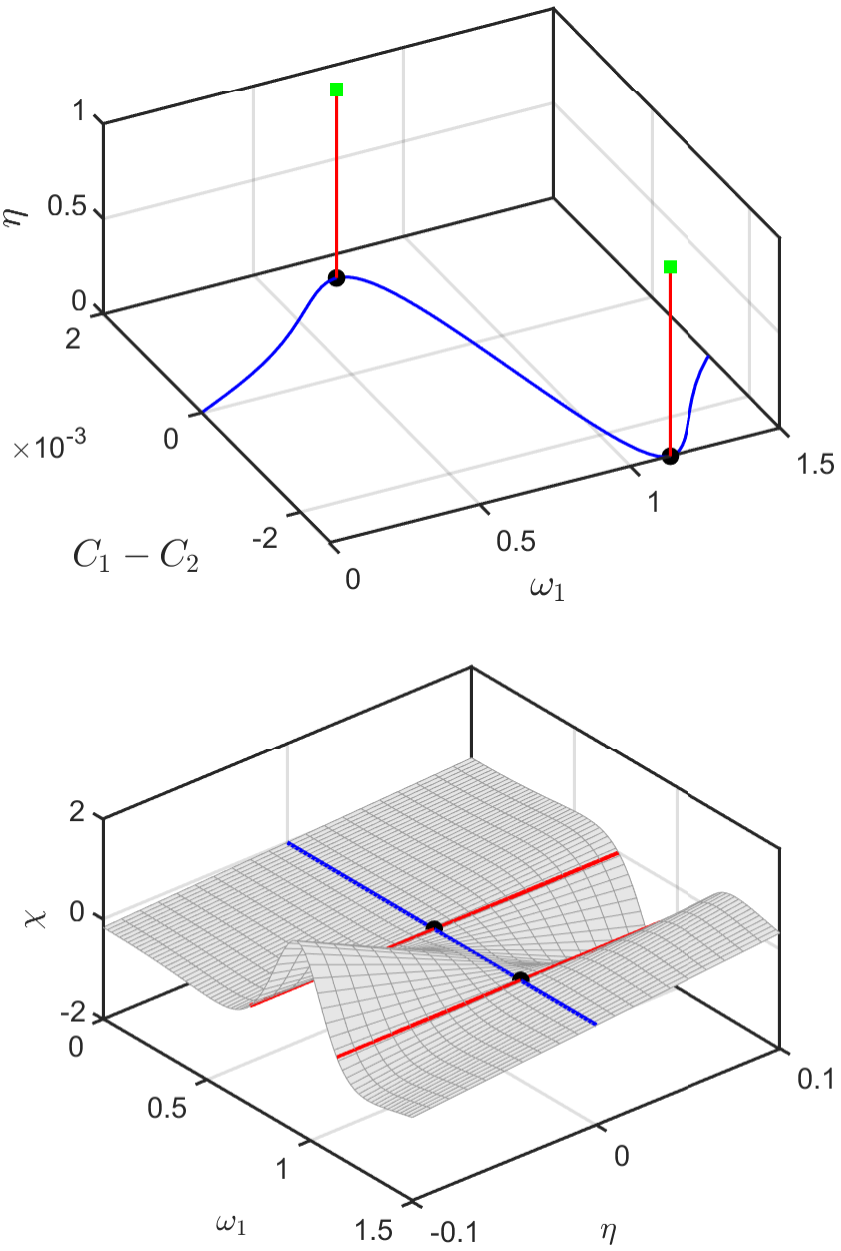

Figure 2.3: (top) Projections of solution branches with vanishing (solid blue) and non-vanishing (solid red) Lagrange multipliers for the problem $\mathbf{P}$ for locating extrema of $C_1 - C_2$ with fixed $(\epsilon, \zeta) = (0.001, 0.3)$. The intersections (filled circles) correspond to local extrema of $C_1 - C_2$ and are singular points of $\mathbf{P}$. The green squares represent solutions with $\eta = 1$. (bottom) Projection of the two-dimensional solution manifold of the problem $\mathbf{P}^*$ with fixed $(\epsilon, \zeta) = (0.001, 0.3)$. The blue and red straight lines correspond to the identically-colored curves in the left panel and lie in the zero level set of χ on the solution manifold. The intersections (black filled circles) are regular points of $\mathbf{P}^*$.

- the substitution of

$$\eta - \lambda_3 + 2\zeta\lambda_1(0) - \dot{\lambda}_1(0) = 0,\ -\eta - \lambda_6 + 2\zeta\lambda_2(0) - \dot{\lambda}_2(0) = 0 \tag{2.41}$$

  in lieu of (2.28) to generate a problem **P** with nominal dimensional deficit equal to one, but with a singular point at the intersection of two one-dimensional curves of solutions $(x_1(\cdot), \omega_1, \theta_1, x_2(\cdot), \omega_2, \theta_2, \eta, \lambda_1(\cdot), \lambda_2(\cdot), \lambda_3, \ldots, \lambda_9)$; followed by

- subtraction of $\epsilon\chi$ from the left-hand side of (2.33) to obtain a problem $\mathbf{P}^*$ with dimensional deficit equal to two and with all regular points on the corresponding solution manifold near (and including) the singular point of **P** (obtained when $\chi = 0$).

2.2.3 The COCO formalism

The discussion in the previous section highlights the merits of considering problem construction separately from problem analysis. First decide what you want to do. Then figure out how to do it. The description of the COCO construction framework in this section continues in this spirit.

In the general case, we consider continuation problems **P** of the form

$$\Phi(u) = 0 \tag{2.42}$$

for some Frechét differentiable operator $\Phi : \mathcal{U}_\Phi \to \mathcal{R}_\Phi$ with Banach space domain $\mathcal{U}_\Phi$ and range $\mathcal{R}_\Phi$. At this level of abstraction, there are no distinguishing features of either domain or range. We do not unnecessarily presuppose a dimensional deficit nor assume a particular decomposition of $\mathcal{U}_\Phi$. Instead, we design a general continuation methodology that is accommodating of different dimensional deficits and independent of any substructure of $\mathcal{U}_\Phi$.

A specialized form of the continuation problem **P** in (2.42) that self-referentially contains

the form in (2.42) is given by the extended continuation problem **E** [32], [88] of the form

$$\begin{pmatrix} \Phi(u) \\ \Psi(u) - \mu \end{pmatrix} = 0 \tag{2.43}$$

in terms of the *zero functions* Φ, *continuation variables* $u \in \mathcal{U}_\Phi$, *monitor functions* $\Psi : \mathcal{U}_\Phi \to \mathbb{R}^{n_\Psi}$, and *continuation parameters* $\mu \in \mathbb{R}^{n_\Psi}$. In the special case that Ψ projects onto a finite subspace of $\mathcal{U}_\Phi$, the corresponding μ amount only to a labeling of these components. More generally, μ tracks a finite number of solution metrics and, when fixed, restricts attention to a subset of solutions to the *zero problem* $\Phi(u) = 0$. The restriction $\mathbf{E}\big|_{\mathbb{I}}$ obtained by fixing a subset $\mathbb{I}$ of continuation parameters is equivalent to a reduced continuation problem **R** in terms of the continuation variables and the remaining continuation parameters. Assuming a dimensional deficit of the zero problem equal to d, the number of possible reduced continuation problems equals $2^{\min(d, n_\Psi)}$.

The examples in Section 2.2.1 illustrate these principles. Each fits the form of (2.42) given some association of unknowns with a space $\mathcal{U}_\Phi$ and constraints with Φ. Of course, every such choice, for example those differing by whether ζ is fixed or free to vary, requires a distinct formulation. In contrast, (2.43) is designed to support every possible choice by including among the monitor functions projections onto all variables that may or may not be designated as fixed during continuation. The decision to hold ζ fixed may thus be deferred to the moment of analysis, rather than imposed at the time of construction.

The constrained optimization examples in Section 2.2.1 actually point to a further extension to (2.43) that recognizes the linearity and homogeneity of the modified adjoint conditions in the various Lagrange multipliers, η, and χ. Additional study also of constrained optimization problems with inequality constraints [35] inspires the definition of an augmented

continuation problem **A** of the form

$$\begin{pmatrix} \Phi(u) \\ \Psi(u) - \mu \\ \Lambda^*(u)\lambda \\ \Xi(u, \lambda, v) \\ \Theta(u, \lambda, v) - \nu \end{pmatrix} = 0 \tag{2.44}$$

in terms of the *zero functions* Φ, *monitor functions* Ψ, *adjoint functions* Λ^*, *complementary zero functions* Ξ, and *complementary monitor functions* Θ, as well as collections of *continuation variables* u, *continuation parameters* μ, *continuation multipliers* λ, *complementary continuation variables* v, and *complementary continuation parameters* ν. The form (2.44) again self-referentially contains both (2.42) and (2.43) with μ and ν designated as variables that may be fixed or allowed to vary at the moment of analysis.

The augmented continuation problem in (2.44) is a generalization of Eq. (30) in [35] for locating solutions to constrained optimization problems with equality and inequality constraints using continuation techniques:

$$\begin{pmatrix} \Phi(u) \\ \Psi(u) - \mu \\ (D\Phi(u))^* \lambda + (D\Psi(u))^* \eta + (DG(u))^* \sigma \\ \eta - \nu \\ K(\sigma, -G(u)) - \kappa \end{pmatrix} = 0, \tag{2.45}$$

where a finite subset of elements of Ψ evaluate to the inequality function G. Here, the complementarity conditions of Karush-Kuhn-Tucker theory [89] are expressed in terms of complementarity functions K that must vanish at extrema. We obtain (2.45) as a special case of (2.44) by defining Λ^* in terms of the collection of adjoint operators $(D\Phi(u))^*$, $(D\Psi(u))^*$, and $(DG(u))^*$, and by designating the collection of Lagrange multipliers (λ, η, σ)

as the corresponding vector of continuation multipliers. Linearity follows from the additive decomposition of the constraint Lagrangian into terms coupling individual constraints with the corresponding adjoint variables. In this notation, (ν, κ) are complementary continuation parameters and the last two rows of (2.45) define the corresponding complementary monitor functions Θ. In practice, we often substitute relaxed complementarity functions that are smooth everywhere (the complementarity functions used in [35] are nonsmooth at the origin). Such relaxed functions are then parameterized by additional complementary continuation variables that, in turn, may be associated with complementary continuation parameters in order to consider variations that stiffen the constraint. We do not consider inequality constraints in this study, but will have use for both Ξ and Θ in later sections.

Suitably discretized, the augmented continuation problem $\mathbf{A}$ in (2.44) is the most general type of continuation problem supported by the most recent release of the COCO platform [74]. Here, $u \in \mathbb{R}^{n_u}$, $\lambda \in \mathbb{R}^{n_\lambda}$, $v \in \mathbb{R}^{n_v}$, $\mu \in \mathbb{R}^{n_\Psi}$ and $\nu \in \mathbb{R}^{n_\Theta}$, while $\Phi : \mathbb{R}^{n_u} \to \mathbb{R}^{n_\Phi}$, $\Psi : \mathbb{R}^{n_u} \to \mathbb{R}^{n_\Psi}$, $\Lambda : \mathbb{R}^{n_u} \to \mathbb{R}^{n_\lambda \times n_\Lambda}$, $\Xi : \mathbb{R}^{n_u} \times \mathbb{R}^{n_\lambda} \times \mathbb{R}^{n_v} \to \mathbb{R}^{n_\Xi}$, and $\Theta : \mathbb{R}^{n_u} \times \mathbb{R}^{n_\lambda} \times \mathbb{R}^{n_v} \to \mathbb{R}^{n_\Theta}$, and $\Lambda^* = \Lambda^{\mathrm{T}}$. We obtain a restricted continuation problem $\mathbf{A}\big|_{\mathbb{I}_\mu, \mathbb{I}_\nu}$ by designating subsets $\{\mu_i,\, i \in \mathbb{I}_\mu\}$ and $\{\nu_i,\, i \in \mathbb{I}_\nu\}$ as fixed. The resulting restricted continuation problem then has nominal dimensional deficit equal to $n_u + n_\lambda + n_v - n_\Phi - n_\Lambda - n_\Xi - |\mathbb{I}_\mu| - |\mathbb{I}_\nu|$.

While there may be some merit in the level of abstraction of the augmented continuation problem purely from an organizational viewpoint, it truly comes into its own when coupled with a systematic paradigm of problem construction. This is one of the features of the COCO software platform, as described in the context of the extended continuation problem (2.43) in Chapter 3 of [32].

It is a truism that a given (finite-dimensional) augmented continuation problem $\mathbf{A}$ may be interpreted as the largest element of a chain

$$\emptyset = \mathbf{A}_0 \dot{\subseteq} \mathbf{A}_1 \dot{\subseteq} \cdots \dot{\subseteq} \mathbf{A}_N = \mathbf{A} \tag{2.46}$$

of augmented continuation problems $\mathbf{A}_i$, where $\tilde{\mathbf{A}} \trianglelefteq \hat{\mathbf{A}}$ if

$$\tilde{n}_{u/\lambda/v/\Phi/\Psi/\Lambda/\Xi/\Theta} \leq \hat{n}_{u/\lambda/v/\Phi/\Psi/\Lambda/\Xi/\Theta}, \tag{2.47}$$

$$\hat{\Phi}_{(1:\tilde{n}_\Phi)}(u) = \tilde{\Phi}\left(u_{(1:\tilde{n}_u)}\right), \; \hat{\Psi}_{(1:\tilde{n}_\Psi)}(u) = \tilde{\Psi}\left(u_{(1:\tilde{n}_u)}\right), \tag{2.48}$$

$$\hat{\Lambda}_{(1:\tilde{n}_\lambda,1:\tilde{n}_\Lambda)}(u) = \tilde{\Lambda}\left(u_{(1:\tilde{n}_u)}\right), \; \hat{\Lambda}_{(1:\tilde{n}_\lambda,\tilde{n}_\Lambda+1:\hat{n}_\Lambda)}(u) = 0 \tag{2.49}$$

$$\hat{\Xi}_{(1:\tilde{n}_\Xi)}(u,\lambda,v) = \tilde{\Xi}\left(u_{(1:\tilde{n}_u)}, \lambda_{(1:\tilde{n}_\lambda)}, v_{(1:\tilde{n}_v)}\right), \tag{2.50}$$

$$\hat{\Theta}_{(1:\tilde{n}_\Theta)}(u,\lambda,v) = \tilde{\Theta}\left(u_{(1:\tilde{n}_u)}, \lambda_{(1:\tilde{n}_\lambda)}, v_{(1:\tilde{n}_v)}\right), \tag{2.51}$$

and

$$\hat{\mu}_{(1:\tilde{n}_\Psi)} = \tilde{\mu}, \; \hat{\nu}_{(1:\tilde{n}_\Xi)} = \tilde{\nu}, \tag{2.52}$$

and where $\emptyset$ denotes an *empty* continuation problem with $n_u = n_\lambda = n_v = n_\Phi = n_\Psi = n_\Lambda = n_\Xi = n_\Theta = 0$. The chain in (2.46) represents a sequential embedding of partial realizations of $\mathbf{A}$ into successively larger problems with additional unknowns and additional constraints. Since $\emptyset \trianglelefteq \mathbf{A}$ for any $\mathbf{A}$, we obtain a nontrivial decomposition of $\mathbf{A}$ in the form of (2.46) when at least one of the partial realizations is nonempty and distinct from $\mathbf{A}$. Given an augmented continuation problem $\mathbf{A}$ with $n_\Phi + n_\Psi + n_\Lambda + n_\Xi + n_\Theta > 1$, it is always possible to find a nontrivial decomposition (2.46) for some equivalent augmented continuation problem obtained by reordering the elements of Φ, Ψ, Λ, Ξ, Θ, u, λ, v, μ, and ν.

Given a chain decomposition (2.46), there exists, for each i, four ordered index sets

$$\{n_{u,i-1}+1, \ldots, n_{u,i}\} \subseteq \mathbb{K}_{u,i} \subseteq \{1, \ldots, n_{u,i}\}, \tag{2.53}$$

$$\{n_{\lambda,i-1}+1, \ldots, n_{\lambda,i}\} \subseteq \mathbb{K}_{\lambda,i} \subseteq \{1, \ldots, n_{\lambda,i}\}, \tag{2.54}$$

$$\{n_{\Lambda,i-1}+1, \ldots, n_{\Lambda,i}\} \subseteq \mathbb{K}_{\Lambda,i} \subseteq \{1, \ldots, n_{\Lambda,i}\}, \tag{2.55}$$

$$\{n_{v,i-1}+1, \ldots, n_{v,i}\} \subseteq \mathbb{K}_{v,i} \subseteq \{1, \ldots, n_{v,i}\}, \tag{2.56}$$

such that

$$\Phi_{\left(n_{\Phi,i-1}+1:n_{\Phi,i}\right)}(u) = \mathfrak{phi}^{(i)}\left(u_{\mathbb{K}_{u,i}}\right), \tag{2.57}$$

$$\Psi_{\left(n_{\Psi,i-1}+:n_{\Psi,i}\right)}(u) = \mathfrak{psi}^{(i)}\left(u_{\mathbb{K}_{u,i}}\right), \tag{2.58}$$

$$\Lambda_{\left(n_{\lambda,i-1}+1:n_{\lambda,i},\mathbb{K}_{\Lambda,i}\right)}(u) = \mathfrak{lambda}^{(i)}\left(u_{\mathbb{K}_{u,i}}\right), \tag{2.59}$$

$$\Xi_{\left(n_{\Xi,i-1}+1:n_{\Xi,i}\right)}(u,\lambda,v) = \mathfrak{xi}^{(i)}\left(u_{\mathbb{K}_{u,i}}, \lambda_{\mathbb{K}_{\lambda,i}}, v_{\mathbb{K}_{v,i}}\right), \tag{2.60}$$

$$\Theta_{\left(n_{\Theta,i-1}+1:n_{\Theta,i}\right)}(u,\lambda,v) = \mathfrak{theta}^{(i)}\left(u_{\mathbb{K}_{u,i}}, \lambda_{\mathbb{K}_{\lambda,i}}, v_{\mathbb{K}_{v,i}}\right), \tag{2.61}$$

and

$$\Lambda_{\left(n_{\lambda,i-1}+1:n_{\lambda,i},\{1,\ldots,n_{\Lambda,i}\}\setminus\mathbb{K}_{\Lambda,i}\right)}(u) = 0 \tag{2.62}$$

for some functions $\mathfrak{phi}^{(i)} : \mathbb{R}^{|\mathbb{K}_{u,i}|} \to \mathbb{R}^{n_{\Phi,i}-n_{\Phi,i-1}}$, $\mathfrak{psi}^{(i)} : \mathbb{R}^{|\mathbb{K}_{u,i}|} \to \mathbb{R}^{n_{\Psi,i}-n_{\Psi,i-1}}$, $\mathfrak{lambda}^{(i)} : \mathbb{R}^{|\mathbb{K}_{u,i}|} \to \mathbb{R}^{(n_{\lambda,i}-n_{\lambda,i-1})\times|\mathbb{K}_{\Lambda,i}|}$, $\mathfrak{xi}^{(i)} : \mathbb{R}^{|\mathbb{K}_{u,i}|} \times \mathbb{R}^{|\mathbb{K}_{\lambda,i}|} \times \mathbb{R}^{|\mathbb{K}_{v,i}|} \to \mathbb{R}^{n_{\Xi,i}-n_{\Xi,i-1}}$, and $\mathfrak{theta}^{(i)} : \mathbb{R}^{|\mathbb{K}_{u,i}|} \times \mathbb{R}^{|\mathbb{K}_{\lambda,i}|} \times \mathbb{R}^{|\mathbb{K}_{v,i}|} \to \mathbb{R}^{n_{\Theta,i}-n_{\Theta,i-1}}$. We refer to these functions as representations of the corresponding left-hand sides and to $\mathbb{K}_{u,i}$, $\mathbb{K}_{\lambda,i}$, $\mathbb{K}_{\Lambda,i}$, and $\mathbb{K}_{v,i}$ as the corresponding dependency index sets.

We now arrive at a paradigm of decomposition of an augmented continuation problem $\mathbf{A}$ through a sequence of partial realizations $\mathbf{A}_i$ constructed sequentially in terms of the representations $\mathfrak{phi}^{(i)}$, $\mathfrak{psi}^{(i)}$, $\mathfrak{lambda}^{(i)}$, $\mathfrak{xi}^{(i)}$, and $\mathfrak{theta}^{(i)}$ and the dependency index sets $\mathbb{K}_{u,i}$, $\mathbb{K}_{\lambda,i}$, $\mathbb{K}_{\Lambda,i}$, and $\mathbb{K}_{v,i}$. Since we must associate an initial solution guess (u_0, λ_0, v_0) to $\mathbf{A}$, we may construct the dependency index sets $\mathbb{K}_{u,i}$, $\mathbb{K}_{\lambda,i}$, and $\mathbb{K}_{v,i}$ in terms of the index sets

$$\mathbb{K}^{\mathrm{o}}_{u,i} = \mathbb{K}_{u,i} \setminus \{n_{u,i-1}+1, \ldots, n_{u,i-1}+(n_{u,i}-n_{u,i-1})\}, \tag{2.63}$$

$$\mathbb{K}^{\mathrm{o}}_{\lambda,i} = \mathbb{K}_{\lambda,i} \setminus \{n_{\lambda,i-1}+1, \ldots, n_{\lambda,i-1}+(n_{\lambda,i}-n_{\lambda,i-1})\}, \tag{2.64}$$

$$\mathbb{K}^{\mathrm{o}}_{v,i} = \mathbb{K}_{v,i} \setminus \{n_{v,i-1}+1, \ldots, n_{v,i-1}+(n_{v,i}-n_{v,i-1})\}, \tag{2.65}$$

and the cardinalities $|u_{0,n_{u,i-1}+1:n_{u,i}}| = n_{u,i} - n_{u,i-1}$, $|\lambda_{0,n_{\lambda,i-1}+1:n_{\lambda,i}}| = n_{\lambda,i} - n_{\lambda,i-1}$, and

$|v_{0,n_{v,i-1}+1:n_{v,i}}| = n_{v,i} - n_{v,i-1}$, respectively. Similarly, we obtain the index set $\mathbb{K}_{\Lambda,i}$ from the index set

$$\mathbb{K}^{\mathrm{o}}_{\Lambda,i} = \mathbb{K}_{\Lambda,i} \setminus \{n_{\Lambda,i-1} + 1, \ldots, n_{\Lambda,i-1} + (n_{\Lambda,i} - n_{\Lambda,i-1})\} \tag{2.66}$$

and the difference between the number of columns of $\mathfrak{lambda}^{(i)}(\cdot)$ and $\mathbb{K}^{\mathrm{o}}_{\Lambda,i}$, since this must equal $n_{\Lambda,i} - n_{\Lambda,i-1}$.

Rather than considering the decomposition of an existing augmented continuation problem, we may consider its staged construction through the successive application of a sequence of operators on the space of augmented continuation problems. Given an augmented continuation problem $\mathbf{A}$ with initial solution guess (u_0, λ_0, v_0) we construct an augmented continuation problem $\hat{\mathbf{A}}$ with initial solution guess $(\hat{u}_0, \hat{\lambda}_0, \hat{v}_0)$ by the application of the operator

$$\hat{} := \left[\mathfrak{phi}, \mathfrak{psi}, \mathfrak{lambda}, \mathfrak{xi}, \mathfrak{theta}, \mathbb{K}^{\mathrm{o}}_u, \mathbb{K}^{\mathrm{o}}_\lambda, \mathbb{K}^{\mathrm{o}}_\Lambda, \mathbb{K}^{\mathrm{o}}_v, u^{\mathrm{n}}_0, \lambda^{\mathrm{n}}_0, v^{\mathrm{n}}_0\right] \tag{2.67}$$

in terms of the index sets $\mathbb{K}^{\mathrm{o}}_u, \mathbb{K}^{\mathrm{o}}_\lambda, \mathbb{K}^{\mathrm{o}}_\Lambda, \mathbb{K}^{\mathrm{o}}_v$, vectors $u^{\mathrm{n}}_0 \in \mathbb{R}^{k_u}$, $\lambda^{\mathrm{n}}_0 \in \mathbb{R}^{k_\lambda}$, and $v^{\mathrm{n}}_0 \in \mathbb{R}^{k_v}$, functions $\mathfrak{phi} : \mathbb{R}^{|\mathbb{K}^{\mathrm{o}}_u|+k_u} \to \mathbb{R}^{k_\Phi}$, $\mathfrak{psi} : \mathbb{R}^{|\mathbb{K}^{\mathrm{o}}_u|+k_u} \to \mathbb{R}^{k_\Psi}$, $\mathfrak{lambda} : \mathbb{R}^{|\mathbb{K}^{\mathrm{o}}_u|+k_u} \to \mathbb{R}^{k_\lambda \times (|\mathbb{K}^{o}_\Lambda|+k_\Lambda)}$, $\mathfrak{xi} : \mathbb{R}^{|\mathbb{K}^{\mathrm{o}}_u|+k_u} \times \mathbb{R}^{|\mathbb{K}^{\mathrm{o}}_\lambda|+k_\lambda} \times \mathbb{R}^{|\mathbb{K}^{\mathrm{o}}_v|+k_v} \to \mathbb{R}^{k_\Xi}$ and $\mathfrak{theta} : \mathbb{R}^{|\mathbb{K}^{\mathrm{o}}_u|+k_u} \times \mathbb{R}^{|\mathbb{K}^{\mathrm{o}}_\lambda|+k_\lambda} \times \mathbb{R}^{|\mathbb{K}^{\mathrm{o}}_v|+k_v} \to \mathbb{R}^{k_\Theta}$, such that $\hat{u}_0 = (u_0, u^{\mathrm{n}}_0)$, $\hat{\lambda}_0 = (\lambda_0, \lambda^{\mathrm{n}}_0)$, and $\hat{v}_0 = (v_0, v^{\mathrm{n}}_0)$, $\mathbb{K}_u = \mathbb{K}^{\mathrm{o}}_u \cup \{n_u + 1, \ldots, n_u + k_u\}$, $\mathbb{K}_\lambda = \mathbb{K}^{\mathrm{o}}_\lambda \cup \{n_\lambda + 1, \ldots, n_\lambda + k_\lambda\}$, $\mathbb{K}_\Lambda = \mathbb{K}^{\mathrm{o}}_\Lambda \cup \{n_\Lambda + 1, \ldots, n_\Lambda + k_\Lambda\}$, and $\mathbb{K}_v = \mathbb{K}^{\mathrm{o}}_v \cup \{n_v + 1, \ldots, n_v + k_v\}$,

$$\hat{\Phi} : \hat{u} \mapsto \begin{pmatrix} \Phi\left(\hat{u}_{(1:n_u)}\right) \\ \mathfrak{phi}\left(\hat{u}_{\mathbb{K}_u}\right) \end{pmatrix}, \tag{2.68}$$

$$\hat{\Psi} : \hat{u} \mapsto \begin{pmatrix} \Psi\left(\hat{u}_{(1:n_u)}\right) \\ \mathfrak{psi}\left(\hat{u}_{\mathbb{K}_u}\right) \end{pmatrix}, \tag{2.69}$$

$$\hat{\Xi} : \left(\hat{u}, \hat{\lambda}, \hat{v}\right) \mapsto \begin{pmatrix} \Xi\left(\hat{u}_{(1:n_u)}, \hat{\lambda}_{(1:n_\lambda)}, \hat{v}_{(1:n_v)}\right) \\ \mathfrak{xi}\left(\hat{u}_{\mathbb{K}_u}, \hat{\lambda}_{\mathbb{K}_\lambda}, \hat{v}_{\mathbb{K}_v}\right) \end{pmatrix}, \tag{2.70}$$

$$\hat{\Theta} : \left(\hat{u}, \hat{\lambda}, \hat{v}\right) \mapsto \begin{pmatrix} \Theta\left(\hat{u}_{(1:n_u)}, \hat{\lambda}_{(1:n_\lambda)}, \hat{v}_{(1:n_v)}\right) \\ \mathfrak{theta}\left(\hat{u}_{\mathbb{K}_u}, \hat{\lambda}_{\mathbb{K}_\lambda}, \hat{v}_{\mathbb{K}_v}\right) \end{pmatrix}, \tag{2.71}$$

and

$$\hat{\Lambda}_{(1:n_\lambda, 1:n_\Lambda)} : \hat{u} \mapsto \Lambda\left(\hat{u}_{(1:n_u)}\right), \tag{2.72}$$

$$\hat{\Lambda}_{(1:n_\lambda, n_\Lambda+1:n_\Lambda+k_\Lambda)} : \hat{u} \mapsto 0, \tag{2.73}$$

$$\hat{\Lambda}_{(n_\lambda+1:n_\lambda+k_\lambda, \mathbb{K}_\Lambda)} : \hat{u} \mapsto \mathfrak{lambda}\left(\hat{u}_{\mathbb{K}_u}\right), \tag{2.74}$$

$$\hat{\Lambda}_{(n_\lambda+1:n_\lambda+k_\lambda, \{1,\ldots,n_\Lambda+k_\Lambda\}\setminus\mathbb{K}_\Lambda)} : \hat{u} \mapsto 0. \tag{2.75}$$

In COCO, an operator of the form (2.67) is called a *constructor*. Its core constructors correspond to the special operators

$$\left[\mathfrak{phi}, \emptyset, \emptyset, \emptyset, \emptyset, \mathbb{K}_u^{\mathrm{o}}, \emptyset, \emptyset, \emptyset, u_0^{\mathrm{n}}, \emptyset, \emptyset\right], \tag{2.76}$$

$$\left[\emptyset, \mathfrak{psi}, \emptyset, \emptyset, \emptyset, \mathbb{K}_u^{\mathrm{o}}, \emptyset, \emptyset, \emptyset, u_0^{\mathrm{n}}, \emptyset, \emptyset\right], \tag{2.77}$$

$$\left[\emptyset, \emptyset, \emptyset, \mathfrak{xi}, \emptyset, \mathbb{K}_u^{\mathrm{o}}, \mathbb{K}_\lambda^{\mathrm{o}}, \emptyset, \mathbb{K}_v^{\mathrm{o}}, \emptyset, \emptyset, v_0^{\mathrm{n}}\right], \tag{2.78}$$

$$\left[\emptyset, \emptyset, \emptyset, \emptyset, \mathfrak{theta}, \mathbb{K}_u^{\mathrm{o}}, \mathbb{K}_\lambda^{\mathrm{o}}, \emptyset, \mathbb{K}_v^{\mathrm{o}}, \emptyset, \emptyset, v_0^{\mathrm{n}}\right], \tag{2.79}$$

and

$$\left[\emptyset, \emptyset, \mathfrak{lambda}, \emptyset, \emptyset, \mathbb{K}_u^{\mathrm{o}}, \emptyset, \mathbb{K}_\Lambda^{\mathrm{o}}, \emptyset, \emptyset, \lambda_0^{\mathrm{n}}, \emptyset\right], \tag{2.80}$$

where, in the last case, $\mathbb{K}_u^{\mathrm{o}}$ equals $\mathbb{K}_u$ for a previous call to one of the first two core constructors. A bipartite graph illustration of these core constructors and their variable dependence is presented in Fig. 2.4. Each call to a core constructor is associated with a unique *function*

identifier allowing subsequent stages of construction, for example, to reference its index sets. Each definition of a (complementary) monitor function is also associated with unique labels for the corresponding (complementary) continuation parameters, allowing each to be fixed or free to vary during the subsequent continuation analysis. Composition of calls to these core constructors defines the space of operators of the form (2.67) that may be realized in COCO.

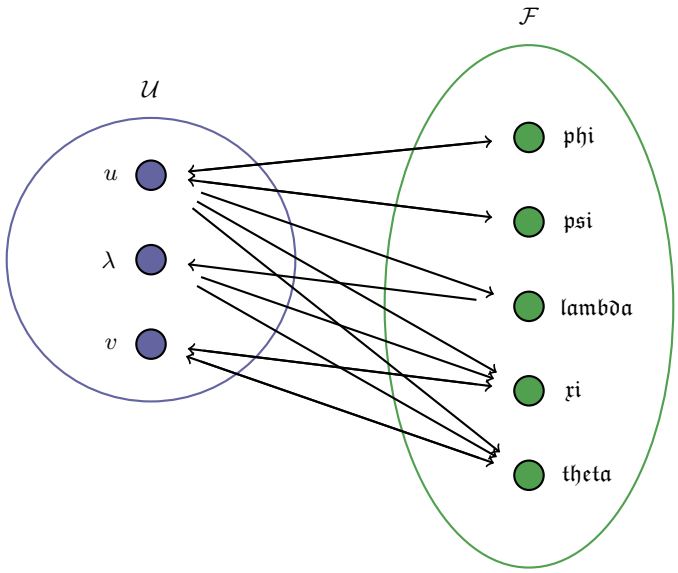

Figure 2.4: A directed bipartite graph illustration of the core constructors in (2.76)-(2.80). Here $\mathcal{U} = \{u, \lambda, v\}$ is a set of variables and $\mathcal{F} = \{\mathfrak{phi}, \mathfrak{psi}, \mathfrak{lambda}, \mathfrak{xi}, \mathfrak{theta}\}$ is a set of functions. A directed edge from node A in $\mathcal{U}$ to node B in $\mathcal{F}$ indicates that a variable of type A is an argument of a function of type B. A directed edge from node C in $\mathcal{F}$ to node D in $\mathcal{U}$ indicates that a new variables of type D can be introduced with the construction of a function of type C.

In the special case that $\mathbb{K}_u^{\text{o}} = \mathbb{K}_\lambda^{\text{o}} = \mathbb{K}_\Lambda^{\text{o}} = \mathbb{K}_v^{\text{o}} = \emptyset$, the augmented continuation problem $\hat{\mathbf{A}}$ obtained by application of the operator $\hat{}$ in (2.67) can be defined as the *canonical sum* of two *uncoupled* augmented continuation problems $\mathbf{A}$ and $\tilde{\mathbf{A}}$, such that $\oplus_{\tilde{\mathbf{A}}}(\mathbf{A}) = \mathbf{A} \oplus \tilde{\mathbf{A}} := \hat{\mathbf{A}}$. An arbitrary augmented continuation problem $\mathbf{A}$ may be constructed as the canonical sum of a sequence of uncoupled augmented continuation problems $\{\mathbf{A}_i\}_{i=1}^N$, glued together by the application of an operator $\mathcal{C}$:

$$\mathbf{A} = \mathcal{C} \circ \oplus_{\mathbf{A}_N} \circ \cdots \circ \oplus_{\mathbf{A}_1}, \tag{2.81}$$

and represented graphically in the left panel of Fig. 2.5. Such a formulation is especially convenient in problems where the individual operators $\oplus_{\mathbf{A}_i}$ may be sampled from a smaller set of operators, for example when modeling multi-segment boundary-value problems, where the $\oplus_{\mathbf{A}_i}$ represent contributions associated with individual segments and $\mathcal{C}$ imposes the corresponding boundary conditions, as well as gluing conditions on the problem parameters. This paradigm of construction is naturally nested and recursive, as suggested in the right panel of Fig. 2.5.

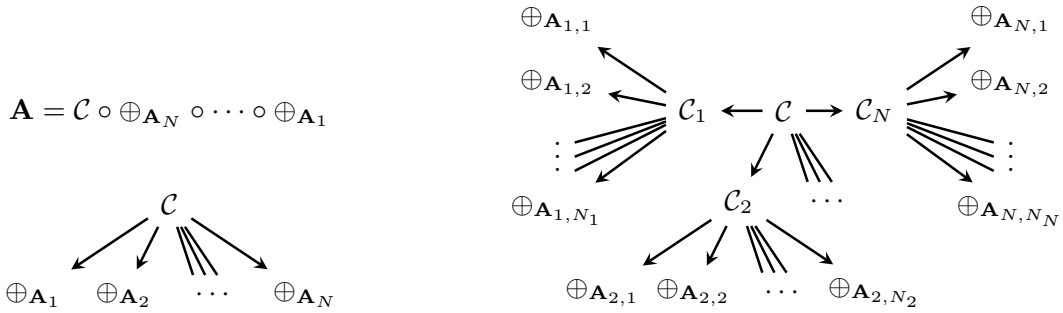

Figure 2.5: (left) A simple tree representation of the construction of the augmented continuation problem $\mathbf{A}$ in terms of a canonical sum of uncoupled problems coupled through the imposition of gluing conditions. (right) A recursive generalization.

The particular choice of core constructors in COCO is not accidental and obviously reflects the unique position of the continuation multipliers λ and complementary continuation variables v in the problem hierarchy. This is best appreciated through examples.

2.3 Data Assimilation

We consider in this section an augmented continuation problem obtained naturally from the optimization of an objective functional in the presence of delay differential constraints adapted from [90]. In contrast to this reference, we emphasize below the form of the resultant necessary conditions and describe a solution strategy similar to that presented in Section 2.2.2.

2.3.1 Problem formulation

From [90] we obtain the data assimilation problem of finding initial values $u(0), p(0)$ for two functions $u, p : [0, T] \mapsto \mathbb{R}^n$ that minimize the cost functional (cf. Fig. 2.6)

$$J := \sum_{k=1}^{M+1} w_k \left| p\big(t_k\big) - \hat{p}_k \right|^2 \tag{2.82}$$

in terms of the given sequence of observations $\hat{p}_k \in \mathbb{R}^n$, non-negative weight vector $w \in \mathbb{R}^{M+1}$, and time sequence $0 = t_1 < \cdots < t_{M+1} = T$ under the differential constraints

$$\dot{u}_j = -j\pi p_j,\ \dot{p}_j = -\zeta_j p_j + j\pi u_j + q_j \tag{2.83}$$

for $t \in (0, \alpha) \cup (\alpha, T)$, continuity conditions

$$\lim_{t \to \alpha -} u(t) = \lim_{t \to \alpha +} u(t),\ \lim_{t \to \alpha -} p(t) = \lim_{t \to \alpha +} p(t), \tag{2.84}$$

and coupling constraints

$$q(t) = \begin{cases} 0, & t \in (0, \alpha), \\ 2\beta F\big(\gamma^{\mathrm{T}} u(t - \alpha)\big), & t \in (\alpha, T) \end{cases} \tag{2.85}$$

for $\beta, \gamma \in \mathbb{R}^n$ and a continuously differentiable function $F : \mathbb{R} \mapsto \mathbb{R}$. We treat this problem using standard techniques from the calculus of variations.

We anticipate discontinuities in the derivative of p at $t = \alpha$ and in the Lagrange multipliers associated with the differential constraints at $t = t_i$ for $i = 2, \ldots, M$. For simplicity, assume that $\alpha = t_I$ for some $2 \leq I \leq M$. For notational convenience, let $T_k := t_{k+1} - t_k$ and

$$\hat{t}_{i,k} := (t_i - t_k + t_I)/T_k \tag{2.86}$$

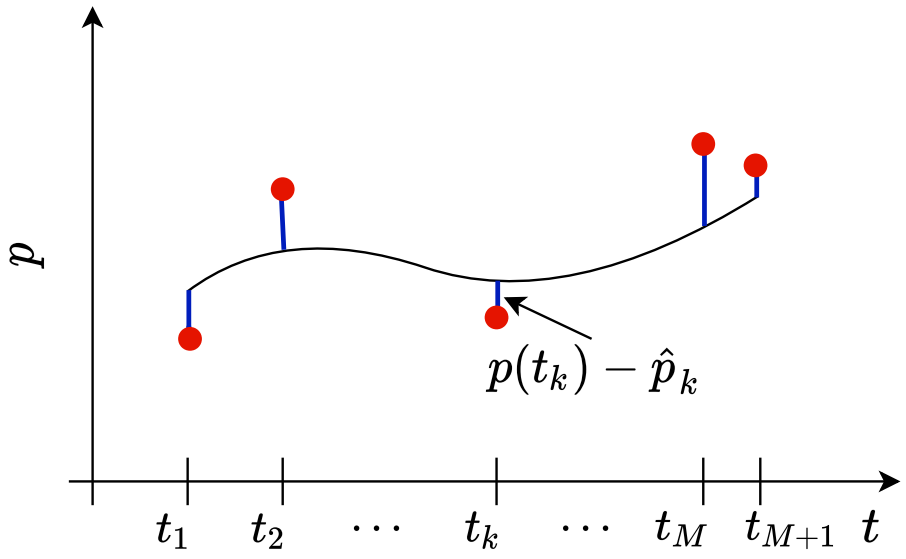

Figure 2.6: Illustration of data assimilation problem in Section 2.3 seeking the optimal selection of $u(0)$ and $p(0)$ to minimize a weighted quadratic sum in the deviations $p(t_k) - \hat{p}_k$.

for $k \geq I$. We then replace (2.83)-(2.85) with a sequential multi-point boundary-value problem for the functions $u^{(k)}, p^{(k)} : [0,1] \to \mathbb{R}^n$ for $k = 1, \ldots, M$ given by

$$\dot{u}_j^{(k)} = T_k \left(-j\pi p_j^{(k)} \right), \; \dot{p}_j^{(k)} = T_k \left(-\zeta_j p_j^{(k)} + j\pi u_j^{(k)} + q_j^{(k)} \right) \tag{2.87}$$

for $t \in (0,1)$ and

$$u^{(k)}(0) = u^{(k-1)}(1), \; p^{(k)}(0) = p^{(k-1)}(1) \tag{2.88}$$

for $k > 1$, with

$$q^{(k)}(t) = 2\beta F \left(\gamma^{\mathrm{T}} u^{(l)} \left(\frac{T_k}{T_l} \left(t - \hat{t}_{l,k} \right) \right) \right) \tag{2.89}$$

for $k \geq I$,

$$l \in \mathbb{I}_k := \{ 1 \leq i \leq M \,\big|\, [0,1] \cap (\hat{t}_{i,k}, \hat{t}_{i+1,k}) \neq \emptyset \} \tag{2.90}$$

and $t \in \left[\max\left(0, \hat{t}_{l,k}\right), \min\left(1, \hat{t}_{l+1,k}\right) \right]$, and $q^{(k)}(t) = 0$ otherwise. In this notation,

$$J = w_1 \left| p^{(1)}(0) - \hat{p}_1 \right|^2 + \sum_{k=2}^{M+1} w_k \left| p^{(k-1)}(1) - \hat{p}_k \right|^2. \tag{2.91}$$

We seek an optimal choice for $u^{(1)}(0)$ and $p^{(1)}(0)$ that corresponds to an extremum of J along the corresponding constraint manifold.

2.3.2 Adjoint conditions

To locate such an extremum, consider the Lagrangian (which differs from [90] in the purposeful introduction of the auxiliary variable μ)

$$\mu + \eta\,(J - \mu) + L_{\mathrm{de}} + L_{\mathrm{ic}} + L_{\mathrm{cp}}, \tag{2.92}$$

where

$$\begin{aligned} L_{\mathrm{de}} := &\sum_{k=1}^{M}\sum_{j=1}^{n}\int_0^1 \kappa_j^{(k)}\left(\dot{u}_j^{(k)} + T_k j\pi p_j^{(k)}\right)\,\mathrm{d}t \\ &+ \sum_{k=1}^{M}\sum_{j=1}^{n}\int_0^1 \lambda_j^{(k)}\left(\dot{p}_j^{(k)} + T_k\zeta_j p_j^{(k)} - T_k j\pi u_j^{(k)} - T_k q_j^{(k)}\right)\,\mathrm{d}t \end{aligned} \tag{2.93}$$

in terms of the Lagrange multiplier functions $\kappa^{(k)}, \lambda^{(k)} : [0,1] \mapsto \mathbb{R}^n$,

$$\begin{aligned} L_{\mathrm{ic}} := &\nu^{(1)\mathrm{T}}\left(u^{(1)}(0) - u_0\right) + \sum_{k=2}^{M}\nu^{(k)\mathrm{T}}\left(u^{(k)}(0) - u^{(k-1)}(1)\right) \\ &+ \omega^{(1)\mathrm{T}}\left(p^{(1)}(0) - p_0\right) + \sum_{k=2}^{M}\omega^{(k)\mathrm{T}}\left(p^{(k)}(0) - p^{(k-1)}(1)\right) \end{aligned} \tag{2.94}$$

in terms of the Lagrange multipliers $\nu^{(k)}, \omega^{(k)} \in \mathbb{R}^n$, and

$$\begin{aligned} L_{\mathrm{cp}} := &\sum_{k<I}\int_0^1 \mu^{(k)\mathrm{T}} q^{(k)}\,\mathrm{d}t \\ &+ \sum_{k\geq I}\sum_{l\in L_k}\int_{\max\left(0,\hat{t}_{l,k}\right)}^{\min\left(1,\hat{t}_{l+1,k}\right)} \mu^{(k)\mathrm{T}}\left(q^{(k)} - 2\beta F\left(\gamma^T u^{(l)}\left(\frac{T_k}{T_l}\left(t - \hat{t}_{l,k}\right)\right)\right)\right)\,\mathrm{d}t \end{aligned} \tag{2.95}$$

in terms of the Lagrange multiplier function $\mu^{(k)} : [0,1] \mapsto \mathbb{R}^n$. Here, the Lagrange multiplier η imposes the relationship between J and the auxiliary variable μ, while the auxiliary variables

u_0 and p_0 are introduced to track $u^{(1)}(0)$ and $p^{(1)}(0)$. We assume below that $\kappa^{(k)}$ and $\lambda^{(k)}$ are continuous and piecewise differentiable, and that $\mu^{(k)}$ is continuous.

For further notational convenience, let

$$\bar{\mathbb{I}}_k := \{1 \le i \le M \,\big|\, [0,1] \cap (\hat{t}_{k,i}, \hat{t}_{k+1,i}) \neq \emptyset\}. \tag{2.96}$$

Independent variations of the constraint Lagrangian with respect to the components of $u^{(k)}(\cdot)$, $p^{(k)}(\cdot)$, $q^{(k)}(\cdot)$, u_0, p_0, and μ then yields the adjoint necessary conditions for an extremum given by

$$-\dot{\kappa}_j^{(k)} - T_k j\pi\lambda_j^{(k)} - 2\gamma_j \mu^{(l)\mathrm{T}} \left(\frac{T_k}{T_l}t + \hat{t}_{k,l}\right) \beta F'\left(\gamma^{\mathrm{T}} u^{(k)}\right) = 0 \tag{2.97}$$

for $t \in \left(\max\left(0, -\hat{t}_{k,l}T_l/T_k\right), \min\left(1, (1-\hat{t}_{k,l})T_l/T_k\right)\right)$ for some $l \in \bar{\mathbb{I}}_k$,

$$-\dot{\kappa}_j^{(k)} - T_k j\pi\lambda_j^{(k)} = 0 \tag{2.98}$$

for $t \notin \left[\max\left(0, -\hat{t}_{k,l}T_l/T_k\right), \min\left(1, (1-\hat{t}_{k,l})T_l/T_k\right)\right]$ for any $l \in \bar{\mathbb{I}}_k$,

$$-\dot{\lambda}_j^{(k)} + T_k\zeta_j\lambda_j^{(k)} + T_k j\pi\kappa_j^{(k)} = 0, \tag{2.99}$$

for $t \in (0,1)$,

$$\mu^{(k)} - T_k\lambda^{(k)} = 0 \tag{2.100}$$

for $t \in [0,1]$,

$$\kappa^{(k-1)}(1) - \nu^{(k)} = 0,\ \lambda^{(k-1)}(1) - \omega^{(k)} + 2\eta w_k\left(p^{(k-1)}(1) - \hat{p}_k\right) = 0, \tag{2.101}$$

$$-\kappa^{(k)}(0) + \nu^{(k)} = 0,\ -\lambda^{(k)}(0) + \omega^{(k)} = 0 \tag{2.102}$$

for $k = 2, \ldots, M$,

$$\kappa^{(M)}(1) = 0,\ \lambda^{(M)}(1) + 2\eta w_{M+1}\left(p^{(M)}(1) - \hat{p}_{M+1}\right) = 0, \tag{2.103}$$

$$-\kappa^{(1)}(0) + \nu^{(1)} = 0,\ -\lambda^{(1)}(0) + \omega^{(1)} + 2\eta w_1\left(p^{(1)}(0) - \hat{p}_1\right) = 0, \tag{2.104}$$

$\nu^{(1)} = \omega^{(1)} = 0$, and $1 - \eta = 0$. As was the case in a previous section, these conditions are linear in the Lagrange multipliers and, apart from the final condition on η, homogeneous.

2.3.3 Problem construction

We obtain an augmented continuation problem **A** of the form in (2.44) by associating

- Φ with the multi-point boundary-value problem in (2.87)-(2.89) in terms of the continuation variables $u^{(k)}$, $p^{(k)}$, and $q^{(k)}$;
- Ψ with the vector $\left(J, u^{(1)}(0), p^{(1)}(0)\right)$ and corresponding continuation parameters μ, u_0, and p_0; and
- Λ^* with the linear operator in (2.97)-(2.104) acting on the continuation multipliers $\kappa^{(k)}$, $\lambda^{(k)}$, $\mu^{(k)}$, $\nu^{(k)}$, $\omega^{(k)}$, and η.

This problem has dimensional deficit $2n + 1$ which reduces to 0 once a solution is found with $\nu^{(1)} = \omega^{(1)} = 0$ and $\eta = 1$.

After suitable discretization, we may construct **A** according to the following algorithm:

Step 1: As k increments from 1 to M, repeatedly invoke the core constructor (2.76) with $\mathfrak{phi}$ encoding the differential constraints (2.87), $\mathbb{K}_u^{\mathrm{o}} = \emptyset$, and u_0^{n} given by an initial solution guess for the continuation variables $u^{(k)}$, $p^{(k)}$, and $q^{(k)}$.

Step 2: As k increments from 2 to M, repeatedly invoke the core constructor (2.76) with $\mathfrak{phi}$ encoding the boundary conditions (2.88), $\mathbb{K}_u^{\mathrm{o}}$ indexing the corresponding continuation variables from **Step 1**, and $u_0^{\mathrm{n}} = \emptyset$.

Step 3: As k increments from 1 to M, repeatedly invoke the core constructor (2.76) with $\mathfrak{phi}$ encoding the coupling (2.89) for $k \geq I$ and the condition $q^{(k)}(t) = 0$ for $k < I$, $\mathbb{K}_u^{\mathrm{o}}$ indexing the corresponding continuation variables from **Step 1**, and $u_0^{\mathrm{n}} = \emptyset$.

Step 4: Invoke the core constructor (2.77) with $\mathfrak{psi}$ encoding the evaluation of J, $u^{(1)}(0)$, and $p^{(1)}(0)$, $\mathbb{K}_u^{\mathrm{o}}$ indexing the corresponding continuation variables from **Step 1**, and $u_0^{\mathrm{n}} = \emptyset$.

Step 5: As k increments from 1 to M, repeatedly invoke the core constructor (2.80) with $\mathfrak{lambda}$ encoding the linear operators acting on $\kappa^{(k)}$ and $\lambda^{(k)}$ in the adjoint conditions (2.97)-(2.104), $\mathbb{K}_u^{\mathrm{o}}$ indexing the continuation variables introduced in the corresponding call in **Step 1**, $\mathbb{K}_\Lambda^{\mathrm{o}} = \emptyset$, and λ_0^{n} given by an initial solution guess for the continuation variables $\kappa^{(k)}$ and $\lambda^{(k)}$.

Step 6: As k increments from 2 to M, repeatedly invoke the core constructor (2.80) with $\mathfrak{lambda}$ encoding the linear operators acting on $\nu^{(k)}$ and $\omega^{(k)}$ in the adjoint conditions (2.97)-(2.104), $\mathbb{K}_u^{\mathrm{o}}$ indexing the continuation variables associated with the corresponding call in **Step 2**, $\mathbb{K}_\Lambda^{\mathrm{o}} \neq \emptyset$, and λ_0^{n} given by an initial solution guess for the continuation variables $\nu^{(k)}$ and $\omega^{(k)}$.

Step 7: As k increments from 1 to M, repeatedly invoke the core constructor (2.80) with $\mathfrak{lambda}$ encoding the linear operators acting on $\mu^{(k)}$ in the adjoint conditions (2.97)-(2.104), $\mathbb{K}_u^{\mathrm{o}}$ indexing the continuation variables associated with the corresponding call in **Step 3**, $\mathbb{K}_\Lambda^{\mathrm{o}} \neq \emptyset$, and λ_0^{n} given by an initial solution guess for the continuation variables $\mu^{(k)}$.

Step 8: Invoke the core constructor (2.80) with $\mathfrak{lambda}$ encoding the linear operators acting on $\nu^{(1)}$, $\omega^{(1)}$, and η in the adjoint conditions (2.97)-(2.104), $\mathbb{K}_u^{\mathrm{o}}$ indexing the continuation variables associated with the corresponding call in **Step 4**, $\mathbb{K}_\Lambda^{\mathrm{o}} \neq \emptyset$, and λ_0^{n} given by an initial solution guess for the continuation variables $\nu^{(1)}$, $\omega^{(1)}$, and η.

One advantage of this algorithm is that steps 5 through 8 can be implemented automatically [1], [14], [35] from information provided in steps 1 through 4, rather than simply using the core constructor (2.76) to implement a general continuation problem **P**. A flowchart representation of this algorithm is presented in Fig. 2.7. This figure also shows a resequenced algorithm for constructing the augmented continuation problem that interlaces construction of adjoint contributions immediately following the construction of the corresponding zero and monitor functions.

2.3.4 Problem analysis

Using a method of successive continuation (originally described in [13] with further developments in [1], [14], [35]), we may reach the desired local extremum through a sequence of intermediate points at the intersection of the solution manifolds to different restricted continuation problem. To this end, invoke the core constructor (2.79) to append complementary monitor functions evaluating to η, $\nu^{(1)}$, and $\omega^{(1)}$ with corresponding complementary continuation parameters φ_η, φ_ν, and φ_ω. Here, $\mathbb{K}_u^{\mathrm{o}} = \mathbb{K}_v^{\mathrm{o}} = v_0^{\mathrm{n}} = \emptyset$ and $\mathbb{K}_\lambda^{\mathrm{o}}$ indexes the corresponding continuation multipliers. We construct the desired sequence of restricted continuation problems by fixing fewer than $2n+1$ (complementary) continuation parameters.

For example, we obtain an augmented continuation problem with dimensional deficit equal to 1 by fixing p_0, all but the first component of u_0, and the first component of φ_ν. A local extremum in μ along a family of solutions to this problem with all vanishing Lagrange multipliers (such a family exists by homogeneity) then coincides with an intersection with a secondary family of solutions along which only the Lagrange multipliers vary. One point along this secondary family has $\eta = 1$. The continuation problem obtained next by fixing φ_η at 1 and allowing, say, the second component of u_0 to vary is satisfied along a tertiary manifold through this point. If we locate a point on this manifold where the second component of φ_ν equals 0, we may use this point to switch to a different restricted continuation problem with the first three components of u_0 allowed to vary and the first two components of φ_ν fixed.

Along the corresponding solution manifold we look for a point where the third component of φ_ν equals 0, and continue in the same fashion until a local extremum is reached.

Alternatively, once the initial point with $\eta = 1$ is reached, denote the corresponding value of $\nu^{(1)}$ by $\nu^{(1)*}$. We may now invoke the core constructor (2.78) to append complementary zero functions that evaluate to all but the first component of the combination

$$\nu^{(1)} - (1 - \chi)\nu^{(1)*} \tag{2.105}$$

in terms of the complementary continuation variable $\chi \in \mathbb{R}$. Here, $\mathbb{K}_u^{\mathrm{o}} = \mathbb{K}_v^{\mathrm{o}} = \emptyset$, $\mathbb{K}_\lambda^{\mathrm{o}}$ indexes the continuation multipliers $\nu^{(1)}$, and v_0^{n} contains an initial solution guess for χ. By again fixing φ_η at 1 and allowing all remaining components of u_0 to vary, we obtain a continuation problem with dimensional deficit equal to 1 and may search along its solution manifold for a point with $\nu^{(1)} = 0$. We drive $\omega^{(1)}$ to 0 following similar principles.

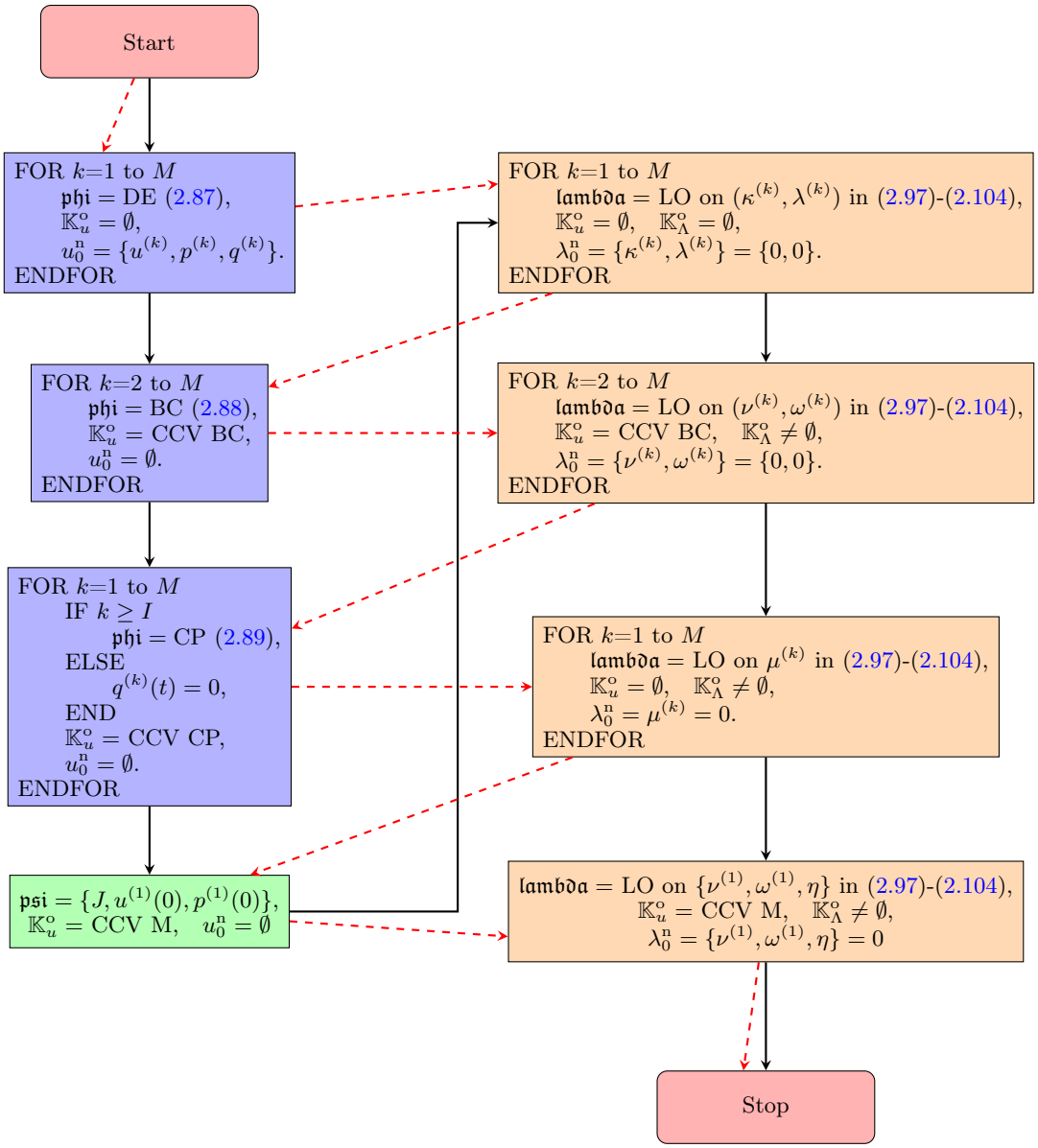

Figure 2.7: A flowchart depicting the construction of the augmented continuation problem **A** associated with the data assimilation problem in Section 2.3. Here rectangles filled with blue, green and orange colors represent core constructors associated with functions of the type $\mathfrak{phi}$, $\mathfrak{psi}$ and $\mathfrak{lambda}$, respectively. The workflow with black solid arrows illustrates the algorithm detailed in Section 2.3.3. In this workflow, adjoint contributions are constructed after the construction of *all* zero and monitor functions. In contrast, in the alternate workflow represented by red dashed arrows, one constructs the adjoint contributions after the introduction of *each* of the corresponding zero or monitor functions. Here, the abbreviations DE, BC, CP, CCV, M, and LO represent differential equations, boundary conditions, coupling conditions, corresponding continuation variables, monitor functions, and linear operators, respectively. In particular, $\mathbb{K}_u^{\text{o}}$ = CCV BC/CP/M denote indexing the corresponding continuation variables for boundary conditions/coupling conditions/monitor functions from the ones defined when constructing the differential constraints.

2.4 Phase response curves of periodic orbits

2.4.1 Linear response theory for closed regular problems

Instead of optimization, as in Section 2.3, we consider in this section the simpler case where the zero problem $\Phi(u) = 0$ for $\Phi : \mathcal{U}_\Phi \to \mathcal{R}_\Phi$ has dimensional deficit equal to 0 and is regular at some solution $\tilde{u}$ (i.e., such that the Frechét derivative $D\Phi(\tilde{u})$ is regular). We choose the case of a scalar-valued monitor function $\Psi : \mathcal{U}_\Phi \mapsto \mathbb{R}$ such that the continuation parameter μ given by $\Psi(u) - \mu = 0$ is also scalar ($\Psi(u)$ is called the *observable*). Let $\mathcal{R}_\Phi^*$ denote the (dual) space of linear functionals on $\mathcal{R}_\Phi$. At extremal points $(\tilde{u}, \tilde{\mu}, \tilde{\lambda}, \tilde{\eta}) \in \mathcal{U}_\Phi \times \mathbb{R} \times \mathcal{R}_\Phi^* \times \mathbb{R}$ of the Lagrangian

$$L(u, \mu, \lambda, \eta) = \mu + \eta(\Psi(u) - \mu) + \lambda\Phi(u) \tag{2.106}$$

the Lagrange multiplier $\tilde{\lambda}$ measures the linear sensitivity of Ψ to changes in Φ. Indeed, by considering vanishing variations of L, it follows that $(\tilde{u}, \tilde{\mu}, \tilde{\lambda}, \tilde{\eta})$ must satisfy

$$\Phi(\tilde{u}) = 0,\ \Psi(\tilde{u}) - \tilde{\mu} = 0,\ \eta D\Psi(\tilde{u}) + \tilde{\lambda} D\Phi(\tilde{u}) = 0 \tag{2.107}$$

and $1 - \eta = 0$, from which we obtain $\tilde{\lambda} = -D\Psi(\tilde{u})\,(D\Phi(\tilde{u}))^{-1}$. For all small perturbations $\delta\Phi \in \mathcal{R}_\Phi$ the perturbed zero problem $\Phi(u) = \delta\Phi$ has a locally unique solution $u = \tilde{u} + \delta u$, where $\delta\Phi = D\Phi(\tilde{u})\delta u + O(\|\delta u\|^2)$. It follows that

$$\delta\Psi = \Psi(u) - \Psi(\tilde{u}) = D\Psi(\tilde{u})\delta u + O(\|\delta u\|^2) = -\tilde{\lambda}\delta\Phi + O(\|\delta\Phi\|^2) \tag{2.108}$$

In this section, we to apply this general observation to the derivation of phase response curves associated with limit cycles in ordinary and delay differential equations.

2.4.2 Phase response curves as linear response

The construction in Section 2.4.1 can be applied to abstract autonomous periodic boundary-value problems and the observable T (the unknown period) to obtain so-called phase response curves [91]–[94].

In the notation of this section, let $\mathcal{U}_\Phi = C^1([0,1];\mathcal{U}) \times \mathbb{R}$ be the space of continuation variables, where $\mathcal{U}$ is some Banach space, and let the zero problem take the form

$$\Phi(u) = (\Phi_{\mathrm{DE}}, \Phi_{\mathrm{BC}}, \Phi_{\mathrm{PS}})((x(\cdot), T)) = (\dot{x}(\cdot) - Tf(x(\cdot)), x(0) - x(1), h(x(0))) \tag{2.109}$$

corresponding to a periodic orbit $\mathbb{R} \ni t \mapsto x(t/T) \in \mathcal{U}$ of period T of an autonomous vector field f and phase determined by the Poincaré condition $h(x(0)) = 0$. We define the monitor function Ψ as the projection onto the scalar component T of $(x(\cdot), T) \in \mathcal{U}_\Phi$ such that $\Psi(x(\cdot), T) = T$. The Lagrangian for the linear response of T, given in (2.106), is then

$$\begin{aligned} L(x(\cdot), T, \mu, \lambda_{\mathrm{DE}}(\cdot), \lambda_{\mathrm{BC}}, \lambda_{\mathrm{PS}}, \eta) &= \mu + \eta(T - \mu) \\ &+ \int_0^1 \lambda_{\mathrm{DE}}(\tau) \left(\dot{x}(\tau) - Tf(x(\tau))\right) \mathrm{d}\tau + \lambda_{\mathrm{BC}} \left(x(0) - x(1)\right) + \lambda_{\mathrm{PS}} h(x(0)) \end{aligned} \tag{2.110}$$

defined on $\mathcal{U}_\Phi \times \mathbb{R} \times \left(C^0\left([0,1];\mathcal{U}\right)\right)^* \times \mathcal{U}^* \times \mathbb{R} \times \mathbb{R}$. In this case, vanishing variations of L with respect to the Lagrange multipliers $\lambda_{\mathrm{DE}}(\cdot)$, λ_{BC}, λ_{PS}, and η at an extremal point $(\tilde{x}(\cdot), \tilde{T}, \tilde{\mu}, \tilde{\lambda}_{\mathrm{DE}}(\cdot), \tilde{\lambda}_{\mathrm{BC}}, \tilde{\lambda}_{\mathrm{PS}}, \tilde{\eta})$ imply that

$$\dot{\tilde{x}}(\tau) - \tilde{T} f(\tilde{x}(\tau)) = 0 \text{ for } \tau \in (0,1),\ \tilde{x}(0) - \tilde{x}(1) = 0,\ h(\tilde{x}(0)) = 0, \tag{2.111}$$

and $\tilde{T} - \tilde{\mu} = 0$, i.e., that $t \mapsto \tilde{x}(t/\tilde{T})$ is a periodic solution with period $\tilde{\mu} = \tilde{T}$ of a dynamical system with autonomous vector field f and with initial condition on the zero-level surface of the function h.

Vanishing variations of L with respect to $x(\cdot)$, T, and μ yield the necessary adjoint

conditions

$$-\dot{\tilde{\lambda}}_{\mathrm{DE}}(\tau) - \tilde{\lambda}_{\mathrm{DE}}(\tau)\tilde{T}Df(\tilde{x}(\tau)) = 0 \text{ for } \tau \in (0,1), \tag{2.112}$$

$$\tilde{\lambda}_{\mathrm{BC}} - \tilde{\lambda}_{\mathrm{DE}}(0) + \tilde{\lambda}_{\mathrm{PS}}Dh(\tilde{x}(0)) = 0, \tag{2.113}$$

$$-\tilde{\lambda}_{\mathrm{BC}} + \tilde{\lambda}_{\mathrm{DE}}(1) = 0, \tag{2.114}$$

$$\eta - \int_0^1 \tilde{\lambda}_{\mathrm{DE}}(\tau) f(\tilde{x}(\tau))\,\mathrm{d}\tau = 0, \tag{2.115}$$

and $1 - \eta = 0$. From (2.111) and (2.112), it follows that $\tilde{\lambda}_{\mathrm{DE}}(\tau)f(\tilde{x}(\tau))$ is constant, i.e., that

$$\tilde{\lambda}_{\mathrm{DE}}(\tau)f(\tilde{x}(\tau)) = 1 \text{ for all } \tau \in [0,1], \tag{2.116}$$

where we used (2.115) and the fact that $\eta = 1$. Moreover, from (2.113) and (2.114), we see that $\tilde{\lambda}_{\mathrm{BC}} = \tilde{\lambda}_{\mathrm{DE}}(1)$ and $\tilde{\lambda}_{\mathrm{PS}}Dh(\tilde{x}(0)) = \tilde{\lambda}_{\mathrm{DE}}(0) - \tilde{\lambda}_{\mathrm{DE}}(1)$. By the periodicity of $\tilde{x}$, it follows that

$$\tilde{\lambda}_{\mathrm{PS}}Dh(\tilde{x}(0))\tilde{T}f(\tilde{x}(0)) = \tilde{\lambda}_{\mathrm{DE}}(0)\tilde{T}f(\tilde{x}(0)) - \tilde{\lambda}_{\mathrm{DE}}(1)\tilde{T}f(\tilde{x}(1)) = 0, \tag{2.117}$$

i.e., that $\tilde{\lambda}_{PS} = 0$ provided that the periodic trajectory $\tilde{x}(\cdot)$ intersects $h = 0$ transversally at $\tilde{x}(0)$. In this case, $t \mapsto \tilde{\lambda}_{\mathrm{DE}}(t/\tilde{T})$ is also periodic with period $\tilde{T}$.

The invertibility of the linearization of (2.111) is equivalent to a simple Floquet multiplier at 1 for the corresponding periodic orbit. This invertibility implies the existence of a unique pair $(x(\cdot), T) \in \mathcal{U}_\Phi$ near $(\tilde{x}(\cdot), \tilde{T})$ for each pair of small perturbations $(\delta_{\mathrm{BC}}, \delta_{\mathrm{PS}})$ such that

$$\dot{x}(\tau) - Tf(x(\tau)) = 0 \text{ for } \tau \in [0,1],\ x(0) - x(1) = \delta_{\mathrm{BC}},\ h(x(0)) = \delta_{\mathrm{PS}}. \tag{2.118}$$

The linear response formula (2.108) from Section 2.4.1 then implies

$$T - \tilde{T} = -\tilde{\lambda}_{\mathrm{DE}}(0)\delta_{\mathrm{BC}} + O\left(\|(\delta_{\mathrm{BC}}, \delta_{\mathrm{PS}})\|^2\right), \tag{2.119}$$

where we have used the fact that $\tilde{\lambda}_{\mathrm{BC}} = \tilde{\lambda}_{\mathrm{DE}}(1) = \tilde{\lambda}_{\mathrm{DE}}(0)$ and $\tilde{\lambda}_{\mathrm{PS}} = 0$. In particular, since

$$\delta_{BC} = x(0) - \tilde{x}(0) + \tilde{x}(1) - x(1), \tag{2.120}$$

it follows that to first order in $\|x(0) - \tilde{x}(0)\|$ and $|T - \tilde{T}|$,

$$\tilde{\lambda}_{\mathrm{DE}}(0)\delta_{\mathrm{BC}} = \tilde{T} - T. \tag{2.121}$$

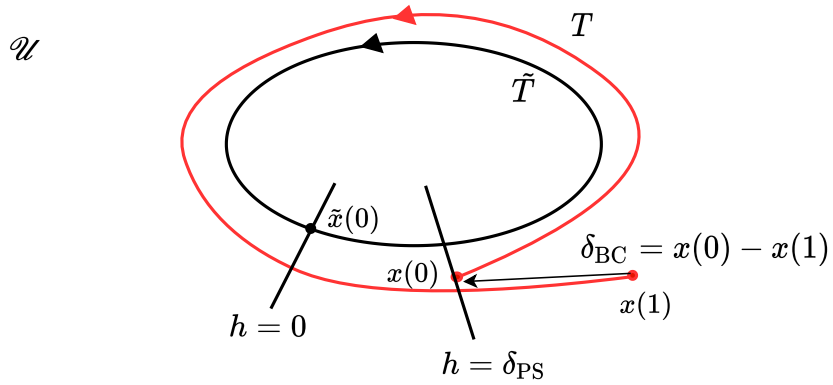

Figure 2.8: The periodic orbit $\mathbb{R} \ni t \mapsto \tilde{x}(t/\tilde{T}) \in \mathcal{U}$ satisfies the Poincaré condition $h(x(0)) = 0$ and periodicity condition $x(0) - x(1) = 0$. A violation by δ_{PS} of the Poincaré condition and by δ_{BC} of the periodicity condition, as shown in the figure, results in a change in the duration T relative to the period $\tilde{T}$ of the periodic orbit by $-\tilde{\lambda}_{\mathrm{DE}}(0)\delta_{\mathrm{BC}}$ to first order in $\|\delta_{\mathrm{BC}}\|$ and $\|\delta_{\mathrm{PS}}\|$. For a stable limit cycle, $\tilde{\lambda}_{\mathrm{DE}}(0)$ equals the Fréchet derivative $D\varphi$ of the asymptotic phase evaluated at $\tilde{x}(0)$.

Consider the special case that the periodic function $\tilde{x}(t/\tilde{T})$ describes a linearly asymptotically stable limit cycle of the vector field $f(x)$. Then, there exists a unique map φ, called the *asymptotic phase* [95], defined on the basin of attraction $\mathcal{B}$ of the limit cycle, such that $\varphi : \mathcal{B} \to [0, \tilde{T})$, $\varphi(\tilde{x}(0)) = 0$, and

$$\lim_{t\to\infty} x(t/T) - \tilde{x}\left((\varphi(x(0)) + t)/\tilde{T}\right) = 0 \tag{2.122}$$

for every solution $x(t)$ to $\dot{x} = Tf(x)$ with $x(0)$ in $\mathcal{B}$. The substitution $t \mapsto s + t$ into this

limit identity shows that ϕ satisfies the

$$\varphi(x(s/T)) = \varphi(x(0)) + s \text{ modulo } \tilde{T} \tag{2.123}$$

for all s, which can also be used as a defining equation for ϕ. In particular, for $s = T$, we obtain

$$\varphi(x(1)) - \varphi(x(0)) = T \text{ modulo } \tilde{T} \tag{2.124}$$

For $x(0) \approx \tilde{x}(0)$ and $T \approx \tilde{T}$, it follows that to first order in $\|x(0) - \tilde{x}(0)\|$ and $|T - \tilde{T}|$,

$$D\varphi(\tilde{x}(0))\delta_{\mathrm{BC}} = \tilde{T} - T, \tag{2.125}$$

i.e., that the Frechét derivative $D\varphi(\tilde{x}(0)) = \tilde{\lambda}_{\mathrm{DE}}(0)$. By considering an arbitrary $t \in [0, \tilde{T})$, we obtain the *phase response functional* $D\varphi(\tilde{x}(t/\tilde{T})) = \tilde{\lambda}_{\mathrm{DE}}(t/\tilde{T})$ for the period-$\tilde{T}$ orbit $\tilde{x}(t/\tilde{T})$ of the vector field $f(x)$.

This phase response functional (or vector in the case of finite-dimensional $\mathcal{U}$) is reduced to the periodic *phase response curve* $\mathrm{PRC}(\tau)$ on $[0, 1]$ for a particular perturbation $\delta_{\mathrm{BC}} \in \mathcal{U}$ by applying the functional to the perturbation at every time τ:

$$\mathrm{PRC}_{\delta_{\mathrm{BC}}} : [0, 1] \ni \tau \mapsto \tilde{\lambda}_{\mathrm{DE}}(\tau)\delta_{\mathrm{BC}} \in \mathbb{R}. \tag{2.126}$$

This measures the first-order shift in the asymptotic phase due to a perturbation of the state $x(\tau)$ at time τ by δ_{BC} (ignoring terms of order $\|(\delta_{\mathrm{BC}}, \delta_{\mathrm{PS}})\|^2$).

2.4.3 Delay differential equations

The results in the previous section apply also to periodic orbits in delay differential equations (DDEs), including the special case of a single discrete delay α, given by

$$\dot{z}(t) = f(z(t), z(t - \alpha)). \tag{2.127}$$

The defining conditions for $\tilde{\lambda}_{DE}(\cdot)$, $\tilde{\lambda}_{BC}$, and $\tilde{\lambda}_{PS}$ may be obtained from the general conditions (2.112)–(2.115) by writing the delay differential equation in the form

$$\dot{z}(t) = f(z(t), \zeta(-\alpha, t)),\ \zeta_{,t}(s,t) = \zeta_{,s}(s,t),\ \zeta(0,t) = z(t) \tag{2.128}$$

in which the delayed term is obtained from the solution of an advective boundary-value problem [96]. Suitable choices of the Banach space $\mathcal{U}$ and of the action of the Lagrange multiplier λ_{DE} yields the corresponding adjoint boundary-value problem after solving the advective problem and its adjoint along characteristics. In this section, we take a different route. We apply the linear response approximation (2.108) from Section 2.4.2 directly to the following form of (2.127):

$$\dot{x}(\tau) = T f(x(\tau), y(\tau)),\ t \in (0,1), \tag{2.129}$$

$$y(\tau) = \begin{cases} x(\tau + 1 - \alpha/T), & \tau \in [0, \alpha/T], \\ x(\tau - \alpha/T), & \tau \in (\alpha/T, 1]. \end{cases} \tag{2.130}$$

where $x(\tau) = z(T\tau)$ and $y(\tau) = z(T\tau - \alpha)$. For this coupled system, we consider vanishing variations of the Lagrangian

$$\begin{aligned} L(x(\cdot), y(\cdot), T, \mu, \lambda_{\mathrm{DE}}(\cdot), \lambda_{\mathrm{CP}}(\cdot), \lambda_{\mathrm{BC}}, \lambda_{\mathrm{PS}}, \eta) &= \mu + \eta(T - \mu) \\ &+ \int_0^1 \lambda_{\mathrm{DE}}^{\mathrm{T}}(t)\left(\dot{x}(t) - T f(x(t), y(t))\right) \mathrm{d}t + \int_0^{\alpha/T} \lambda_{\mathrm{CP}}^{\mathrm{T}}(t)\left(y(t) - x(t + 1 - \alpha/T)\right) \mathrm{d}t \\ &+ \int_{\alpha/T}^1 \lambda_{\mathrm{CP}}^{\mathrm{T}}(t)\left(y(t) - x(t - \alpha/T)\right) \mathrm{d}t + \lambda_{\mathrm{BC}}^{\mathrm{T}}\left(x(0) - x(1)\right) + \lambda_{\mathrm{PS}} h(x(0)) \end{aligned} \tag{2.131}$$

with respect to its arguments at an extremal point. We assume that $x, \lambda_{\mathrm{DE}} \in C^1([0,1]; \mathbb{R}^n)$, while $y, \lambda_{\mathrm{CP}} \in C^0([0,1]; \mathbb{R}^n)$. As in the previous section, variations with respect to the

Lagrange multipliers $\lambda_{\mathrm{DE}}(\cdot)$, $\lambda_{\mathrm{CP}}(\cdot)$, λ_{BC}, λ_{PS}, and η yield the boundary-value problem

$$\dot{\tilde{x}}(t) - \tilde{T} f(\tilde{x}(t), \tilde{y}(t)) = 0 \text{ for } t \in (0,1),\ \tilde{x}(0) - \tilde{x}(1) = 0,\ h(\tilde{x}(0)) = 0, \tag{2.132}$$

and $\tilde{T} - \tilde{\mu} = 0$, where

$$\tilde{y}(t) - \tilde{x}(t + 1 - \alpha/\tilde{T}) = 0 \text{ for } t \in (0, \alpha/\tilde{T}), \tag{2.133}$$

$$\tilde{y}(t) - \tilde{x}(t - \alpha/\tilde{T}) = 0 \text{ for } t \in (\alpha/\tilde{T}, 1). \tag{2.134}$$

It follows that $\tilde{x}(t/\tilde{T})$ is a periodic solution with period $\tilde{\mu} = \tilde{T}$ of the delay differential equation (2.127) and with initial condition on the zero-level surface of the function h.

Vanishing variations of L with respect to $x(\cdot)$, $y(\cdot)$, T, and μ, yields the necessary adjoint differential equations

$$-\dot{\tilde{\lambda}}^{\mathrm{T}}_{\mathrm{DE}}(t) - \tilde{\lambda}^{\mathrm{T}}_{\mathrm{DE}}(t)\tilde{T} D_x f(\tilde{x}(t), \tilde{y}(t)) - \tilde{\lambda}^{\mathrm{T}}_{\mathrm{CP}}(t + \alpha/\tilde{T}) = 0, \tag{2.135}$$

for $t \in (0, 1 - \alpha/\tilde{T})$ and

$$-\dot{\tilde{\lambda}}^{\mathrm{T}}_{\mathrm{DE}}(t) - \tilde{\lambda}^{\mathrm{T}}_{\mathrm{DE}}(t)\tilde{T} D_x f(\tilde{x}(t), \tilde{y}(t)) - \tilde{\lambda}^{\mathrm{T}}_{\mathrm{CP}}(t + \alpha/\tilde{T} - 1) = 0, \tag{2.136}$$

for $t \in (1 - \alpha/\tilde{T}, 1)$, boundary conditions

$$-\tilde{\lambda}^{\mathrm{T}}_{\mathrm{DE}}(0) + \lambda^{\mathrm{T}}_{\mathrm{BC}} + \lambda_{\mathrm{PS}} Dh(x(0)) = 0,\ \tilde{\lambda}^{\mathrm{T}}_{\mathrm{DE}}(1) - \lambda^{\mathrm{T}}_{\mathrm{BC}} = 0, \tag{2.137}$$

coupling conditions

$$-\tilde{\lambda}^{\mathrm{T}}_{\mathrm{DE}}(t)\tilde{T} D_y f(\tilde{x}(t), \tilde{y}(t)) + \tilde{\lambda}^{\mathrm{T}}_{\mathrm{CP}}(t) = 0,\ t \in (0,1) \tag{2.138}$$

integral condition

$$\eta - \int_0^1 \tilde{\lambda}_{\mathrm{DE}}^{\mathrm{T}}(t) f(\tilde{x}(t), \tilde{y}(t))\,\mathrm{d}t - \frac{\alpha}{\tilde{T}^2}\int_0^{\alpha/\tilde{T}} \tilde{\lambda}_{\mathrm{CP}}^{\mathrm{T}}(t)\dot{\tilde{x}}(t+1-\alpha/\tilde{T})\,\mathrm{d}t$$
$$- \frac{\alpha}{\tilde{T}^2}\int_{\alpha/\tilde{T}}^1 \tilde{\lambda}_{\mathrm{CP}}^{\mathrm{T}}(t)\dot{\tilde{x}}(t-\alpha/\tilde{T})\,\mathrm{d}t = 0, \tag{2.139}$$

and $1 - \eta = 0$.

As in the previous section, we show by differentiation and use of (2.132)-(2.134), (2.135)-(2.136), and (2.138) that the function

$$\tilde{\lambda}_{\mathrm{DE}}^{\mathrm{T}}(t) f(\tilde{x}(t), \tilde{y}(t)) + \frac{1}{\tilde{T}}\int_t^{t+\alpha/\tilde{T}} \tilde{\lambda}_{\mathrm{CP}}^{\mathrm{T}}(s)\dot{\tilde{x}}(s-\alpha/\tilde{T})\,\mathrm{d}s \tag{2.140}$$

for $t \in [0, 1-\alpha/\tilde{T})$ and

$$\tilde{\lambda}_{\mathrm{DE}}^{\mathrm{T}}(t) f(\tilde{x}(t), \tilde{y}(t)) + \frac{1}{\tilde{T}}\int_t^1 \tilde{\lambda}_{\mathrm{CP}}^{\mathrm{T}}(s)\dot{\tilde{x}}(s-\alpha/\tilde{T})\,\mathrm{d}s + \frac{1}{\tilde{T}}\int_0^{t-1+\alpha/\tilde{T}} \tilde{\lambda}_{\mathrm{CP}}^{\mathrm{T}}(s)\dot{\tilde{x}}(s-\alpha/\tilde{T})\,\mathrm{d}s \tag{2.141}$$

for $t \in [1-\alpha/\tilde{T}, 1]$ is continuous and constant, such that

$$\tilde{\lambda}_{\mathrm{DE}}^{\mathrm{T}}(1) f(\tilde{x}(1), \tilde{y}(1)) = \tilde{\lambda}_{\mathrm{DE}}^{\mathrm{T}}(0) f(\tilde{x}(0), \tilde{y}(0)). \tag{2.142}$$

From (2.137) it then follows that $\lambda_{\mathrm{PS}} = 0$ provided that the periodic trajectory $\tilde{x}(t)$ intersects $h = 0$ transversally at $\tilde{x}(0)$, since in this case $Dh(x(0))f(x(0), y(0)) \neq 0$. In this case, $\tilde{\lambda}_{\mathrm{DE}}(t/\tilde{T})$ is also periodic with period $\tilde{T}$. By (2.138) this also holds for the function $\tilde{\lambda}_{\mathrm{CP}}(t/\tilde{T})$. It follows that the constant function in (2.140) and (2.141) may be written in the form (2.140) for all t. Integration of this function over $t \in [0, 1]$ and changing the order of integration then

yields

$$\int_0^1 \tilde{\lambda}_{\mathrm{DE}}^{\mathrm{T}}(t) f(\tilde{x}(t), \tilde{y}(t))\,\mathrm{d}t + \frac{1}{\tilde{T}} \int_0^1 \int_t^{t+\alpha/\tilde{T}} \tilde{\lambda}_{\mathrm{CP}}^{\mathrm{T}}(s) \dot{\tilde{x}}(s - \alpha/\tilde{T})\,\mathrm{d}s\,\mathrm{d}t$$
$$= \int_0^1 \tilde{\lambda}_{\mathrm{DE}}^{\mathrm{T}}(t) f(\tilde{x}(t), \tilde{y}(t))\,\mathrm{d}t + \frac{\alpha}{\tilde{T}^2} \int_0^1 \tilde{\lambda}_{\mathrm{CP}}^{\mathrm{T}}(s) \dot{\tilde{x}}(s - \alpha/\tilde{T})\,\mathrm{d}s = 1, \tag{2.143}$$

where we used (2.139), periodicity, and the fact that $\eta = 1$. After substitution for $\dot{\tilde{x}}$ and of the integration variable, we obtain the normalization condition [96]

$$\tilde{\lambda}_{\mathrm{DE}}^{\mathrm{T}}(0) f(\tilde{x}(0), \tilde{y}(0)) + \int_{-\alpha/\tilde{T}}^{0} \tilde{\lambda}_{\mathrm{CP}}^{\mathrm{T}}(s + \alpha/\tilde{T}) f(\tilde{x}(s), \tilde{y}(s))\,\mathrm{d}s = 1. \tag{2.144}$$

As in the previous section, the regularity of the periodic orbit implies the existence of a unique triplet $(x(\cdot), y(\cdot), T)$ near $(\tilde{x}(\cdot), \tilde{y}(t), \tilde{T})$ for each pair of small δ_{BC} and δ_{PS}, such that

$$\dot{x}(t) - T f(x(t), y(t)) = 0 \text{ for } t \in [0, 1], x(0) - x(1) = \delta_{\mathrm{BC}},\ h(x(0)) = \delta_{\mathrm{PS}}, \tag{2.145}$$

where

$$y(t) - x(t + 1 - \alpha/T) = 0 \text{ for } t \in (0, \alpha/T), \tag{2.146}$$
$$y(t) - x(t - \alpha/T) = 0 \text{ for } t \in (\alpha/T, 1). \tag{2.147}$$

From the analysis in Section 2.4.1, we conclude that

$$T - \tilde{T} = -\tilde{\lambda}_{\mathrm{DE}}^{\mathrm{T}}(0) \delta_{\mathrm{BC}} + O\left(\|\delta_{\mathrm{BC}}\|^2\right). \tag{2.148}$$

where we have used the fact that $\tilde{\lambda}_{\mathrm{BC}} = \tilde{\lambda}_{\mathrm{DE}}(1) = \tilde{\lambda}_{\mathrm{DE}}(0)$ and $\tilde{\lambda}_{\mathrm{PS}} = 0$. For an asymptotically stable limit cycle, we may again associate $\tilde{\lambda}_{\mathrm{DE}}^{\mathrm{T}}(0)$ with the Frechét derivative $D\varphi(\tilde{x}(0))$ of the corresponding asymptotic phase [95].

2.4.4 Problem construction and analysis

As in the previous section on optimization, we obtain an augmented continuation problem **A** of the form in (2.44) corresponding to the analysis of a periodic orbit with $\mathcal{U} = \mathbb{R}^n$ by associating

- Φ with the boundary-value problem in (2.111) in terms of the continuation variables x and T;
- Ψ with the scalar T and corresponding continuation parameter μ; and
- Λ^* with the linear operator in (2.112)-(2.115) acting on the continuation multipliers λ_{DE}, λ_{BC}, λ_{PS}, and η.

This problem has dimensional deficit 1 which reduces to 0 once a solution is found with $\eta = 1$.

After suitable discretization, we may construct **A** according to the following algorithm:

Step 1: Invoke the core constructor (2.76) with `phi` encoding the differential constraint in (2.111), $\mathbb{K}_u^{\mathrm{o}} = \emptyset$, and u_0^{n} given by an initial solution guess for the continuation variables x and T.

Step 2: Invoke the core constructor (2.76) with `phi` encoding the periodic boundary conditions in (2.111), $\mathbb{K}_u^{\mathrm{o}}$ indexing the corresponding continuation variables from **Step 1**, and $u_0^{\mathrm{n}} = \emptyset$.

Step 3: Invoke the core constructor (2.76) with `phi` encoding the phase condition in (2.111), $\mathbb{K}_u^{\mathrm{o}}$ indexing the corresponding continuation variables from **Step 1**, and $u_0^{\mathrm{n}} = \emptyset$.

Step 4: Invoke the core constructor (2.77) with `psi` encoding the evaluation of T, $\mathbb{K}_u^{\mathrm{o}}$ indexing the corresponding continuation variable from **Step 1**, and $u_0^{\mathrm{n}} = \emptyset$.

Step 5: Invoke the core constructor (2.80) with `lambda` encoding the linear operators acting on λ_{DE} in the adjoint conditions (2.112)-(2.115), $\mathbb{K}_u^{\mathrm{o}}$ indexing the continuation variables

introduced in the corresponding call in **Step 1**, $\mathbb{K}_{\Lambda}^{\mathrm{o}} = \emptyset$, and λ_0^{n} given by an initial solution guess for the continuation variables λ_{DE}.

Step 6: Invoke the core constructor (2.80) with `lambda` encoding the linear operators acting on λ_{BC} in the adjoint conditions (2.112)-(2.115), $\mathbb{K}_u^{\mathrm{o}}$ indexing the continuation variables associated with the corresponding call in **Step 2**, $\mathbb{K}_{\Lambda}^{\mathrm{o}} \neq \emptyset$, and λ_0^{n} given by an initial solution guess for the continuation variables λ_{BC}.

Step 7: Invoke the core constructor (2.80) with `lambda` encoding the linear operators acting on λ_{PS} in the adjoint conditions (2.112)-(2.115), $\mathbb{K}_u^{\mathrm{o}}$ indexing the continuation variables associated with the corresponding call in **Step 3**, $\mathbb{K}_{\Lambda}^{\mathrm{o}} \neq \emptyset$, and λ_0^{n} given by an initial solution guess for the continuation variables λ_{PS}.

Step 8: Invoke the core constructor (2.80) with `lambda` encoding the linear operators acting on η in the adjoint conditions (2.112)-(2.115), $\mathbb{K}_u^{\mathrm{o}}$ indexing the continuation variables associated with the corresponding call in **Step 4**, $\mathbb{K}_{\Lambda}^{\mathrm{o}} \neq \emptyset$, and λ_0^{n} given by an initial solution guess for the continuation variable η.

As suggested previously, steps 5 through 8 can be implemented automatically from information provided in steps 1 through 4, thereby reducing the task of construction to the definition of the vector field f. To solve for the corresponding phase response curve, we invoke the core constructor (2.78) to append a complementary zero function that evaluates to $1 - \eta$. Here, $\mathbb{K}_u^{\mathrm{o}} = \mathbb{K}_v^{\mathrm{o}} = \emptyset$ and $\mathbb{K}_{\lambda}^{\mathrm{o}}$ indexes the continuation multiplier η.

For the analysis of a periodic orbit of the delay differential equation (2.127), we similarly obtain an augmented continuation problem **A** of the form in (2.44) by associating

- Φ with the boundary-value problem in (2.132)-(2.134) in terms of the continuation variables x, y, and T;
- Ψ with the scalar T and corresponding continuation parameter μ; and

- Λ^* with the linear operator in (2.135)-(2.139) acting on the continuation multipliers λ_{DE}, λ_{CP}, λ_{BC}, λ_{PS}, and η.

This problem again has dimensional deficit 1 which reduces to 0 once a solution is found with $\eta = 1$.

2.5 Conclusions

In this chapter, we reviewed the general style of problem construction amenable to continuation offered by the package COCO. A data assimilation problem and a phase response curve analysis were used to show that the general style of construction can be extended to delay-differential problems and their adjoints. In the next chapter, we consider a technique of successive continuation for solving optimization problems constrained by periodic or quasiperiodic boundary-value problems with delay.

Chapter 3

DESIGN OPTIMIZATION IN PROBLEMS WITH DELAY

In this chapter[1], we generalize a previously-conceived, continuation-based optimization technique for scalar objective functions on constraint manifolds to cases of periodic and quasiperiodic solutions of delay-differential equations. A Lagrange formalism is used to construct adjoint conditions that are linear and homogenous in the unknown Lagrange multipliers. As a consequence, it is shown how critical points on the constraint manifold can be found through several stages of continuation along a sequence of connected one-dimensional manifolds of solutions to increasing subsets of the necessary optimality conditions. Due to the presence of delayed and advanced arguments in the original and adjoint differential equations, care must be taken to determine the degree of smoothness of the Lagrange multipliers with respect to time. Such considerations naturally lead to a formulation in terms of multi-segment boundary-value problems (BVPs), including the possibility that the number of segments may change, or that their order may permute, during continuation. The methodology is illustrated using the software package COCO on periodic orbits of both linear and nonlinear delay-differential equations, keeping in mind that closed-form solutions are not typically available even in the linear case. Finally, we demonstrate optimization on a family of quasiperiodic invariant tori in an example unfolding of a Hopf bifurcation with delay and parametric forcing.

We first motivate our interest and approach with the problem of optimization of the

[1]The content of this chapter is reproduced from Ahsan, Dankowicz and Sieber, "Optimization along families of periodic and quasiperiodic orbits in dynamical systems with delay," *Nonlinear Dynamics*, **99**(1), 837–854, 2020 [1], and included here with permission from the publisher.

response amplitude of a harmonically-forced, scalar, linear, delay-differential equation in Section 3.1. The general framework for problems with single delays is then considered in Section 3.2, first for periodic orbits and subsequently for families of two-dimensional quasiperiodic invariant tori. As discussed in detail, the latter optimization problem falls into the category of constrained optimization for partial differential equations (PDEs) [97]–[99], for which the necessary optimality conditions take the form of coupled, piecewise-defined PDEs with non-local coupling, as well as associated boundary and interval conditions representing periodicity in one dimension and rotation in the other. Subsections of Section 3.2 consider example applications to the search for a saddle of the response amplitude of a harmonically-forced Duffing oscillator subject to delayed feedback control and a geometric fold along a family of quasiperiodic trajectories for constant rotation number. Analysis using the COCO software package validates the successive continuation approach, as well as the simultaneous discretization of the dynamic constraints and adjoint equations.

3.1 Motivating Example

We illustrate the general framework for optimization along families of solutions to delay-differential equations (DDEs) by first considering periodic responses $z(t)$ of frequency ω for a harmonically-forced, scalar, linear, delay-differential equation

$$\dot{z} = -z - z\,(t-1) + \cos\omega t, \tag{3.1}$$

where we omit (here, and throughout the chapter) functional arguments when they are obvious from the context. It follows from the method of undetermined coefficients that such responses are of the harmonic form

$$z(t) = r(\omega)\cos(\omega t - \theta(\omega)), \tag{3.2}$$

where

$$r(\omega) = \left[2 + \omega^2 - 2\omega \sin\omega + 2\cos\omega\right]^{-1/2} \tag{3.3}$$

and

$$\cos\theta(\omega) = -\frac{1+\cos\omega}{r^3(\omega)},\ \sin\theta(\omega) = \frac{\sin\omega - \omega}{r^3(\omega)}. \tag{3.4}$$

Let us consider the optimization problem of finding the forcing frequency ω for which such a periodic response has maximum amplitude. It follows from (3.3) that the maximum amplitude $r_{\text{crit}} \doteq r(\omega_{\text{crit}}) \approx 0.89$ is achieved for $\omega_{\text{crit}} \approx 1.72$ (cf. Fig. 3.1), and that $z(t_{\text{crit}}) = r_{\text{crit}}$ at time $t_{\text{crit}} \doteq \theta(\omega_{\text{crit}})/\omega_{\text{crit}} \approx 2.24$ (up to multiples of the period $T_{\text{crit}} \doteq 2\pi/\omega_{\text{crit}} \approx 3.65$). Hence, for this simple optimization problem all components of the solution are known exactly, enabling a comparison with the results of numerical algorithms.

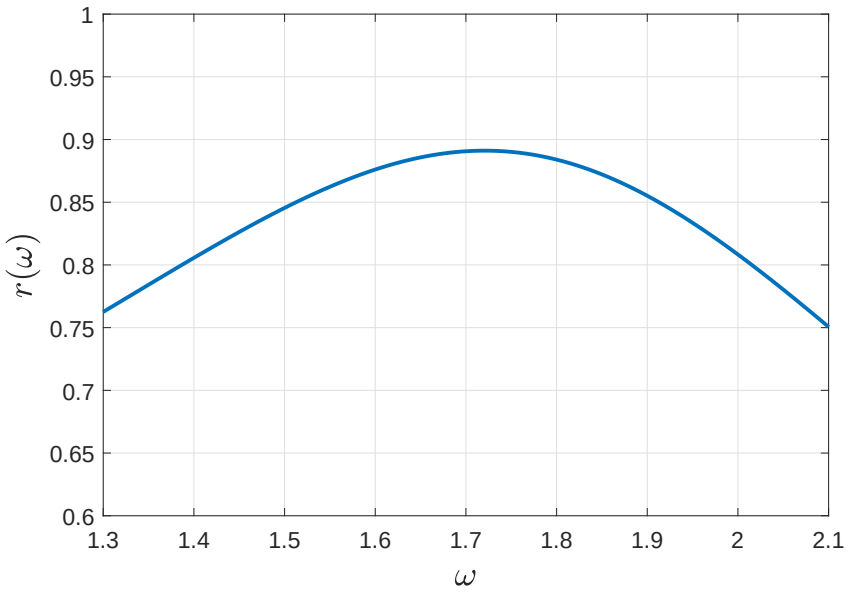

Figure 3.1: Frequency-response diagram for the steady-state periodic solutions of the harmonically-forced, scalar, linear delay-differential equation (3.1). The maximum value of the amplitude is $r_{\text{crit}} \approx 0.8911$ which occurs for $\omega = \omega_{\text{crit}} \approx 1.7207$ ($T = T_{\text{crit}} \approx 3.6516$).

3.1.1 Formulation as a constrained optimization problem

We transform the above optimization problem into a format suitable for a general numerical solver by introducing the excitation period $T = 2\pi/\omega$ as an unknown (T replaces ω) and rescaling time (calling the new time τ) such that $x(\tau) \doteq z(T\tau + T\phi/2\pi)$. Here, the free phase ϕ is to be chosen so as to shift the time on the interval $[0, 1]$ when the periodic solution x has a critical point to $\tau = 0$. Thus, we are seeking a solution to the constrained optimization problem

$$\text{maximize} \quad \mu_A = x(0) \tag{3.5}$$

with respect to a continuous function x on $[0, 1]$, as well as the variables T and ϕ, subject to the equality constraints

$$x' = -Tx - Tx\,(\tau + 1 - 1/T) + T\cos(2\pi\tau + \phi) \quad \text{for } \tau \in (0, 1/T), \tag{3.6}$$

$$x' = -Tx - Tx\,(\tau - 1/T) + T\cos(2\pi\tau + \phi) \quad \text{for } \tau \in (1/T, 1), \tag{3.7}$$

$$0 = x(0) - x(1), \tag{3.8}$$

$$0 = x(0) + x(1 - 1/T) - \cos\phi. \tag{3.9}$$

Here, the constraints (3.6) and (3.7) impose the original delay-differential equation on the interval $(0, 1)$. They rely on periodicity to wrap the delayed argument back into this interval assuming that $T > 1$. The constraints (3.8) and (3.9) are boundary conditions. Constraint (3.8) imposes periodicity also on the interval boundary, while (3.9) is a phase condition that ensures that $x'(0) = 0$, consistent with x having a critical point at $\tau = 0$ and justifying the maximization of $x(0)$ as a substitute for the amplitude. By continuity of x on $[0, 1]$ and (3.8) it follows that x is, in fact, a smooth function on $[0, 1]$. Indeed, from the explicit solution in the previous section, it follows that $x(\tau) = r(2\pi/T)\cos 2\pi\tau$ and $\phi = \theta(2\pi/T)$ and, in particular, that optimality is obtained for $x(\tau) = x_{\text{crit}}(\tau) \doteq r_{\text{crit}}\cos 2\pi\tau$ and $\phi = \phi_{\text{crit}} \doteq \theta(2\pi/T_{\text{crit}})$ for $T = T_{\text{crit}}$.

The constrained optimization problem (3.5)–(3.9) gives rise to the Lagrangian

$$
\begin{aligned}
&L\left(x(\cdot),\phi,T,\mu_A,\lambda_1(\cdot),\lambda_2,\lambda_3,\eta_A\right)=\mu_A+\eta_A\left(x\left(0\right)-\mu_A\right)\\
&+\int_0^{1/T}\lambda_1\left[x'+T\left[x+x\left(\tau+1-1/T\right)-\cos\left(2\pi\tau+\phi\right)\right]\right]\,\mathrm{d}\tau\\
&+\int_{1/T}^{1-2/T}\lambda_1\left[x'+T\left[x+x\left(\tau-1/T\right)-\cos\left(2\pi\tau+\phi\right)\right]\right]\,\mathrm{d}\tau\\
&+\int_{1-2/T}^{1-1/T}\lambda_1\left[x'+T\left[x+x\left(\tau-1/T\right)-\cos\left(2\pi\tau+\phi\right)\right]\right]\,\mathrm{d}\tau\\
&+\int_{1-1/T}^{1}\lambda_1\left[x'+T\left[x+x\left(\tau-1/T\right)-\cos\left(2\pi\tau+\phi\right)\right]\right]\,\mathrm{d}\tau\\
&+\lambda_2\left(x\left(0\right)-x\left(1\right)\right)+\lambda_3\left(x\left(0\right)+x\left(1-1/T\right)-\cos\left(\phi\right)\right),
\end{aligned}
\tag{3.10}
$$

where the Lagrange multipliers are $\lambda_1(\tau)$ (a function on $[0,1]$) for the DDE constraints (3.6) and (3.7), λ_2 and λ_3 for the boundary conditions (3.8) and (3.9), and η_A for the relationship between the fitness μ_A and $x(0)$ in (3.5).

In (3.10), the integral for the pairing between λ_1 and the DDE constraints has been split into 4 parts, one for each of the intervals $(0,1/T)$, $(1/T,1-2/T)$, $(1-2/T,1-1/T)$, and $(1-1/T,1)$, reflecting different functional forms of the differential equations (3.6) and (3.7) for x on $(0,1/T)$ and $(1/T,1)$, respectively, and anticipating possible discontinuities in λ_1 and λ_1'. For example, the split at $\tau=1-1/T$ is in anticipation of a potential discontinuity of the Lagrange multiplier λ_1 at this instant caused by the imposition of a constraint on x evaluated at this time in (3.9). This discontinuity implies a potential discontinuity of λ_1' at $\tau=1-2/T$. For the same reason, the appearances of $x(0)$ in (3.5) and (3.9) suggest that $\lambda_1(0)\neq\lambda_1(1)$ resulting in a potential discontinuity of λ_1' at $\tau=1-1/T$. All functions are assumed to be continuously differentiable on the partition implied by the integrals in (3.10). The ordering of the discontinuity points assumes that $T>3$ (Fig. 3.1 shows that the optimal

T is in this range).

Imposing vanishing variations of the Lagrangian L with respect to variations in all its arguments recovers the original constraints (3.5)–(3.9) and the following *adjoint system* determining the Lagrange multipliers. Specfically, vanishing variations with respect to x imply

$$-\lambda_1' + T\lambda_1 + T\lambda_1\left(\tau + 1/T\right) = 0 \tag{3.11}$$

for $\tau \in (0, 1/T) \cup (1/T, 1-2/T) \cup (1-2/T, 1-1/T)$ and

$$-\lambda_1' + T\lambda_1 + T\lambda_1\left(\tau - 1 + 1/T\right) = 0 \tag{3.12}$$

for $\tau \in (1-1/T, 1)$. Boundary and interface conditions for these equations are obtained by considering variations with respect to $x(0)$, $x(1/T)$, $x(1-2/T)$, $x(1-1/T)$, and $x(1)$, corresponding in that order to

$$0 = -\lambda_1(0) + \lambda_2 + \lambda_3 + \eta_A, \tag{3.13}$$

$$0 = \lambda_1(1/T)_- - \lambda_1(1/T)_+, \tag{3.14}$$

$$0 = \lambda_1(1-2/T)_- - \lambda_1(1-2/T)_+, \tag{3.15}$$

$$0 = \lambda_1(1-1/T)_- - \lambda_1(1-1/T)_+ + \lambda_3, \tag{3.16}$$

$$0 = \lambda_1(1) - \lambda_2, \tag{3.17}$$

using the convention that $\lambda_1(\tau^*)_\pm \doteq \lim_{\tau\to\tau^*\pm} \lambda_1(\tau)$ and recalling that $x(\tau)$ is continuous on $[0,1]$. Vanishing variations with respect to ϕ and T imply the integral constraints

$$0 = \int_0^1 T\lambda_1 \sin\left(2\pi\tau + \phi\right)\, \mathrm{d}\tau + \lambda_3 \sin\left(\phi\right) \tag{3.18}$$

and

$$
\begin{aligned}
0 = &\int_0^{1/T} \lambda_1 \left(x(\tau + 1 - 1/T) + x'(\tau + 1 - 1/T)/T\right) \,\mathrm{d}\tau \\
&+ \int_{1/T}^{1} \lambda_1 \left(x(\tau - 1/T) + x'(\tau - 1/T)/T\right) \,\mathrm{d}\tau \\
&+ \int_0^{1} \lambda_1 \left(x - \cos(2\pi\tau + \phi)\right) \,\mathrm{d}\tau + \lambda_3 T^{-2} x'(1 - 1/T),
\end{aligned} \tag{3.19}
$$

respectively. Finally, vanishing variation with respect to μ_A implies that

$$
1 - \eta_A = 0. \tag{3.20}
$$

In summary, the system of original contraints (3.5)–(3.9) and adjoint equations (3.11)–(3.20) is a nonlinear integro-differential boundary-value problem (BVP) defining the critical points of the Lagrangian L and the constrained optimization problem (3.5)–(3.9).

In this example, the dimension of the manifold on which the constrained optimization problem is posed equals 1, corresponding to the numbers of degrees of freedom of the nonlinear subsystem (3.5)–(3.9) (with variables x, T and ϕ). In contrast, the full system (3.5)–(3.9), (3.11)–(3.20) has no such degrees of freedom and, consequently, generically has only isolated solutions. Several properties put it beyond the reach of "off-the-shelf" BVP solvers:

1. It consists of differential equations on multiple intervals (thus, the problem is called a *multi-segment* BVP) with differential functional forms and continuous "right-hand sides". The number and length of these intervals is strongly problem dependent, and may even change during the optimization process.

2. The differential equations evaluate their right-hand sides at times deviating from τ (delayed or advanced arguments).

3. The second point leads to nonlocal coupling across segments that is not restricted to coupling at the boundaries of the intervals. For example, (3.11) couples the values of λ_1 in $(1-2/T, 1-1/T)$ to values of λ_1 in $(1-1/T, 1)$.

On the other hand, the system (3.5)–(3.9), (3.11)–(3.20) has some additional structure that aids both in its construction and solution:

1. The equations are only forward coupled in that a solution to the original constraints (3.5)–(3.9) can be obtained independently of the values of the Lagrange multipliers, while a solution to the adjoint equations (3.11)–(3.20) requires knowledge of x, T, and ϕ, and generically exists, at best, only for isolated choices of x, T, and ϕ.

2. The adjoint equations (3.11)–(3.19) (thus excluding (3.20)) are linear and homogeneous in the Lagrange multipliers λ_j $(j = 1, 2, 3)$ and η_A. A trivial solution of this subset of the adjoint system is therefore given by vanishing Lagrange multipliers for any x, T, and ϕ.

3. The adjoint equation (3.20) is trivial both in construction and solution. Imposing its solution ($\eta_A = 1$) on the remaining adjoint system, however, renders the latter nonhomogeneous.

This structure will also be present for more general cases than the example and can be exploited in the search for solutions, as well as to generate the adjoint equations (3.11)–(3.19) automatically during a staged construction of the optimization problem similar to [14].

In this example, a few facts about the Lagrange multipliers may be deduced directly from the adjoint equations. It follows immediately from (3.14) and (3.15) that λ_1 is continuous at $\tau = 1/T$ and $\tau = 1 - 2/T$, and from (3.11) that λ_1' is continuous at $\tau = 1/T$. Moreover, using the explicitly known solution for x, it follows that the Lagrange multiplier λ_3 must equal 0 at a local extremum. Indeed, substitution of the modified phase condition

$$\delta = x\,(0) + x\,(1 - 1/T) - \cos\phi \tag{3.21}$$

in lieu of (3.9) implies that

$$\mu_A = \left(\cos\phi + \cos(\omega+\phi) + \omega\sin\phi\right)/r(\omega), \tag{3.22}$$

where ϕ is implicitly determined by

$$\delta = \omega\left(\sin\phi + \sin(\omega+\phi) - \omega\cos\phi\right)/r(\omega) \tag{3.23}$$

for $\delta \approx 0$. Implicit differentiation of both conditions with respect to the residual δ shows that the rate of change of μ_A with respect to δ equals 0 at $\delta = 0$. This, in turn, implies that that $\lambda_3 = 0$ at an extremum, i.e., that λ_1 is, in fact, continuous also at $\tau = 1 - 1/T$ and, consequently, continuously differentiable also at $\tau = 1 - 2/T$. In contrast, λ_1' experiences a discontinuity at $\tau = 1 - 1/T$ for nonzero $\eta_A = \lambda_1(0) - \lambda_1(1)$.

3.1.2 Simple continuation

According to the properties enumerated above, a solution to (3.5)–(3.9), (3.11)–(3.20) may be sought using a method of *successive continuation* [13], [14] with an embedded multi-segment boundary-value problem implementation that permits evaluation of the right-hand side at arguments shifted by arbitrary times. Specifically, this method overcomes the problem of initializing a nonlinear solver for the full system by defining a sequence of continuation problems with one-dimensional solution manifolds that connect an initial solution guess with Lagrange multipliers all equal to 0 with the sought critical point for which η_A must equal 1.

To this end, we consider the system given by the relationship between μ_A and $x(0)$ in (3.5), the boundary-value problem constraints (3.6)–(3.9), and the adjoint integral-differential boundary-value problem (3.11)–(3.19), but purposely omit the algebraic constraint (3.20). Although we anticipate that λ_3 will equal 0 throughout the analysis, we keep λ_3 as an unknown and monitor its value during continuation. By linearity and homogeneity of the adjoint subsystem in the Lagrange multipliers λ_j and η_A, it follows that solutions to the

full system lie on either of two one-dimensional manifolds. The first of these consists of functions $x(\tau) = r(2\pi/T)\cos 2\pi\tau$ with corresponding T, ϕ, and $\mu_A = x(0) = r(2\pi/T)$, and with vanishing Lagrange multipliers. The second manifold consists of the periodic solution $x_{\text{crit}}(\tau) = r_{\text{crit}}\cos 2\pi\tau$ with corresponding $T = T_{\text{crit}}$, $\phi = \phi_{\text{crit}}$, and $\mu_A = r_{\text{crit}}$, and with varying Lagrange multipliers proportional to η_A. The two manifolds clearly intersect at the local extremum of μ_A along the first manifold. The sought solution to the complete set of equations (3.5)–(3.9), (3.11)–(3.20) corresponds to the point along the second manifold where $\eta_A = 1$.

In this example, the solutions along the first manifold are known explicitly. In other cases, an initial periodic response may be approximately obtained from the dynamically stable solution by direct simulation. Given such an initial solution guess for x, T, and ϕ, a nonlinear solver may be employed to converge to a point on the manifold. A numerical continuation algorithm (e.g., pseudo-arclength continuation) may then be used to generate a sequence of points along the manifold, meanwhile monitoring for local extrema of μ_A and singular points for the system Jacobian (corresponding to branch points on the manifold). As shown above, and true also in the general case, these coincide. Using standard techniques, numerical continuation may proceed from such a branch point along the secondary manifold with the help of a candidate direction of continuation, for example, one that is i) transversal to the tangent direction to the original solution manifold and ii) in the plane spanned by the tangent directions to the two manifolds at the branch point.

Continuation using such an implementation in the COCO software package [74] approximately locates an extremum (in the form of a fold point in μ_A along the solution manifold) at $T \approx 3.6515$ as shown in Fig. 3.2. Branch switching from the nearby branch point (exact coincidence is lost due to discretization) and continuation until $\eta_A = 1$ yields the graphs of $x(\tau)$ and $\lambda_1(\tau)$ shown in Fig. 3.3. As seen in the bottom panel, $\lambda_1(\tau)$ is approximately continuous at $1 - 1/T \approx 0.73$, albeit with discontinuous derivative at this point, since $\lambda_1(0) - \lambda_1(1) = 1$.

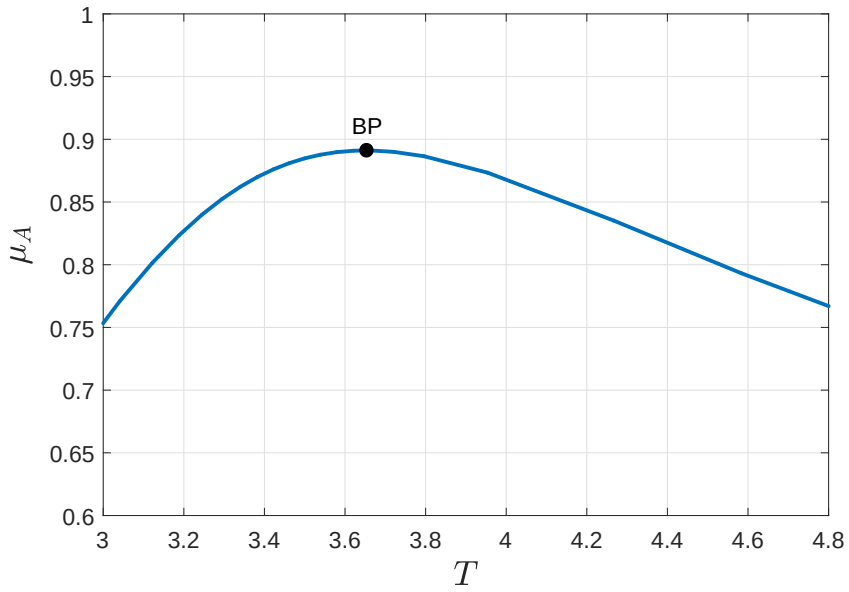

Figure 3.2: Results from numerical continuation with vanishing Lagrange multipliers. The maximum value of μ_A is located at $T \approx 3.6515$ and is here identified by the label BP, since it approximately coincides with a branch point.

3.2 General Optimization Framework

In this section, we discuss the general methodology for optimization on periodic and quasiperiodic solutions $z(t) \in \mathbb{R}^n$ of delay-differential equations with a single delay of the form

$$\dot{z} = f\left(t, z, z\left(t-\alpha\right), p\right), \tag{3.24}$$

where $f : \mathbb{R}^1 \times \mathbb{R}^n \times \mathbb{R}^n \times \mathbb{R}^q \to \mathbb{R}^n$ is periodic in its first argument with period T. Here, α and p denote the time delay and the problem parameters (excluding T), respectively.

As the motivating example in the previous section illustrates, the problem Lagrangian and, by implication, the adjoint equations are linear in the Lagrange multipliers. The adjoint equations may therefore be constructed term-by-term by successively deriving the contributions from disjoint collections of constraints from the corresponding *partial Lagrangians* associated with a subset of the Lagrange multipliers. Until the full set of constraints has been

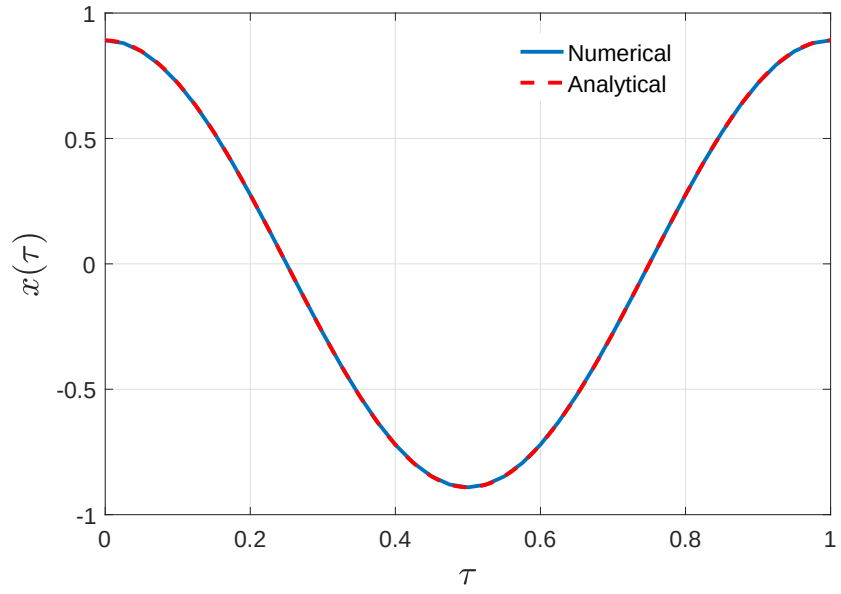

(a)

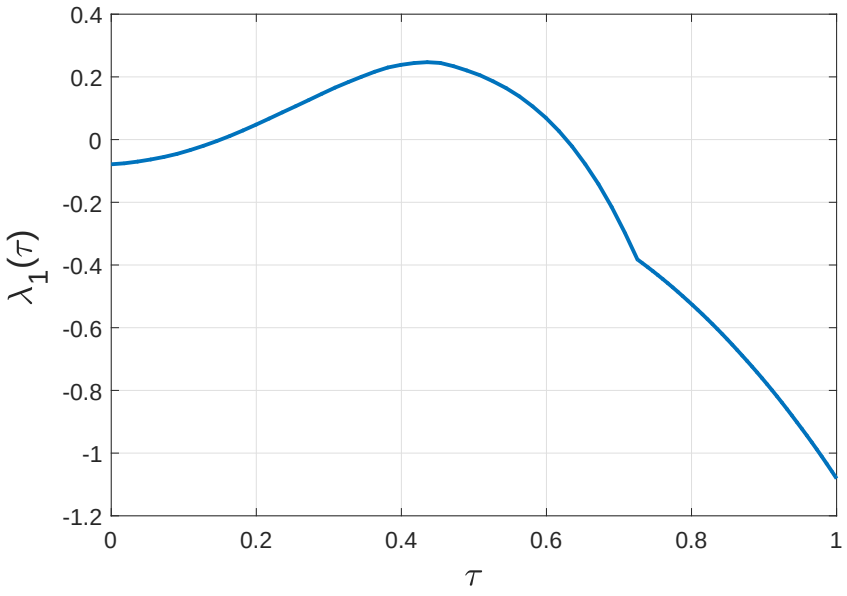

(b)

Figure 3.3: (a) $x(\tau)$ and (b) $\lambda_1(\tau)$ at the terminal point of the second stage of continuation with $\eta_A = 1$. The upper panel shows a comparison between the numerical solution and the analytical solution at the extremum. The bottom panel shows the Lagrange multiplier associated with the imposition of the DDE admitting a slope discontinuity at $\tau = 1 - 1/T$.

considered, the adjoint equations are not completely known. The following subsections discuss the partial Lagrangians and the implied contributions to the adjoint equations resulting from the DDE constraints and boundary conditions associated with periodic and quasiperiodic orbits. For particular examples, we indicate the additional contributions associated with problem-specific constraints that complete the construction of the adjoint equations. In all cases, the contribution from the objective function to the Lagrangian implies the algebraic adjoint condition that the corresponding Lagrange multiplier (η_A in the previous section) must equal 1 at a stationary point.

3.2.1 Periodic orbits

Suppose first that $T > \alpha$ and consider the problem of optimizing a scalar-valued objective functional on a family of continuous solutions $x(\tau)$ to the differential equations

$$x' = Tf\left(T\tau, x, x\left(\tau + 1 - \alpha/T\right), p\right) \quad \text{for } \tau \in (0, \alpha/T), \tag{3.25}$$

$$x' = Tf\left(T\tau, x, x\left(\tau - \alpha/T\right), p\right) \quad \text{for } \tau \in (\alpha/T, 1), \tag{3.26}$$

and the boundary conditions

$$x\left(0\right) - x\left(1\right) = 0. \tag{3.27}$$

By a rescaling of the independent variable by T, such solutions correspond to periodic solutions of (3.24) with period T. By continuity and periodicity, such solutions must be continuously differentiable to all orders.

Suppose, in fact, that $T > 3\alpha$ and that the objective functional and any additional constraints depend on pointwise values of $x(\tau)$ only at $\tau = 0$, $\tau = 1$, and $\tau = \beta$ for some $\beta = \beta(\alpha, T)$ such that

$$2\alpha/T < \beta < 1 - \alpha/T. \tag{3.28}$$

As we show below, such dependence results in an additional adjoint equation associated with

variations with respect to $x(\beta)$. Other pointwise dependencies of the objective functional would be treated similarly, while dependence on an integral over the entire interval $[0,1]$ of a function of x would not result in additional adjoint equations. We may formulate a corresponding partial Lagrangian

$$\begin{aligned} &L_{\mathrm{BVP}}\left(x(\cdot),\alpha,T,p,\lambda_f(\cdot),\lambda_{\mathrm{bc}}\right) = \\ &\quad \lambda_{\mathrm{bc}}^{\mathrm{T}}\left(x(0)-x(1)\right) + \int_0^{\alpha/T} \lambda_f^{\mathrm{T}}\left(x'-Tf_1\right)\,\mathrm{d}\tau \\ &\quad + \int_{\alpha/T}^{\beta-\alpha/T} \lambda_f^{\mathrm{T}}\left(x'-Tf_0\right)\,\mathrm{d}\tau + \int_{\beta-\alpha/T}^{\beta} \lambda_f^{\mathrm{T}}\left(x'-Tf_0\right)\,\mathrm{d}\tau \\ &\quad + \int_{\beta}^{1-\alpha/T} \lambda_f^{\mathrm{T}}\left(x'-Tf_0\right)\,\mathrm{d}\tau + \int_{1-\alpha/T}^{1} \lambda_f^{\mathrm{T}}\left(x'-Tf_0\right)\,\mathrm{d}\tau, \end{aligned} \tag{3.29}$$

where $f_j(\tau) = f\left(T\tau, x\left(\tau\right), x\left(\tau+j-\alpha/T\right), p\right)$. Here, $\lambda_f(\tau)$ and λ_{bc} are the Lagrange multipliers associated with the imposition of the differential equations and boundary conditions, respectively, and each integrand is assumed to be continuously differentiable on the corresponding interval. The splitting of the integral is here motivated by an anticipated discontinuity of λ_f at $\tau=\beta$ and, consequently, of λ_f' at $\tau=\beta-\alpha/T$, the different functional forms of the original DDEs on the intervals $(0,\alpha/T)$ and $(\alpha/T,1)$, and an anticipated discontinuity in λ_f' also at $\tau=1-\alpha/T$.

By the stated assumptions on the objective function and any additional constraints, it is easy to show that, at a stationary point of the total Lagrangian, $\lambda_f(\tau)$ must be continuous at $\tau=\alpha/T$, $\tau=\beta-\alpha/T$, and $\tau=1-\alpha/T$. Using the notation

$$f_{j,k}(\tau) = \partial_k f(T\tau, x(\tau), x(\tau+j-\alpha/T), p), \tag{3.30}$$

$$f_{j,q}(\tau) = \frac{\mathrm{d}}{\mathrm{d}\,q} f\left(T\tau, x\left(\tau\right), x\left(\tau+j-\alpha/T\right), p\right) \tag{3.31}$$

for $j=0,1$ and $q=\alpha,T$ ($\partial_k f$ is the partial derivative of f with respect to its kth argument,

$\mathrm{d}/\mathrm{d}q$ is the total derivative of an expression with respect to q), the contributions to the necessary adjoint conditions for a stationary point of the total Lagrangian are given by

$$-\lambda_f'^{\mathrm{T}} - T\lambda_f^{\mathrm{T}} f_{1,2} - T\lambda_f^{\mathrm{T}}\left(\tau + \alpha/T\right) f_{0,3}\left(\tau + \alpha/T\right) \tag{3.32}$$

for variations with respect to $x(\tau)$ on $\tau \in (0, \alpha/T)$;

$$-\lambda_f'^{\mathrm{T}} - T\lambda_f^{\mathrm{T}} f_{0,2} - T\lambda_f^{\mathrm{T}}\left(\tau + \alpha/T\right) f_{0,3}\left(\tau + \alpha/T\right) \tag{3.33}$$

for variations with respect to $x(\tau)$ on $\tau \in (\alpha/T, \beta - \alpha/T) \cup (\beta - \alpha/T, \beta) \cup (\beta, 1 - \alpha/T)$;

$$-\lambda_f'^{\mathrm{T}} - T\lambda_f^{\mathrm{T}} f_{0,2} - T\lambda_f^{\mathrm{T}}\left(\tau + \alpha/T - 1\right) f_{1,3}\left(\tau + \alpha/T - 1\right) \tag{3.34}$$

for variations with respect to $x(\tau)$ on $\tau \in (1 - \alpha/T, 1)$;

$$-\lambda_f^{\mathrm{T}}(0) + \lambda_{\mathrm{bc}}^{\mathrm{T}}, \quad \lambda_f^{\mathrm{T}}(\beta)_- - \lambda_f^{\mathrm{T}}(\beta)_+, \quad \lambda_f^{\mathrm{T}}(1) - \lambda_{\mathrm{bc}}^{\mathrm{T}}, \tag{3.35}$$

for variations with respect to $x(0)$, $x(\beta)$, and $x(1)$, respectively;

$$-\int_0^{\alpha/T} \lambda_f^{\mathrm{T}} T f_{1,\alpha}\,\mathrm{d}\tau - \int_{\alpha/T}^1 \lambda_f^{\mathrm{T}} T f_{0,\alpha}\,\mathrm{d}\tau \tag{3.36}$$

for variations with respect to α;

$$-\int_0^{\alpha/T} \lambda_f^{\mathrm{T}}\left(f_1 + T f_{1,T}\right)\mathrm{d}\tau - \int_{\alpha/T}^1 \lambda_f^{\mathrm{T}}\left(f_0 + T f_{0,T}\right)\mathrm{d}\tau \tag{3.37}$$

for variations with respect to T; and

$$-\int_0^{\alpha/T} \lambda_1^{\mathrm{T}} T f_{1,4}\,\mathrm{d}\tau - \int_{\alpha/T}^1 \lambda_1^{\mathrm{T}} T f_{0,4}\,\mathrm{d}\tau \tag{3.38}$$

for variations with respect to p. The terms $f_{j,T}$ and $f_{j,\alpha}$ in (3.36) and (3.37) both contain

time derivatives x' with delayed or advanced arguments, since T and α both appear in the evaluation of x in the third arguments of f_0 and f_1.

As previously anticipated, the explicit dependence of the Lagrangian on the internal state point $x(\beta)$ results in a potential discontinuity of the Lagrange multiplier $\lambda_f(\tau)$ at $\tau = \beta$. Continuous differentiability of $x(\tau)$ on $[0, 1]$ and of $\lambda_f(\tau)$ on $(0, \beta - \alpha/T)$, $(\beta - \alpha/T, \beta)$, $(\beta, 1 - \alpha/T)$, and $(1 - \alpha/T, 1)$ implies that the necessary conditions for an extremum are in the form of a multi-segment boundary-value problem in a single trajectory segment for $x(\tau)$ and four coupled trajectory segments for $\lambda_f(\tau)$. A similar result is obtained, for example, in the limiting case when $\beta = 1 - \alpha/T$. This case specializes to the example discussed in the previous section, since there $\alpha = 1$, $\beta = 1 - 1/T$, and $T > 3$. In contrast, when β is either 0 or 1, i.e., when there is no dependence of the objective function or any additional constraints on an internal point, then we obtain a single trajectory segment for $x(\tau)$ and three coupled trajectory segments for $\lambda_f(\tau)$ with both variables continuous throughout the interval $[0, 1]$.

3.2.2 A Duffing oscillator with delayed PD control

As an application of the general methodology when $\beta = 0$, consider the harmonically-forced Duffing oscillator with delayed state (proportional and derivative; PD) feedback given by the DDE

$$\ddot{z} + 2\zeta\dot{z} + z + \mu z^3 = 2az\,(t - \alpha) + 2b\dot{z}\,(t - \alpha) + \gamma\,\cos\,(2\pi t/T)\,. \tag{3.39}$$

Inspired by [100], for fixed ζ, μ, a, b, and γ, we seek a delay α that minimizes the maximum amplitude of oscillation along a family of periodic responses of this system under variations in the excitation period T. Since the optimization problem involves minimizing a maximum, it corresponds to the search for a saddle point in the value of the oscillation amplitude on the two-dimensional constraint manifold.

Following Section 3.1.1, let $x_1(\tau) \doteq z(T\tau + T\phi/2\pi)$ and $x_2(\tau) \doteq \dot{z}(T\tau + T\phi/2\pi)$ represent

the displacement and velocity, respectively, on the rescaled time interval $[0, 1]$. The phase ϕ is again to be chosen so as to shift the time on this interval when the oscillator reaches its maximum displacement to $\tau = 0$. It follows that the objective functional is given by

$$\mu_A = x_1(0) \tag{3.40}$$

for solutions of (3.25)–(3.27) subject to the phase condition

$$x_2(0) = 0 \tag{3.41}$$

and corresponding to the vector field

$$f(t, u, v, p) = \begin{pmatrix} u_2 \\ -2\zeta u_2 - u_1 - \mu u_1^3 \end{pmatrix} + \begin{pmatrix} 0 \\ 2av_1 + 2bv_2 + \gamma \cos(2\pi t/T + \phi) \end{pmatrix}, \tag{3.42}$$

where $p = \phi$.

The partial Lagrangian for the objective functional and phase condition is

$$L_{\text{opt}}(x(\cdot), \mu_A, \lambda_{\text{ph}}, \eta_A) = \mu_A + \lambda_{\text{ph}} x_2(0) + \eta_A(x_1(0) - \mu_A), \tag{3.43}$$

where λ_{ph} and η_A are additional Lagrange multipliers. This partial Lagrangian adds the term $(\eta_A, \lambda_{\text{ph}})^{\text{T}}$ to the variation with respect to $x(0)$ in (3.35) (first term) and results in the algebraic adjoint constraint

$$0 = 1 - \eta_A, \tag{3.44}$$

assuming no additional dependence of the problem Lagrangian on μ_A.

Since neither the objective functional nor the additional phase condition depend on x evaluated at an interior point of the interval $[0, 1]$, it follows that λ_f is continuous on the

entire interval. This simplifies the partial Lagrangian L_{BVP} in (3.29) as the two integrals with boundary β can be combined, and the resulting adjoint DDE contribution (3.33) can be applied on the combined interval $(\alpha/T, 1-\alpha/T)$, such that $\lambda_f(\tau)$ is in fact continuously differentiable on $(0, 1-\alpha/T)$. Correspondingly, the middle adjoint condition in (3.35) can be omitted. Moreover, like in the motivating example in Section 3.1.1, it is easy to see that the rate of change of $\mu_A = x_1(0)$ with respect to $\delta = x_2(0)$ vanishes at $\delta = 0$. We conclude that $\lambda_{\mathrm{ph}} = 0$ at a stationary point of the Lagrangian. This implies that $\lambda_{f,2}(1) = \lambda_{f,2}(0)$ and, by inspection of (3.33) and (3.34), that both components of λ_f are actually continuously differentiable throughout the interval $[0, 1]$.

Since the dimension n_{opt} of the optimization manifold equals 2, the successive continuation approach proposed by Kernévez and Doedel [13] requires multiple stages (in contrast to the motivating example in Section 3.1.1, where $n_{\mathrm{opt}} = 1$): one initially optimizes only with respect to one variable, following a curve in the optimization manifold, keeping $n_{\mathrm{opt}} - 1$ variables fixed. At each successive stage of continuation one releases one further optimization variable, until all variables are free. In this analysis, we propose to keep α fixed during the initial stage of continuation, corresponding to the imposition of a constraint on the set of unknowns. To this end, we consider the additional partial Lagrangian

$$L_{\mathrm{sc}}(\alpha, \mu_\alpha, \eta_\alpha) = \eta_\alpha(\alpha - \mu_\alpha). \tag{3.45}$$

This partial Lagrangian adds the constraint

$$\alpha = \mu_\alpha \tag{3.46}$$

and the algebraic adjoint equation (for vanishing variation with respect to μ_α)

$$0 = \eta_\alpha, \tag{3.47}$$

and adds η_α to the adjoint variations with respect to α in (3.36). The total problem Lagrangian is now given by

$$L\left(x(\cdot),\alpha,T,p,\mu_A,\mu_\alpha,\lambda_f(\cdot),\lambda_{\mathrm{bc}},\lambda_{\mathrm{ph}},\eta_A,\eta_\alpha\right) = \\ L_{\mathrm{BVP}}\left(x(\cdot),\alpha,T,p,\lambda_f(\cdot),\lambda_{\mathrm{bc}}\right) + L_{\mathrm{opt}}\left(x(\cdot),\mu_A,\lambda_{\mathrm{ph}},\eta_A\right) + L_{\mathrm{sc}}(\alpha,\mu_\alpha,\eta_\alpha). \tag{3.48}$$

The necessary conditions for an extremum of the total Lagrangian are then given by (i) the original differential equations and boundary conditions, (3.25)–(3.27), (3.40), (3.41), and (3.46), and (ii) the various adjoint equations, including (3.44) and (3.47), assembled in stages as constraints and variables are added, setting the sums of all resulting contributions equal to 0. Although we anticipate that λ_{ph} will equal 0 throughout the analysis, we keep λ_{ph} as an unknown and monitor its value during continuation.

As in the previous section, we may locate an extremum of L by several successive stages of continuation, in each stage omitting one or both of the adjoint conditions (3.44) and (3.47). In particular, by holding μ_α fixed and letting η_A vary freely, we may arrive at a solution with $\eta_A = 1$ in two stages of continuation: first, by continuing along a one-dimensional manifold with vanishing Lagrange multipliers, and next by branch-switching at a local extremum of μ_A to a secondary branch along which only the Lagrange multipliers vary and, in fact, do so proportionally to η_A. A final stage of continuation then proceeds from the point on this second manifold where $\eta_A = 1$, but this time with η_A fixed at 1 and μ_α free to vary. A sought extremum is obtained when $\eta_\alpha = 0$.

An example of such an analysis for the case when $\zeta = 0.05$, $\mu = 0.05$, $a = 0.05$, $b = -0.05$, and $\gamma = 0.5$ is shown in Fig. 3.4 (projected into the $(\alpha, 2\pi/T, \mu_A)$ space). Here, the full integro-differential boundary-value problem is discretized and analyzed using the COCO [74] package following the methodology discussed in [32] in terms of continuous, piecewise-polynomial approximants on a uniform partition of every solution segment into $N = 10$ mesh intervals, resulting in a large system of nonlinear algebraic equations. The successive continuation

approach then proceeds along the following stages:

- *Initial guess.* An initial solution guess for $x(\tau)$ near the first manifold is first constructed using direct simulation with $\alpha = 0.1$ and $T = 2\pi$, after which ϕ is adjusted such that the maximum of x_1 occurs at $\tau \approx 0$. We finally let $\mu_A = x_1(0)$ and $\mu_\alpha = \alpha$.

- *Stage 1: Continuation along manifold with vanishing Lagrange multipliers.* The delay α is held constant by fixing μ_α at its initial value. Continuation proceeds along the blue curve in Fig. 3.4, monitoring for branch points (coincident with extrema in μ_A up to discretization errors).

- *Stage 2: Continuation along manifold with varying Lagrange multipliers.* Branch off at the discovered branch point (labeled BP in Fig. 3.4) with μ_α still fixed, stopping when η_A reaches 1. During this continuation all primary variables $x(\cdot)$, ϕ, T, α stay constant. Only Lagrange multipliers change their values. This continuation does not change any coordinates in Fig. 3.4 (we remain at the point BP).

- *Stage 3: Continuation with varying μ_α.* Fix η_A at 1 and allow μ_α (and, consequently, α) to vary. Continue while monitoring η_α for zero crossings (red curve in Fig. 3.4). The point where $\eta_\alpha = 0$ along the red curve is labelled "Local Optimum". At this point all necessary conditions for a stationary point of L are satisfied, including $\eta_A = 1$ and $\eta_\alpha = 0$.

The end point of stage 3 corresponds to a critical point at $\alpha \approx 0.7824$, $\phi \approx 1.488$, and $T \approx 5.88$ (which Fig. 3.4 confirms to be a saddle point). We may compare the resulting optimal delay with the prediction from a first-order multiple-scales perturbation analysis for the weakly nonlinear (small μ), weakly damped (small ζ), and weakly forced (small γ) case, which predicts a maximal (with respect to T) response amplitude

$$\frac{\gamma}{2|\zeta + a\sin\alpha - b\cos\alpha|}, \tag{3.49}$$

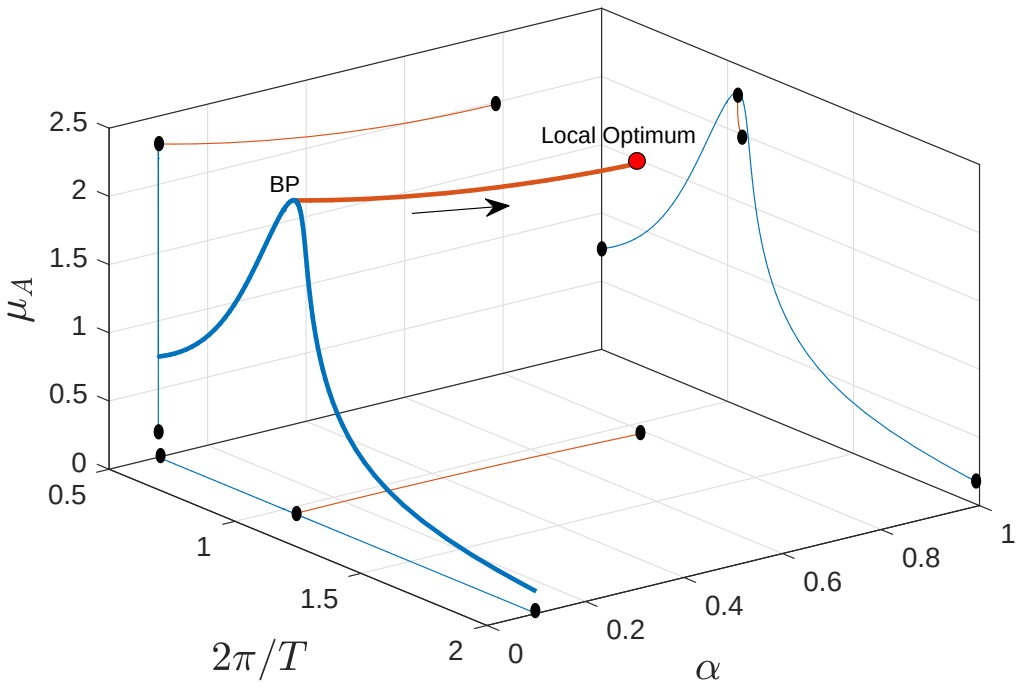

Figure 3.4: Optimization of the displacement amplitude along periodic orbits of the harmonically-excited Duffing oscillator with $\zeta = 0.05$, $\mu = 0.05$, $a = 0.05$, $b = -0.05$, and $\gamma = 0.5$ under variations in α and T. Three successive stages of continuation connect the sought saddle point with an initial solution guess with vanishing Lagrange multipliers. Stages 1 (blue) and 3 (red) described in the text are visible in the $(\alpha, 2\pi/T, \mu_A)$ space. In Stage 1, a peak in the displacement amplitude is approximately detected in close proximity to a branch point for the corresponding continuation problem. The second stage involves branch switching to a branch along which only the Lagrange multipliers vary (not visible). The red curve shows the final stage of continuation with fixed $\eta_A = 1$. The optimal delay and corresponding period obtained at the terminal point with $\eta_\alpha = 0$ equal 0.7824 and 5.88, respectively. At this point $\mu_A = 1.9852$.

(independent of μ, see the appendix A for intermediate steps and [100], [101]). The computed optimal delay $\alpha \approx 0.7824$ is in close agreement with the predicted optimal delay $\pi/4 \approx 0.7854$ obtained from (3.49) for the case that $b = -a$. The optimal displacement profile $x_1(\tau)$ and the components of $\lambda_f(\tau)$ are shown in Fig. 3.5. The top panel shows close agreement between the results obtained using continuation and the harmonic response obtained from the perturbation analysis, at the computed optimal values of α, T, and ϕ. Panel (b) of Fig. 3.5 shows the functional Lagrange multipliers λ_f, confirming that they are approximately smooth

in this example (since the objective does not depend on $\beta \in (0,1)$) but with $\lambda_{f,1}(1) \neq \lambda_{f,1}(0)$ and $\lambda_{f,2}(1) \approx \lambda_{f,2}(0)$ (since the objective functional and the phase constraint depend on $x(0)$ and $\lambda_{\text{ph}} \approx 0$).

Further comparisons between the results obtained using the successive continuation approach and those predicted by the perturbation analysis are shown in Figs. 3.6 and 3.7 for the case when the oscillator is only subjected to displacement feedback, i.e., when $b = 0$, with weak ($\mu = 0.05$) and strong ($\mu = 1$) nonlinearity, respectively. In each case, the perturbation analysis predicts a saddle in the response amplitude for $\alpha = \pi/2 \approx 1.5708$, while the computational results are $\alpha \approx 1.4712$ and 0.8712, respectively. For the case of weak nonlinearity depicted in Fig. 3.6, there is still close agreement between the optimal time histories for $x_1(\tau)$, while this is no longer true for the case of strong nonlinearity shown in Fig. 3.7. The frequency-response curves shown in the lower panels of Figs. 3.6 and 3.7 were obtained using numerical continuation for the computed and predicted critical values of α. In the case of the weak nonlinearity, we note a weak dependence on the location and magnitude of the peak on the value of the delay, while the differences are stark in the case of the strong nonlinearity. In the latter case, the optimal delay predicted by the perturbation analysis produces a peak amplitude more than 50% larger than that obtained using the numerical method.

3.2.3 Quasiperiodic Orbits

We proceed to consider the problem of optimizing a scalar-valued objective functional on a family of quasiperiodic solutions of (3.24), for which there exists an irrational *rotation number* ϱ and a smooth function $Z : \mathbb{S} \times \mathbb{S} \to \mathbb{R}^n$ (here, $\mathbb{S}$ denotes the unit circle) such that

$$z(t) = Z\left(\theta_1(t), \theta_2(t)\right), \dot{\theta}_1 = \varrho\Omega, \text{ and } \dot{\theta}_2 = \Omega \doteq 2\pi/T \tag{3.50}$$

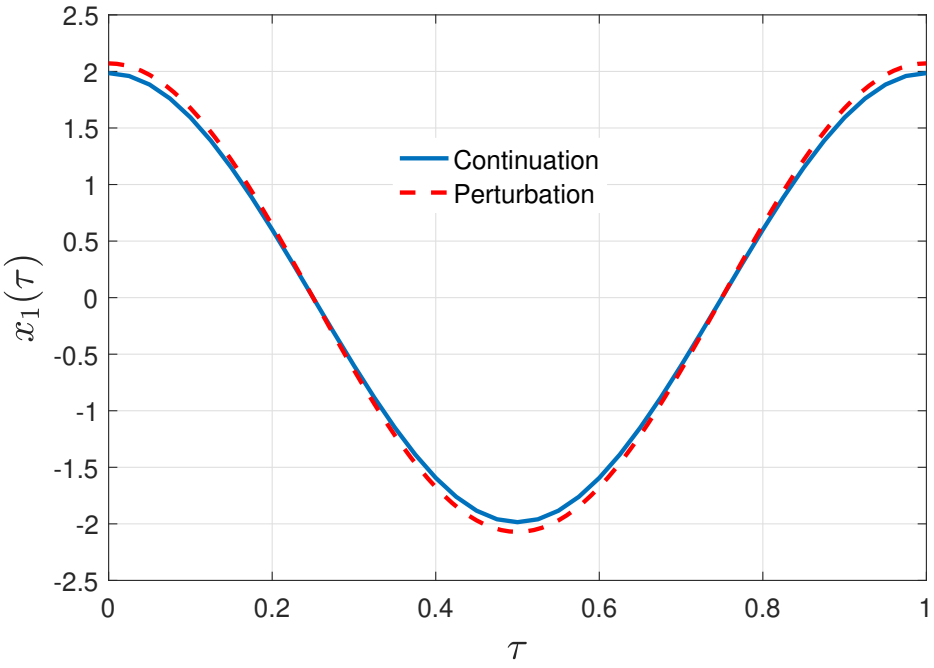

(a)

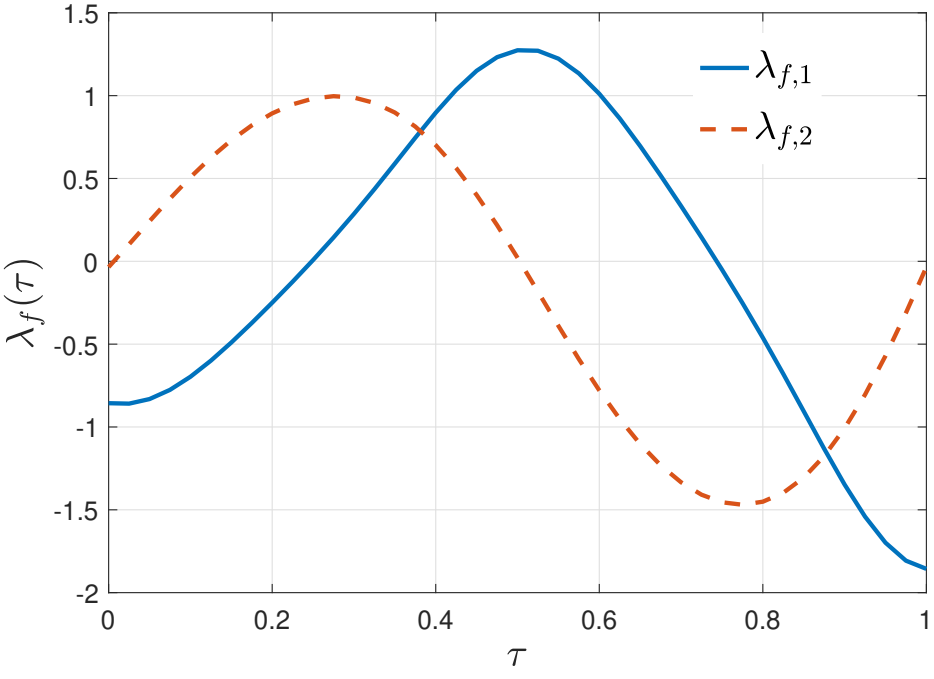

(b)

Figure 3.5: (a) $x_1(\tau)$ and (b) $\lambda_{f,1}(\tau)$ and $\lambda_{f,2}(\tau)$ at the terminal point of the third stage of continuation illustrated in Fig. 3.4. The upper panel shows a comparison between the numerical solutions obtained using continuation at the computed optimal value of α, with a first-order multiple-scales perturbation analysis at the predicted optimal value of α.

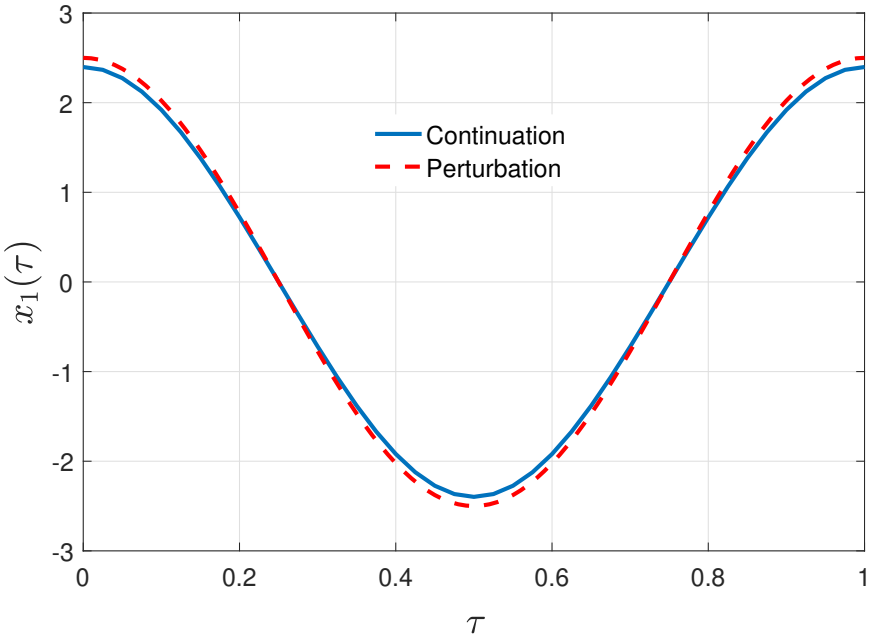

(a)

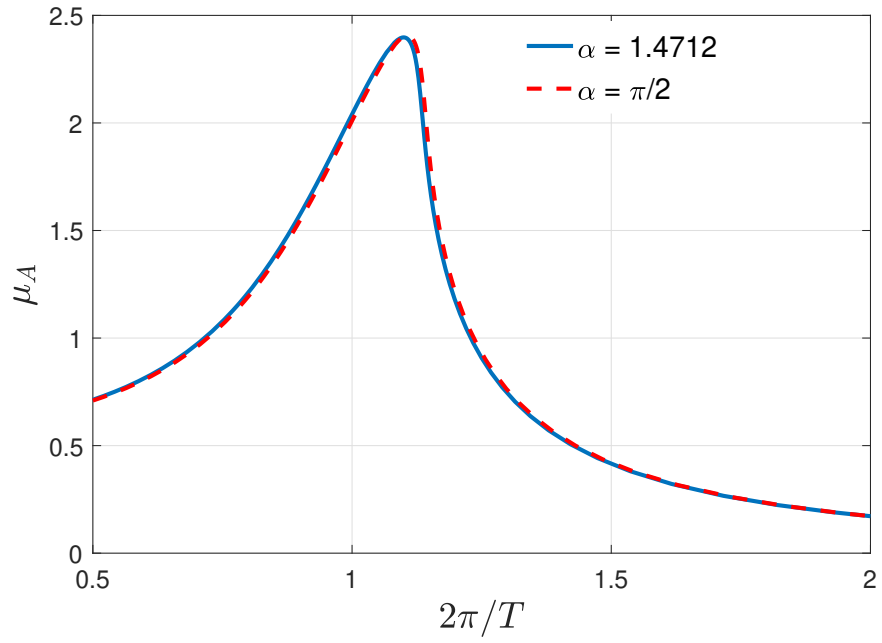

(b)

Figure 3.6: Optimization of the displacement amplitude along periodic orbits of the harmonically-excited, weakly-nonlinear Duffing oscillator with $\zeta = 0.05$, $\mu = 0.05$, $a = 0.05$, $b = 0$, and $\gamma = 0.5$ under variations in α and T. (a) Comparison of the displacement profile obtained from continuation at the computed optimal delay $\alpha \approx 1.4712$ and period $T \approx 5.7151$ with the results predicted by perturbation analysis. (b) Frequency-response diagrams for the computed and predicted critical delay values 1.4712 and $\pi/2$, respectively.

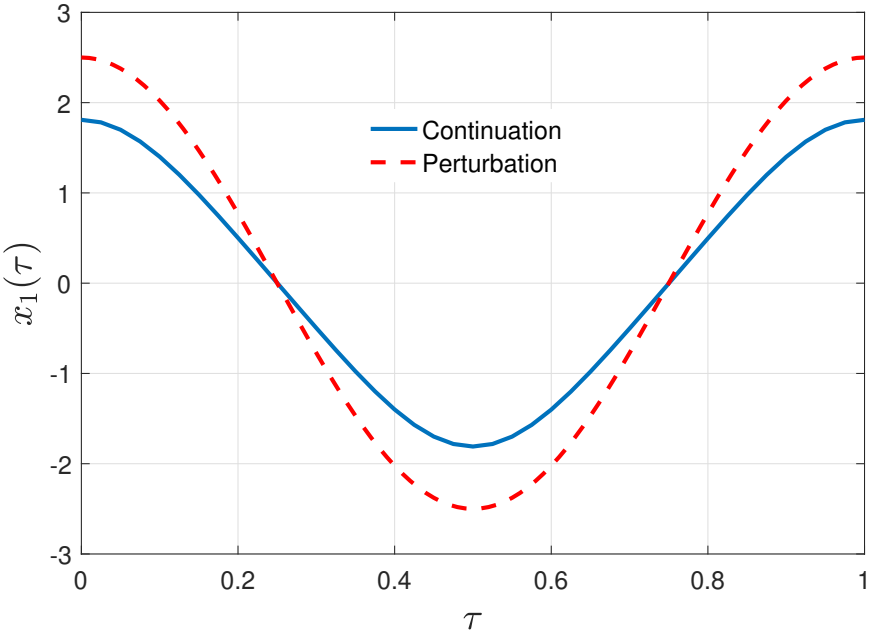

(a)

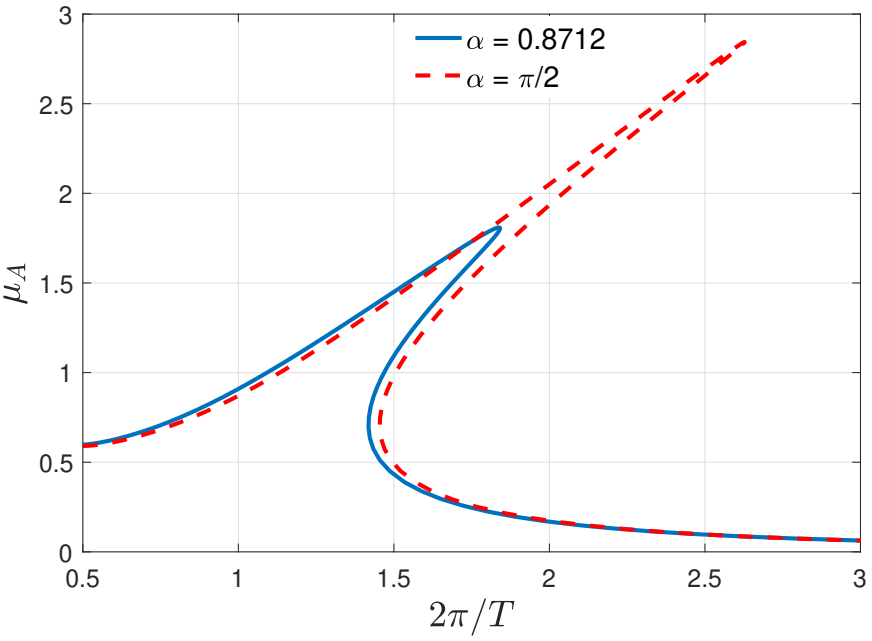

(b)

Figure 3.7: Optimization of the displacement amplitude along periodic orbits of the harmonically-excited, strongly nonlinear Duffing oscillator with $\zeta = 0.05$, $\mu = 1$, $a = 0.05$, $b = 0$, and $\gamma = 0.5$ under variations in α and T. (a) Comparison of the displacement profile obtained from continuation at the computed optimal delay $\alpha \approx 0.8712$ and period $T \approx 3.4192$ with the results predicted by perturbation analysis. (b) Frequency-response diagrams for the computed and predicted critical delay values 0.8712 and $\pi/2$, respectively.

in terms of the period T of the vector field f in its first argument. Let subscripts $_{\theta_1}$ and $_{\theta_2}$ denote partial derivatives with respect to the corresponding arguments. Substitution into the governing equation then yields the partial differential equation (PDE)

$$\varrho\Omega Z_{\theta_1} + \Omega Z_{\theta_2} = f\left(t, Z, Z\left(\theta_1 - \varrho\Omega\alpha, \theta_2 - \Omega\alpha\right), p\right) \tag{3.51}$$

on the two-dimensional torus $\mathbb{S} \times \mathbb{S}$.

We decompose this PDE along its characteristics. To this end, consider the continuous function $V : \mathbb{S} \times [0,1] \to \mathbb{R}^n$ given by

$$V(\varphi, \tau) \doteq Z(\varphi + 2\pi\varrho\tau, 2\pi\tau), \tag{3.52}$$

such that $\tau = t/T$, $\theta_1(0) = \varphi$, and without loss of generality $\theta_2(0) = 0$. Shifting and wrapping of arguments between and along characteristics will occur several times below. To simplify notation, suppose that $T > \alpha$ and introduce the wrapping operation W for a function V on $\mathbb{S} \times [0,1]$ as

$$\left[W_a^j V\right](\varphi, \tau) = V(\varphi - 2\pi j\rho, \tau - a + j),\ j = -1, 0, 1 \tag{3.53}$$

for $\tau - a + j \in [0,1]$ and all $\varphi \in \mathbb{S}$. It follows by periodicity that

$$Z(\varphi + 2\pi\varrho(\tau - a), 2\pi(\tau - a)) = \left[W_a^j V\right](\varphi, \tau) \tag{3.54}$$

for $\tau - a + j \in [0,1]$ and all $\varphi \in \mathbb{S}$. Differentiation and use of (3.51) then implies that

$$V_\tau = Tf\left(T\tau, V, W^1_{\alpha/T} V, p\right),\ (\varphi, \tau) \in \mathbb{S} \times (0, \alpha/T), \tag{3.55}$$

$$V_\tau = Tf\left(T\tau, V, W^0_{\alpha/T} V, p\right),\ (\varphi, \tau) \in \mathbb{S} \times (\alpha/T, 1), \tag{3.56}$$

along with the boundary conditions

$$V(\varphi, 1) - V(\varphi + 2\pi\varrho, 0) = 0,\ \varphi \in \mathbb{S}. \tag{3.57}$$

Equations (3.55)–(3.57) are a family of coupled DDE BVPs in time τ, parametrized by the continuous periodic angle φ. A family of orbit segments $\mathbb{S} \times [0, 1] \ni (\varphi, \tau) \mapsto V(\varphi, \tau) \in \mathbb{R}^n$ solving this family of BVPs then spans the sought quasiperiodic invariant torus. Such a family is unique only up to a shift of its argument $\varphi \in \mathbb{S}$. We isolate a locally unique solution by introducing the integral phase condition

$$\int_0^{2\pi} \left(V(\varphi, 0) - V^*(\varphi)\right)^{\mathrm{T}} V_\varphi^*(\varphi)\, \mathrm{d}\varphi = 0 \tag{3.58}$$

in terms of a given continuously-differentiable reference function $V^* : \mathbb{S} \to \mathbb{R}^n$ that is either fixed throughout the analysis or updated as appropriate. For fixed values of the problem delay α, excitation period T, and problem parameters p, the resultant integro-differential BVP (3.55)–(3.58) defining the quasiperiodic response is over-determined (recall that the rotation number ϱ is fixed) such that one has to leave at least one system parameter free to vary to obtain isolated solutions. For example, for fixed α, we thus expect to obtain a one-dimensional manifold of quasiperiodic invariant tori under simultaneous variations in T and a single element of p.

We now apply the construction of the Lagrangian and adjoint equations to this family of DDE BVPs to formulate optimization problems with constraints of the form (3.55)–(3.58), following the procedure from Section 3.2.1. We assume that neither the objective functional nor any additional constraints depend on V evaluated for τ on the interior of the interval $[0, 1]$, and that they only depend on V on the boundaries $\tau = 0$ and $\tau = 1$ through integrals over φ. In this case, the Lagrange multipliers λ_f for the DDE constraint (3.55) will be continuous on the domain $\mathbb{S} \times [0, 1]$ (including periodicity in their first argument φ). The partial Lagrangian

for the constraints (3.55)–(3.58) is then given by

$$
\begin{aligned}
&L_{\mathrm{BVP}}(V(\cdot,\cdot),\alpha,T,p,\lambda_f(\cdot,\cdot),\lambda_{\mathrm{rot}}(\cdot),\lambda_{\mathrm{ph}}) = \\
&\int_{\varphi}\int_{0}^{\alpha/T} \mathrm{d}\tau \left[\lambda_f^{\mathrm{T}}\left(V_\tau - T f_1\right)\right] + \int_{\varphi}\int_{\alpha/T}^{1-\alpha/T} \mathrm{d}\tau \left[\lambda_f^{\mathrm{T}}\left(V_\tau - T f_0\right)\right] + \int_{\varphi}\int_{1-\alpha/T}^{1} \mathrm{d}\tau \left[\lambda_f^{\mathrm{T}}\left(V_\tau - T f_0\right)\right] \\
&+ \int_{\varphi} \lambda_{\mathrm{rot}}^{\mathrm{T}}(\varphi)\left(V\left(\varphi,1\right) - V\left(\varphi + 2\pi\varrho, 0\right)\right) + \lambda_{\mathrm{ph}} \int_{\varphi} \left(V(\varphi,0) - V^*(\varphi)\right)^{\mathrm{T}} V_\varphi^*(\varphi),
\end{aligned}
\tag{3.59}
$$

where we abbreviate $\int_\varphi = \int_0^{2\pi} \mathrm{d}\phi$ and, similarly to Section 3.2.1, let the notation $f_j(\varphi,\tau) = f(T\tau, V, W^j_{\alpha/T}V, p)$. The vector-valued functions $\lambda_f(\varphi,\tau)$ and $\lambda_{\mathrm{rot}}(\varphi)$, and the scalar λ_{ph} are the Lagrange multipliers associated with the imposition of the differential equations (3.55) and (3.56), boundary conditions (3.57), and the integral phase condition (3.58), respectively. Each integrand is assumed to be continuously differentiable on the corresponding interval, and λ_f and λ_{rot} are assumed to be continuous and, hence, periodic in φ for all τ. It is again straightforward to show that λ_f must be continuous in τ on $\tau = \alpha/T$ and $\tau = 1 - \alpha/T$ at a stationary point of the total Lagrangian. In this case, λ_f is continuously differentiable in τ everywhere except at $\tau = 1 - \alpha/T$, where a slope discontinuity is anticipated from the boundary conditions (3.57).

Analogously to Section 3.2.1, consider the notation

$$
f_{j,k}(\varphi,\tau) = \partial_k f(T\tau, V(\varphi,\tau), [W^j_{\alpha/T}V](\varphi,\tau), p), \tag{3.60}
$$

$$
f_{j,q}(\varphi,\tau) = \frac{\mathrm{d}}{\mathrm{d}\,q} f\left(T\tau, V(\varphi,\tau), [W^j_{\alpha/T}V](\varphi,\tau), p\right), \tag{3.61}
$$

for $j = 0, 1$ and $q = \alpha, T$. Then, the contributions to the necessary adjoint conditions for a stationary point of the total Lagrangian are given by

$$
-\lambda_{f,\tau}^{\mathrm{T}} - T\lambda_f^{\mathrm{T}} f_{1,2} - T\left(W^0_{-\alpha/T}\,\lambda_f\right)^{\mathrm{T}} W^0_{-\alpha/T} f_{0,3} \tag{3.62}
$$

for variations with respect to $V(\varphi,\tau)$ on $(\varphi,\tau)\in\mathbb{S}\times(0,\alpha/T)$;

$$-\lambda_{f,\tau}^{\mathrm{T}}-T\lambda_{f}^{\mathrm{T}}f_{0,2}-T\left(W_{-\alpha/T}^{0}\,\lambda_{f}\right)^{\mathrm{T}}W_{-\alpha/T}^{0}f_{0,3} \tag{3.63}$$

for variations with respect to $V(\varphi,\tau)$ on $(\varphi,\tau)\in\mathbb{S}\times(\alpha/T,1-\alpha/T)$;

$$-\lambda_{f,\tau}^{\mathrm{T}}-T\lambda_{f}^{\mathrm{T}}f_{0,2}-T\left(W_{-\alpha/T}^{-1}\,\lambda_{f}\right)^{\mathrm{T}}W_{-\alpha/T}^{-1}f_{1,3} \tag{3.64}$$

for variations with respect to $V(\varphi,\tau)$ on $(\varphi,\tau)\in\mathbb{S}\times(1-\alpha/T,1)$;

$$\lambda_{f}^{\mathrm{T}}\left(\varphi,0\right)+\lambda_{\mathrm{rot}}^{\mathrm{T}}\left(\varphi-2\pi\varrho\right)+\lambda_{\mathrm{ph}}V_{\varphi}^{*\top}(\varphi) \tag{3.65}$$

for variations with respect to $V(\varphi,0)$ on $\varphi\in\mathbb{S}$;

$$\lambda_{f}^{\mathrm{T}}\left(\varphi,1\right)+\lambda_{\mathrm{rot}}^{\mathrm{T}}\left(\varphi\right) \tag{3.66}$$

for variations with respect to $V(\varphi,1)$ on $\varphi\in\mathbb{S}$;

$$-\int_{\varphi}\int_{0}^{\alpha/T}\mathrm{d}\tau\left[\lambda_{f}^{\mathrm{T}}Tf_{1,\alpha}\right]-\int_{\varphi}\int_{\alpha/T}^{1}\mathrm{d}\tau\left[\lambda_{f}^{\mathrm{T}}Tf_{0,\alpha}\right] \tag{3.67}$$

for variations with respect to α;

$$-\int_{\varphi}\int_{0}^{\alpha/T}\mathrm{d}\tau\left[\lambda_{f}^{\mathrm{T}}\left(Tf_{1,T}+f_{1}\right)\right]-\int_{\varphi}\int_{\alpha/T}^{1}\mathrm{d}\tau\left[\lambda_{f}^{\mathrm{T}}\left(Tf_{0,T}+f_{0}\right)\right] \tag{3.68}$$

for variations with respect to T; and

$$-\int_{\varphi}\int_{0}^{\alpha/T}\mathrm{d}\tau\left[\lambda_{f}^{\mathrm{T}}Tf_{1,4}\right]-\int_{\varphi}\int_{\alpha/T}^{1}\mathrm{d}\tau\left[\lambda_{f}^{\mathrm{T}}Tf_{0,4}\right] \tag{3.69}$$

for variations with respect to p.

3.2.4 A Hopf unfolding with delay and forcing

Consider, for example, the problem of finding a local maximum in ω along a family of quasiperiodic invariant tori of the vector field

$$f\left(t,u,v,p\right)=\left(\begin{array}{c}-\omega u_2+v_1\left(1+r\left(\cos 2\pi t/T-1\right)\right)\\ \omega u_1+v_2\left(1+r\left(\cos 2\pi t/T-1\right)\right)\end{array}\right), \tag{3.70}$$

where $r=\sqrt{u_1^2+u_2^2}$, $\alpha=1$, and $p=\omega$. Notably, an example in the tutorial for the COCO trajectory segment toolbox [74] shows that no such local maximum exists when $\alpha=0$, since then $\omega T=2\pi\varrho$. In the present case, we consider the optimization problem

$$\text{maximize}\quad \mu_\omega=\omega \tag{3.71}$$

subject to the constraints (3.55)–(3.58) (the coupled DDEs with boundary conditions and phase condition, depending on φ). The problem Lagrangian is then given by

$$\begin{aligned}&L(V(\cdot,\cdot),T,p,\mu_\omega,\lambda_f(\cdot,\cdot),\lambda_{\text{rot}}(\cdot),\lambda_{\text{ph}},\eta_\omega)\\&\quad=\mu_\omega+\eta_\omega(\omega-\mu_\omega)+L_{\text{BVP}}\left(V(\cdot,\cdot),1,T,p,\lambda_f(\cdot,\cdot),\lambda_{\text{rot}}(\cdot),\lambda_{\text{ph}}\right),\end{aligned} \tag{3.72}$$

where L_{BVP} is given in (3.59) and η_ω is the additional Lagrange multiplier. The necessary conditions for an extremum of the total Lagrangian are then given by (i) the original differential equations and boundary conditions (3.55)–(3.58); (ii) the adjoint conditions (excluding (3.67)) obtained by appending η_ω to the variation with respect to p (3.69) and setting all the resulting contributions equal to 0; and (iii) the condition that $\eta_\omega=1$.

As in previous examples, we immediately note that λ_{ph} must equal 0 at a stationary point of the Lagrangian, since the objective function is clearly independent of the particular choice

of family $(\varphi, \tau) \mapsto V(\varphi, \tau)$ selected by the phase condition. The adjoint boundary conditions (3.65) and (3.66) then imply that

$$\lambda_f^{\mathrm{T}}(\varphi, 1) - \lambda_f^{\mathrm{T}}(\varphi + 2\pi\varrho, 0) = 0. \tag{3.73}$$

Moreover, direct computation using (3.70) and the boundary condition (3.57) shows that

$$f_{0,3}(\varphi, 1) - f_{1,3}(\varphi + 2\pi\varrho, 0) = 0. \tag{3.74}$$

It follows from (3.63) and (3.64) that

$$\lambda_{f,\tau}^{\mathrm{T}}(\varphi, 1 - 1/T)_+ - \lambda_{f,\tau}^{\mathrm{T}}(\varphi, 1 - 1/T)_- = 0, \tag{3.75}$$

i.e., that λ_f is continuously differentiable in τ on the entire interval $[0, 1]$.

We proceed to locate an extremum by applying the successive continuation technique to the set of equations obtained by omitting the trivial adjoint condition that $\eta_\omega = 1$. To this end, we approximate $V(\varphi, \tau)$, $\lambda_f(\varphi, \tau)$, and $\lambda_{\mathrm{rot}}(\varphi)$ by truncated Fourier series in φ with τ-dependent Fourier coefficient functions, as appropriate, approximated by continuous piecewise-polynomial interpolants on the interval $[0, 1]$. Although we anticipate that λ_{ph} will equal 0 throughout continuation, we keep λ_{ph} as an unknown and monitor its value during continuation. We first continue along a one-dimensional manifold along which the Lagrange multipliers always equal 0, and then branch switch at a local maximum of μ_ω to a secondary branch along which the family V remains unchanged, while the Lagrange multipliers vary linearly in η_ω. The solution to the necessary conditions for a local stationary point is then obtained once $\eta_\omega = 1$ along the secondary branch.

The results of such an analysis using COCO is shown in Figs. 3.8-3.10 for the case that $\varrho \approx 0.6618$. Here, dependence on φ is approximated using a Fourier series truncated at the fifth harmonic corresponding to 11 trajectory segments on the torus based at $\varphi = (i - 1)/11$,

$i = 1, \ldots, 11$. Each τ dependent Fourier coefficient is discretized using polynomials of degree 4 on a uniform mesh with 10 intervals. The one-dimensional family of quasiperiodic orbits in Fig. 3.8 along the first manifold with vanishing Lagrange multipliers indicates the existence of a local maximum in $\mu_\omega \approx 0.43685$ for $T \approx 5.3153$. Branch switching from the nearby branch point (as before, exact coincidence is lost due to discretization) and continuing until $\eta_\omega = 1$ yields the approximate torus and the corresponding Lagrange multipliers λ_{rot}, λ_f shown in Fig. 3.9 and Fig. 3.10 respectively.

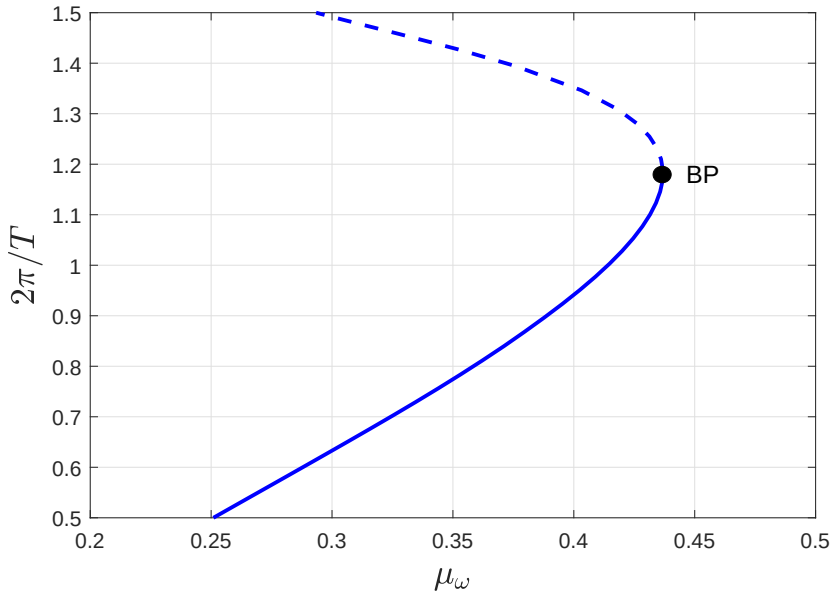

Figure 3.8: One-dimensional manifold obtained from the first stage of continuation along a family of approximate quasiperiodic invariant tori with vanishing Lagrange multipliers for the case that $\varrho \approx 0.6618$. The local maximum $\mu_\omega \approx 0.43685$ when $T \approx 5.3153$ approximately coincides with a branch point (BP). Solid and dashed lines denote dynamically stable and unstable tori, respectively.

As an aside, direct numerical simulation using initial conditions predicted by the continuation analysis suggest that quasiperiodic tori found on the lower half of the one-dimensional family shown in Fig. 3.8 are stable to sufficiently small perturbations, while the tori found on the upper half are unstable, with a critical loss of stability coincident with the peak value of μ_ω.

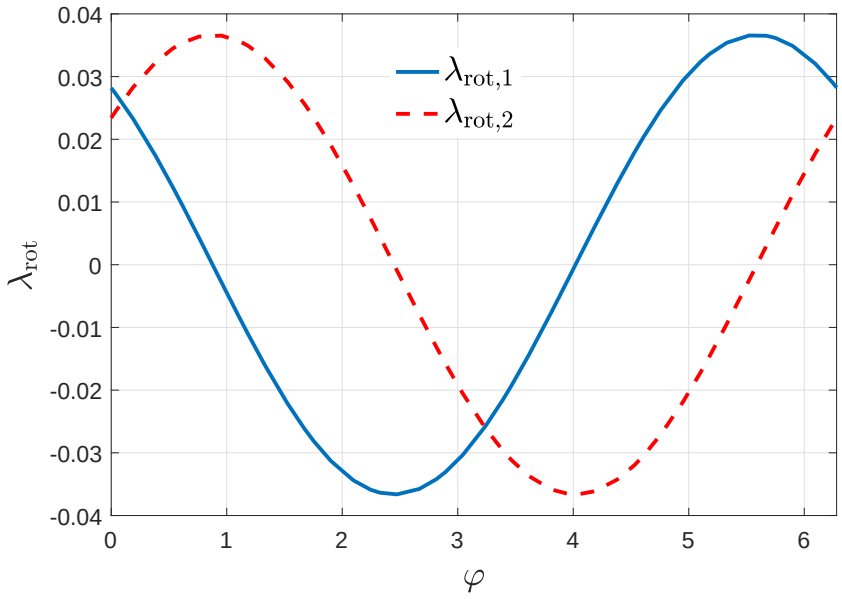

Figure 3.9: Lagrange multiplier λ_{rot} at the optimum point for the quasiperiodic invariant torus optimization problem.

3.3 Conclusions

In this chapter, we generalized a technique of successive parameter continuation to also enable solving constrained optimal design problems with delays. In the next chapter, motivated by the problem construction paradigm discussed in Chapter 2, we propose a toolbox template that can handle a broad class of delay-coupled, multi-segment boundary-value problems.

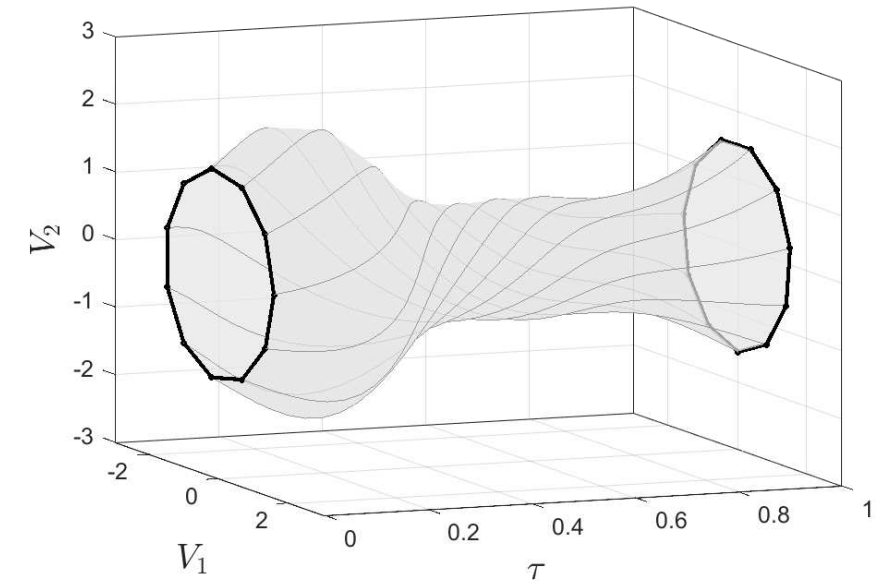

(a)

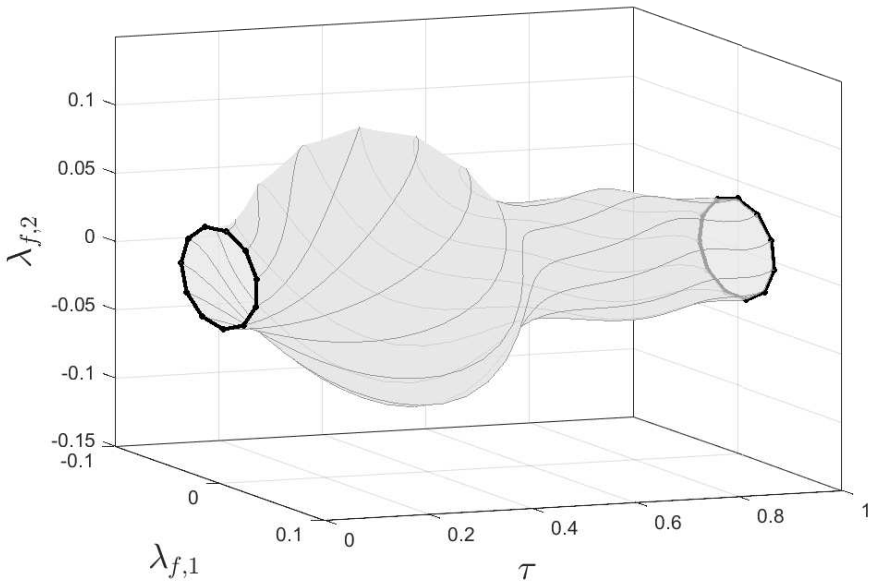

(b)

Figure 3.10: Optimal quasiperiodic invariant torus (a) and corresponding representation of λ_f (b) obtained at the terminal point ($\eta_\omega = 1$) of the second stage of continuation with $\varrho \approx 0.6618$. Solid grey curves denote the discretization of $V(\varphi, \tau)$ and $\lambda_f(\varphi, \tau)$ using trajectory segments based at $\varphi = (i-1)/11$, for $i = 1, \ldots, 11$.

Chapter 4

A TOOLBOX FOR DELAY-COUPLED BOUNDARY-VALUE PROBLEMS

The examples on data assimilation and phase response curves in Sections 2.3 and 2.4 demonstrated how advanced examples of augmented continuation problems may be constructed through repeated calls to the core COCO constructors. Motivated by these examples and the generalization of the continuation-based optimization technique to delay-coupled problems in Chapter 3, this chapter[1] develops a general COCO-compatible toolbox template for a large family of delay-coupled, multi-segment boundary value problems, including those describing periodic orbits, quasiperiodic orbits, connecting orbits, initial-value problems, and optimal control problems. A suite of numerical examples illustrate the generality provided by the proposed toolbox for a variety of boundary-value problems with delay.

4.1 Toolbox construction

4.1.1 Composite construction

A COCO constructor of the form (2.67) with $\mathbb{K}_u^{\mathrm{o}} = \emptyset$, $\mathbb{K}_\lambda^{\mathrm{o}} = \emptyset$, $\mathbb{K}_\Lambda^{\mathrm{o}} = \emptyset$, and $\mathbb{K}_v^{\mathrm{o}} = \emptyset$ and with its remaining arguments defined according to an abstract paradigm is called a *toolbox constructor*. We often use this terminology also to describe constructors whose index sets $\mathbb{K}_u^{\mathrm{o}}$, $\mathbb{K}_\lambda^{\mathrm{o}}$, $\mathbb{K}_\Lambda^{\mathrm{o}}$, and $\mathbb{K}_v^{\mathrm{o}}$ are associated with a preceding application of a toolbox constructor

[1] The content of this chapter is reproduced from Ahsan, Dankowicz, Li and Sieber, "Methods of Continuation and their Implementation in the COCO Software Platform with Application to Delay Differential Equations," *Nonlinear Dynamics*, **107**(4), 3181–3243, 2022 [2], and included here with permission from the publisher.

and whose remaining arguments are defined by the same abstract paradigm. A collection of toolbox constructors is called a (COCO-compatible) toolbox. A paradigm for toolbox construction using the COCO platform is described in Part II of textbook [32].

As an example, a toolbox constructor may be designed to construct the zero problem and monitor functions associated with analyzing equilibria of an arbitrary autonomous vector field in terms of its problem parameters. In this case, the functions $\mathfrak{phi}$ and $\mathfrak{psi}$ may be defined to include calls to user-defined encodings of the vector field and its derivatives without assuming a particular state space dimension or a particular number of problem parameters. In the COCO-compatible toolbox `'ep'` (see EP-Tutorial.pdf in [74]), for example, the toolbox constructors `ode_isol2ep` and `ode_ep2ep` accomplish this task using data provided by the user and data stored from a previous analysis, respectively.

For constrained optimization along manifolds of equilibria, it is necessary to construct the contributions to the adjoint conditions corresponding to the equilibrium constraints. In the `'ep'` toolbox, this is accomplished with the `adjt_isol2ep` and `adjt_ep2ep` toolbox constructors, provided that the equilibrium constraint was constructed using `ode_isol2ep` and `ode_ep2ep`, respectively. Since the vector field, the state space dimension, and the number of problem parameters were provided already to the latter constructors, the adjoint constructors `adjt_isol2ep` and `adjt_ep2ep` require no further user data. This observation simplifies the calling syntax to these operators.

These same principles apply also to the constructors associated with the COCO-compatible `'coll'` (see COLL-Tutorial.pdf in [74]) and `'po'` (see PO-Tutorial.pdf in [74]) toolboxes that are included with the COCO release. For example, given a vector field, a sequence of time instants, a corresponding array of state-space vectors, and an array of numerical values for the problem parameters, the toolbox constructor `ode_isol2coll` constructs a discretization of the trajectory problem

$$\dot{x} = f(t, x, p),\ t \in [T_0, T_0 + T] \tag{4.1}$$

in terms of the unknown values of $x(t)$ for a finite set of values of $t \in [T_0, T_0 + T]$, un-

known values of p, and unknown initial time T_0 and duration T. Given a preceding call to `ode_isol2coll`, the corresponding adjoint contributions may be appended to the augmented continuation problem using the `adjt_isol2coll` toolbox constructor. As before, no additional information about the problem is required in this call. Additional constructors associated with the `coll` toolbox encode multi-segment boundary-value problems and the corresponding contributions to the adjoint necessary conditions. The `'po'` toolbox encodes the special case of periodic boundary conditions, also for piecewise-defined vector fields and hybrid dynamical systems, according to the same fundamental paradigm.

By definition, we arrive at a toolbox constructor by recognizing a universality among a class of individual problems and by encoding an abstract representation of this universality in suitable constructors. We see elements of such universality represented in the examples in Sections 2.3 and 2.4 and proceed in the remainder of this section to derive the mathematical formalism of a corresponding toolbox.

4.1.2 Delay graphs

The data assimilation example in Section 2.3 may be abstractly represented according to a graph-theoretic framework [102]. Specifically, let the term *segment* here refer to a variable $x : [-\hat{\alpha}, T] \to \mathbb{R}^n$ in terms of a *maximal past* $\hat{\alpha}$ and *duration* T such that $\dot{x} = f(x(t), x(t-\alpha))$ for $t \in (0, T)$ in terms of a vector field f and *delay* $\alpha \leq \hat{\alpha}$. For a collection of M segments, we use a subscript $k = 1, \ldots, M$ to identify individual segments. In the example in Section 2.3, $x_k(T_k\alpha) = (u^{(k)}(\alpha), p^{(k)}(\alpha))$ with $\alpha_k = 0$ for $k < I$ and $\alpha_k = \alpha$ for $k \geq I$.

In this section, we say that the i-th and j-th segments are *coupled*, in that order, if there exists a coupling matrix $B_{i,j}$ such that

$$x_i(s) = B_{i,j} x_j(T_j + s) \text{ for all } s \in [-\hat{\alpha}_i, 0] \tag{4.2}$$

and, in particular, that $x_i(0) = B_{i,j} x_j(T_j)$. Clearly, this is possible only if $-\hat{\alpha}_j \leq T_j - \hat{\alpha}_i$. We

say that the j-th segment is a *predecessor* of the i-th segment. For a consistent definition, we require that there be at most one predecessor for each segment, but allow a segment to be a predecessor of multiple nodes. We naturally arrive at a directed graph with nodes representing segments and directed edges representing predecessor coupling. For a segment that is not a predecessor of any other segment, we may assume without loss of generality that $\hat{\alpha}_i = \alpha_i$. Similarly, for a segment that is not preceded by another segment, we may assume without loss of generality that $\hat{\alpha}_i = 0$. It is not the case, however, that $\hat{\alpha}_j$ may be assumed to equal 0 for a segment with $\alpha_j = 0$, since the former is involved in coupling conditions of the form (4.2) with other segments.

The example in Section 2.3 may be described in terms of the directed graph in Fig. 4.1, in which the k-th segment is the unique predecessor to the $k+1$-th segment with coupling matrix I_n. By definition

$$\sum_{k=1}^{I-1} T_k = \alpha, \sum_{k=1}^{M} T_k = T. \tag{4.3}$$

From this graph, we see that $x_k(s) = x_{k-1}(T_{k-1} + s)$ for all $s \in [-\hat{\alpha}_k, 0]$. Provided that $T_{k-1} - \alpha_k \geq 0$, we may evaluate the delayed term $x_k(t - \alpha_k)$ for all $t \in (0, T_k)$ without further reference to the graph. If, instead, $T_{k-1} - \alpha_k < 0$, we may use the fact that $x_{k-1}(s) = x_{k-2}(T_{k-2} + s)$ for all $s \in [-\hat{\alpha}_{k-1}, 0]$ to obtain $x_k(s) = x_{k-2}(T_{k-2} + T_{k-1} + s)$ for $s \in [-\hat{\alpha}_k, -T_{k-1}]$. Provided that $T_{k-2} + T_{k-1} - \alpha_k \geq 0$, we may evaluate the delayed term $x_k(t - \alpha_k)$ for all $t \in (0, T_k)$ without further reference to the graph. If not, then we proceed iteratively until the sum $\sum_{l=1}^{L} T_{k-l}$ equals or exceeds α_k for some $L < k$.

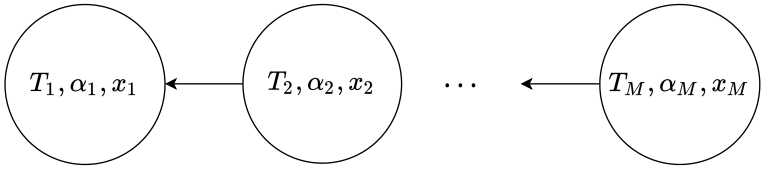

Figure 4.1: Directed graph representation of the data assimilation problem with M segments. In the special case in the text, $M = 5$, the segment lengths are $T_1 = T_3 = T_4 = 0.2T, T_2 = 0.3T, T_5 = 0.1T$ and the delays equal $\alpha_1 = \alpha_2 = 0$, $\alpha_3 = \alpha_4 = \alpha_5 = \alpha := 0.5T$.

As an example, suppose that $M = 5$, $\alpha = 0.5T$, $T_1 = T_3 = T_4 = 0.2T$, $T_2 = 0.3T$, and

$T_5 = 0.1T$. The algorithm in the previous paragraph shows that

$$x_5(s) = x_2(T_2 + T_3 + T_4 + s),\ s \in [-\alpha_5, T_5 - \alpha_5], \tag{4.4}$$

$$x_4(s) = x_2(T_2 + T_3 + s),\ s \in [-\alpha_4, T_4 - \alpha_4], \tag{4.5}$$

$$x_3(s) = x_1(T_1 + T_2 + s),\ s \in [-\alpha_3, T_3 - \alpha_3], \tag{4.6}$$

and, consequently,

$$x_5(t - \alpha_5) = x_2(T_2 + T_3 + T_4 - \alpha_5 + t),\ t \in [0, T_5], \tag{4.7}$$

$$x_4(t - \alpha_4) = x_2(T_2 + T_3 - \alpha_4 + t),\ t \in [0, T_4], \tag{4.8}$$

$$x_3(t - \alpha_3) = x_1(T_1 + T_2 - \alpha_3 + t),\ t \in [0, T_3]. \tag{4.9}$$

It follows, for example, that

$$u^{(5)}\left(t - \frac{\alpha_5}{T_5}\right) = u^{(2)}\left(\frac{T_2 + T_3 + T_4 - \alpha_5}{T_2} + \frac{T_5}{T_2}t\right),\ t \in [0, 1] \tag{4.10}$$

in agreement with the general expression in (2.89).

From the general form of the adjoint contributions in Section 2.3, it may be correctly surmised that the directed graph in Fig. 4.1 contains all the information required to construct these expressions for any number of segments M, time delay α, and interval durations T_k. This is analogous to the possible application of the adjoint constructors `adjt_isol2coll` and `adjt_isol2po` in the `'coll'` and `'ep'` toolboxes, respectively, without requiring additional information than that provided to `ode_isol2coll` and `ode_isol2po`, respectively.

We recognize in this construction of constraints and adjoint contributions a universal paradigm for multi-segment boundary-value problems with discrete delays. In the next section, we formulate an abstract toolbox template that is sufficiently flexible to handle a broad class of such problems. Several examples illustrate the reduction of the abstract framework to problems involving periodic and quasiperiodic orbits.

4.2 A toolbox template for delay-coupled differential equations

4.2.1 An abstract zero problem

Consider a collection of non-autonomous vector fields $f_i : \mathbb{R} \times \mathbb{R}^n \times \mathbb{R}^n \times \mathbb{R}^q \to \mathbb{R}^n$, for $i = 1, \ldots, M$, governing the time histories of M *differential state variables* $x_i \in C^1([0,1], \mathbb{R}^n)$ according to the *differential constraints*

$$x_i'(\tau) = T_i f_i\left(T_{0,i} + T_i\tau, x_i(\tau), y_i(\tau), p\right), \ \tau \in (0,1), \tag{4.11}$$

in terms of the individual *initial times* $T_{0,i} \in \mathbb{R}$, individual *durations* $T_i \in \mathbb{R}$, and shared *problem parameters* $p \in \mathbb{R}^q$. For a subset of indices i, we assume the imposition of *boundary conditions*

$$x_i(0) = \sum_{j=1}^{M} B_{i,j}(p) \cdot x_j(1) \tag{4.12}$$

in terms of (possibly zero) *coupling matrices* $B_{i,j}(p)$.

The collection of *algebraic state variables* $y_i \in C^0([0,1], \mathbb{R}^n)$ provide exogenous excitation to the system dynamics (4.11). For indices i such that f_i depends explicitly on y_i, we obtain a closed abstract model by specifying C_i *coupling conditions* on a partition of $[0,1]$ into subintervals $[\gamma_{\mathrm{b},i,k}, \gamma_{\mathrm{e},i,k}]$ with

$$0 = \gamma_{\mathrm{b},i,1} \leq \gamma_{\mathrm{e},i,1} = \gamma_{\mathrm{b},i,2} \leq \cdots \leq \gamma_{\mathrm{e},i,C_i-1} = \gamma_{\mathrm{b},i,C_i} \leq \gamma_{\mathrm{e},i,C_i} = 1 \tag{4.13}$$

according to the expressions

$$y_i(\tau) = \sum_{s=1}^{S_{i,k}} A_{i,k,s}(p) \cdot x_{j_{i,k,s}}\left(\frac{T_i}{T_{j_{i,k}}}\left(\tau - \Delta_{i,k}\right)\right), \ \tau \in [\gamma_{\mathrm{b},i,k}, \gamma_{\mathrm{e},i,k}] \tag{4.14}$$

for $k = 1, \ldots, C_i$ and $j_{i,k}, j_{i,k,s} \in \{1, \ldots, M\}$, and where

$$0 \leq \xi_{\mathrm{b},i,k} := \frac{T_i}{T_{j_{i,k}}} \left(\gamma_{\mathrm{b},i,k} - \Delta_{i,k}\right) \leq \xi_{\mathrm{e},i,k} := \frac{T_i}{T_{j_{i,k}}} \left(\gamma_{\mathrm{e},i,k} - \Delta_{i,k}\right) \leq 1 \tag{4.15}$$

for all i and k. In particular, the *coupling delays* $\Delta_{i,k}$ and interval boundaries $\gamma_{\mathrm{b},i,k}$, and $\gamma_{\mathrm{e},i,k}$ are constrained such that

$$\xi_{\mathrm{e},i,k} = 1,\ k = 1, \ldots, C_i - 1, \tag{4.16}$$

$$\xi_{\mathrm{b},i,k} = 0,\ k = 2, \ldots, C_i, \tag{4.17}$$

and the *composite coupling matrices* $A_{i,k,s}$ are chosen so that continuity of y_i across $\tau = \gamma_{\mathrm{e},i,k} = \gamma_{\mathrm{b},i,k+1}$ for $k = 1, \ldots, C_i - 1$ is implied by the boundary conditions (4.12). It is clear that the functions y_i are completely determined by the coupling conditions. Consequently, no additional constraints on the algebraic state variables can be added to the continuation problem.

In practice, additional problem-specific algebraic constraints relate the quantities $T_{0,i}$, T_i, and $\gamma_{\mathrm{e},i,1}$ for $i = 1, \ldots, M$ to each other and/or the problem parameters p. Per the additive principles of the constrained optimization paradigm, we omit consideration of such dependencies in the abstract framework, but make the relationships explicit in the context of particular examples.

4.2.2 Examples

As a first example, suppose that $M = 1$, $C_1 = 2$, and $S_{1,1} = S_{1,2} = j_{1,1,1} = j_{1,2,1} = j_{1,1} = j_{1,2} = 1$, and let

$$B_{1,1} = A_{1,1,1} = A_{1,2,1} = I_n,\ \gamma_{\mathrm{e},1,1} = \frac{\alpha}{T} \tag{4.18}$$

with $T_1 = T$ in terms of the problem parameters α and T, where $0 \leq \alpha \leq T$. It follows that

$$\gamma_{\mathrm{b},1,2} = \Delta_{1,2} = \frac{\alpha}{T},\ \Delta_{1,1} = \frac{\alpha}{T} - 1. \tag{4.19}$$

We obtain the equations

$$\begin{aligned} x'(\tau) &= T f\left(T_0 + T\tau, x(\tau), y(\tau), p\right),\ \tau \in (0,1), \\ y(\tau) &= \begin{cases} x\left(\tau + 1 - \alpha/T\right), & \tau \in (0, \alpha/T), \\ x\left(\tau - \alpha/T\right), & \tau \in (\alpha/T, 1), \end{cases} \end{aligned} \tag{4.20}$$

where we omitted the trivial subscript (cf. the governing boundary-value problem in the derivation of the phase response functional in Section 2.4.3 for an autonomous vector field). Here, the boundary condition $x(0) = x(1)$ implies continuity of $y(\tau)$ across $\tau = \alpha/T$, while evaluation of the coupling conditions at $\tau = 0$ and $\tau = 1$ shows that $y(0) = y(1)$. With $z(t) := x\left((t - T_0)/T\right)$ and $\tilde{z}(t) := y\left((t - T_0)/T\right)$, the coupling conditions may be condensed using the modulo operator to yield

$$\tilde{z}(t) = z\left(t - \alpha\big|_{\mathrm{mod}[T_0, T_0+T)}\right),\ t \in [T_0, T_0 + T), \tag{4.21}$$

from which we conclude that the abstract problem corresponds to the existence of a continuously-differentiable, T-periodic solution $z(t)$ of the delay differential equation

$$\dot{z}(t) = f(t, z(t), z(t-\alpha), p) \tag{4.22}$$

provided that f is periodic with period T in its first argument.

As a second example, suppose that $M = C_1 = C_2 = 2$, $S_{1,1} = S_{1,2} = S_{2,1} = S_{2,2} = 1$,

$j_{1,1,1} = j_{2,2,1} = j_{1,1} = j_{2,2} = 2$, and $j_{1,2,1} = j_{2,1,1} = j_{1,2} = j_{2,1} = 1$, and let

$$B_{1,1} = B_{2,2} = 0_n,\ B_{1,2} = B_{2,1} = A_{1,1,1} = A_{1,2,1} = A_{2,1,1} = A_{2,2,1} = I_n,$$
$$\gamma_{\mathrm{e},1,1} = \frac{\alpha}{\beta},\ \gamma_{\mathrm{e},2,1} = \frac{\alpha}{T-\beta} \tag{4.23}$$

with $T_1 = \beta$, $T_2 = T - \beta$ in terms of the problem parameters α, β, and T, where $0 \leq \alpha < \beta < T - \alpha$. It follows that

$$\gamma_{\mathrm{b},1,2} = \frac{\alpha}{\beta},\ \gamma_{\mathrm{b},2,2} = \frac{\alpha}{T-\beta},\ \Delta_{1,1} = \frac{\alpha - T + \beta}{\beta},$$
$$\Delta_{1,2} = \frac{\alpha}{\beta},\ \Delta_{2,1} = \frac{\alpha - \beta}{T-\beta},\ \Delta_{2,2} = \frac{\alpha}{T-\beta}. \tag{4.24}$$

Then, if $T_{0,1} = T_0$ and $T_{0,2} = T_0 + \beta$, we obtain the equations

$$x_1'(\tau) = \beta f_1\left(T_0 + \beta\tau, x_1(\tau), y_1(\tau), p\right),\ \tau \in (0,1), \tag{4.25}$$

$$x_2'(\tau) = (T-\beta)\, f_2\left(T_0 + \beta + (T-\beta)\,\tau, x_2(\tau), y_2(\tau), p\right),\ \tau \in (0,1), \tag{4.26}$$

$$y_1(\tau) = \begin{cases} x_2\left(\beta\tau/(T-\beta) + 1 - \alpha/(T-\beta)\right), & \tau \in (0, \alpha/\beta), \\ x_1\left(\tau - \alpha/\beta\right), & \tau \in (\alpha/\beta, 1), \end{cases} \tag{4.27}$$

$$y_2(\tau) = \begin{cases} x_1\left((T-\beta)\tau/\beta + 1 - \alpha/\beta\right), & \tau \in (0, \alpha/(T-\beta)), \\ x_2\left(\tau - \alpha/(T-\beta)\right), & \tau \in (\alpha/(T-\beta), 1). \end{cases} \tag{4.28}$$

Here, the boundary conditions $x_1(0) = x_2(1)$ and $x_1(1) = x_2(0)$ imply continuity of $y_1(\tau)$ across $\tau = \alpha/\beta$ and of $y_2(\tau)$ across $\tau = \alpha/(T-\beta)$, respectively, while evaluation of the coupling conditions at $\tau = 0$ and $\tau = 1$ shows that $y_1(0) = y_2(1)$ and $y_1(1) = y_2(0)$. With $z_1(t) := x_1\left((t - T_0)/\beta\right)$, $z_2(t) := x_2\left((t - T_0 - \beta)/(T-\beta)\right)$, $\tilde{z}_1(t) := y_1\left((t - T_0)/\beta\right)$, and $\tilde{z}_2(t) := y_2\left((t - T_0 - \beta)/(T-\beta)\right)$, the coupling conditions may now be condensed using the

modulo operator to yield

$$\tilde{z}_1(t) = \begin{cases} z_2\left(t - \alpha\big|_{\mathrm{mod}[T_0,T_0+T]}\right), & t \in [T_0, T_0+\alpha], \\ z_1\left(t - \alpha\big|_{\mathrm{mod}[T_0,T_0+T]}\right), & t \in [T_0+\alpha, T_0+\beta], \end{cases} \tag{4.29}$$

$$\tilde{z}_2(t) = \begin{cases} z_1\left(t - \alpha\big|_{\mathrm{mod}[T_0,T_0+T]}\right), & t \in [T_0+\beta, T_0+\alpha+\beta], \\ z_2\left(t - \alpha\big|_{\mathrm{mod}[T_0,T_0+T]}\right), & t \in [T_0+\alpha+\beta, T_0+T], \end{cases} \tag{4.30}$$

from which we conclude that the abstract problem corresponds to the existence of a continuous, T-periodic, piecewise differentiable function $z(t)$ of the system of delay differential equations

$$\dot{z}(t) = f_1(t, z(t), z(t-\alpha), p),\ t\big|_{\mathrm{mod}[T_0,T_0+T)} \in (T_0, T_0+\beta), \tag{4.31}$$

$$\dot{z}(t) = f_2(t, z(t), z(t-\alpha), p),\ t\big|_{\mathrm{mod}[T_0,T_0+T)} \in (T_0+\beta, T_0+T) \tag{4.32}$$

provided that f_1 and f_2 are periodic with period T in their first argument.

As a final example inspired by the analysis of quasiperiodic invariant tori [1], suppose that M equals an odd integer, and that $C_i = 2$, $S_{i,1} = M$, $S_{i,2} = 1$, $j_{i,1,1} = 1, \ldots, j_{i,1,M} = j_{i,1} = M$, and $j_{i,2,1} = j_{i,2} = i$ for $i = 1, \ldots, M$. For each i, let

$$B_{i,j} = A_{i,1,j} = A_{i,j},\ j = 1, \ldots, M \tag{4.33}$$

and

$$A_{i,2,1} = I_n,\ \gamma_{\mathrm{e},i,1} = \frac{\alpha}{T} \tag{4.34}$$

with $T_1 = \cdots = T_M = T$ in terms of the problem parameters α and T, where $0 \leq \alpha \leq T$. It follows that

$$\gamma_{\mathrm{b},i,2} = \frac{\alpha}{T},\ \Delta_{i,1} = \frac{\alpha}{T} - 1,\ \Delta_{i,2} = \frac{\alpha}{T}. \tag{4.35}$$

Then, if $T_{0,1} = \cdots = T_{0,M} = T_0$ and $f_1 = \cdots = f_M = f$, we obtain

$$\begin{aligned} x_i'(\tau) &= Tf\left(T_0 + T\tau, x_i(\tau), y_i(\tau), p\right), \ \tau \in (0,1), \\ y_i(\tau) &= \begin{cases} \sum_{s=1}^{M} A_{i,s} \cdot x_s\left(\tau + 1 - \alpha/T\right), & \tau \in (0, \alpha/T), \\ x_i\left(\tau - \alpha/T\right), & \tau \in (\alpha/T, 1). \end{cases} \end{aligned} \tag{4.36}$$

Here, the boundary conditions

$$x_i(0) = \sum_{j=1}^{M} A_{i,j} \cdot x_j(1), \tag{4.37}$$

imply continuity of $y_i(\tau)$ across $\tau = \alpha/T$, while evaluation of the coupling conditions at $\tau = 0$ and $\tau = 1$ shows that

$$y_i(0) = \sum_{j=1}^{M} A_{i,j} \cdot y_j(1). \tag{4.38}$$

We specialize to the case with $A_{i,s}$ given by the (i,s)-th $n \times n$ block in the $Mn \times Mn$ matrix $(F \otimes I_n)^{-1}((RF) \otimes I_n)$, where F denotes the symmetric square matrix whose (i,j)-th entry equals $e^{-2\pi \mathrm{j}(i-1)(j-1)/M}$ and R denotes the diagonal matrix whose diagonal elements equal $1, e^{-2\pi\rho}, \ldots, e^{-2\pi\lfloor M/2 \rfloor \rho}, e^{2\pi\lfloor M/2 \rfloor \rho}, \ldots, e^{2\pi\rho}$ in terms of the *rotation number* ρ. Then, if $x_i(\tau) = x\left(\varphi_i, \tau\right)$ and $y_i(\tau) = y\left(\varphi_i, \tau\right)$ in terms of some functions

$$x\left(\varphi, \tau\right) := \sum_{m=-\lfloor M/2 \rfloor}^{\lfloor M/2 \rfloor} c_{x,m}(\tau) e^{\mathrm{j}m\varphi}, \ y\left(\varphi, \tau\right) := \sum_{m=-\lfloor M/2 \rfloor}^{\lfloor M/2 \rfloor} c_{y,m}(\tau) e^{\mathrm{j}m\varphi}, \tag{4.39}$$

and $\varphi_i = 2\pi(i-1)/M$, it follows from the coupling conditions that the discrete Fourier transform of $y(\varphi, \tau)$ sampled at $\varphi = \varphi_i$ equals the discrete Fourier transform of $x(\varphi - 2\pi\rho, \tau + 1 - \alpha/T)$ sampled at $\varphi = \varphi_i$ when $\tau \in [0, \alpha/T]$ and, consequently, that

$$y(\varphi, \tau) = \begin{cases} x(\varphi - 2\pi\rho, \tau + 1 - \alpha/T), & \tau \in (0, \alpha/T), \\ x(\varphi, \tau - \alpha/T), & \tau \in (\alpha/T, 1). \end{cases} \tag{4.40}$$

In this case, continuity of $y(\varphi,\tau)$ across $\tau=\alpha/T$ requires that $x(\varphi,0)=x(\varphi-2\pi\rho,1)$, while evaluation at $\tau=0$ and $\tau=1$ shows that $y(\varphi,0)=y(\varphi-2\pi\rho,1)$. Suppose now, additionally, that

$$x_{,\tau}(\varphi,\tau)=Tf(T_0+T\tau,x(\varphi,\tau),y(\varphi,\tau),p),\ \tau\in(0,1) \tag{4.41}$$

for all $\varphi\in\mathbb{S}$ rather than only at $\varphi=\varphi_i$. Then, with

$$\tilde{z}(\theta_1(t),\theta_2(t)):=x\left(\theta_1(t)-\rho\theta_2(t),\frac{\theta_2(t)}{2\pi}\right),\ \theta_1(t)=\varphi+2\pi\rho\frac{t-T_0}{T},\ \theta_2(t)=2\pi\frac{t-T_0}{T}, \tag{4.42}$$

we obtain

$$\begin{aligned}\frac{d}{dt}\tilde{z}(\theta_1(t),\theta_2(t))&=\frac{1}{T}x_{,\tau}\left(\theta_1(t)-\rho\theta_2(t),\frac{\theta_2(t)}{2\pi}\right)\\&=f\left(t,z(\theta_1(t),\theta_2(t)),z\left(\theta_1(t)-\frac{2\pi\rho\alpha}{T},\theta_2(t)-\frac{2\pi\alpha}{T}\right),p\right)\end{aligned} \tag{4.43}$$

and, consequently, that the function $z(t)=\tilde{z}(\theta_1(t),\theta_2(t))$ describes a continuously-differentiable, quasiperiodic solution with angular frequencies $2\pi/T$ and $2\pi\rho/T$ of the delay differential equation

$$\dot{z}(t)=f(t,z(t),z(t-\alpha),p) \tag{4.44}$$

provided that f is periodic with period T in its first argument and ρ is irrational.

An example of the use of (4.36)-(4.37) to approximate a quasiperiodic invariant torus for a two-dimensional equation of the form (4.44) (taken from [1]) using a finite collection of trajectory segments is shown in Fig. 4.2. The boundary conditions (4.37) correspond to a discretized representation of a relative rotation by $2\pi\rho$ between the intersections of the torus with the $t=0$ and $t=T$ (here, $T=2\pi$) surfaces, as is also the case for problems without delay [32]. In the presence of delay, the history for each segment is obtained by Fourier interpolation over the family of trajectory segments, rotated by $2\pi\rho$ and shifted by T.

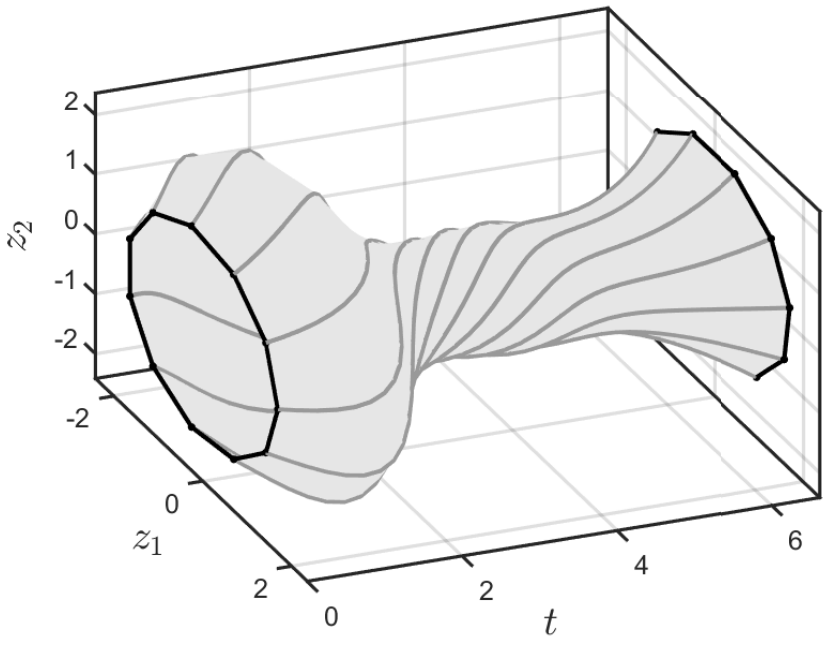

Figure 4.2: A discretized representation of a quasiperiodic invariant torus for a two-dimensional non-autonomous equation of the form (4.44) using the multi-segment formalism described in (4.36)-(4.37) with $M = 11$ and $T = 2\pi$.

4.2.3 Adjoint conditions

We proceed to consider the problem of optimizing a scalar valued function of the differential state variables x_i, algebraic state variables y_i, initial times $T_{0,i}$, durations T_i, coupling delays $\Delta_{i,k}$, interval limits $\gamma_{\mathrm{b},i,k}$ and $\gamma_{\mathrm{e},i,k}$, and problem parameters p, subject to the proposed differential constraints (4.11), boundary conditions (4.12), mesh conditions (4.13), coupling conditions (4.14), and algebraic conditions (4.16)-(4.17). In this section, we derive the corresponding contributions to the necessary adjoint conditions for stationary points. Several examples of such optimization problems may be found in [1] and are revisited here in the context of the abstract framework.

By analogy with the i-th differential constraint (4.11) and boundary conditions (4.12)

(when applicable), consider the partial Lagrangian

$$\int_0^1 \lambda^{\mathrm{T}}(\tau) \cdot \left(x'(\tau) - Tf\left(T_0 + T\tau, x(\tau), y(\tau), p\right)\right) \mathrm{d}\tau + \zeta^{\mathrm{T}} \cdot \left(x(0) - \sum_{j=1}^{M} B_{i,j}(p) x_j(1)\right) \quad (4.45)$$

in terms of the Lagrange multipliers $\lambda : \mathbb{R} \to \mathbb{R}^n$ and $\zeta \in \mathbb{R}^n$. We obtain additive contributions to the necessary adjoint conditions by considering independent variations with respect to $x(\cdot)$, $x_j(1)$, $y(\cdot)$, T_0, T, and p, followed by identification of the coefficients of $\delta x(\cdot)$, $\delta x_j(1)$, $\delta y(\cdot)$, δT_0, δT, and δp, respectively. For example, using integration by parts, we obtain the contributions

$$-\lambda'^{\mathrm{T}}(\tau) - T\lambda^{\mathrm{T}}(\tau) \cdot f_{,x}\left(T_0 + T\tau, x(\tau), y(\tau), p\right), \quad (4.46)$$

corresponding to variations $\delta x(\tau)$ for $\tau \in (0, 1)$, and

$$\zeta^{\mathrm{T}} - \lambda^{\mathrm{T}}(0), \quad \lambda^{\mathrm{T}}(1) \quad (4.47)$$

for variations $\delta x(0)$ and $\delta x(1)$, respectively. Similarly, contributions corresponding to $\delta y(\tau)$ for $\tau \in [0, 1]$, δT_0, δT, δp and $\delta x_j(1)$ are given by

$$-T\lambda^{\mathrm{T}}(\tau) \cdot f_{,y}\left(T_0 + T\tau, x(\tau), y(\tau), p\right), \quad (4.48)$$

$$-T\int_0^1 \lambda^{\mathrm{T}}(\tau) \cdot f_{,t}\left(T_0 + T\tau, x(\tau), y(\tau), p\right) \mathrm{d}\tau, \quad (4.49)$$

$$-\int_0^1 \lambda^{\mathrm{T}}(\tau) \cdot \left(\tau T f_{,t}\left(T_0 + T\tau, x(\tau), y(\tau), p\right) + f\left(T_0 + T\tau, x(\tau), y(\tau), p\right)\right) \mathrm{d}\tau, \quad (4.50)$$

$$-T\int_0^1 \lambda^{\mathrm{T}}(\tau) \cdot f_{,p}\left(T_0 + T\tau, x(\tau), y(\tau), p\right) \mathrm{d}\tau - \zeta^{\mathrm{T}} \cdot \sum_{j=1}^{M} \left(B_{i,j}(p) x_j(1)\right)_{,p}, \quad (4.51)$$

$$-\zeta^{\mathrm{T}} \cdot B_{i,j}(p), \quad (4.52)$$

respectively.

Next, by analogy with the mesh conditions in (4.13) and C_i coupling conditions in (4.14),

consider the partial Lagrangian

$$\sum_{k=1}^{C} \int_{\gamma_{\mathrm{b},k}}^{\gamma_{\mathrm{e},k}} \mu^{\mathrm{T}}(\tau) \cdot \left(y(\tau) - \sum_{s=1}^{S_k} A_{k,s}(p) \cdot x_{j_{k,s}} \left(\frac{T}{T_{j_k}} (\tau - \Delta_k) \right) \right) \mathrm{d}\tau + \eta_1 \gamma_{\mathrm{b},1} + \sum_{k=1}^{C-1} \eta_{k+1} \left(\gamma_{\mathrm{b},k+1} - \gamma_{\mathrm{e},k} \right) + \eta_{C+1} \left(1 - \gamma_{\mathrm{e},C} \right) \tag{4.53}$$

in terms of the Lagrange multipliers $\mu : \mathbb{R} \to \mathbb{R}^n$ and $\eta_k \in \mathbb{R}$ for $k = 1, \ldots, C+1$. We obtain additive contributions to the necessary adjoint conditions by considering independent variations with respect to $y(\cdot)$, p, and T, as well as T_{j_k}, Δ_k, $x_{j_{k,s}}(\cdot)$, $\gamma_{\mathrm{b},k}$, and $\gamma_{\mathrm{e},k}$ for $s = 1, \ldots, S_k$ and $k = 1, \ldots, C$, followed by identification of the coefficients of $\delta y(\cdot)$, δp, and δT, as well as δT_{j_k}, $\delta \Delta_k$, $\delta x_{j_{k,s}}(\cdot)$, $\delta \gamma_{\mathrm{b},k}$, and $\delta \gamma_{\mathrm{e},k}$, for $s = 1, \ldots, S_k$ and $k = 1, \ldots, C$, respectively. In order, these equal

$$\mu^{\mathrm{T}}(\tau),\ \tau \in [0,1]\,, \tag{4.54}$$

$$-\sum_{k=1}^{C} \int_{\gamma_{\mathrm{b},k}}^{\gamma_{\mathrm{e},k}} \mu^{\mathrm{T}}(\tau) \cdot \sum_{s=1}^{S_k} \left(A_{k,s}(p) \cdot x_{j_{k,s}} \left(\frac{T}{T_{j_k}} (\tau - \Delta_k) \right) \right)_{,p} \mathrm{d}\tau, \tag{4.55}$$

$$-\sum_{k=1}^{C} \frac{1}{T_{j_k}} \int_{\gamma_{\mathrm{b},k}}^{\gamma_{\mathrm{e},k}} (\tau - \Delta_k) \mu^{\mathrm{T}}(\tau) \cdot \sum_{s=1}^{S_k} A_{k,s}(p) \cdot x'_{j_{k,s}} \left(\frac{T}{T_{j_k}} (\tau - \Delta_k) \right) \mathrm{d}\tau, \tag{4.56}$$

$$\frac{T}{T_{j_k}^2} \int_{\gamma_{\mathrm{b},k}}^{\gamma_{\mathrm{e},k}} (\tau - \Delta_k) \mu^{\mathrm{T}}(\tau) \cdot \sum_{s=1}^{S_k} A_{k,s}(p) \cdot x'_{j_{k,s}} \left(\frac{T}{T_{j_k}} (\tau - \Delta_k) \right) \mathrm{d}\tau,\ k = 1, \ldots, C, \tag{4.57}$$

$$\frac{T}{T_{j_k}} \int_{\gamma_{\mathrm{b},k}}^{\gamma_{\mathrm{e},k}} \mu^{\mathrm{T}}(\tau) \cdot \sum_{s=1}^{S_k} A_{k,s}(p) \cdot x'_{j_{k,s}} \left(\frac{T}{T_{j_k}} (\tau - \Delta_k) \right) \mathrm{d}\tau,\ k = 1, \ldots, C, \tag{4.58}$$

$$-\frac{T_{j_k}}{T} \mu^{\mathrm{T}} \left(\frac{T_{j_k}}{T} \tau + \Delta_k \right) \cdot A_{k,s}(p),\ \tau \in (\xi_{\mathrm{b},k}, \xi_{\mathrm{e},k})\,,\ s = 1, \ldots, S_k,\ k = 1, \ldots, C \tag{4.59}$$

and, by the assumed continuity of $y(\tau)$, the sequences

$$\eta_1, \ldots, \eta_C, \quad \text{and} \quad -\eta_2, \ldots, -\eta_{C+1}, \tag{4.60}$$

respectively. When several subscripts j_k evaluate to the same integer, the corresponding

contributions may be added to each other to obtain the adjoint contributions associated with a particular differential state variable or duration. Consistent with the smoothness assumptions on x and y, we assume that λ and μ are continuous, piecewise-differentiable and continuous, respectively.

Finally, by analogy with the additional conditions (4.16) and (4.17) on the quantities $\xi_{\mathrm{b},k}$ and $\xi_{\mathrm{e},k}$, consider the partial Lagrangian

$$\sum_{k=1}^{C-1} \chi_{\mathrm{e},k} \left(\frac{T}{T_{j_k}} \left(\gamma_{\mathrm{e},k} - \Delta_k \right) - 1 \right) + \sum_{k=2}^{C} \chi_{\mathrm{b},k} \left(\frac{T}{T_{j_k}} \left(\gamma_{\mathrm{b},k} - \Delta_k \right) \right), \tag{4.61}$$

in terms of the Lagrange multipliers $\chi_{\mathrm{e},k}$ for $k = 1, \ldots, C-1$ and $\chi_{\mathrm{b},k}$ for $k = 2, \ldots, C$. We obtain additive contributions to the necessary adjoint conditions by considering independent variations with respect to T, T_{j_k} and Δ_k for $k = 1, \ldots, C$, $\gamma_{\mathrm{e},k}$ for $k = 1, \ldots, C-1$, and $\gamma_{\mathrm{b},k}$ for $k = 2, \ldots, C$. For example, identification of the coefficient of δT yields the contribution

$$\sum_{k=1}^{C-1} \chi_{\mathrm{e},k} \frac{\gamma_{\mathrm{e},k} - \Delta_k}{T_{j_k}} + \sum_{k=2}^{C} \chi_{\mathrm{b},k} \frac{\gamma_{\mathrm{b},k} - \Delta_k}{T_{j_k}}. \tag{4.62}$$

We find the contributions

$$-\chi_{\mathrm{e},1} \frac{T}{T_{j_1}^2} \left(\gamma_{\mathrm{e},1} - \Delta_k \right), \; -\chi_{\mathrm{e},1} \frac{T}{T_{j_1}} \tag{4.63}$$

by considering coefficients of δT_{j_1} and $\delta \Delta_1$,

$$-\chi_{\mathrm{b},C} \frac{T}{T_{j_C}^2} \left(\gamma_{\mathrm{b},C} - \Delta_C \right), \; -\chi_{\mathrm{b},C} \frac{T}{T_{j_C}} \tag{4.64}$$

by considering coefficients of δT_{j_C} and $\delta \Delta_C$, and

$$-\left(\chi_{\mathrm{e},k} \gamma_{\mathrm{e},k} + \chi_{\mathrm{b},k} \gamma_{\mathrm{b},k} \right) \frac{T}{T_{j_k}^2}, \; -\left(\chi_{\mathrm{e},k} + \chi_{\mathrm{b},k} \right) \frac{T}{T_{j_k}} \tag{4.65}$$

by considering coefficients of δT_{j_k} and $\delta \Delta_k$ for $k = 2, \ldots, C-1$, respectively. As before

contributions may be added to each other when several subscripts j_k evaluate to the same integer. Finally, identification of the coefficients of $\delta\gamma_{\mathrm{e},k}$ for $k = 1, \ldots, C-1$ and $\delta\gamma_{\mathrm{b},k}$ for $k = 2, \ldots, C$ yields the contributions

$$\chi_{\mathrm{e},k}\frac{T}{T_{j_k}} \tag{4.66}$$

and

$$\chi_{\mathrm{b},k}\frac{T}{T_{j_k}}, \tag{4.67}$$

respectively.

4.2.4 Examples, continued

For the first example in Section 4.2.2, we obtain the adjoint contributions

$$-\lambda'^{\mathrm{T}}(\tau) - T\lambda^{\mathrm{T}}(\tau)\cdot f_{,x}\left(T_0 + T\tau, x(\tau), y(\tau), p\right) - \mu^{\mathrm{T}}\left(\tau + \frac{\alpha}{T}\right),\ \tau \in \left(0, 1 - \frac{\alpha}{T}\right), \tag{4.68}$$

$$-\lambda'^{\mathrm{T}}(\tau) - T\lambda^{\mathrm{T}}(\tau)\cdot f_{,x}\left(T_0 + T\tau, x(\tau), y(\tau), p\right) - \mu^{\mathrm{T}}\left(\tau + \frac{\alpha}{T} - 1\right),\ \tau \in \left(1 - \frac{\alpha}{T}, 1\right), \tag{4.69}$$

corresponding to variations $\delta x(\tau)$ for $\tau \in (0,1)$, and

$$-T\lambda^{\mathrm{T}}(\tau)\cdot f_{,y}(T_0 + T\tau, x(\tau), y(\tau), p) + \mu^{\mathrm{T}}(\tau),\ \tau \in [0,1] \tag{4.70}$$

corresponding to variations $\delta y(\tau)$ for $\tau \in [0,1]$. All three of these must equal zero in the absence of any additional constraints involving $x(\tau)$ on $(0,1)$ or $y(\tau)$ on $[0,1]$. In this case,

$$\begin{aligned}\lim_{\tau\uparrow 1-\frac{\alpha}{T}} \lambda'^{\mathrm{T}}(\tau) - \lim_{\tau\downarrow 1-\frac{\alpha}{T}} \lambda'^{\mathrm{T}}(\tau) &= \mu^{\mathrm{T}}(0) - \mu^{\mathrm{T}}(1)\\ &= T\lambda^{\mathrm{T}}(0)\cdot f_{,y}(T_0, x(0), y(0), p)\\ &\quad - T\lambda^{\mathrm{T}}(1)\cdot f_{,y}(T_0 + T, x(1), y(1), p).\end{aligned} \tag{4.71}$$

Since by continuity $y(0) = y(1)$ and $x(0) = x(1)$, the right-hand side equals

$$T\left(\lambda^{\mathrm{T}}(0) - \lambda^{\mathrm{T}}(1)\right) \cdot f_{,y}(T_0, x(0), y(0), p) \tag{4.72}$$

in the case that f is periodic in its first argument with period T. In general, this is nonzero and a discontinuity in the derivative of λ occurs at $\tau = 1 - \alpha/T$.

For the second example in Section 4.2.2, we obtain the adjoint contributions

$$-\lambda_1'^{\mathrm{T}}(\tau) - \beta\lambda_1^{\mathrm{T}}(\tau) \cdot f_{1,x}\left(T_0 + \beta\tau, x_1(\tau), y_1(\tau), p\right) - \mu_1^{\mathrm{T}}\left(\tau + \frac{\alpha}{\beta}\right), \tau \in \left(0, 1 - \frac{\alpha}{\beta}\right), \tag{4.73}$$

$$-\lambda_1'^{\mathrm{T}}(\tau) - \beta\lambda_1^{\mathrm{T}}(\tau) \cdot f_{1,x}\left(T_0 + \beta\tau, x_1(\tau), y_1(\tau), p\right) - \frac{\beta}{T-\beta}\mu_2^{\mathrm{T}}\left(\frac{\beta}{T-\beta}\tau + \frac{\alpha-\beta}{T-\beta}\right), \tau \in \left(1 - \frac{\alpha}{\beta}, 1\right), \tag{4.74}$$

$$-\lambda_2'^{\mathrm{T}}(\tau) - (T-\beta)\lambda_2^{\mathrm{T}}(\tau) \cdot f_{2,x}\left(T_0 + \beta + (T-\beta)\tau, x_2(\tau), y_2(\tau), p\right) - \mu_2^{\mathrm{T}}\left(\tau + \frac{\alpha}{T-\beta}\right), \tau \in \left(0, 1 - \frac{\alpha}{T-\beta}\right), \tag{4.75}$$

$$-\lambda_2'^{\mathrm{T}}(\tau) - (T-\beta)\lambda_2^{\mathrm{T}}(\tau) \cdot f_{2,x}\left(T_0 + \beta + (T-\beta)\tau, x_2(\tau), y_2(\tau), p\right) - \frac{T-\beta}{\beta}\mu_1^{\mathrm{T}}\left(\frac{T-\beta}{\beta}\tau + \frac{\alpha-T+\beta}{\beta}\right), \tau \in \left(1 - \frac{\alpha}{T-\beta}, 1\right), \tag{4.76}$$

corresponding to variations $\delta x_1(\tau)$ and $\delta x_2(\tau)$ for $\tau \in (0, 1)$, and

$$-\beta\lambda_1^{\mathrm{T}}(\tau) \cdot f_{1,y}(T_0 + \beta\tau, x_1(\tau), y_1(\tau), p) + \mu_1^{\mathrm{T}}(\tau), \tau \in [0, 1], \tag{4.77}$$

$$-(T-\beta)\lambda_2^{\mathrm{T}}(\tau) \cdot f_{2,y}(T_0 + \beta + (T-\beta)\tau, x_2(\tau), y_2(\tau), p) + \mu_2^{\mathrm{T}}(\tau), \tau \in [0, 1], \tag{4.78}$$

corresponding to variations $\delta y_1(\tau)$ and $\delta y_2(\tau)$ for $\tau \in [0, 1]$. All six of these must equal zero in the absence of any additional constraints involving $x_1(\tau)$ or $x_2(\tau)$ on $(0, 1)$ or $y_1(\tau)$ or $y_2(\tau)$ on $[0, 1]$.

4.2.5 Discretization

We proceed to describe a natural discretization of the governing zero problem and adjoint contributions, first as an identity in spaces of piecewise polynomials and then in terms of the resulting large systems of algebraic equations with unknowns in $\mathbb{R}^{\hat{N}}$ with $\hat{N} \gg 1$. Given such a discretization, we may formulate Jacobians with respect to the set of discrete unknowns, but omit their explicit expressions in this text.

4.2.6 Abstract formulation of collocation discretization

Given a partition τ_{pt} with $0 = \tau_{\mathrm{pt},1} < \ldots < \tau_{\mathrm{pt},N+1} = 1$ of the interval $[0,1]$, two spaces of, potentially discontinuous, piecewise-polynomial functions are relevant to our discussion, namely

$$\mathcal{P}_m \ := \left\{ x : [0,1] \to \mathbb{R}^n : x|_{[\tau_{\mathrm{pt},j}, \tau_{\mathrm{pt},j+1}]} \text{ is polynomial of degree } m \text{ for } j = 1, \ldots, N \right\},$$

and the subspace $\mathcal{P}_{m,0} := \{x \in \mathcal{P}_m : x(0) = 0\}$. In particular, $\mathcal{P}_{0,0}$ is the space of piecewise-constant functions that equal 0 at $t = 0$. Elements of $\mathcal{P}_m$ are permitted to be discontinuous and multivalued on the interior partition points $\{\tau_{\mathrm{pt},j}\}_{j=2}^{N}$ and we use the notation $x(\tau_{\mathrm{pt},j}^{\pm})$ to distinguish between left- and right-sided limits. The spaces depend on the partition τ_{pt} (of length N), the degree m and space dimension n. Specifically, $\dim \mathcal{P}_m = nN(m+1)$, while $\dim \mathcal{P}_{m,0} = nN(m+1) - n$ (we use the space $\mathcal{P}_{0,0}$ of piecewise constant functions with $x(0) = 0$, which has $\dim \mathcal{P}_{0,0} = n(N-1)$). We observe that differentiation maps $\mathcal{P}_m$ into $\mathcal{P}_{m-1}$.

Our proposed discretization (consistent with the approach in the COCO-compatible `'coll'` toolbox) is expressed in terms of four projections into the spaces $\mathcal{P}_m$ and $\mathcal{P}_{0,0}$, using interpolation at either the collection of Gauss-Legendre points of degree $m-1$ on each subinterval, $\{\tau_{\mathrm{cn},j}\}_{j=1}^{Nm}$, a mesh of $N(m+1)$ base points, $\{\tau_{\mathrm{bp},j}\}_{j=1}^{N(m+1)}$, or the interior partition

points $\{\tau_{\mathrm{pt},j}\}_{j=2}^{N}$:

$$\begin{aligned}
P_{\mathrm{cn}} &: (x : [0,1] \to \mathbb{R}^n) \mapsto \tilde{x} \in \mathcal{P}_{m-1} \text{ with } \tilde{x}(\tau_{\mathrm{cn},j}) = x(\tau_{\mathrm{cn},j}) \text{ for all } j = 1, \ldots, Nm. \\
P_{\mathrm{bp}} &: (x : [0,1] \to \mathbb{R}^n) \mapsto \tilde{x} \in \mathcal{P}_{m} \quad \text{with } \tilde{x}(\tau_{\mathrm{bp},j}) = x(\tau_{\mathrm{bp},j}) \text{ for all } j = 1, \ldots, N(m+1), \\
P_{\mathrm{cont}}^{\pm} &: (x : [0,1] \to \mathbb{R}^n) \mapsto \tilde{x} \in \mathcal{P}_{0,0} \quad \text{with } \tilde{x}(\tau_{\mathrm{pt},j}^{+}) = x(\tau_{\mathrm{pt},j}^{\pm}) \text{ for all } j = 2, \ldots, N.
\end{aligned} \tag{4.79}$$

Note the use of the right limit $\tilde{x}(\tau_{\mathrm{pt},j}^{+})$ for the result $\tilde{x}$ for both projections $P_{\mathrm{cont}}^{\pm}$ (which will enforce continuity of the solution in (4.86) below). All projections depend on the partition τ_{pt}, collection of base points τ_{bp}, and space dimension n (without indicating these dependencies as subscripts). They can be applied to functions that are continuous on each partition interval and have well-defined left and right limits.

For the i-th segment (omitting the i subscript), let $S := \sum_{k=1}^{C} S_k$ and $J_k := (\gamma_{\mathrm{b},k}, \gamma_{\mathrm{e},k})$. Recall the differential constraint (4.11)

$$x'(\tau) = T f(T_0 + T\tau, x(\tau), y(\tau), p),\ \tau \in (0,1) \tag{4.80}$$

and coupling conditions (4.14), which are of the form

$$y(\tau) = \sum_{\ell=1}^{S} a_\ell(\tau) z_\ell\left(b_\ell \tau - c_\ell\right),\ \tau \in [0,1], \tag{4.81}$$

where

$$a_\ell(\tau) := A_{k(\ell),s(\ell)}(p) \mathbb{1}_{J_{k(\ell)}}(\tau),\ z_\ell(\tau) := x_{j_{k(\ell),s(\ell)}}(\tau),\ b_\ell := \frac{T}{T_{j_k}},\ c_\ell := \frac{T}{T_{j_k}} \Delta_k \tag{4.82}$$

and

$$k(\ell) := \min\left\{\nu : \sum_{j=1}^{\nu} S_j \geq \ell\right\},\ s(\ell) := \ell - \sum_{j=1}^{k-1} S_j, \tag{4.83}$$

in terms of the unknown differential and algebraic state variables $x(\cdot)$ and $y(\cdot)$.

We included the indicator function $\mathbb{1}_{J_{k(\ell)}}(\tau)$ in the definition of $a_\ell(\tau)$ to make explicit that the functions $x_{j_{k(\ell),s(\ell)}}$ are only evaluated on the subinterval $J_{k(\ell)}$. The unknowns x and y and z_ℓ are continuous (or more regular) functions on the interval $[0,1]$. Our chosen method of discretization looks for functions $\tilde{x}, \tilde{y} \in \mathcal{P}_m$, coupled to $\tilde{z}_\ell \in \mathcal{P}_m$ from possibly other segments, that satisfy the finite-dimensional constraints

$$\tilde{x}' = P_{\mathrm{cn}} T f\left(T_0 + (\cdot)T, \tilde{x}(\cdot), \tilde{y}(\cdot), p\right) \tag{4.84}$$

corresponding to the discretized ODE in $\mathcal{P}_{m-1}$ of dimension nNm,

$$\tilde{y} = P_{\mathrm{bp}} \sum_{\ell=1}^{S} a_\ell(\cdot)\tilde{z}_\ell((\cdot)b_\ell - c_\ell), \tag{4.85}$$

corresponding to the discretized algebraic constraint in $\mathcal{P}_m$ of dimension $nN(m+1)$, and

$$P^-_{\mathrm{cont}}\,\tilde{x} = P^+_{\mathrm{cont}}\,\tilde{x} \tag{4.86}$$

corresponding to zero gaps for $\tilde{x}$ in $\mathcal{P}_{0,0}$, of dimension $n(N-1)$.

Equation (4.84) is an identity between discontinuous piecewise polynomials of degree $m-1$, while (4.85) is an identity between discontinuous piecewise polynomials of degree m, and (4.86) is an identity between piecewise constant functions that are 0 in $t=0$. The equations (4.84)–(4.86) have a dimensional deficit n (considering $\tilde{x}$ and $\tilde{y}$ as the variables). Evaluation of f, the time shift and scaling $\tilde{z}_\ell \mapsto \tilde{z}_\ell((\cdot)b_\ell - c_\ell)$ and multiplication by the piecewise continuous function $a_\ell(\cdot)$ are exact such that an approximation is only performed when the respective projections P_{cn} and P_{bp} are applied in (4.84) and (4.85).

In lieu of the Lagrange multipliers, we seek functions $\tilde{\lambda}, \tilde{\mu} \in \mathcal{P}_m$. The equations resulting from vanishing variations with respect to x are projected by P_{cn}, giving piecewise polynomial identities in $\mathcal{P}_{m-1}$, while equations from vanishing variations with respect to y are projected by P_{bp}, giving piecewise polynomial identities in $\mathcal{P}_m$. Thus, continuity has to be enforced

only for $\tilde{\lambda}$ (by imposing $P^-_{\text{cont}}\,\tilde{\lambda} = P^+_{\text{cont}}\,\tilde{\lambda}$). Integrals over subintervals J of $[0,1]$ occurring in finite-dimensional adjoint contributions, such as (4.57) and (4.58), are approximated using P_{cn} on the expression truncated by the indicator function. Specifically, for arbitrary $g \in C([0,1];\mathbb{R}^j)$, the integral $\int_J g(\tau)\mathrm{d}\tau$ is approximated as $\int_0^1 P_{\text{cn}}\left[\mathbb{1}_J(\cdot)g(\cdot)\right](\tau)\mathrm{d}\tau$.

The polynomial identities (4.84)– (4.86) and the corresponding contributions to the adjoint conditions have to be evaluated for all segments $i = 1,\ldots,M$. The identities in the spaces of piecewise polynomials, $\mathcal{P}_m$, $\mathcal{P}_{m-1}$ and $\mathcal{P}_{0,0}$, are reduced to algebraic equations in $\mathbb{R}^{nN(m+1)}$, $\mathbb{R}^{nNm}$ and $\mathbb{R}^{n(N-1)}$ by evaluating them on the meshes τ_{bp}, τ_{cn} and the interior partition points $\{\tau^+_{\text{pt},j}\}_{j=2}^N$, respectively.

Before proceeding to consider a detailed implementation of the abstract discretization scheme presented in this section, we conclude with a comment on convergence analysis. Indeed, it is notable that rigorous convergence analysis—showing that solutions of (4.84)–(4.86) converge to solutions of (4.80) and (4.81) under appropriate regularity assumptions—is an open problem. Even for autonomous single-segment periodic boundary-value problems with delay, a complete convergence proof has only been presented recently [103]. The difficulty with this analysis is the non-differentiability of the discretized nonlinear system with respect to many unknowns away from the solution (for example, the period T, the delay α and the quantities b_ℓ, c_ℓ in (4.82)). Similar concerns apply to the convergence analysis for the Lagrange multipliers. In our framework, we use discretizations of the adjoints of the infinite-dimensional problem (4.80)-(4.81), not the adjoints of the discretized problem (4.84)–(4.86) (which are different and possibly not well defined away from the solution manifold; the same concern applies to Jacobians of all equations).

4.2.7 Implementation as large systems of algebraic equations

We now describe a COCO-implementable form of the zero problems and contributions to adjoint conditions derived in Sections 4.2.1 and 4.2.3, and their discretization as polynomials described in Section 4.2.6. As in the abstract discussion above, we consider an arbitrary

segment i, but omit the index i in the description below. Where possible, we rely on vectorized notation to suppress a jungle of indices. For example, we use the $\mathfrak{vec}$ operator to convert its argument into a one-dimensional array of scalars. If A is an array of possible values for the argument of a function f, then $f(A)$ is an array of the same size as A of values of f applied to each element of A.

Consistent with the abstract discussion and following [32], let N and m be two positive integers and define the uniform partition $\tau_{\mathrm{pt},j} = (j-1)/N$, for $j = 1, \ldots, N+1$, and time sequence

$$\tau_{\mathrm{bp},(m+1)(j-1)+k} = \tau_{\mathrm{pt},j} + \frac{k-1}{Nm},\ j = 1, \ldots, N,\ k = 1, \ldots, m+1. \tag{4.87}$$

In particular, $\tau_{\mathrm{bp},1} = \tau_{\mathrm{pt},1} = 0$, $\tau_{\mathrm{bp},N(m+1)} = \tau_{\mathrm{pt},N} + 1/N = \tau_{\mathrm{pt},N+1} = 1$, and

$$\tau_{\mathrm{bp},(m+1)j+1} = \tau_{\mathrm{pt},j+1} = \tau_{\mathrm{bp},(m+1)(j-1)+m+1} = \tau_{\mathrm{bp},(m+1)j},\ j = 1, \ldots, N-1. \tag{4.88}$$

We represent the discretized differential state variable $\tilde{x}(\cdot)$ as the one-dimensional array $x_{\mathrm{bp}} := \tilde{x}(\tau_{\mathrm{bp}})$ of $N(m+1)$ vectors in $\mathbb{R}^n$ and proceed, similarly, to represent the discretized algebraic state variable $y(\cdot)$ and Lagrange multipliers $\lambda(\cdot)$ and $\mu(\cdot)$ as the one-dimensional arrays $y_{\mathrm{bp}} := \tilde{y}(\tau_{\mathrm{bp}})$, $\lambda_{\mathrm{bp}} := \tilde{\lambda}(\tau_{\mathrm{bp}})$, and $\mu_{\mathrm{bp}} := \tilde{\mu}(\tau_{\mathrm{bp}})$, respectively, of $N(m+1)$ vectors in $\mathbb{R}^n$ each. In this representation the continuity equation (4.86) (and its correspondent for $\tilde{\lambda}$) takes the form of $2(N-1)n$ continuity conditions

$$x_{\mathrm{bp}} \cdot \mathcal{C} = \lambda_{\mathrm{bp}} \cdot \mathcal{C} = 0. \tag{4.89}$$

Since the base points include the partition points according to (4.88), the j-th column of the $N(m+1) \times (N-1)$ matrix $\mathcal{C}$ equals $\mathbf{e}_{(m+1)j+1} - \mathbf{e}_{(m+1)j}$ in the standard basis of $\mathbb{R}^{N(m+1)}$. Equivalently, in vectorized form, we write $Q \cdot \mathfrak{vec}(x_{\mathrm{bp}}) = Q \cdot \mathfrak{vec}(\lambda_{\mathrm{bp}}) = 0$ with the $(N-1)n \times N(m+1)n$ matrix $Q = \mathcal{C}^{\mathrm{T}} \otimes I_n$. Since the discretized coupling conditions (4.85) and their adjoint contributions with respect to variations $\delta y(\cdot)$ are imposed in $\mathcal{P}_m$, there is

no need to impose explicit continuity conditions for y_{bp} and μ_{bp}.

It is convenient to define an index function that maps times τ to the corresponding subinterval indices for the partition of $\mathcal{P}_m$. This is useful, for example, when applying the time scale and -shift operator $\tilde{x}(\cdot) \mapsto \tilde{x}((\cdot)b - c)$ on piecewise polynomials in $\mathcal{P}_m$ in the discretized coupling conditions in (4.85). To this end, given a partition σ of $[0, 1]$ into P intervals, let $\tau \mapsto \iota(\tau; \sigma)$ denote the linear interpolation of the pairing $\sigma \to \{1, \ldots, P+1\}$ at τ. In terms of the floor function $\lfloor \cdot \rfloor$,

$$\tau \in [\sigma_p, \sigma_{p+1}) \Rightarrow \pi(\tau; \sigma) := \lfloor \iota(\tau; \sigma) \rfloor = p \tag{4.90}$$

for any $p = 1, \ldots, P$. Then, with $\pi(\tau; \sigma) = 1$ for $\tau < 0$ and $\pi(\tau; \sigma) = P$ for $\tau \geq 1$, the piecewise-constant, non-decreasing index function $\pi(\cdot; \sigma)$ maps $(-\infty, \infty)$ to $\{1, \ldots, P\}$. Consider, for example, the sequence $\{\mathcal{L}_l\}_{l=1}^{m+1}$ of m-th degree Lagrange polynomials defined on the uniform partition of $[-1, 1]$, such that

$$\mathcal{L}_l\left(-1 + 2\frac{k-1}{m}\right) = \delta_{l,k},\ k = 1, \ldots, m+1. \tag{4.91}$$

Then, since

$$\lim_{\tau \to \tau_{\text{pt},j}-} \mathcal{L}_l\left(2N\tau + 1 - 2\pi(\tau; \tau_{\text{pt}})\right) = \delta_{l,m+1},\ \lim_{\tau \to \tau_{\text{pt},j}+} \mathcal{L}_l\left(2N\tau + 1 - 2\pi(\tau; \tau_{\text{pt}})\right) = \delta_{l,1}, \tag{4.92}$$

the continuous, piecewise-polynomial interpolants given by

$$\tau \mapsto \sum_{l=1}^{m+1} \mathcal{L}_l \left(2N\tau + 1 - 2\pi(\tau;\tau_{\mathrm{pt}})\right) x_{\mathrm{bp},(m+1)(\pi(\tau;\tau_{\mathrm{pt}})-1)+l}, \tag{4.93}$$

$$\tau \mapsto \sum_{l=1}^{m+1} \mathcal{L}_l \left(2N\tau + 1 - 2\pi(\tau;\tau_{\mathrm{pt}})\right) y_{\mathrm{bp},(m+1)(\pi(\tau;\tau_{\mathrm{pt}})-1)+l}, \tag{4.94}$$

$$\tau \mapsto \sum_{l=1}^{m+1} \mathcal{L}_l \left(2N\tau + 1 - 2\pi(\tau;\tau_{\mathrm{pt}})\right) \lambda_{\mathrm{bp},(m+1)(\pi(\tau;\tau_{\mathrm{pt}})-1)+l}, \tag{4.95}$$

$$\tau \mapsto \sum_{l=1}^{m+1} \mathcal{L}_l \left(2N\tau + 1 - 2\pi(\tau;\tau_{\mathrm{pt}})\right) \mu_{\mathrm{bp},(m+1)(\pi(\tau;\tau_{\mathrm{pt}})-1)+l} \tag{4.96}$$

allow us to evaluate the piecewise polynomials $\tilde{x}(\tau)$, $\tilde{y}(\tau)$, $\tilde{\lambda}(\tau)$, and $\tilde{\mu}(\tau)$ and, as appropriate, their derivatives at arbitrary τ in $[0,1]$ in terms of linear combinations of the elements of x_{bp}, y_{bp}, λ_{bp}, and μ_{bp}, respectively. As a special case, let z denote the one-dimensional array of m-th order Gauss-Legendre quadrature nodes on the interval $[-1,1]$ in increasing order, and define the time sequence

$$\tau_{\mathrm{cn},m(j-1)+k} = \tau_{\mathrm{pt},j} + \frac{1+z_k}{2N},\ j = 1,\ldots,N,\ k = 1,\ldots,m, \tag{4.97}$$

such that $2N\tau_{\mathrm{cn}} - 2\pi\left(\tau_{\mathrm{cn}};\tau_{\mathrm{pt}}\right) = J_{N,1} \otimes (z-1)$. Then,

$$\tilde{x}\left(\tau_{\mathrm{cn}}\right) = x_{\mathrm{cn}} := x_{\mathrm{bp}} \cdot \mathcal{L}_{\mathrm{cn}},\ \tilde{x}'\left(\tau_{\mathrm{cn}}\right) = x'_{\mathrm{cn}} := 2N x_{\mathrm{bp}} \cdot \mathcal{L}'_{\mathrm{cn}},\ \tilde{y}\left(\tau_{\mathrm{cn}}\right) = y_{\mathrm{cn}} := y_{\mathrm{bp}} \cdot \mathcal{L}_{\mathrm{cn}}, \tag{4.98}$$

$$\tilde{\lambda}\left(\tau_{\mathrm{cn}}\right) = \lambda_{\mathrm{cn}} := \lambda_{\mathrm{bp}} \cdot \mathcal{L}_{\mathrm{cn}},\ \tilde{\lambda}'\left(\tau_{\mathrm{cn}}\right) = \lambda'_{\mathrm{cn}} := 2N\lambda_{\mathrm{bp}} \cdot \mathcal{L}'_{\mathrm{cn}},\ \tilde{\mu}\left(\tau_{\mathrm{cn}}\right) = \mu_{\mathrm{cn}} := \mu_{\mathrm{bp}} \cdot \mathcal{L}_{\mathrm{cn}}, \tag{4.99}$$

where

$$\mathcal{L}_{\mathrm{cn},(m+1)(a-1)+c,m(b-1)+d} = \delta_{a,b}\mathcal{L}_c(z_d),\ \mathcal{L}'_{\mathrm{cn},(m+1)(a-1)+c,m(d-1)+d} = \delta_{a,b}\mathcal{L}'_c(z_d) \tag{4.100}$$

for $a,b = 1,\ldots,N$, $c = 1,\ldots,m+1$, and $d = 1,\ldots,m$. Equivalently, we write $\mathfrak{vec}\left(x_{\mathrm{cn}}\right) = W \cdot \mathfrak{vec}\left(x_{\mathrm{bp}}\right)$, $\mathfrak{vec}\left(x'_{\mathrm{cn}}\right) = 2NW' \cdot \mathfrak{vec}\left(x_{\mathrm{bp}}\right)$, $\mathfrak{vec}\left(y_{\mathrm{cn}}\right) := W \cdot \mathfrak{vec}\left(y_{\mathrm{bp}}\right)$, $\mathfrak{vec}\left(\lambda_{\mathrm{cn}}\right) = W \cdot \mathfrak{vec}\left(\lambda_{\mathrm{bp}}\right)$,

$\mathfrak{vec}\,(\lambda'_{\rm cn}) = 2NW' \cdot \mathfrak{vec}\,(\lambda_{\rm bp})$, and $\mathfrak{vec}\,(\mu_{\rm cn}) = W \cdot \mathfrak{vec}\,(\mu_{\rm bp})$ in terms of the $Nmn \times N(m+1)n$ matrices $W = \mathcal{L}_{\rm cn}^{\rm T} \otimes I_n$ and $W' = \mathcal{L}_{\rm cn}'^{\rm T} \otimes I_n$.

We use evaluation at $\tau_{\rm cn}$ to represent the discretization (4.84) of differential constraint (4.11) as the vectorized algebraic constraints

$$0 = \mathfrak{vec}\,(x'_{\rm cn} - T f_{\rm cn}) = 2NW' \cdot \mathfrak{vec}\,(x_{\rm bp}) - T\mathfrak{vec}\,(f_{\rm cn})\,, \tag{4.101}$$

where $f_{\rm cn} := f(T_0 + T\tau_{\rm cn}, x_{\rm cn}, y_{\rm cn}, p)$ is a one-dimensional array of Nm vectors in $\mathbb{R}^n$. By a similar use of notation and evaluation at $\tau_{\rm cn}$, we represent the discretizations of the corresponding contributions in (4.46) to the necessary adjoint conditions associated with variations $\delta x(\tau)$ for $\tau \in (0,1)$ as the vectorized algebraic expression

$$-\mathfrak{vec}\,(\lambda'_{\rm cn}) - T\mathfrak{diag}\,(f_{x,{\rm cn}})^{\rm T} \cdot \mathfrak{vec}\,(\lambda_{\rm cn}) = \left(-2NW' - T\mathfrak{diag}\,(f_{x,{\rm cn}})^{\rm T} \cdot W\right) \cdot \mathfrak{vec}\,(\lambda_{\rm bp})\,, \tag{4.102}$$

where $f_{x,{\rm cn}} := f_{,x}(T_0 + T\tau_{\rm cn}, x_{\rm cn}, y_{\rm cn}, p)$ is a one-dimensional array of Nm matrices in $\mathbb{R}^{n\times n}$ and $\mathfrak{diag}\,(f_{x,{\rm cn}})$ is an $Nmn \times Nmn$ block-diagonal matrix with the elements of $f_{x,{\rm cn}}$ along the diagonal. The discretized contributions from the Lagrangian (4.45) associated with variations $\delta x(0)$ and $\delta x(1)$ are similarly given by $\zeta - \begin{pmatrix} I_n & 0 & \cdots & 0 \end{pmatrix} \cdot \mathfrak{vec}\,(\lambda_{\rm bp})$ and $\begin{pmatrix} 0 & \cdots & 0 & I_n \end{pmatrix} \cdot \mathfrak{vec}\,(\lambda_{\rm bp})$, while that corresponding to $\delta x_j(1)$ equals $-(B_{i,j}(p))^{\rm T} \cdot \zeta$. By replacing the x subscript with y and cn with bp, evaluation at $\tau_{\rm bp}$ yields the discretization of the contributions in (4.48) to the necessary adjoint condition associated with variations $\delta y(\tau)$ for $\tau \in [0,1]$ in terms of the vectorized algebraic expression

$$-T\mathfrak{diag}\,(f_{y,{\rm bp}})^{\rm T} \cdot \mathfrak{vec}\,(\lambda_{\rm bp})\,. \tag{4.103}$$

Finally, Gaussian quadrature on the partition $\tau_{\rm pt}$ with collocation nodes at $\tau_{\rm cn}$ and with t or p subscripts in place of x or y yields the discretization of the contributions to the necessary adjoint conditions in (4.49), (4.50), and (4.51) associated with variations δT_0, δT, and δp,

given in order by the vectorized algebraic expressions

$$-\frac{T}{2N}\,\mathfrak{vec}\left(f_{t,\mathrm{cn}}\right)^{\mathrm{T}}\cdot\Omega_{\mathrm{cn}}\cdot W\cdot\mathfrak{vec}\left(\lambda_{\mathrm{bp}}\right) \tag{4.104}$$

$$-\frac{1}{2N}\left(\mathfrak{vec}\left(f_{\mathrm{cn}}\right)+T\left(\mathfrak{diag}\left(\tau_{\mathrm{cn}}\right)\otimes I_n\right)\cdot\mathfrak{vec}\left(f_{t,\mathrm{cn}}\right)\right)^{\mathrm{T}}\cdot\Omega_{\mathrm{cn}}\cdot W\cdot\mathfrak{vec}\left(\lambda_{\mathrm{bp}}\right), \tag{4.105}$$

$$\begin{aligned}-\frac{T}{2N}\mathfrak{transp}\left(f_{p,\mathrm{cn}}\right)^{\mathrm{T}}\cdot\Omega_{\mathrm{cn}}\cdot W\cdot\mathfrak{vec}\left(\lambda_{\mathrm{bp}}\right)-\\ \sum_{j=1}^{M}\left(\mathfrak{vec}\left(B_{i,j}(p)\right)_{,p}\right)^{\mathrm{T}}\cdot\left(\begin{pmatrix}0&\cdots&0&I_n\end{pmatrix}\cdot\mathfrak{vec}\left(x_{j,\mathrm{bp}}\right)\otimes I_n\right)\cdot\zeta\end{aligned} \tag{4.106}$$

in terms of the $Nmn\times Nmn$ matrix $\Omega_{\mathrm{cn}}=I_N\otimes\mathfrak{diag}(\omega)\otimes I_n$, the one-dimensional array ω of m-th order quadrature weights associated with the nodes $z_1,\ldots,z_m$, and the $Nmn\times q$ block-vertical matrix $\mathfrak{transp}\left(f_{p,\mathrm{cn}}\right)$ with the elements of $f_{p,\mathrm{cn}}$ stacked vertically.

For the discretization (4.85) of the coupling conditions in (4.14) and the corresponding adjoint contributions in (4.55)-(4.59), it is necessary to consider interpolation at time instants defined by the arguments of the differential state variables $x_{j_{k,s}}$ and Lagrange multiplier μ for $\tau\in\tau_{\mathrm{bp}}$ or τ_{cn}. In contrast to interpolation at τ_{cn}, the corresponding interpolation matrices by necessity depend on the durations T and T_{j_k}, coupling delays Δ_k, and mesh limits $\gamma_{\mathrm{b},k}$ and $\gamma_{\mathrm{e},k}$. For example, let $k_{\mathrm{bp}}=\pi(\tau_{\mathrm{bp}};\{0,\gamma_{\mathrm{b},2}\ldots,\gamma_{\mathrm{b},C},1\})$ as a non-decreasing sequence of coupling interval indices associated with the elements of the τ_{bp} array. For each subarray of successive elements τ_{bp}^k that share an interval index $k\in k_{\mathrm{bp}}$, associate the shifted time instants

$$\tau_{\mathrm{bp}\downarrow\mathrm{sh}}^k:=\frac{T}{T_{j_k}}\left(\tau_{\mathrm{bp}}^k-J_{|\tau_{\mathrm{bp}}^k|,1}\otimes\Delta_k\right) \tag{4.107}$$

with the non-decreasing sequence $j_{\mathrm{bp}\downarrow\mathrm{sh}}^k=\pi\left(\tau_{\mathrm{bp}\downarrow\mathrm{sh}}^k,\tau_{\mathrm{pt}}\right)$ of interval indices j. For each such k, the coupling conditions (4.14) discretized at τ_{bp}^k then take the form

$$y_{\mathrm{bp}}^k-\sum_{s=1}^{S_k}A_{k,s}(p)\cdot x_{j_{k,s},\mathrm{bp}}\cdot\mathcal{L}_{\mathrm{bp}\downarrow\mathrm{sh}}^k=0, \tag{4.108}$$

where y^k_{bp} denotes the corresponding elements of y_{bp} and

$$\mathcal{L}^k_{\mathrm{bp}\downarrow\mathrm{sh},(m+1)(a-1)+c,b} = \delta_{a,j^k_{\mathrm{bp}\downarrow sh,b}} \mathcal{L}_c \left(2N\tau^k_{\mathrm{bp}\downarrow\mathrm{sh},b} + 1 - 2j^k_{\mathrm{bp}\downarrow sh,b}\right), \tag{4.109}$$

for $a = 1, \ldots, N$, $c = 1, \ldots, m+1$, and $b = 1, \ldots, |\tau^k_{\mathrm{bp}}|$. Equivalently, in vectorized form,

$$\mathfrak{vec}\left(y^k_{\mathrm{bp}}\right) - \sum_{s=1}^{S_k} \left(\left(\mathcal{L}^k_{\mathrm{bp}\downarrow\mathrm{sh}}\right)^{\mathrm{T}} \otimes A_{k,s}(p)\right) \cdot \mathfrak{vec}\left(x_{j_{k,s},\mathrm{bp}}\right) = 0. \tag{4.110}$$

For the adjoint contributions in (4.59) associated with variations $\delta x_{j_{k,s}}(\cdot)$ and discretized at τ_{cn}, we obtain nonzero contributions only on the subset $\tau^k_{\mathrm{cn}} \subseteq \tau_{\mathrm{cn}}$ of time instances in $(\xi_{\mathrm{b},k}, \xi_{\mathrm{e},k})$, corresponding to the non-decreasing sequence $j^k_{\mathrm{cn}\uparrow\mathrm{sh}} = \pi\left(\tau^k_{\mathrm{cn}\uparrow\mathrm{sh}}, \tau_{\mathrm{pt}}\right)$ of interval indices for $\tau^k_{\mathrm{cn}\uparrow\mathrm{sh}} := T_{j_k}\tau^k_{\mathrm{cn}}/T + \Delta_k$. The corresponding vectorized expression is now given by

$$-\frac{T_{j_k}}{T}\left(\left(\mathcal{L}^k_{\mathrm{cn}\uparrow\mathrm{sh}}\right)^{\mathrm{T}} \otimes A^{\mathrm{T}}_{k,s}(p)\right) \cdot \mathfrak{vec}\left(\mu_{\mathrm{bp}}\right), \tag{4.111}$$

where

$$\mathcal{L}^k_{\mathrm{cn}\uparrow\mathrm{sh},(m+1)(a-1)+c,b} = \delta_{a,j^k_{\mathrm{cn}\uparrow sh,b}} \mathcal{L}_c \left(2N\tau^k_{\mathrm{cn}\uparrow\mathrm{sh},b} + 1 - 2j^k_{\mathrm{cn}\uparrow sh,b}\right), \tag{4.112}$$

for $a = 1, \ldots, N$, $c = 1, \ldots, m+1$, and $b = 1, \ldots, |\tau^k_{\mathrm{cn}\uparrow\mathrm{sh}}|$.

For the adjoint contributions in (4.54) associated with variations $\delta y(\cdot)$ and discretized at τ_{bp}, the vectorization is simply given by $\mathfrak{vec}\left(\mu_{\mathrm{bp}}\right)$. In contrast, for the adjoint contributions in (4.55)-(4.58) associated with variations δp, δT, δT_{j_k}, and $\delta\Delta_k$ and discretized using quadrature on the partition τ_{pt} with collocation nodes at τ_{cn}, let $k_{\mathrm{cn}} = \pi\left(\tau_{\mathrm{cn}}; \{0, \gamma_{\mathrm{b},2}, \ldots, \gamma_{\mathrm{b},C}, 1\}\right)$ be a non-decreasing sequence of coupling interval indices associated with the elements of the τ_{cn} array. For each subarray of successive elements τ^k_{cn} that share an interval index $k \in k_{\mathrm{cn}}$, let Ω^k_{cn} denote the corresponding subset of Ω_{cn} and associate the shifted time instants

$$\tau^k_{\mathrm{cn}\downarrow\mathrm{sh}} := \frac{T}{T_{j_k}}\left(\tau^k_{\mathrm{cn}} - J_{|\tau^k_{\mathrm{cn}}|,1} \otimes \Delta_k\right) \tag{4.113}$$

with the non-decreasing sequence $j^k_{\mathrm{cn}\downarrow\mathrm{sh}} = \pi\left(\tau^k_{\mathrm{cn}\downarrow\mathrm{sh}}, \tau_{\mathrm{pt}}\right)$ of interval indices j. The sought vectorized contributions are then given by

$$-\sum_{k=1}^{C}\left(\sum_{s=1}^{S_k}\left(\mathfrak{vec}\left(A_{k,s}(p)\right)_{,p}\right)^{\mathrm{T}}\cdot\left(x_{j_{k,s},\mathrm{bp}}\cdot\mathcal{L}^k_{\mathrm{cn}\downarrow\mathrm{sh}}\otimes I_n\right)\right)\cdot\Omega^k_{\mathrm{cn}}\cdot\mathfrak{vec}\left(\mu^k_{\mathrm{cn}}\right), \tag{4.114}$$

$$-\frac{1}{T}\sum_{k=1}^{C}\left(\sum_{s=1}^{S_k}\mathfrak{vec}\left(x_{j_{k,s},\mathrm{bp}}\right)^{\mathrm{T}}\cdot\left(\mathcal{L}'^k_{\mathrm{cn}\downarrow\mathrm{sh}}\otimes A^{\mathrm{T}}_{k,s}(p)\right)\right)\cdot \left(\mathfrak{diag}(\tau^k_{\mathrm{cn}\downarrow\mathrm{sh}})\otimes I_n\right)\cdot\Omega^k_{\mathrm{cn}}\cdot\mathfrak{vec}\left(\mu^k_{\mathrm{cn}}\right), \tag{4.115}$$

$$\frac{1}{T_{j_k}}\left(\sum_{s=1}^{S_k}\mathfrak{vec}\left(x_{j_{k,s},\mathrm{bp}}\right)^{\mathrm{T}}\cdot\left(\mathcal{L}'^k_{\mathrm{cn}\downarrow\mathrm{sh}}\otimes A^{\mathrm{T}}_{k,s}(p)\right)\right)\cdot\left(\mathfrak{diag}(\tau^k_{\mathrm{cn}\downarrow\mathrm{sh}})\otimes I_n\right)\cdot\Omega^k_{\mathrm{cn}}\cdot\mathfrak{vec}\left(\mu^k_{\mathrm{cn}}\right), \tag{4.116}$$

$$\frac{T}{T_{j_k}}\left(\sum_{s=1}^{S_k}\mathfrak{vec}\left(x_{j_{k,s},\mathrm{bp}}\right)^{\mathrm{T}}\cdot\left(\mathcal{L}'^k_{\mathrm{cn}\downarrow\mathrm{sh}}\otimes A^{\mathrm{T}}_{k,s}(p)\right)\right)\cdot\Omega^k_{\mathrm{cn}}\cdot\mathfrak{vec}\left(\mu^k_{\mathrm{cn}}\right), \tag{4.117}$$

where μ^k_{cn} denote the corresponding elements of μ_{cn} and

$$\mathcal{L}'^k_{\mathrm{cn}\downarrow\mathrm{sh},(m+1)(a-1)+c,b} = \delta_{a,j^k_{\mathrm{cn}\downarrow sh,b}}\mathcal{L}'_c\left(2N\tau^k_{\mathrm{cn}\downarrow\mathrm{sh},b}+1-2j^k_{\mathrm{cn}\downarrow sh,b}\right), \tag{4.118}$$

for $a = 1,\ldots,N$, $c = 1,\ldots,m+1$, and $b = 1,\ldots,|\tau^k_{\mathrm{cn}\uparrow\mathrm{sh}}|$.

4.2.8 Dimensional deficit

The dimensional deficit of the zero problem in Section 4.2.1 equals $M(n+2)+q-Kn+G$, where K is the total number of boundary conditions (4.12) and G is the number of segments with f_i explicitly dependent on y_i. With the imposition of the adjoint conditions, the dimensional deficit is reduced by $M(n+2)+q-Kn+G$ for a net value of 0.

The discretization in the previous section is consistent with these counts, since i) there the $(M+G)N(m+1)n$ unknown components of x_{bp} and y_{bp} are constrained by $M(N-1)n$ continuity conditions, $MNmn$ discretized differential conditions, and $GN(m+1)n$ discretized coupling conditions, and ii) the $(M+G)N(m+1)n$ unknown components of λ_{bp} and μ_{bp} are constrained by $M(N-1)n$ continuity conditions, $MNmn$ discretized adjoint differential

conditions, $GN(m+1)n$ discretized adjoint coupling conditions, and $2Mn$ adjoint boundary conditions.

In the first example in Section 4.2.2, we supplement with the algebraic constraints $T_{0,1} = T_0$, $T_1 = T$, and $\gamma_{\mathrm{e},1,1} = \alpha/T$ resulting in a composite zero problem with dimensional deficit q provided that $T, T_0, \alpha \in p$. Similarly, in the second example, we supplement with the algebraic constraints $\gamma_{\mathrm{e},1,1} = \alpha/\beta$, $\gamma_{\mathrm{e},2,1} = \alpha/(T-\beta)$, $T_1 = \beta$, $T_2 = T - \beta$, $T_{0,1} = T_0$, and $T_{0,2} = T_0 + \beta$ resulting in a composite zero problem with dimensional deficit q provided that $\alpha, \beta, T, T_0 \in p$. Finally, in the last example in this section, we supplement with the algebraic constraints $\gamma_{\mathrm{e},i,1} = \alpha/T$, $T_i = T$, and $T_{0,i} = T_0$ for $i = 1, \ldots, M$ resulting in a composite zero problem with dimensional deficit q provided that $\alpha, T, T_0 \in p$.

4.2.9 Toolbox construction

We may pattern the development of a COCO-compatible toolbox on the abstract template introduced in Section 4.2.1 and the corresonding contributions to adjoint conditions in Section 4.2.3. A zero problem constructor naturally decomposes into repeated calls to a toolbox constructor for the differential constraint (4.11) (the `ode_isol2coll` toolbox constructor already accomplishes this for vector fields that do not depend on an algebraic state variable), followed by a constructor for the boundary conditions (4.12), followed or interspersed by repeated calls to a constructor for the mesh conditions (4.13), coupling conditions (4.14), and algebraic conditions (4.16)-(4.17). Assuming, as is typically the case, that the constructor for the differential constraint assumes independent problem parameters in each constructor call, it is necessary to introduce additional algebraic constraints (a.k.a. *gluing conditions*) to ensure that the problem parameters are shared across all segments. Similar considerations may also apply to the construction of the coupling conditions.

A flow chart similar in character to that in Section 2.3.3 corresponding here to the construction of an augmented continuation problem per the abstract toolbox template is shown in Fig. 4.3. Since the i-th coupling condition depends on segments $x_{j_{i,k,s}}$, for

$s = 1, \ldots, S_k$ and $k = 1, \ldots, C_i$, it must be constructed after the corresponding differential constraints have been appended to the continuation problem. It is not necessary, however, to wait until all differential constraints have been introduced. Similar considerations apply to the constructors for the contributions to the adjoint conditions. These may be invoked only after the entire zero problem has been constructed, or at opportune moments following the construction of the corresponding zero functions.

In the next section, we proceed to illustrate the application of such a COCO-compatible toolbox through several numerical examples. These demonstrate the versatility of the tool and the opportunity to use such a toolbox, and the COCO construction paradigm described in Section 2.2.3, to build sophisticated special-purpose toolboxes, dedicated to particular classes of delay differential equations, say.

4.3 Numerical examples

4.3.1 Generalizations of the abstract framework

Before we consider numerical examples illustrating the ability of the proposed toolbox to perform continuation and constrained optimization for boundary-value problems with delay, we consider two possible generalizations that allow one to handle initial-value problems and unknown exogenous driving, as well as problems involving multiple discrete delays.

Consider, for example, the initial-value problem

$$\dot{z}(t) = f(t, z(t), z(t-\alpha), p), \; t \in (T_0, T_0 + T), \tag{4.119}$$

$$z(t) = g(t + \alpha - T_0, p), \; t \in [T_0 - \alpha, T_0] \tag{4.120}$$

for some known function $g(s, p)$, for $s \in [0, \alpha]$. The substitution $x(\tau) = z(T_0 + T\tau)$ then

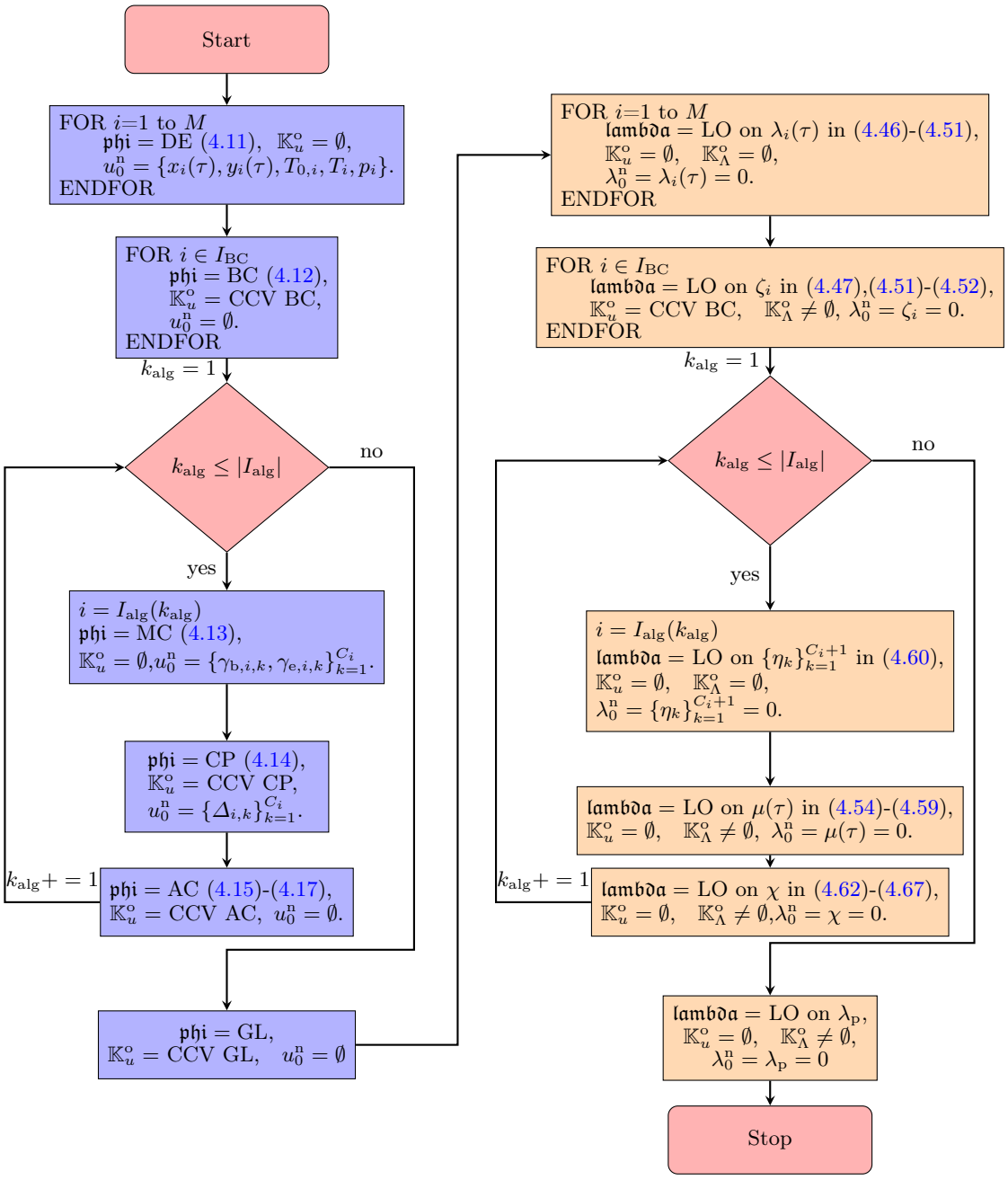

Figure 4.3: A flowchart depicting the construction of the abstract zero problem in Section 4.2.1 and corresponding contributions to adjoint conditions in Section 4.2.3. Here rectangles filled with blue and orange colors represent core constructors associated with functions of the type $\mathfrak{phi}$ and $\mathfrak{lambda}$, respectively. The abbreviations DE, BC, MC, CP, CCV, AC, GL, and LO represent diff. eqns, boundary conditions, mesh conditions, coupling conditions, corresponding continuation variables, algebraic conditions, glue conditions, and linear operators, respectively. In particular, $\mathbb{K}_u^{\text{o}}$ = CCV BC/CP/AC/GL denote indexing the corresponding continuation variables for boundary conditions/coupling conditions/algebraic conditions/glue conditions from the ones defined when constructing the differential constraints. $I_{\text{BC}} \subset \{1, \cdots, M\}$ gives the set of differential state variables involving boundary conditions. $I_{\text{alg}} \subset \{1, \cdots, M\}$ gives the collection of algebraic state variables involving coupling conditions. $k_{\text{alg}} += 1$ should be interpreted as $k_{\text{alg}} = k_{\text{alg}} + 1$.

yields

$$x'(\tau) = Tf\left(T_0 + T\tau, x(\tau), y(\tau), p\right), \ \tau \in (0,1),$$
$$y(\tau) = \begin{cases} g\left(T\tau, p\right), & \tau \in (0, \alpha/T), \\ x\left(\tau - \alpha/T\right), & \tau \in (\alpha/T, 1). \end{cases} \tag{4.121}$$

Inspired by this example, we consider coupling conditions of the form

$$y_i(\tau) = g_{i,k}\left(T_i\tau - \Delta_{i,k,1}, p\right), \tau \in (\gamma_{\mathrm{b},i,k}, \gamma_{\mathrm{e},i,k}) \tag{4.122}$$

for some $g_{i,k} : \mathbb{R} \times \mathbb{R}^q \to \mathbb{R}^n$ as an alternative to the form given in (4.14).

A further generalization of the framework introduced in Section 4.1 is support for vector fields of the form $f : \mathbb{R} \times \mathbb{R}^n \times \mathbb{R}^{n\times n_\delta} \times \mathbb{R}^q \to \mathbb{R}^n$ with coupling conditions of the form (4.14) for each column of the $n \times n_\delta$ matrix of algebraic state variables. This may be used to analyze problems with multiple discrete time delays. In combination with the implementation of coupling conditions of the form (4.122), it allows for analysis of problems with or without delay and with unknown exogenous driving terms to be determined through the optimization of an objective function, as in the theory of optimal control.

Both of these techniques are illustrated through the sequence of examples below.

4.3.2 Connecting orbits

The dynamical system

$$\dot{z}(t) = f(z(t), z(t-\alpha), p) := \begin{pmatrix} z_2(t) \\ z_1(t) - z_1(t)z_1\left(t-\alpha\right) + p_2 z_2(t) + p_1 z_1(t) z_2(t) \end{pmatrix} \tag{4.123}$$

admits equilibrium solutions at $(z_1, z_2) = (0,0)$ and $(1,0)$ for all values of the parameters p_1 and p_2 and delay α. The equilibrium at the origin is always a saddle, while that at $(1,0)$

undergoes a Hopf bifurcation with angular frequency ω provided that

$$\cos \alpha\omega = \omega^2, \sin \alpha\omega = -(p_1 + p_2)\omega. \tag{4.124}$$

For $\alpha = 0.8255$ and $p_1 = 0.5$ (cf. [104]), the bifurcation occurs for $p_2 = p_{2,\mathrm{HB}} \approx -1.257$ with $\omega \approx 0.868$. A supercritical family of limit cycles of approximate limiting form $(z_1(t) - 1, z_2(t)) \sim \sqrt{p_2 - p_{2,\mathrm{HB}}}(\omega^{-1} \sin \omega t, \cos \omega t)$ grows out of this point as p_2 increases past the critical value $p_{2,\mathrm{HB}}$.

We obtain a continuation problem for single-segment periodic orbits of the form developed in the first example in Section 4.2.2 by straightforward substitution. Since the vector field is autonomous, we let $T_0 = 0$ without loss of generality and impose the condition $x_2(0) = 0$ to fix the solution phase. We use interpolation according to (4.93) to impose the condition $x_2(\tau_{\mathrm{cr}}) = 0$ in terms of the additional continuation variable τ_{cr}. Finally, we introduce monitor functions evaluating to p_1, p_2, α, T, and τ_{cr} and denote the corresponding continuation parameters by μ_{p_1}, μ_{p_2}, μ_α, μ_T and $\mu_{\tau_{\mathrm{cr}}}$. An initial solution guess is then given by $(x_1(\tau), x_2(\tau)) = (1, 0) + 0.01(0.868^{-1} \sin(2\pi\tau - \pi/2), \cos(2\pi\tau - \pi/2))$, $T = 2\pi/0.868$, $p_1 = 0.5$, $p_2 = -1.257$, $\alpha = 0.8255$, and $\tau_{\mathrm{cr}} = 0.5$.

With $N = 100$, one-dimensional continuation with μ_{p_1} and μ_α fixed and μ_{p_2}, μ_T, and $\mu_{\tau_{\mathrm{cr}}}$ free to vary yields the one-dimensional family of limit cycles sampled in the top panel of Fig. 4.4. Notably, as seen in the bottom panel, the period T increases without bound as p_2 approaches a number close to -1.0782, suggestive of the existence of a homoclinic connecting orbit based at the saddle equilibrium at the origin, as also evident in the top panel. We may consider the periodic orbit with $T = 20$ as a first-order approximation to such a connecting orbit.

We proceed to construct a continuation problem for locating and tracking an approximate family of such connecting orbits under variations in the problem parameters and delay by

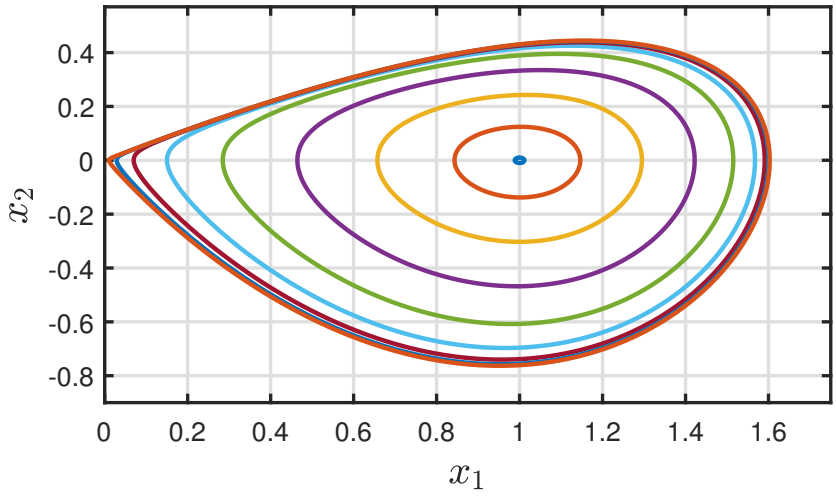

(a)

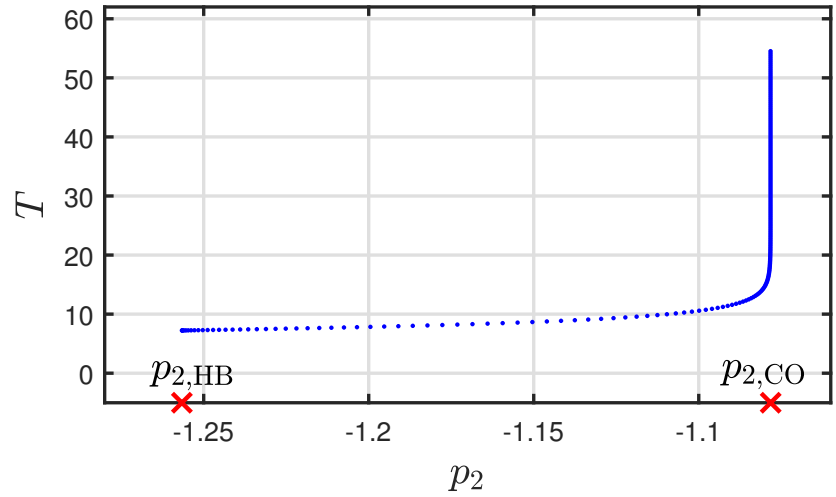

(b)

Figure 4.4: (Top) A family of periodic orbits of the dynamical system in (4.123) born from a Hopf bifurcation at $p_2 = p_{2,\mathrm{HB}}$ with fixed $p_1 = 0.5$ and $\alpha = 0.8255$ and varying T and p_2. (Bottom) The corresponding period T shows unbounded growth as a function of p_2 as a homoclinic bifurcation at $p_2 \approx p_{2,\mathrm{CO}}$ is approached.

replacing the single-segment periodic orbit coupling conditions with the equations

$$y(\tau) = \begin{cases} \epsilon v e^{\ell T(\tau - \alpha/T)}, & \tau \in (0, \alpha/T)\,, \\ x\left(\tau - \alpha/T\right), & \tau \in (\alpha/T, 1)\,, \end{cases} \tag{4.125}$$

and the periodic boundary condition with $x(0) = \epsilon v$ in terms of an unknown scalar ϵ and a normalized right eigenvector v of the Jacobian

$$A = \begin{pmatrix} 0 & 1 \\ 1 & p_2 \end{pmatrix} \tag{4.126}$$

of the linearization at the origin corresponding to the unstable eigenvalue ℓ. We impose the additional boundary condition

$$w^{\mathrm{T}} x\left(1\right) = 0 \tag{4.127}$$

in terms of a normalized left eigenvector w of A in order to ensure that the end point $x(1)$ lies in the stable eigenspace of the equilibrium at the origin. We again let $T_0 = 0$ and use interpolation according to (4.93) to impose the condition $x_2(\tau_{\mathrm{cr}}) = 0$ in terms of the additional continuation variable τ_{cr}. We introduce monitor functions evaluating to p_1, p_2, α, T, τ_{cr}, and ϵ and denote the corresponding continuation parameters by μ_{p_1}, μ_{p_2}, μ_α, μ_T, $\mu_{\tau_{\mathrm{cr}}}$, and μ_ϵ.

For fixed μ_T, μ_{p_1}, μ_{p_2}, μ_α, $\mu_{\tau_{\mathrm{cr}}}$, and μ_ϵ we obtain a continuation problem with dimensional deficit -2. We proceed to first allow μ_{p_2} and μ_ϵ to vary and obtain a unique solution by applying a nonlinear solver (`atlas_0d` in COCO) with initial solution guess given by the periodic orbit with $T = 20$, the corresponding values of p_1, p_2, α, and τ_{cr}, and $\epsilon = 10^{-3}$. Next, we fix μ_ϵ, and allow additionally μ_{p_1}, μ_α, and μ_T to vary in order to obtain a two-dimensional solution manifold and seed `atlas_kd` with the unique solution found in the previous step. The top panel of Fig. 4.5 shows the approximate homoclinic obtained with $p_1 = 0.5$ and $\alpha = 0.8255$, while the bottom panel shows the corresponding two-dimensional homoclinic bifurcation surface under simultaneous variations in p_1, p_2, and α.

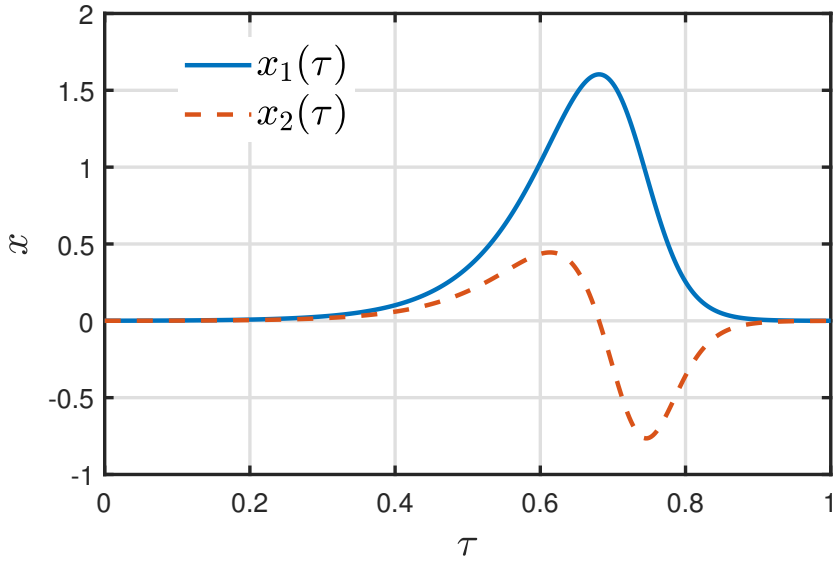

(a)

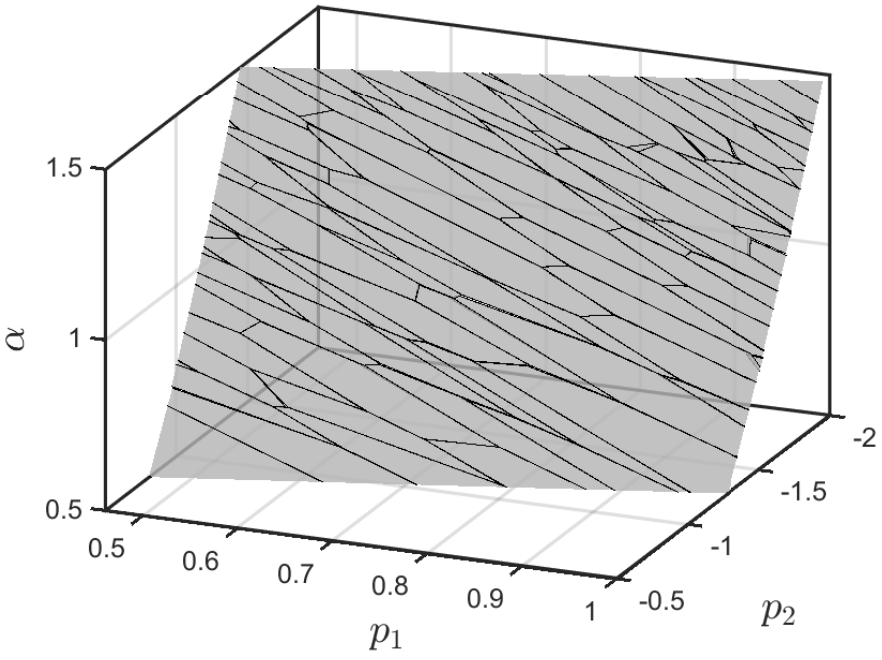

(b)

Figure 4.5: (a) Approximate connecting orbit of the delay differential equation (4.123) obtained using the proposed framework for $\alpha = 0.8255$, $p_1 = 0.5$, $p_2 \approx -1.0782$, $T = 20$, $\tau_{\text{cr}} \approx 0.6756$, $\epsilon \approx 1.3907 \times 10^{-3}$. (b) Homoclinic bifurcation surface obtained using two-dimensional continuation with COCO.

4.3.3 Phase response curves

We use the methodology in Section 2.4.1 to compute the phase response curve of a stable limit cycle of the Mackey-Glass equation [105]

$$\dot{z}(t) = \frac{az\,(t-\alpha)}{1+z^b\,(t-\alpha)} - z(t), \tag{4.128}$$

an oft-used model for the dynamics of physiological systems such as respiratory dynamics [106] and the production of white blood cells [107]. Specifically, a family of such limit cycles is born from the equilibrium at $z = (a-1)^{1/b}$ for $a = 2$ and $b = 10$ when α increases through a Hopf bifurcation at $\alpha_{\text{HB}} \approx 0.4708$ as shown in Fig. 4.6. We proceed to analyze the phase response curve for the orbit obtained with $\alpha = 0.7$.

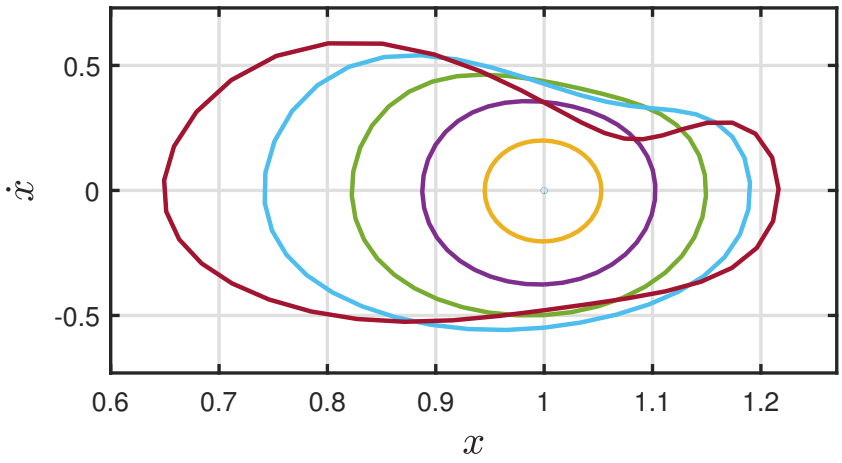

Figure 4.6: Sample orbits from a family of limit cycles of the Mackey-Glass system (4.128) with $a = 2$ and $b = 10$ emanating from a supercritical Hopf bifurcation under variations in the delay α past the critical value $\alpha_{\text{HB}} \approx 0.4708$.

With the decomposition in Section 4.2.2, we obtain

$$\begin{aligned} x'(\tau) &= T\left(\frac{ay(\tau)}{1+y^b(\tau)} - x(\tau)\right), \ \tau \in (0,1), \\ y(\tau) &= \begin{cases} x(\tau + 1 - \alpha/T), & \tau \in (0, \alpha/T), \\ x(\tau - \alpha/T), & \tau \in (\alpha/T, 1). \end{cases} \end{aligned} \tag{4.129}$$

The toolbox developed in Section 4.1 may be applied out of the box to construct the corresponding zero problems and adjoint contributions provided that we append the algebraic conditions $\gamma_{\mathrm{e},1,1} = \alpha/T$, $T_0 = 0$, and the periodicity condition $x(0) = x(1)$. Since the vector field is autonomous, we append the phase condition $x(0) = 1$ to remove the invariance to time shifts.

We proceed to append monitor functions that evaluate to T, α, a, and b with corresponding continuation parameter μ_T, μ_α, μ_a, and μ_b, respectively. We denote the continuation multipliers associated with the corresponding adjoint contributions by η_T, η_α, η_a, and η_b. Then, the phase response curve is obtained from the continuation multiplier $\lambda_{\mathrm{DE}}(\cdot)$ associated with the differential constraint at a solution to the augmented continuation problem with $\eta_T = 1$. To locate such a solution, we append a complementary zero function that evaluates to $\eta_T - 1$.

With μ_T, μ_α, μ_a, and μ_b fixed, we obtain a reduced continuation problem with dimensional deficit -1. With the Lagrange multipliers initially set to 0, we allow μ_T to vary and obtain the graphs of $x(\cdot)$ and $\lambda_{\mathrm{DE}}(\cdot)$ shown in Fig. 4.7. These agree with phase-shifted versions of the curves obtained in [96] using backward integration. A family of phase response curves computed using one-dimensional continuation under simultaneous variations of μ_T and μ_b is shown in Fig. 4.8.

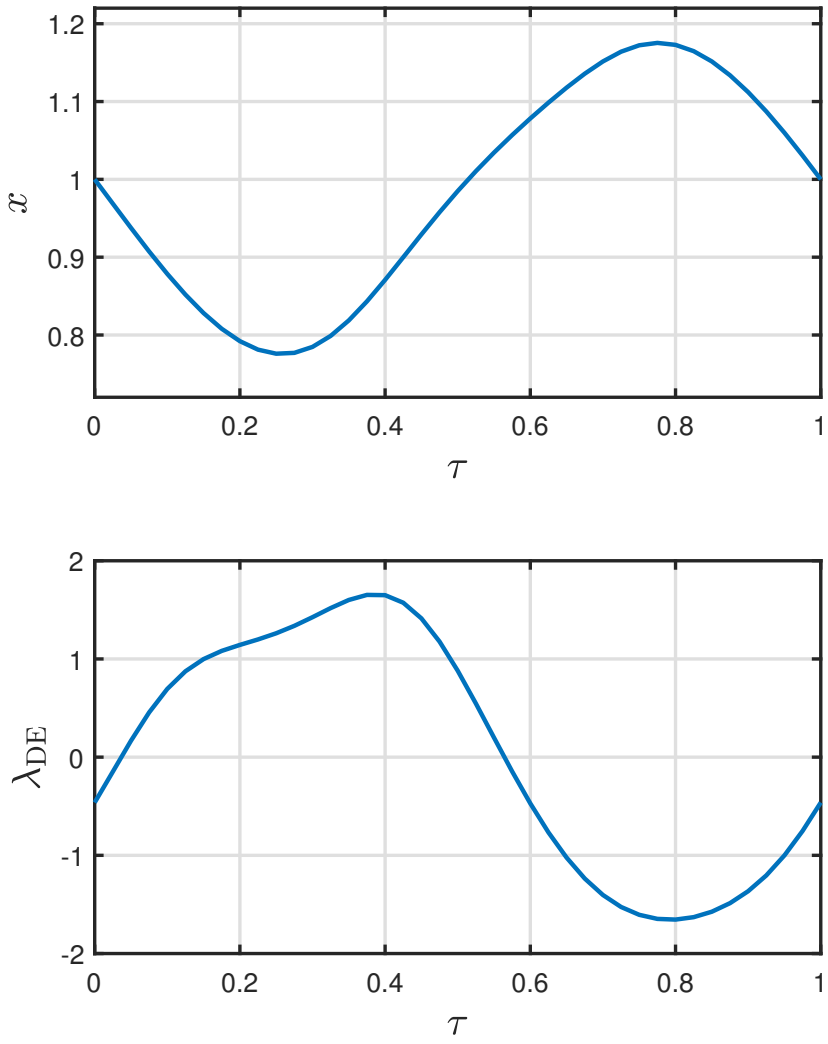

Figure 4.7: Time histories for the differential variable $x(\cdot)$ and corresponding phase response curve $\lambda_{\mathrm{DE}}(\cdot)$ for a limit cycle of the delay differential equation (4.128) with $a = 2$, $b = 10$, $\alpha = 0.7$, and $T \approx 2.2958$.

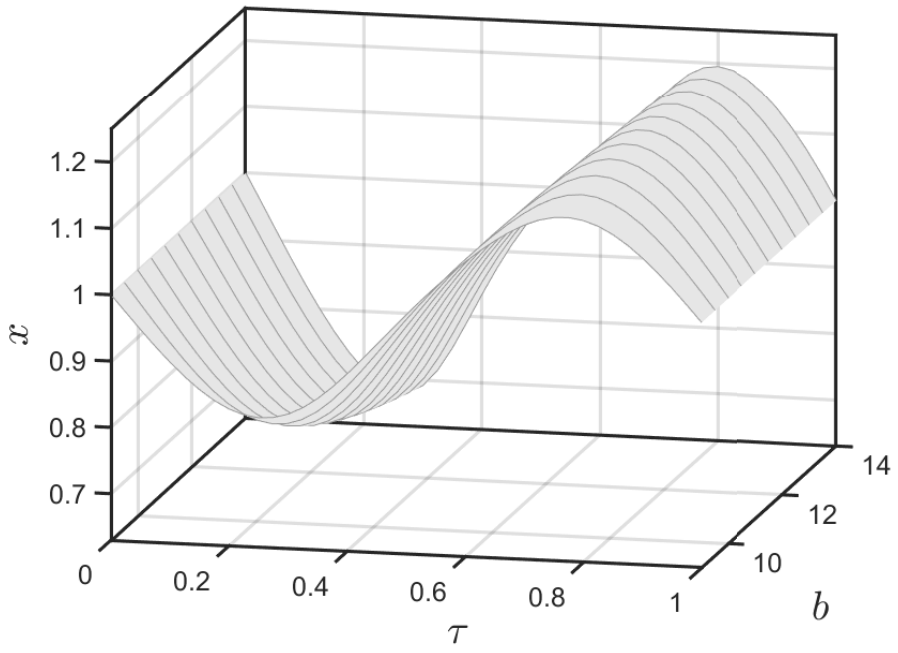

(a)

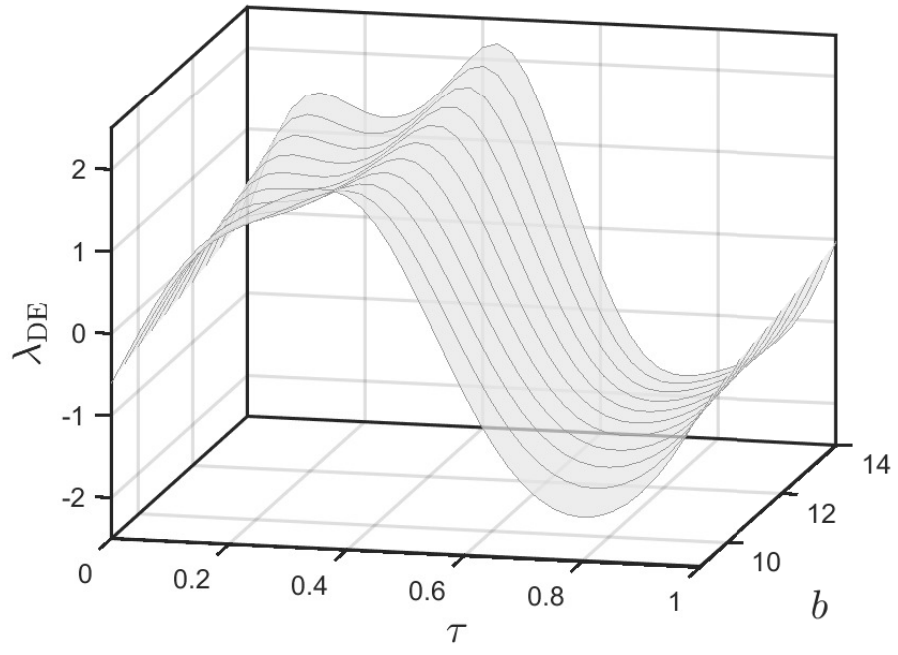

(b)

Figure 4.8: A one-parameter family of time histories for (a) the differential state variable $x(\cdot)$ and (b) corresponding phase response curve $\lambda_{\mathrm{DE}}(\cdot)$ of the delay differential equation (4.128) with $a = 2$ and $\alpha = 0.7$ under variations in b.

4.3.4 Optimal control problems

From [108], we obtain the problem of choosing a control input $u(t) \in \mathbb{R}$ that minimizes the objective functional

$$J = \int_0^2 \left(z^2 + u^2\right) \mathrm{d}t \tag{4.130}$$

subject to the initial-value problem

$$\begin{aligned} \dot{z} = tz + z\left(t-1\right) + u\left(t\right),\ t \in (0,2), \\ z\left(t\right) = 1,\ t \in [-1,0]. \end{aligned} \tag{4.131}$$

We parameterize the sought optimal control input in terms of a truncated expansion of normalized Chebyshev polynomials of the first kind $T_{c,j}$ defined on the interval $[-1,1]$. Specifically, with $x(\tau) := z(2\tau)$, we obtain

$$x'(\tau) = 4\tau x(\tau) + 2y^{(1)}(\tau) + 2y^{(2)}(\tau),\ \tau \in (0,1)\,, \tag{4.132}$$

$$y^{(1)}\left(\tau\right) = \begin{cases} 1, & \tau \in (0,1/2)\,, \\ x\left(\tau - 1/2\right), & \tau \in (1/2,1)\,, \end{cases} \tag{4.133}$$

$$y^{(2)}\left(\tau\right) = \sum_{j=1}^{q} p_j T_{c,j}(2\tau - 1),\ \tau \in (0,1)\,, \tag{4.134}$$

and boundary condition $x(0) = 1$ in terms of the *a priori* unknown coefficients p_j. With the generalization described in Section 4.3.1 for matrix-valued algebraic state variables, the toolbox developed in Section 4.1 may be applied out of the box to construct the corresponding zero problems and adjoint contributions provided that we append the algebraic conditions $\gamma_{\mathrm{e},1,1}^{(1)} = 1/2$, $T_0 = 0$, $T = 2$.

In order to search for optimal choices of the expansion coefficients, we append monitor functions that evaluate to J and $\{p_j\}_{j=1}^q$, as well as the corresponding contributions to the adjoint conditions. We denote the continuation parameters associated with J and $\{p_j\}_{j=1}^q$ by

μ_J and $\{\mu_{p_j}\}_{j=1}^q$ and the corresponding continuation multipliers by η_J and $\{\eta_{p_j}\}_{j=1}^q$. Next, we introduce additional complementary monitor functions that evaluate to η_J and $\{\eta_{p_j}\}_{j=1}^q$ and denote the corresponding complementary continuation parameters by ν_J and $\{\nu_{p_j}\}_{j=1}^q$. At the sought extremum, $\nu_J = 1$ and $\nu_{p_j} = 0$ for $j = 1, \ldots, q$. We construct an initial solution guess for the discretization of the differential state variables by integrating the initial-value problem (4.131) using the *dde23* solver in MATLAB. We use linear interpolation to construct an initial solution guess for the discretization of $y^{(1)}(\cdot)$ and initially let $p_j = 0$ for $j = 1, \ldots, q$. Finally, the Lagrange multipliers are all initialized with zero values.

With μ_J, $\{\mu_{p_j}\}_{j=1}^q$, and $\{\nu_{p_j}\}_{j=1}^q$ fixed, the dimensional deficit equals $-q-1$. We obtain the two-dimensional solution manifold in Fig. 4.9 by allowing μ_J, ν_J, μ_{p_1}, and $\{\nu_{p_j}\}_{j=1}^q$ to vary while holding $\{\mu_{p_j}\}_{j=2}^q$ fixed. We select the point with $\nu_J = 1$ and ν_{p_1} closest to 0 as initial solution guess for a second stage of continuation obtained by fixing ν_J and ν_{p_1} to 1 and 0, respectively, and allowing μ_{p_2} to vary. If we locate a point with $\nu_{p_2} = 0$ along the corresponding one-dimensional manifold, then we may continue from this point along a new one-dimensional manifold obtained by fixing ν_{p_2} at 0 and allowing μ_{p_3} to vary. Continuing in this fashion, we locate the sought extremum.

Figure 4.10 shows the locally optimal solution obtained using this methodology with $q = 8$ (here, $N = 10$ and $m = 4$). At this solution, $J = J_8 \approx 4.797$, is in excellent agreement with the minimum reported in [108] using stochastic optimization. Table 4.1 demonstrates the rapid convergence of the locally optimal value $J = J_q$ with the expansion order q anticipated from the use of Chebyshev polynomials and the smoothness of the optimal solution.

Table 4.1: The error $E = |(J_q - J_8)/J_8|$ decays rapidly with increasing truncation order q for the optimal control problem (4.130)-(4.131).

q	1	2	3	4	5	6	7
E	4.3×10^{-1}	4.8×10^{-3}	9.7×10^{-6}	2.6×10^{-5}	2.7×10^{-5}	2.8×10^{-5}	8×10^{-6}

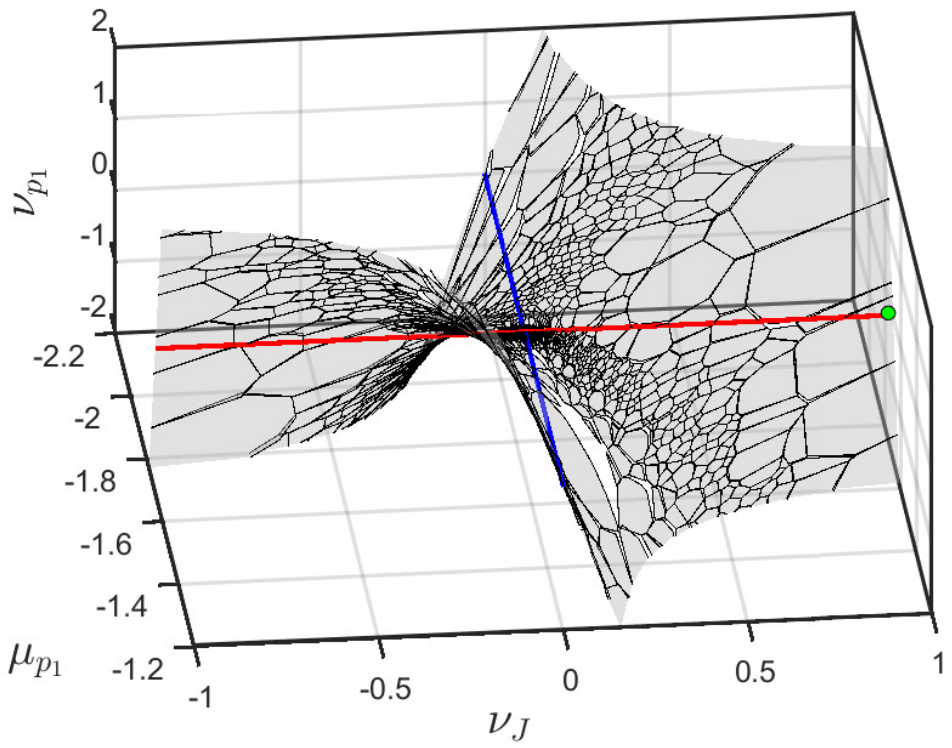

Figure 4.9: Projection of a two-dimensional solution manifold for the optimal control problem (4.130–4.131) and the corresponding adjoint equations obtained using the `atlas_kd` atlas algorithm by allowing μ_J, ν_J, μ_{p_1}, and $\{\nu_{p_j}\}_{j=1}^{q}$ to vary while holding $\{\mu_{p_j}\}_{j=2}^{q}$ fixed. As in Section 2.2.1, the zero-level curves of ν_{p_1} on this manifold are two straight lines with $\nu_J = 0$ (blue) and μ_{p_1} (red) constant, respectively, that intersect at a stationary point of μ_J along the first curve. The solution with $\nu_J = 1$ and $\nu_{p_1} = 0$ (green circle) can be located (to within desired tolerance) by continuation along the first of these straight lines, followed by branch switching and continuation along the second of these lines. Alternatively, it may be approximated by the solution point on the intersection of the two-dimensional manifold with the $\nu_J = 1$ coordinate plane (located within desired tolerance) with ν_{p_1} closest to zero.

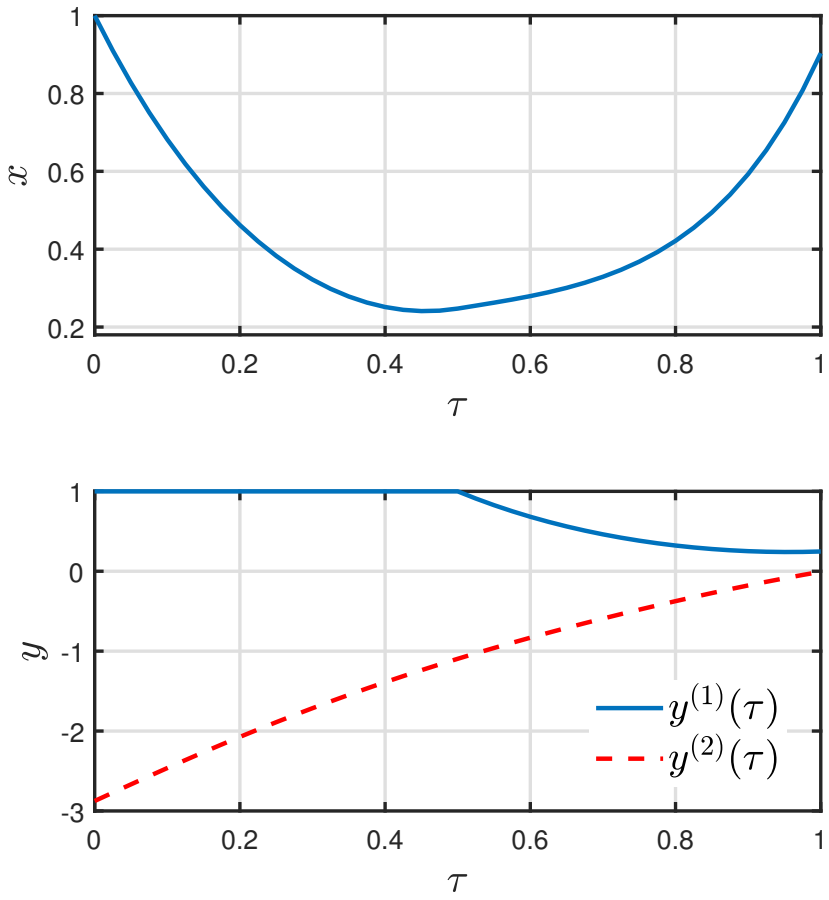

Figure 4.10: State variables at a local minimum for the optimal control problem (4.130–4.131).

4.3.5 Quasiperiodic orbits

As a final example, studied previously in [1], we consider the problem of locating stationary values of ω along a family of quasiperiodic invariant tori of the delay differential equations

$$\dot{z}(t) = f(t, z(t), z(t-\alpha), p) := \begin{pmatrix} -\omega z_2(t) + z_1(t-\alpha)\left(1 + r(t)\left(\cos 2\pi t/T - 1\right)\right) \\ \omega z_1(t) + z_2(t-\alpha)\left(1 + r(t)\left(\cos 2\pi t/T - 1\right)\right) \end{pmatrix} \quad (4.135)$$

with $r = \sqrt{z_1^2 + z_2^2}$. By applying the analysis of the third example in Section 4.2.2 in reverse, we obtain the delay-coupled multi-segment boundary-value problem in (4.36)-(4.37). The toolbox developed in Section 4.1 may be applied out of the box to construct the corresponding zero problem and adjoint contributions provided that we append the algebraic conditions

$T_{0,i} = 0$, $T_i = T$, and $\gamma^{(1)}_{\mathrm{e},i,1} = \alpha/T$ for $i = 1, \ldots, M$. The additional phase condition $x_{1,2}(0) = 1$ restricts attention to a unique family of trajectory segments discretizing a quasiperiodic invariant torus.

In order to search for extremal values of ω, we proceed to append monitor functions that evaluate to ω, T and α, respectively, and denote the corresponding continuation parameters by μ_ω, μ_T, and μ_α. We denote the continuation multipliers associated with the corresponding adjoint contributions by η_ω, η_T and η_α. Next, we introduce complementary monitor functions that evaluate to $\eta_\omega, \eta_T, \eta_\alpha$ and denote the corresponding complementary continuation parameters by ν_ω, ν_T and ν_α. At a stationary point of ω, we must have $\nu_\omega = 1, \nu_T = \nu_\alpha = 0$.

For the special case with $\alpha = 0$ (this case is considered in the tutorial documentation for the COCO-compatible `coll` toolbox), a one-parameter family of quasiperiodic orbits covering an invariant torus for the delay differential equation (4.135) is given by

$$z(T_0 + T\tau; \varphi) = x(\varphi, \tau) = \left(r\left(\tau\right)\cos\left(2\pi\varrho\tau + \varphi\right), r\left(\tau\right)\sin\left(2\pi\varrho\tau + \varphi\right)\right), \ \varphi \in \mathbb{S} \tag{4.136}$$

where

$$r\left(\tau\right) = \frac{1 + \Omega^2}{1 + \Omega^2 - \cos 2\pi\tau - \Omega \sin 2\pi\tau}, \tag{4.137}$$

$\Omega = 2\pi/T$, and ϱ is an irrational number. With the substitution $x_i(\tau) = x(2\pi(i-1)/M, \tau)$ we obtain an initial solution guess for the i-th trajectory segment of the corresponding boundary-value problem. Here, we initialize continuation with $\omega = 1$ and $\Omega = 1.5$ and set the rotation number ρ to 0.6618. We use the initial guess for the problem with $\alpha = 0$ along with continuation in α to obtain the differential state variables for nonzero α.

With $\mu_\omega, \mu_T, \mu_\alpha, \nu_\omega, \nu_T, \nu_\alpha$ fixed, the problem has a dimensional deficit of -3. We obtain a dimensional deficit of 1 by allowing $\mu_\omega, \mu_T, \nu_\omega, \nu_\alpha$ to vary. The dashed-dotted line in Fig. 4.11(a) shows the corresponding solution manifold with trivial Lagrange multipliers obtained with $\mu_\alpha = 0.75$. Through the local maximum in ω (denoted by the red sphere) at $(\mu^\star_\omega, \mu^\star_T, \mu^\star_\alpha) \approx (0.773, 3.601, 0.75)$ runs a secondary branch of solutions along which ν_ω (and

the other Lagrange multipliers) vary. We locate a unique point on this branch with $\nu_\omega = 1$. Continuation along the one-dimensional solution manifold through this point obtained by fixing ν_ω at 1 and allowing μ_α to vary yields a family of local maxima of ω under variations in T (solid black curve in Fig. 4.11(a)). Within the chosen computational domain, we do not find a point along this manifold where $\nu_\alpha = 0$.

The successive continuation approach used here may yield different families of stationary points depending on the initial solution guess and the order in which initially-fixed continuation parameters are allowed to vary. For example, if we repeat the above analysis with an initial value of $\mu_\alpha = 1.2$, then the one-dimensional solution manifold with trivial Lagrange multipliers has two local maxima and one local minimum in μ_ω within the computational domain, as depicted by the dashed-dotted line in Fig. 4.11(b) and Fig. 4.12. The red sphere in Fig. 4.11(b) denotes one such local maximum at $(\mu_\omega^\star, \mu_T^\star, \mu_\alpha^\star) \approx (0.305, 6.62, 1.2)$. We may again switch to a secondary branch through this point in order to locate a point with $\nu_\omega = 1$ and then continue along a one-dimensional manifold with ν_ω fixed at 1 and varying μ_α corresponding to a family of stationary points of μ_ω under variations in μ_T. The latter manifold is found to equal that obtained in the previous paragraph. The identical methodology applied to the other stationary points on the original solution branch located at $(\mu_\omega^\star, \mu_T^\star, \mu_\alpha^\star) \approx (0.202, 4.229, 1.2)$ and $(0.181, 4.724, 1.2)$ (black spheres in Fig. 4.12) yields a single curve of stationary points (solid red curve in Fig. 4.12) of μ_ω under variations in μ_T. Although μ_ω achieves a local maximum along this manifold, ν_α does not equal 0 at any point along this curve, and we again conclude that there does not exist a stationary point of μ_ω with respect to variations in both μ_T and μ_α within the chosen computational domain.

The same conclusion is obtained by holding μ_T fixed initially while allowing μ_α to vary along a one-dimensional manifold with trivial Lagrange multipliers. For example, with μ_T fixed at 8.37, we locate a local minimum and a local maximum in the value of μ_ω at $\mu_\alpha = 2.04$ and 2.49. Through each of these points runs a secondary branch along which ν_ω varies. The unique point with $\nu_\omega = 1$ on each of these secondary branches may be used to continue

along a one-dimensional solution manifold with ν_ω fixed at 1 and μ_T allowed to vary. Such a manifold corresponds to a curve of stationary points of μ_ω with respect to μ_α. As shown in Fig. 4.13, we obtain a single such curve which does not intersect the curve of stationary points of μ_ω with respect to μ_T at any point in the computational domain. These observations are consistent with the visualization in Fig. 4.14 of the two-dimensional solution manifold obtained by allowing μ_ω, μ_α, and μ_T to vary.

4.4 Conclusions

In this chapter, we proposed a COCO-compatible toolbox template for a large class of delay-coupled, multi-segment boundary-value problems. Extensions of this template that consider adaptive remeshing of the discretized equations and automated encapsulation of the required toolbox data from user defined input is discussed in Chapter 7. In the next chapter, we take a different turn and consider the analysis of uncertainty quantification problems using adjoints.

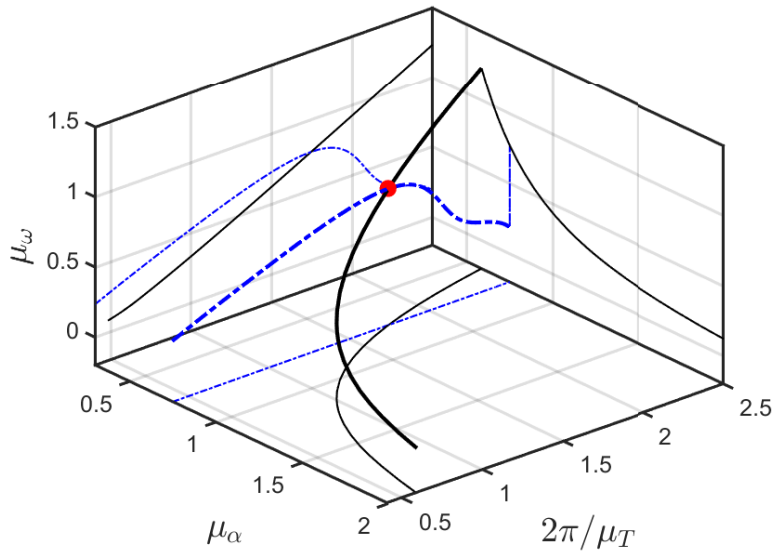

(a)

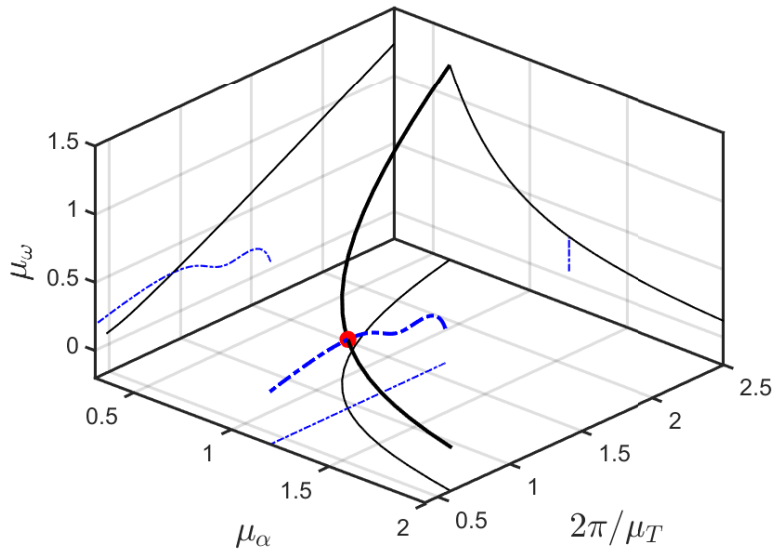

(b)

Figure 4.11: Curves (solid) of local stationary points of μ_ω with respect to variations in μ_T along approximate families of quasiperiodic invariant tori for the delay differential equation (4.135) obtained by first continuing along a one-dimensional manifold with trivial Lagrange multipliers and fixed μ_α (dashed), then switching at a local stationary point to a branch with varying Lagrange multipliers, and finally fixing ν_ω at 1 and allowing μ_T to vary. (a) Initial continuation with $\mu_\alpha = 0.75$ and branch switching at a unique local maximum. (b) Initial continuation with $\mu_\alpha = 1.2$ and branch switching at one of the two local maxima. The final manifold coincides with that obtained in (a).

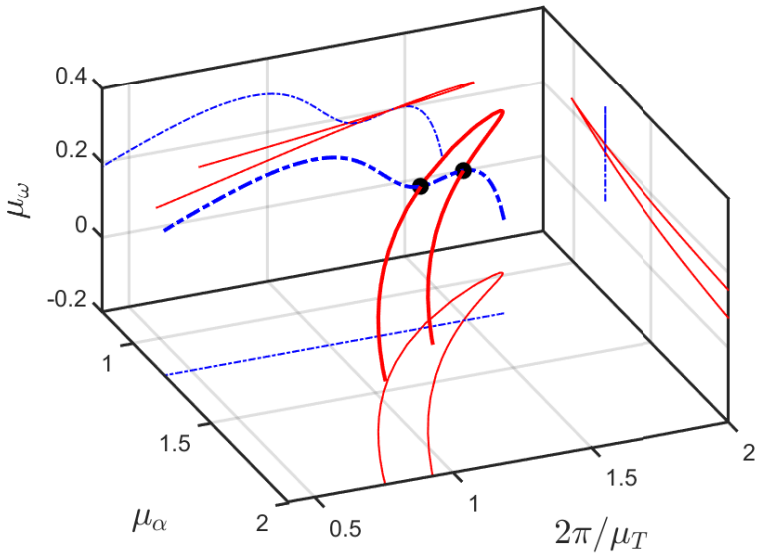

Figure 4.12: Curves (solid) of local stationary points of μ_ω with respect to variations in μ_T along approximate families of quasiperiodic invariant tori for the delay differential equation (4.135) obtained by first continuing along a one-dimensional manifold with trivial Lagrange multipliers and fixed μ_α (dashed), then switching at a local stationary point to a branch with varying Lagrange multipliers, and finally fixing ν_ω at 1 and allowing μ_T to vary. Initial continuation with $\mu_\alpha = 1.2$ and branch switching at either of the local minimum or other local maximum. The final manifolds obtained in these two cases coincide.

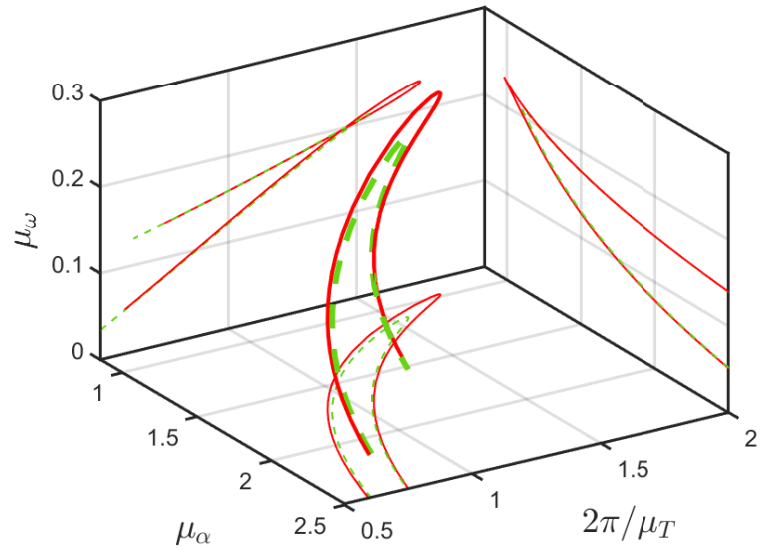

Figure 4.13: Curves of stationary points of μ_ω with respect to μ_T (solid) and μ_α (dashed) along approximate families of quasiperiodic invariant tori for the delay differential equation (4.135). The two curves never intersect within the chosen computational domain.

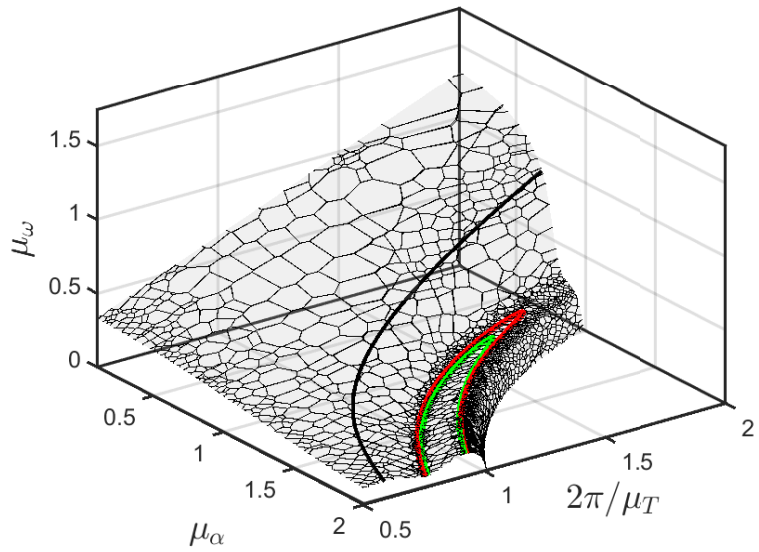

(a) View 1

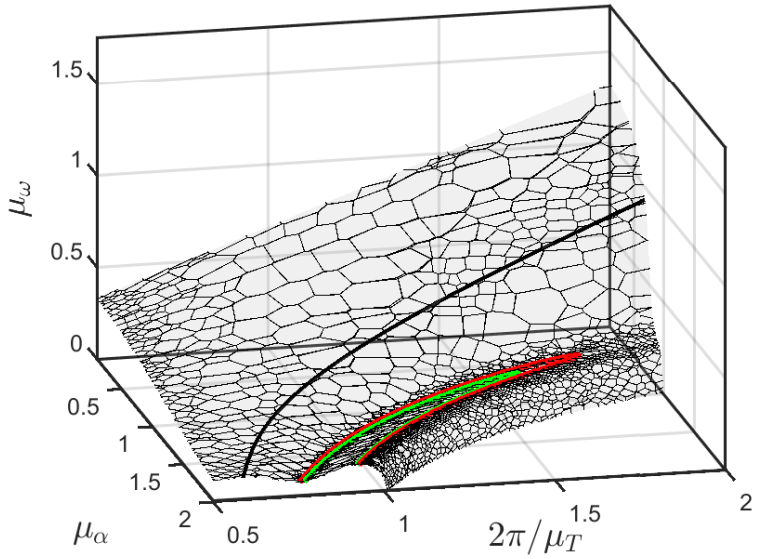

(b) View 2

Figure 4.14: An approximate family of quasiperiodic invariant tori for the delay differential equation (4.135) obtained using two-dimensional continuation in COCO. Highlighted curves consist of stationary points of μ_ω with respect to μ_T (red and black) and stationary points of μ_ω with respect to μ_α (green) located using the corresponding augmented continuation problem.

Chapter 5

NOISE INDUCED BEHAVIOR NEAR DETERMINISTIC LIMIT CYCLES

In this chapter[1], we derive a covariance boundary-value problem that captures the effects of noise on the local behavior near stable periodic orbits of some deterministic dynamical system. The formulation relies on suitably constructed adjoint variables to project the dynamics onto locally transversal hyperplanes and ensures the existence of a unique solution. For each such hyperplane, the computed covariance matrix describes an approximately Gaussian, stationary distribution that highlights directions away from the limit cycle of particular sensitivity to noise. In contrast to previous formulations, the boundary-value problem analyzed in this study makes predictions in the original state-space variables rather than in terms of a reduced set of local coordinates for hyperplanes perpendicular to the local vector field. The formulation is compatible with the general form of an augmented continuation problem for the software package COCO; a non-adaptive version has been implemented as a general-purpose constructor for the periodic-orbit toolbox included in the COCO release. We illustrate the efficacy of the proposed formulation and toolbox by analyzing noise-induced behavior near limit cycles in two examples of nonlinear dynamical systems with autonomous drift terms.

In contrast to previous chapters, here we make use of adjoints for uncertainty quantification near periodic orbits. Section 5.1 deals with the mathematical preliminaries to project the dynamics onto hyperplanes defined by the adjoint variables. We show that on each of these

[1]The content of this chapter is partially reproduced from [51] Ahsan, Kuehn, and Dankowicz, 2022, "A covariance boundary value problem for stochastically perturbed limit cycles", Proceedings of the IDETC-CIE, St. Louis, Missouri, August 14-17, 2022, ASME (accepted manuscript).

hyperplanes there exists a unique covariance matrix. Next, in Section 5.2, we propose a corresponding boundary-value problem that may be solved for the covariance function along the periodic orbit and be embedded in a continuation problem for studying the effects of parameter variations. The theory is applied in Section 5.3 to a planar stochastic differential equation (SDE), for which explicit expressions may be obtained and verified against numerical simulations. Key implementation aspects of our formulation in the context of the software package COCO are presented in Section 5.4. This implementation is then used to perform further numerical study of the planar problem, as well as of an SDE governing noise-induced dynamics near a limit-cycle oscillation of a nonlinear mechanical oscillator network.

5.1 Mathematical preliminaries

Consider the Itô SDE

$$\mathrm{d}x = f\left(x\right)\mathrm{d}t + \sigma F\left(x\right)\mathrm{d}W_t, \tag{5.1}$$

in terms of an autonomous *drift* $f : \mathbb{R}^n \mapsto \mathbb{R}^n$ and *dispersion matrix* $F : \mathbb{R}^n \mapsto \mathbb{R}^{n\times m}$, noise level σ, and m-dimensional vector W_t of independent standard Brownian motions. In the absence of noise, we assume that the system has an asymptotically stable limit cycle $\tilde{x}(t)$ of period $\tilde{T}$, i.e., such that the eigenvalues of the corresponding monodromy matrix all lie within the unit circle.

As illustrated in Fig. 5.1, when a reasonably small amount of noise is present in the system, we expect that trajectories will be more likely to stay close to $\tilde{x}(t)$. Provided that we are concerned only with the local behavior in the vicinity of the limit cycle and given some distribution for the initial perturbation away from some point $\tilde{x}(0)$ on the limit cycle, we anticipate convergence of intersections in any sufficiently transversal hyperplane through any arbitrary point along the limit cycle to a stationary distribution that is approximately Gaussian with mean given by the corresponding point on the limit cycle. It follows that the likelihood of finding sample paths near any such point may be determined by a suitably defined

positive-definite covariance matrix. Once this is computed, we may construct concentric tubular neighborhoods about the limit cycle that intersect the corresponding hyperplanes in multi-dimensional ellipsoids with axes defined by the eigenvectors and eigenvalues of the corresponding covariance matrices. An example of such a tubular neighborhood is sketched in Fig. 5.1 (c) in terms of a size h. We expect that the probability of finding a sample path inside such a tubular neighborhood remains unchanged by a scaling $\sigma \mapsto \alpha\sigma$, $h \mapsto h/\alpha$.

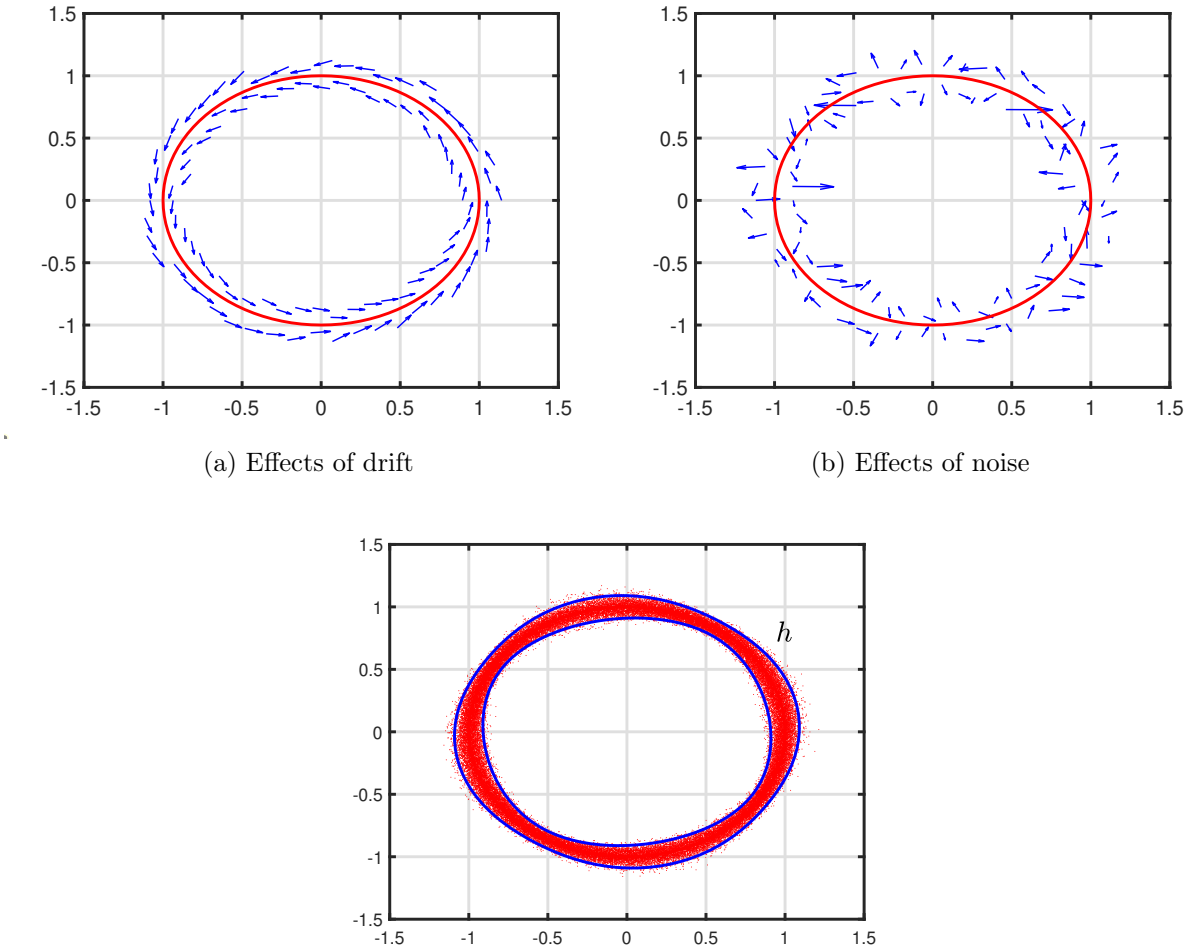

(a) Effects of drift

(b) Effects of noise

(c) Stochastic trajectories

Figure 5.1: Schematic representation of the competition between the stabilization due to eigenvalues and the destabilizing effects of noise for a planar limit cycle (red circle). Illustration of (a) the stabilizing effects of the drift, (b) the destabilizing effects of noise and (c) the resultant stochastic trajectories near the limit cycle that lie within high likelihood within some annular neighborhood.

In contrast to a previously documented formalism [47] in terms of projections onto hyperplanes perpendicular to the local vector field along the limit cycle, we here choose a continuous family of hyperplanes perpendicular to the solution $\tilde{\lambda}$ of the adjoint boundary-value problem

$$0 = -\dot{\lambda}^{\mathrm{T}}(t) - \lambda^{\mathrm{T}}(t)\partial_x f(\tilde{x}(t)), \tag{5.2}$$

$$0 = \lambda^{\mathrm{T}}(\tilde{T}) - \lambda_{\mathrm{bc}}^{\mathrm{T}}, \tag{5.3}$$

$$0 = -\lambda^{\mathrm{T}}(0) + \lambda_{\mathrm{bc}}^{\mathrm{T}} + \lambda_{\mathrm{ps}} h_x(x(0)), \tag{5.4}$$

$$0 = \eta_T - \lambda_{\mathrm{bc}}^{\mathrm{T}} f(x(\tilde{T})), \tag{5.5}$$

with $\eta_T = 1$. As seen in Section 2.4, provided that $h_x(\tilde{x}(0))f(\tilde{x}(0)) \neq 0$, this is equivalent to the periodic boundary-value problem

$$0 = -\dot{\lambda}^{\mathrm{T}}(t) - \lambda^{\mathrm{T}}(t)\partial_x f(\tilde{x}(t)),\ \lambda(\tilde{T}) = \lambda(0), \tag{5.6}$$

where $\lambda^{\mathrm{T}}(t)f(\tilde{x}(t)) = 1$ must hold. It follows that the operator [109]

$$\tilde{Q}(t) = I - f(\tilde{x}(t))\tilde{\lambda}^{\mathrm{T}}(t) \tag{5.7}$$

is a projection along $f(\tilde{x}(t))$ onto a plane perpendicular to $\tilde{\lambda}(t)$, since $\tilde{Q}^2(t) = \tilde{Q}(t)$, $\tilde{\lambda}^{\mathrm{T}}(t)\tilde{Q}(t) = 0$ and $\tilde{Q}(t)f(\tilde{x}(t)) = 0$. For later reference, we obtain

$$\dot{\tilde{Q}} = \partial_x f(\tilde{x})\tilde{Q} - \tilde{Q}\partial_x f(\tilde{x}) \tag{5.8}$$

Indeed, as also shown in [109], if $\tilde{X}(t)$ satisfies the variational problem

$$\dot{X}(t) = \partial_x f(\tilde{x}(t))X(t),\ X(0) = I \tag{5.9}$$

then

$$\tilde{X}(t)f(\tilde{x}(0) = f(\tilde{x}(t)) \tag{5.10}$$

and

$$\tilde{\lambda}^{\mathrm{T}}(t)\tilde{X}(t) \equiv \tilde{\lambda}^{\mathrm{T}}(0) = \tilde{\lambda}^{\mathrm{T}}(\tilde{T}) = \tilde{\lambda}^{\mathrm{T}}(\tilde{T})\tilde{X}(\tilde{T}), \tag{5.11}$$

i.e., that $\tilde{\lambda}(\tilde{T})$ and $f(\tilde{x}(\tilde{T}))$, respectively, span the left and right eigenspaces of the monodromy matrix $\tilde{X}(\tilde{T})$ corresponding to the eigenvalue 1. It follows that

$$\begin{aligned}\tilde{X}^{-1}(t)\tilde{Q}(t) &= \tilde{X}^{-1}(t) - \tilde{X}^{-1}(t)f(\tilde{x}(t))\tilde{\lambda}^{\mathrm{T}}(t) \\ &= \tilde{X}^{-1}(t) - f(\tilde{x}(0))\tilde{\lambda}^{\mathrm{T}}(0)\tilde{X}^{-1}(t) = \tilde{Q}(0)\tilde{X}^{-1}(t),\end{aligned} \tag{5.12}$$

and consequently that

$$\tilde{Q}(t)\tilde{X}(t) = \tilde{X}(t)\tilde{Q}(0) \tag{5.13}$$

i.e., that the family of hyperplanes is invariant under the linearized flow.

As shown in [109], for $x(t) \approx \tilde{x}(\tau)$ for some τ, the scalar equation

$$\tilde{\lambda}^{\mathrm{T}}(\varpi(t))(x(t) - \tilde{x}(\varpi(t)) = 0 \tag{5.14}$$

defines $\varpi(t)$ uniquely on a neighborhood of τ, such that $\varpi(t) = \tau$ if $x(t) = \tilde{x}(\tau)$. It follows that there exists a unique $x_{\mathrm{tr}}(t) := x(t) - \tilde{x}(\varpi(t))$, such that $\tilde{Q}(\varpi(t))x_{\mathrm{tr}}(t) = x_{\mathrm{tr}}(t)$. Moreover, by generalizing a result from [109] for the deterministic case, we obtain

$$\mathrm{d}x_{\mathrm{tr}} = \partial_x f(\tilde{x}(t))x_{\mathrm{tr}}\mathrm{d}t + \sigma\tilde{Q}(t)F(\tilde{x}(t))\mathrm{d}W_t \tag{5.15}$$

to lowest order in σ and the deviation $x_{\rm tr}$. This may be solved explicitly to yield

$$\begin{aligned} x_{\rm tr}(t) &= \tilde{X}(t)x_{\rm tr}(0) + \sigma\tilde{X}(t)\int_0^t \tilde{X}^{-1}(\tau)\tilde{Q}(\tau)F(\tilde{x}(\tau))\mathrm{d}W_\tau \\ &= \tilde{X}(t)x_{\rm tr}(0) + \sigma\tilde{Q}(t)\tilde{X}(t)\int_0^t G(\tau)\mathrm{d}W_\tau, \end{aligned} \tag{5.16}$$

where $G(\tau) = \tilde{X}^{-1}(\tau)F(\tilde{x}(\tau))$.

We proceed to define the rescaled covariance matrix

$$C(t) = \frac{1}{\sigma^2}\mathbb{E}\left[x_{\rm tr}(t)x_{\rm tr}^{\rm T}(t)\right], \tag{5.17}$$

such that $\tilde{\lambda}^{\rm T}(t)C(t)\tilde{\lambda}(t) = 0$ by (5.14). It follows from the definition and the invariance condition (5.13) that

$$C(t) = \tilde{X}(t)C(0)\tilde{X}^{\rm T}(t) + \tilde{Q}(t)\tilde{X}(t)\left(\int_0^t G(\tau)G^{\rm T}(\tau)\mathrm{d}\tau\right)\tilde{X}^{\rm T}(t)\tilde{Q}^{\rm T}(t) \tag{5.18}$$

where we used the stochastic equalities [110]

$$\mathbb{E}\left[\int_0^T Y(\tau)\mathrm{d}W_\tau\right] = 0 \tag{5.19}$$

and

$$\mathbb{E}\left[\int_0^t Y(\tau)\mathrm{d}W_\tau\int_0^t Z^{\rm T}(\tau)\mathrm{d}W_\tau\right] = \int_0^t Y(\tau)Z^{\rm T}(\tau)\mathrm{d}\tau. \tag{5.20}$$

By the anticipated asymptotic convergence toward a stationary probability distribution, it now follows that we seek a solution to this integral equation, such that $C(\tilde{T}) = C(0)$, i.e., a solution to the linear algebraic system

$$C(0) = \tilde{X}(\tilde{T})C(0)\tilde{X}^{\rm T}(\tilde{T}) + \tilde{Q}(\tilde{T})\tilde{X}(\tilde{T})\left(\int_0^{\tilde{T}} G(\tau)G^{\rm T}(\tau)\mathrm{d}\tau\right)\tilde{X}^{\rm T}(\tilde{T})\tilde{Q}(\tilde{T}) \tag{5.21}$$

that also satisfies the condition

$$\tilde{\lambda}^{\mathrm{T}}(0)C(0)\tilde{\lambda}(0) = 0. \tag{5.22}$$

Indeed, the existence and uniqueness of a solution $C(0)$ such that the function $C(t)$ satisfies $\tilde{\lambda}^{\mathrm{T}}(t)C(t)\tilde{\lambda}(t) = 0$ may be shown as follows. First, note that since $\tilde{\lambda}^{\mathrm{T}}\tilde{Q} = 0$ and $\tilde{\lambda}^{\mathrm{T}}\tilde{X} = \tilde{\lambda}^{\mathrm{T}}(0)$,

$$\begin{aligned}\tilde{\lambda}^{\mathrm{T}}(t)C(t)\tilde{\lambda}(t) &= \tilde{\lambda}^{\mathrm{T}}(t)\tilde{X}(t)C(0)\tilde{X}^{\mathrm{T}}(t)\tilde{\lambda}(t) \\ &\quad + \tilde{\lambda}^{\mathrm{T}}(t)\tilde{Q}(t)\tilde{X}(t)\left(\int_0^t G(\tau)G^{\mathrm{T}}(\tau)\mathrm{d}\tau\right)\tilde{X}^{\mathrm{T}}(t)\tilde{Q}^{\mathrm{T}}(t)\tilde{\lambda}(t) \\ &= \tilde{\lambda}^{\mathrm{T}}(0)C(0)\tilde{\lambda}(0),\end{aligned} \tag{5.23}$$

i.e., that $\tilde{\lambda}^{\mathrm{T}}(t)C(t)\tilde{\lambda}(t)$ is constant. Next, for large k, it follows from [109] that

$$\tilde{X}(k\tilde{T}) = f(\tilde{x}(0))\tilde{\lambda}^{\mathrm{T}}(0) + \mathcal{O}\left(\exp(-k/\tau_{\mathrm{tr}})\right), \tag{5.24}$$

where τ_{tr} is a positive constant. Then, since $C(k\tilde{T}) = C(0)$, it follows that

$$C(0) = \tilde{X}(k\tilde{T})C(0)\tilde{X}^{\mathrm{T}}(k\tilde{T}) + \tilde{Q}(0)\tilde{X}(k\tilde{T})\left(\int_0^{k\tilde{T}} G(\tau)G^{\mathrm{T}}(\tau)\mathrm{d}\tau\right)\tilde{X}^{\mathrm{T}}(k\tilde{T})\tilde{Q}(0), \tag{5.25}$$

for any k, since $\tilde{Q}(k\tilde{T}) = \tilde{Q}(0)$. Here,

$$\begin{aligned}\int_0^{k\tilde{T}} G(\tau)G^{\mathrm{T}}(\tau)\mathrm{d}\tau &= \sum_{l=1}^{k}\int_{(l-1)\tilde{T}}^{l\tilde{T}} G(\tau)G^{\mathrm{T}}(\tau)\mathrm{d}\tau \\ &= \sum_{l=1}^{k}\tilde{X}^{-1}((l-1)\tilde{T})\left(\int_0^{\tilde{T}} G(\rho)G^{\mathrm{T}}(\rho)\mathrm{d}\rho\right)\tilde{X}^{-1,\mathrm{T}}((l-1)\tilde{T}) \\ &= \sum_{n=1}^{k}\tilde{X}^{-1}((k-n)\tilde{T})\left(\int_0^{\tilde{T}} G(\rho)G^{\mathrm{T}}(\rho)\mathrm{d}\rho\right)\tilde{X}^{-1,\mathrm{T}}((k-n)\tilde{T}),\end{aligned} \tag{5.26}$$

since $G(\tau) = \tilde{X}^{-1}(\tau)F(\tilde{x}(\tau))$ and $\tilde{X}((l-1)\tilde{T}+\rho) = \tilde{X}(\rho)\tilde{X}((l-1)\tilde{T})$. For sufficiently large

k, the right-hand side of (5.25) is then approximately equal to

$$\sum_{n=1}^{\infty} \tilde{Q}(0)\tilde{X}(n\tilde{T}) \left(\int_0^{\tilde{T}} G(\rho)G^{\mathrm{T}}(\rho)\mathrm{d}\rho \right) \tilde{X}^{\mathrm{T}}(n\tilde{T})\tilde{Q}^{\mathrm{T}}(0) \tag{5.27}$$

which converges to a finite value, since

$$\tilde{Q}(0)\tilde{X}(n\tilde{T}) \left(\int_0^{\tilde{T}} G(\rho)G^{\mathrm{T}}(\rho)\mathrm{d}\rho \right) \tilde{X}^{\mathrm{T}}(n\tilde{T})\tilde{Q}^{\mathrm{T}}(0) = \mathcal{O}(\exp(-2n/\tau_{\mathrm{tr}})) \tag{5.28}$$

for large n.

5.2 Covariance boundary value problem

By differentiation of (5.18), we obtain

$$\dot{C} = \partial_x f(\tilde{x})C + C\partial_x f^{\mathrm{T}}(\tilde{x}) + \tilde{Q}F(\tilde{x})F^{\mathrm{T}}(\tilde{x})\tilde{Q}^{\mathrm{T}} \tag{5.29}$$

The corresponding boundary-value problem obtained by imposing periodicity $C(\tilde{T}) = C(0)$ and the initial condition $\tilde{\lambda}^{\mathrm{T}}(0)C(0)\tilde{\lambda}(0) = 0$ has a unique solution but appears over-determined as the nominal dimensional deficit equals -1. To resolve this conundrum and inspired by a well-known technique for continuation of periodic orbits in conservatives systems [111], we resort to introducing an additional auxiliary unknown into the differential equation by adding the term $\alpha f(\tilde{x})f^{\mathrm{T}}(\tilde{x})$, which we anticipate will lead to a non-degenerate solution with $\alpha = 0$. Indeed, with this addition,

$$\frac{\mathrm{d}}{\mathrm{d}t} \left(\tilde{\lambda}^{\mathrm{T}}(t)C(t)\tilde{\lambda}(t) \right) = \alpha, \tag{5.30}$$

but since both $\tilde{\lambda}$ and C are periodic, α must equal 0.

It follows that the covariance matrix for a given point $\tilde{x}(t)$ along the limit cycle and relative to a hyperplane perpendicular to the vector $\tilde{\lambda}(t)$ may be obtained from a solution

$\left(\tilde{x}(t), \tilde{T}, \tilde{\lambda}(t), \tilde{C}(t), \tilde{\alpha}\right)$ to the boundary-value problem

$$0 = \dot{x} - f(x,p), \tag{5.31}$$

$$0 = x(0) - x(T), \tag{5.32}$$

$$0 = h(x(0),p), \tag{5.33}$$

$$0 = \dot{\lambda}^{\mathsf{T}} + \lambda^{\mathsf{T}} \partial_x f(x,p), \tag{5.34}$$

$$0 = \lambda^{\mathsf{T}}(0) - \lambda^{\mathsf{T}}(T), \tag{5.35}$$

$$1 = \lambda^{\mathsf{T}}(0) f(x(0),p), \tag{5.36}$$

$$\begin{aligned} 0 = \dot{C} &- \partial_x f(x,p) C - C \partial_x f^{\mathsf{T}}(x,p) \\ &- Q F(x,p) F^{\mathsf{T}}(x,p) Q^{\mathsf{T}} \\ &- \alpha f(x,p) f^{\mathsf{T}}(x,p), \end{aligned} \tag{5.37}$$

$$0 = C(0) - C(T), \tag{5.38}$$

$$0 = \lambda^{\mathsf{T}}(0) C(0) \lambda(0). \tag{5.39}$$

Here (5.31-5.33) is the periodic boundary value problem that yields $\tilde{x}(t)$ and $\tilde{T}$. Eqs. (5.34-5.35) is the boundary-value problem, equivalent to the corresponding adjoint conditions associated with the periodic orbit, that must be solved to obtain $\tilde{\lambda}(t)$. The periodic orbit and the adjoint variables are then used in the covariance formulation (5.37-5.39) to obtain the unique covariance matrix associated with hyperplanes along the orbit.

The formulation outlined here differs from that employed in the past by the purposeful introduction of the projection Q in (5.37), the imposition of the non-degeneracy condition (5.39), and the introduction of the corresponding "damping" parameter α in (5.37). This formalism sidesteps entirely the need to derive an $n-1$-dimensional basis for planes transversal to the limit cycle. We have chosen to use a projection defined by the solution $\tilde{\lambda}(t)$ to the adjoint boundary-value problem (5.34)-(5.36) and, consequently, associated with planes orthogonal to $\tilde{\lambda}(t)$ rather than $f(\tilde{x}(t))$, since this is a natural decomposition that respects

the spectral properties of the solution $\tilde{X}(t)$ to the variational problem.

5.3 Hopf Normal Form

Consider, as a first example, the deterministic vector field

$$f(x) = \begin{pmatrix} x_1 - x_2 - x_1(x_1^2 + x_2^2) \\ x_1 + x_2 - x_2(x_1^2 + x_2^2) \end{pmatrix}. \tag{5.40}$$

It is straightforward to show that an orbitally asymptotically stable periodic orbit with period 2π and initial condition on the Poincaré section $x_2 = 0$ is given by

$$\tilde{x}(t) = \begin{pmatrix} \cos t \\ \sin t \end{pmatrix} \tag{5.41}$$

and that the solution to the corresponding variational initial-value problem equals

$$\tilde{X}(t) = \begin{pmatrix} e^{-2t}\cos t & -\sin t \\ e^{-2t}\sin t & \cos t \end{pmatrix}. \tag{5.42}$$

In particular, the monodromy matrix $\tilde{X}(2\pi)$ has eigenvalues 1 and $e^{-4\pi}$.

Given $\tilde{x}(t)$, the solution to the adjoint boundary-value problem is given by

$$\tilde{\lambda}(t) = \begin{pmatrix} -\sin t \\ \cos t \end{pmatrix}, \tag{5.43}$$

which here coincides with $f(\tilde{x}(t))$. It follows that

$$\tilde{Q}(t) = \begin{pmatrix} \cos^2 t & \cos t \sin t \\ \cos t \sin t & \sin^2 t \end{pmatrix} \tag{5.44}$$

and

$$\tilde{X}^{-1}(t)\tilde{Q}(t) = \begin{pmatrix} e^{2t}\cos t & e^{2t}\sin t \\ 0 & 0 \end{pmatrix}. \tag{5.45}$$

Now let

$$F(\tilde{x}, p) = \begin{pmatrix} \tilde{F}_{11} & \tilde{F}_{12} \\ \tilde{F}_{21} & \tilde{F}_{22} \end{pmatrix}. \tag{5.46}$$

By substitution in (5.37), integration over a full period, and substitution into the equality $\tilde{C}(0) = \tilde{C}(2\pi)$, it follows that

$$\tilde{C}(0) = \begin{pmatrix} c_{11}(0) & 0 \\ 0 & 0 \end{pmatrix}, \tag{5.47}$$

where

$$c_{11}(0) = \frac{\mathcal{I}(2\pi)}{e^{8\pi} - 1} \tag{5.48}$$

and

$$\mathcal{I}(t) = \int_0^t e^{4s}\big((\tilde{F}_{11}\cos s + \tilde{F}_{21}\sin s)^2 + (\tilde{F}_{12}\cos s + \tilde{F}_{22}\sin s)^2\big)\,\mathrm{d}s. \tag{5.49}$$

We conclude that

$$\tilde{C}(t) = e^{-4t}\left(\mathcal{I}(t) + \frac{\mathcal{I}(2\pi)}{e^{8\pi} - 1}\right)\begin{pmatrix} \cos^2 t & \cos t \sin t \\ \cos t \sin t & \sin^2 t \end{pmatrix}. \tag{5.50}$$

An alternative derivation is possible by transforming to polar coordinates, i.e., with $x_1 = r\cos\theta$ and $x_2 = r\sin\theta$, in which case, to $\mathcal{O}(\sigma)$, we obtain the decoupled SDEs

$$\mathrm{d}r = r\left(1 - r^2\right)\mathrm{d}t + \sigma\left(F_{11}\cos\theta + F_{21}\sin\theta\right)\mathrm{d}W_{1,t} + \sigma\left(F_{12}\cos\theta + F_{22}\sin\theta\right)\mathrm{d}W_{2,t} \tag{5.51}$$

and

$$\mathrm{d}\theta = \mathrm{d}t - \frac{\sigma}{r}\left(F_{11}\sin\theta - F_{21}\cos\theta\right)\mathrm{d}W_{1,t} - \frac{\sigma}{r}\left(F_{12}\sin\theta - F_{22}\cos\theta\right)\mathrm{d}W_{2,t}. \tag{5.52}$$

At this order of approximation, we find that the deterministic limit cycle is here given by $\tilde{r} \equiv 1$ and $\tilde{\theta}(t) = t$. In particular, the covariance boundary-value problem describing the linearized response of the radial variable r near $r = \tilde{r}$ is then given by

$$\dot{c}_r = -4c_r + \left(\tilde{F}_{11}\cos t + \tilde{F}_{21}\sin t\right)^2 + \left(\tilde{F}_{12}\cos t + \tilde{F}_{22}\sin t\right)^2 \tag{5.53}$$

and

$$c_r(2\pi) = c(0), \tag{5.54}$$

from which we obtain

$$\tilde{c}_r(t) = e^{-4t}\left(\mathcal{I}(t) + \frac{\mathcal{I}(2\pi)}{e^{8\pi} - 1}\right). \tag{5.55}$$

We recover $\tilde{C}(t)$ in (5.50) by only considering variations in x_1 and x_2 associated with variations in r:

$$\begin{aligned}\tilde{C}(t) &= \begin{pmatrix}\delta r\cos t\\ \delta r\sin t\end{pmatrix}\begin{pmatrix}\delta r\cos t & \delta r\sin t\end{pmatrix}\\ &= (\delta r)^2\begin{pmatrix}\cos^2 t & \cos t\sin t\\ \cos t\sin t & \sin^2 t\end{pmatrix},\end{aligned} \tag{5.56}$$

where $(\delta r)^2 = \tilde{c}_r$.

To verify our analysis, we compare its predictions in the case when $\sigma = 0.1$ to the statistics obtained from sample paths of the original Itô SDE obtained using an explicit Euler-Maruyama integrator [112] in MATLAB. Specifically, given the drift f in (5.40), we

consider the dispersion matrix

$$F(x) = \begin{pmatrix} x_1^2 & 0 \\ 0 & x_2^2 \end{pmatrix} \Rightarrow F(\tilde{x}) = \begin{pmatrix} \cos^2 t & 0 \\ 0 & \sin^2 t \end{pmatrix} \tag{5.57}$$

and assume two independent Brownian increments $\mathrm{d}W_{t,1}$ and $\mathrm{d}W_{t,2}$. In this case, we find

$$\mathcal{I}(t) = \frac{e^{4t}\left(10 + 3\cos 4t + 3\sin 4t\right) - 13}{64} \tag{5.58}$$

and, consequently, that the nontrivial eigenvalue of $\tilde{C}(t)$ equals

$$\tilde{\gamma}(t) := \frac{10 + 3\cos 4t + 3\sin 4t}{64}. \tag{5.59}$$

We graph the corresponding function, multiplied by $\sigma^2 = 0.01$ in Fig. 5.2.

We proceed to generate sample trajectories with a fixed time step $\mathrm{d}t = 10^{-4}$ and Brownian increments generated using the `randn` command in Matlab. In each case, we run simulations based at the initial condition $\tilde{x}(0)$ for a total duration of $1,000$ periods of the underlying limit cycle. For each sample trajectory, we detect crossings near $\tilde{x}(\phi)$ with the transversal section

$$\Sigma_\phi : \left(x_2 - \tilde{x}_2(\phi)\right)\cos\phi - \left(x_1 - \tilde{x}_1(\phi)\right)\sin\phi = 0 \tag{5.60}$$

corresponding, locally, to the image of $\tilde{Q}(\phi)$. When such a crossing is detected, we use linear interpolation based at the nearest points on either side of Σ_ϕ to compute an approximate intersection of the sample trajectory with Σ_ϕ. Given the nontrivial Floquet multiplier $e^{-4\pi} \approx 3.5 \times 10^{-6}$, we anticipate that transients die down quickly and that convergence to the stationary distribution may be anticipated within a few periods. We denote the covariance matrix of intersections computed using this approach by $C_{\mathrm{EM}}(\phi)$.

As an example, with $\phi = 0$ and, consequently, Σ_0 given by the x_1 axis, we obtain the

approximate covariance matrix

$$C_{\mathrm{EM}}(0) = \begin{pmatrix} 0.00203 & 0 \\ 0 & 0 \end{pmatrix} \tag{5.61}$$

from the last 990 intersections with Σ_0. As a comparison, using (5.50), we obtain

$$\sigma^2 \tilde{C}\,(0) = \begin{pmatrix} 0.00206 & 0 \\ 0 & 0 \end{pmatrix} \tag{5.62}$$

in excellent agreement. Repeating this calculation for other values of ϕ and computing the corresponding nonzero eigenvalue yields the data shown in Fig. 5.2. We attribute the differences between the simulated data and the predictions from (5.50) to the low order of accuracy of the Euler-Maruyama integrator, errors incurred through interpolation across Σ_ϕ, the relatively small sample of intersections, and the finite size of σ.

In Fig. 5.3, we show the complete picture by projecting the stochastic trajectories along the normalized radial eigenvector $e(\phi) = (\cos\phi, \sin\phi)^{\mathrm{T}}$ corresponding to the nonzero eigenvalue of the covariance matrix. To obtain the projections, for each point on the stochastic trajectory $x(t)$, we use the hyperplane definition (5.14) to compute the corresponding value of ϕ. We then project the perturbation $x(t) - \tilde{x}(\phi)$ onto $e(\phi)$. These results are compared with the one and two standard deviation predictions computed from the square root of the eigenvalue expression (5.59). We can clearly observe that the predicted and the numerical results are in great agreement with each other.

5.4 Implementation

It is not generally possible to derive closed-form expressions for the covariance function as was done for the Hopf normal form in the previous section. Instead, we numerically solve the corresponding boundary-value problem in COCO. As discussed in Chapter 2, a unique

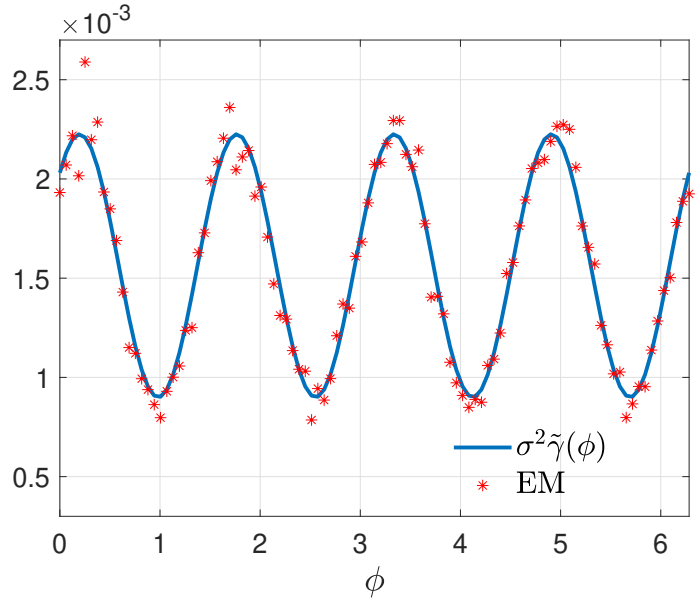

Figure 5.2: The variance as a function of the limit cycle phase for the Hopf normal form SDE. Blue solid line is obtained from (5.59) and red dots are the result of integration using the explicit Euler-Maruyama solver. Here, $\sigma = 0.1$.

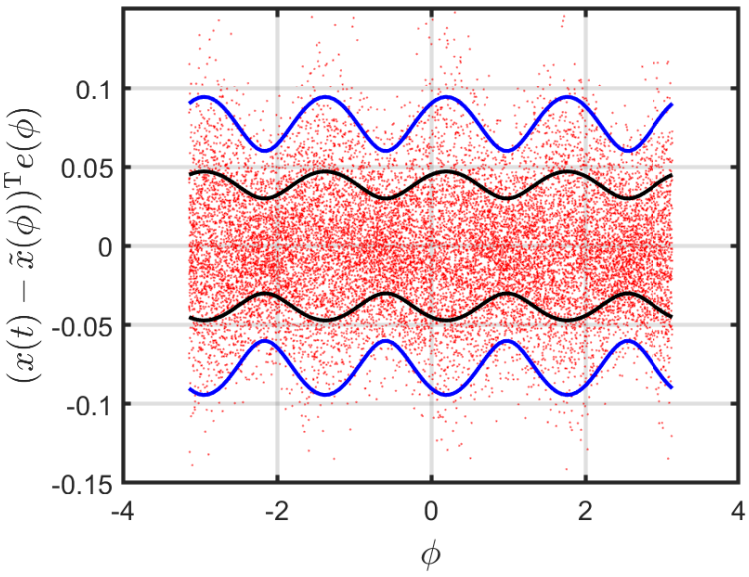

Figure 5.3: Comparison of theoretical and numerical results for the Hopf normal form SDE. Black and blue lines represent deviations equal to one and two standard deviations, respectively, from the limit cycle, computed using (5.59) and plotted as a function of the limit cycle phase. Red dots denote projections of the deviations from the limit cycle of points along the stochastic trajectories onto the normalized radial eigenvector $e(\phi) = (\cos\phi, \sin\phi)^{\mathrm{T}}$.

feature of this package is the staged style of problem construction. This general staged style of construction fits perfectly for our formulation. In particular, we rely on an instance of the collocation discretization of the periodic orbit boundary-value problem in Eqs. (5.31)-(5.33), a collocation discretization of the adjoint boundary-value problem in Eqs. (5.34)-(5.36), and a collocation discretization of the covariance boundary-value problem in Eqs. (5.37)-(5.39).

We first use the already available `po` toolbox constructor to implement the discretization of the periodic boundary-value problem (5.31-5.33) as a zero problem in terms of the vector of continuation variables $u = (x, T, p)$, and to append monitor functions that evaluate to the period length T and the problem parameters p, as well as the associated continuation parameters μ_T and μ_p. In lieu of a Poincaré phase condition of the form (5.33), we rely on a built-in integral phase condition. An initial solution guess may be obtained from forward simulation.

In the next stage of construction, we use the adjoint constructors in the `po` toolbox to append the adjoint contributions associated with the constraints (5.31-5.33) and the monitor functions in terms of the adjoint variables λ, λ_{bc}, λ_{ps}, η_T, and η_p. The toolbox also associates complementary continuation parameters ν_T and ν_p with complementary monitor functions that evaluate to η_T and η_p. We fix ν_T to 1 and use vanishing adjoint variables as the initial solution guess.

In the final stage of construction, we use the COCO complementary zero function constructor to append a discretization of the boundary-value problem (5.37-5.39) for the covariance function in terms of the complementary continuation variables $\upsilon = (C, \alpha)$. We initialize the search with $C \equiv 0$ and $\alpha = 0$.

5.5 Examples

In this section, we discuss the results obtained from the implementation in COCO of the covariance boundary-value problem as described in Section 5.4. For all the computations, a

uniform mesh is used with the number of collocation nodes in each interval fixed to 4. The number of discretization intervals used are 10 unless specified otherwise.

5.5.1 Hopf Normal SDE

For the purpose of illustration, as a first example we recall the Hopf normal form SDE with the drift vector field

$$f(x) = \begin{pmatrix} x_1 - x_2 - x_1(x_1^2 + x_2^2) \\ x_1 + x_2 - x_2(x_1^2 + x_2^2) \end{pmatrix}. \tag{5.63}$$

The initial guess for the periodic boundary-value problem is obtained from the explicit solution (5.41), whereas both the adjoint variables and the covariance variables are initialized with zeros. With μ_T released and ν_T fixed to unity, we perform a zero dimensional continuation to obtain the desired covariance matrix. Figure 5.4 shows a comparison of the non-trivial eigenvalue of the covariance matrix obtained using COCO and the analytical expression (5.59). The results are in excellent agreement with each other.

5.5.2 Coupled Network System

As a second example, we consider the stochastically perturbed nonlinear network model illustrated in Fig. 5.5 and governed by the coupled Itô SDEs

$$\mathrm{d}y = z\,\mathrm{d}t, \;\; \mathrm{d}z = -(Ky + \epsilon G(y)\, z)\,\mathrm{d}t + \sigma F \mathrm{d}W_t \tag{5.64}$$

with stiffness matrix

$$K = \begin{pmatrix} 3 & -1 & 0 & -1 \\ -1 & 4 & -1 & -1 \\ 0 & -1 & 2 & 0 \\ -1 & -1 & 0 & 3 \end{pmatrix}, \tag{5.65}$$

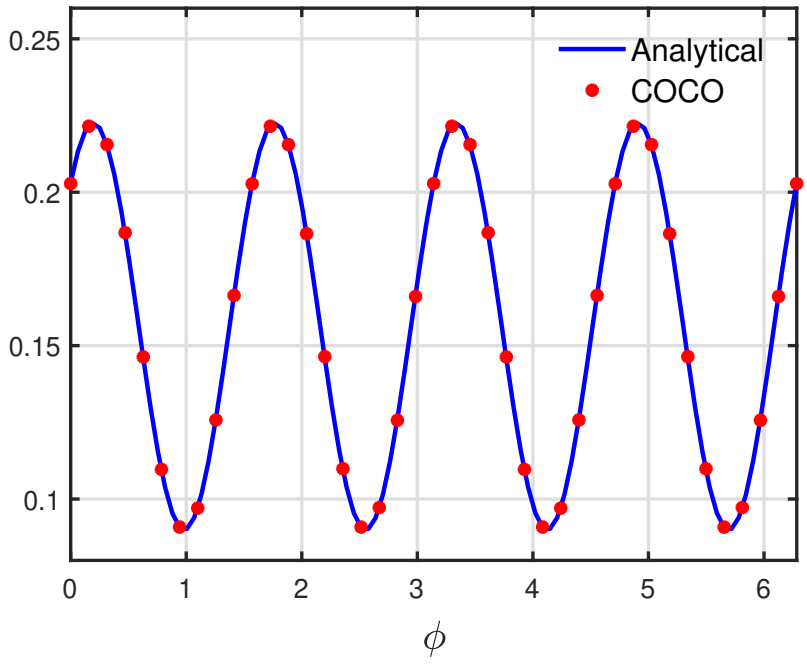

Figure 5.4: Comparison of the non-trivial eigenvalue of the covariance matrix for the Hopf normal form obtained using a boundary-value problem implementation in COCO and the analytical expression reported in (5.59), respectively.

damping matrix

$$G(y) = \begin{pmatrix} -1 - 10y_1^2(t) + 10y_1^4(t) & 0 & 0 & 0 \\ 0 & 1 & 0 & 0 \\ 0 & 0 & 1 & 0 \\ 0 & 0 & 0 & \zeta \end{pmatrix}, \tag{5.66}$$

and diagonal dispersion matrix F. It is assumed that $\epsilon, \zeta > 0$ and $\epsilon \ll 1$.

In the absence of noise, the corresponding deterministic system has a trivial equilibrium which undergoes a subcritical Hopf bifurcation for ζ near unity [113]. To leading order in ϵ, the branch of periodic orbits born at the Hopf bifurcation may be described in terms of the normal mode

$$\tilde{y}(t) = A\sin(2t + \psi)\, e_1,\ \tilde{z}(t) = 2A\cos(2t + \psi)\, e_1, \tag{5.67}$$

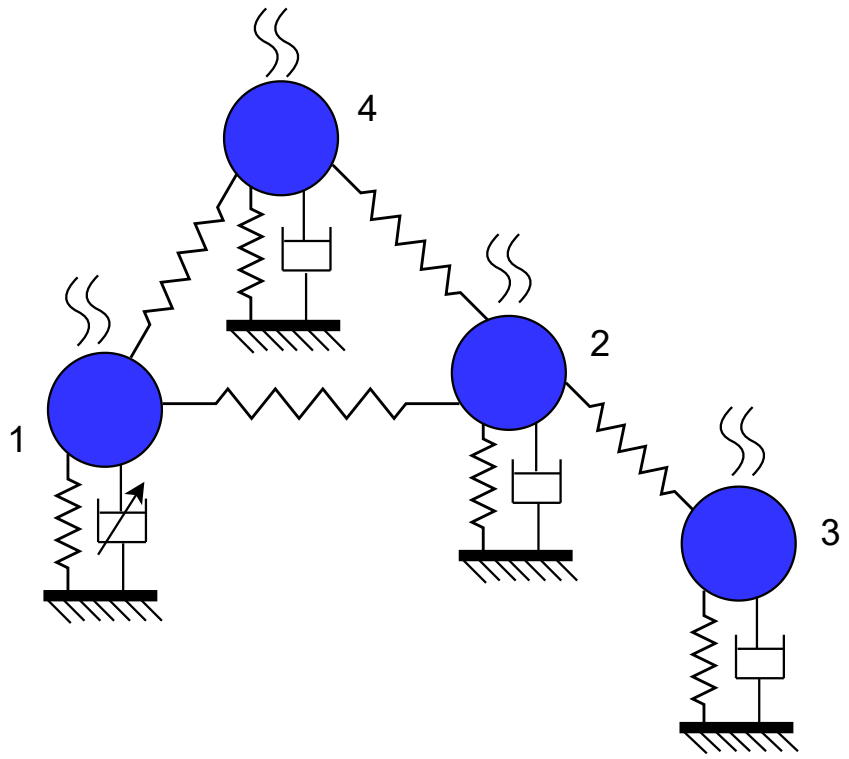

Figure 5.5: Schematic representation of a coupled four-node oscillator model operating in a stochastic environment. Here, nonlinearity appears only in the damping of node 1.

where $e_1 = \begin{pmatrix} 1 & 0 & 0 & -1 \end{pmatrix}^{\mathsf{T}} / \sqrt{2}$,

$$A^2 = 2 \pm 2\sqrt{\frac{9 - 4\zeta}{5}} \tag{5.68}$$

and ψ is arbitrary. In particular, periodic orbits are found for $\zeta < 9/4$ as shown in Fig. 5.6. To this order of approximation, the corresponding adjoint functions are then given by

$$\tilde{\lambda}_y(t) = \frac{1}{2A}\cos(2t + \psi)\, e_1,\ \tilde{\lambda}_z(t) = -\frac{1}{4A}\sin(2t + \psi)\, e_1. \tag{5.69}$$

Using a multiple-scales analysis, one finds that the local stability of the periodic orbits born at the Hopf bifurcation is governed by the stability of the corresponding equilibria for

the slow-flow amplitude equation

$$4A' = (1-\zeta)\,A + \frac{5}{4}A^3 - \frac{5}{16}A^5, \tag{5.70}$$

where $(')$ denotes differentiation with respect to the slow time scale ϵt. In particular, as also suggested in Fig. 5.6, the periodic orbits along the lower branch are unstable, while those along the upper branch are asymptotically stable. Here, we investigate the effects of noise on the local behavior near the limit cycle on the upper branch.

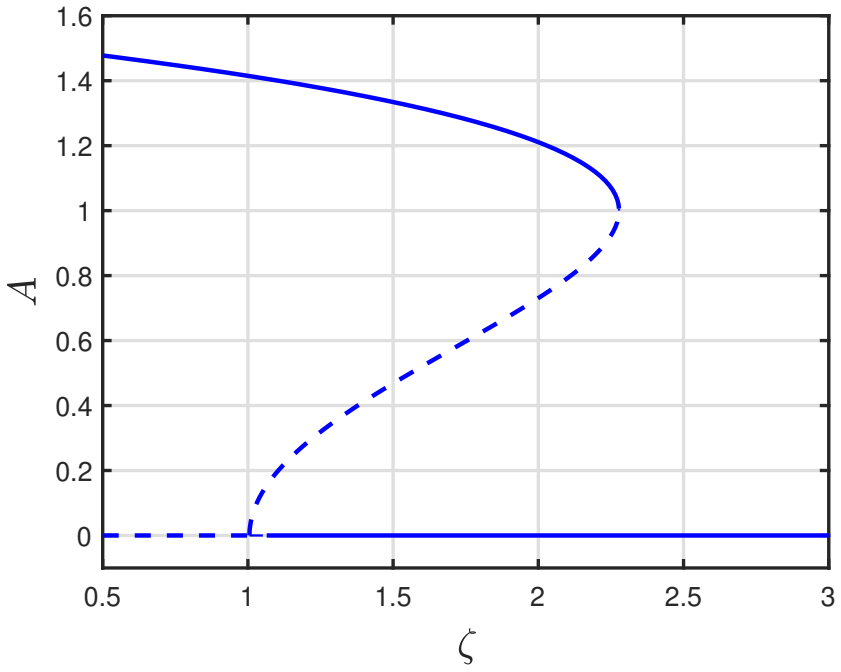

Figure 5.6: Bifurcation diagram for the four-node network oscillator model reported in [113]. The variable A denotes the amplitude of the first oscillator.

For this problem, since we have the approximate periodic orbit (5.67) and the corresponding adjoint solution (5.69), we may construct a leading-order approximation of the projection $\tilde{Q}(t)$. It follows that, given a leading order approximation of the inverse $\tilde{X}^{-1}(t)$, one can perform a similar analysis to that in a previous section to obtain an approximate analytical expression for $\tilde{C}(t)$. While that is, in fact, possible, the analytical expressions are cumbersome and no simple formula results for the eigenvalues of $\tilde{C}(t)$.

Instead of such an analytical study, we numerically solve the corresponding boundary-value problem in COCO. For the periodic boundary-value problem instance, we fix $\epsilon = 0.05$ and $\zeta = 1.2565$ and assign F to be the identity matrix. The initial guess for this instance is obtained from the multiple-scale approximation, whereas the adjoint and the covariance variables are all initialized with zero values. With $\mu_T, \nu_\epsilon, \nu_\zeta$ released and ν_T fixed to unity we perform a zero dimensional continuation to solve the covariance boundary-value problem. As expected, we find that $\tilde{\alpha} \approx 0$ to within the default accuracy of the Newton solver used by COCO. In Fig. 5.7, we graph the square root of the largest eigenvalue of $\sigma^2\tilde{C}(\phi)$ for $\sigma = 0.005$.

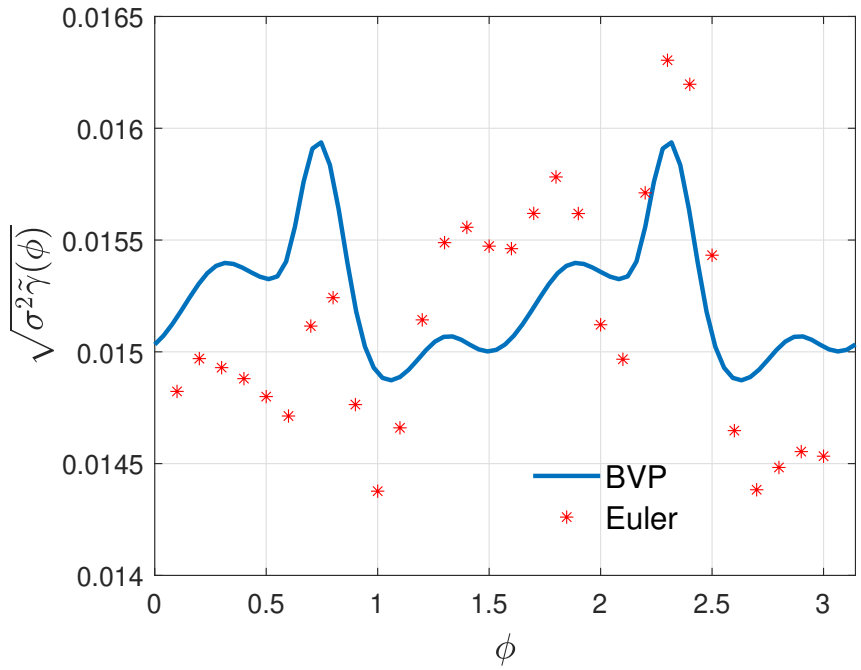

Figure 5.7: Comparison of predicted and numerical values for the square root of the maximum eigenvalue $\sigma^2\tilde{\gamma}(\phi)$ of the covariance matrix $\sigma^2\tilde{C}(\phi)$ as a function of ϕ for the four-node oscillator network problem with $\epsilon = 0.05$, $\sigma = 0.005$ and $\zeta = 1.2565$. Here, the solid blue line is obtained from the solution to the covariance boundary-value problem while the red dots were obtained from points along stochastic trajectories generated with the Euler-Maruyama integrator.

To verify these predictions, we again use the explicit Euler-Maruyama integrator to numerically simulate sample trajectories of the network SDEs (5.64) based at the initial condition $u(0) = \tilde{u}(0)$ and $v(0) = \tilde{v}(0)$. Here, we consider intersections with the transversal

section

$$\Sigma_\phi : \tilde{\lambda}_y^{\mathsf{T}}(\phi)\,(y - \tilde{y}(\phi)) + \tilde{\lambda}_z^{\mathsf{T}}(\phi)\,(z - \tilde{z}(\phi)) = 0 \tag{5.71}$$

obtained using the leading order expressions for $\tilde{y}$, $\tilde{z}$, $\tilde{\lambda}_y$, and $\tilde{\lambda}_z$ corresponding, locally, to the image of the leading order expression for $\tilde{Q}(\phi)$. As before, we approximate such intersections by linear interpolation based at the nearest points on either side of Σ_ϕ. The simulations are performed for 1,000 periods of the limit cycle and with $\mathrm{d}t = 10^{-4}$. The corresponding statistics produce the preliminary results represented by the dots in Fig. 5.7, which agree in order of magnitude with the theoretical predictions. Discrepancies are here related to effects of transients, finite size of σ, finite size of ϵ (recall that Σ_ϕ was here defined from the leading-order analysis in ϵ), and finite sample sizes.

Finally, in Fig. 5.8, we vary the parameter ζ, while keeping all other parameters fixed. The graph shows the maximum of the square root of the largest eigenvalue of $\sigma^2\tilde{C}(\phi)$ for $\phi \in [0, 2\pi)$. As the saddle-node point is approached, this quantity grows with the inverse distance to the saddle-node. Consequently, the effects of noise become more pronounced as the bifurcation is approached.

5.6 Conclusions

In this chapter, we proposed a novel adjoint-based, boundary-value problem formulation for capturing the effects of Brownian noise near limit cycles in terms of covariance matrix functions that describe a stationary probability distribution that is locally Gaussian. Conveniently, several of the required ingredients for a computational implementation were already available in existing software. The next chapter deals with the extension of this formulation to stochastic trajectories near quasiperiodic tori.

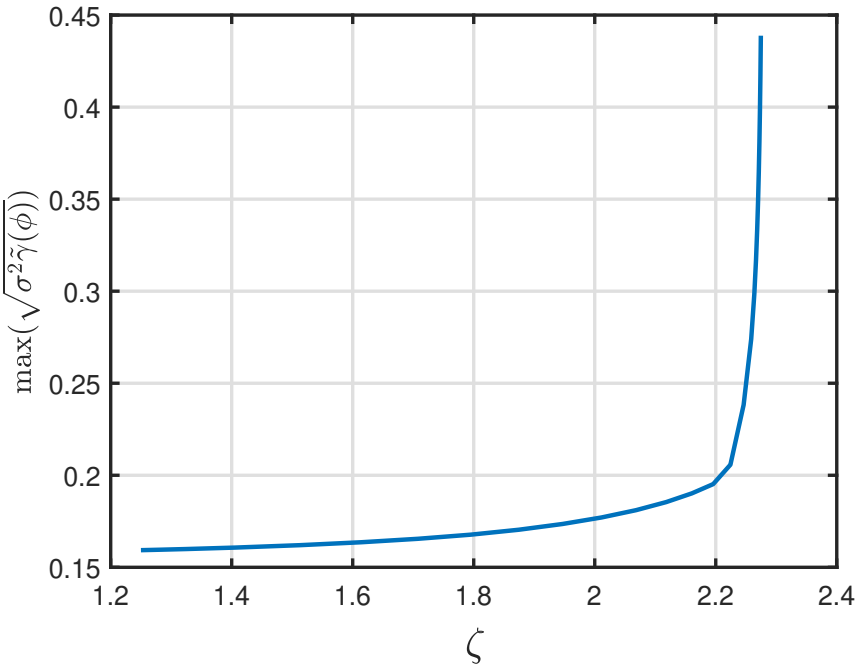

Figure 5.8: Variation of the square root of the maximum eigenvalue of the covariance matrix $\sigma^2\tilde{C}(\phi)$ with the parameter ζ. The maximum eigenvalue increases as ζ approaches the saddle node point $\zeta^* \approx 2.2779$. Here $\sigma = 0.05$.

Chapter 6

NOISE INDUCED BEHAVIOR NEAR DETERMINISTIC QUASIPERIODIC ORBITS

In this chapter, we generalize the boundary-value problem formulation from the previous chapter to obtain a similar uncertainty quantification of noise-induced dynamics near transversally stable quasiperiodic tori. As in the case of limit cycles, the formulation relies on the computation of adjoints, here obtained from a quasiperiodic boundary-value problem, to project the dynamics onto hyperplanes locally transversal to the torus. On each of these hyperplanes, the underlying steady-state distribution of stochastic intersections is again Gaussian, and a unique covariance matrix associated with each point on the torus may be obtained from a partial differential equation boundary-value problem.

The chapter is organized as follows. Section 6.1 generalizes the construction of families of local projections to the quasiperiodic case and shows that a unique covariance matrix may be associated with each corresponding hyperplane. The corresponding boundary-value problem is given in Section 6.2 and its implementation in COCO is described in Section 6.3. Validation of this methodology is illustrated for a stochastically perturbed coupled Van-der-Pol oscillator system in Section 6.4.

6.1 Mathematical Preliminaries

From [109], we obtain the defining boundary-value problem for a quasiperiodic invariant torus

$$\partial_t v(\phi,t) = f(v(\phi,t),\, v(\phi,T) = v(\phi+\rho,0) \tag{6.1}$$

in terms of a function $v : \mathbb{S}\times[0,T]\to\mathbb{R}^n$ for an *a priori* unknown T, and irrational rotation number ρ. We denote a solution of this boundary-value problem by $\tilde{v}(\phi,t)$ and $\tilde{T}$ and assume from here on that the corresponding torus is transversally stable. As shown in [109], the solutions to the adjoint boundary-value problem

$$0 = -\partial_t \lambda^{\mathrm{T}}(\phi,t) - \lambda^{\mathrm{T}}(\phi,t)\,\partial_x f\left(\tilde{v}(\phi,t)\right) + \lambda_{\mathrm{ps}}^{\mathrm{T}}\partial_v h\left(\tilde{v}(\cdot,\cdot)\right) \tag{6.2}$$

$$0 = \lambda^{\mathrm{T}}(\phi,T) - \lambda_{\mathrm{bc}}^{\mathrm{T}}(\phi) \tag{6.3}$$

$$0 = -\lambda^{\mathrm{T}}(\phi,0) + \lambda_{\mathrm{bc}}^{\mathrm{T}}(\phi-\rho) \tag{6.4}$$

$$0 = \eta_T - \int_{\mathbb{S}} \lambda_{\mathrm{bc}}^{\mathrm{T}}(\phi)\, f\left(\tilde{v}(\phi,T)\right)\mathrm{d}\phi \tag{6.5}$$

$$0 = \eta_\rho + \int_{\mathbb{S}} \lambda_{\mathrm{bc}}^{\mathrm{T}}(\phi)\partial_\phi\tilde{v}(\phi+\rho,0)\mathrm{d}\phi. \tag{6.6}$$

with $(\eta_T,\eta_\rho) = (1,0)$ and $(0,1)$, respectively, may be used to construct a projection operator, as was done in Chapter 5. Specifically, under certain non-degeneracy conditions on h, these equations imply that $\lambda_{\mathrm{ps}} = 0$ and $\lambda(\phi,T) = \lambda(\phi+\rho,0)$. Moreover,

$$\begin{aligned}
&\lambda_T^{\mathrm{T}}(\phi,t)\partial_t\tilde{v}(\phi,t) = 1,\ \lambda_T^{\mathrm{T}}(\phi,t)\partial_\phi\tilde{v}(\phi,t) = 0,\\
&\lambda_\rho^{\mathrm{T}}(\phi,t)\partial_t\tilde{v}(\phi,t) = 0,\ \lambda_\rho^{\mathrm{T}}(\phi,t)\partial_\phi\tilde{v}(\phi,t) = -1,
\end{aligned} \tag{6.7}$$

where λ_T denotes any solution obtained with $(\eta_T,\eta_\rho) = (1,0)$ and λ_ρ denotes any solution obtained with $(\eta_T,\eta_\rho) = (0,1)$. In fact, by the transversal stability of the torus, it follows

that there exist unique solutions $\tilde{\lambda}_T$ and $\tilde{\lambda}_\rho$, from which we obtain the projection

$$\tilde{Q}(\phi,t) = I_n - \partial_t\tilde{v}(\phi,t)\tilde{\lambda}_T^{\mathrm{T}}(\phi,t) + \partial_\phi\tilde{v}(\phi,t)\tilde{\lambda}_\rho^{\mathrm{T}}(\phi,t) \tag{6.8}$$

along the tangent plane to the torus at $\tilde{v}(\phi,t)$, spanned by the vectors $\partial_t\tilde{v}(\phi,t)$ and $\partial_\phi\tilde{v}(\phi,t)$, onto a plane perpendicular to $\tilde{\lambda}_T^{\mathrm{T}}(\phi,t)$ and $\tilde{\lambda}_\rho^{\mathrm{T}}(\phi,t)$. Indeed, here, $\tilde{Q}^2(\phi,t) = \tilde{Q}(\phi,t)$, $\tilde{\lambda}_T^{\mathrm{T}}(\phi,t)\tilde{Q}(\phi,t) = \tilde{\lambda}_\rho^{\mathrm{T}}(\phi,t)\tilde{Q}(\phi,t) = 0$ and $\tilde{Q}(\phi,t)\partial_t\tilde{v}(\phi,t) = \tilde{Q}(\phi,t)\partial_\phi\tilde{v}(\phi,t) = 0$.

Also, as shown in [109], if $\tilde{X}(\phi,t)$ satisfies the variational problem

$$\partial_t X = \partial_x f\left(\tilde{v}\right) X, X\left(\cdot,0\right) = I_n \tag{6.9}$$

then

$$\partial_\phi\tilde{v}\left(\phi,t\right) = \tilde{X}\left(\phi,t\right)\partial_\phi\tilde{v}\left(\phi,0\right), \tag{6.10}$$

$$\partial_t\tilde{v}\left(\phi,t\right) = \tilde{X}\left(\phi,t\right)\partial_t\tilde{v}\left(\phi,0\right) \tag{6.11}$$

and

$$\tilde{\lambda}_{T/\rho}^{\mathrm{T}}(\phi,t)\tilde{X}(\phi,t) = \tilde{\lambda}_{T/\rho}^{\mathrm{T}}(\phi,0). \tag{6.12}$$

It follows that

$$\tilde{X}^{-1}(\phi,t)\tilde{Q}(\phi,t) = \tilde{X}^{-1}(\phi,t)\Big(I_n - \partial_t\tilde{v}(\phi,t)\tilde{\lambda}_T^{\mathrm{T}}(\phi,t) + \partial_\phi\tilde{v}(\phi,t)\tilde{\lambda}_\rho^{\mathrm{T}}(\phi,t)\Big), \tag{6.13}$$

which simplifies to

$$\tilde{X}^{-1}(\phi,t)\tilde{Q}(\phi,t) = \tilde{Q}(\phi,0)\tilde{X}^{-1}(\phi,t) \Longleftrightarrow \tilde{Q}(\phi,t)\tilde{X}(\phi,t) = \tilde{X}(\phi,t)\tilde{Q}(\phi,0) \tag{6.14}$$

i.e., that the family of hyperplanes is invariant under the linearized flow.

As further shown in [109], for $x(t) \approx \tilde{v}(\phi, \tau)$ for some ϕ and τ, the scalar equations

$$\tilde{\lambda}_T^{\mathrm{T}}\left(\psi(t), \varpi(t)\right)\left(x\left(t\right) - \tilde{v}\left(\psi(t), \varpi(t)\right)\right) = 0, \tag{6.15}$$

$$\tilde{\lambda}_\rho^{\mathrm{T}}\left(\psi(t), \varpi(t)\right)\left(x\left(t\right) - \tilde{v}\left(\psi(t), \varpi(t)\right)\right) = 0, \tag{6.16}$$

define $\psi(t)$ and $\varpi(t)$ uniquely on a neighborhood of ϕ and τ, such that $\psi(t) = \phi, \varpi(t) = \tau$ if $x(t) = \tilde{v}(\phi, \tau)$. It follows that there exists a unique $x_{\mathrm{tr}}(t) \coloneqq x(t) - \tilde{v}(\psi(t), \varpi(t))$, such that $\tilde{Q}(\psi(t), \varpi(t))x_{\mathrm{tr}}(t) = x_{\mathrm{tr}}(t)$. Moreover by generalizing a result from [109] for the deterministic case, we obtain

$$\mathrm{d}x_{\mathrm{tr}} = \partial_x f\left(\tilde{v}\left(\phi, t\right)\right) x_{\mathrm{tr}} \mathrm{d}t + \sigma \tilde{Q}(\phi, t) F\left(\tilde{v}\left(\phi, t\right)\right) \mathrm{d}W_t \tag{6.17}$$

to lowest order in σ and deviations x_{tr}. This may be solved explicitly to yield

$$\begin{aligned} x_{\mathrm{tr}}\left(t\right) &= \tilde{X}\left(\phi, t\right) x_{\mathrm{tr}}\left(0\right) + \sigma \int_0^t \left(\tilde{X}\left(\phi, t\right) \tilde{X}^{-1}\left(\phi, \tau\right)\right) \tilde{Q}(\phi, \tau) F\left(\tilde{v}\left(\phi, \tau\right)\right) \mathrm{d}W_\tau \\ &= \tilde{X}\left(\phi, t\right) x_{\mathrm{tr}}\left(0\right) + \sigma \tilde{Q}(\phi, t) \tilde{X}\left(\phi, t\right) \int_0^t G(\phi, \tau) \mathrm{d}W_\tau, \end{aligned} \tag{6.18}$$

where $G(\phi, \tau) = \tilde{X}^{-1}\left(\phi, \tau\right) F\left(\tilde{v}\left(\phi, \tau\right)\right)$.

As in the previous chapter, we proceed to define the rescaled covariance matrix

$$C\left(\phi, t\right) = \frac{1}{\sigma^2} \mathbb{E}\left[x_{\mathrm{tr}}(t) x_{\mathrm{tr}}^{\mathrm{T}}(t)\right], \tag{6.19}$$

such that

$$\left(\beta_T \tilde{\lambda}_T^{\mathrm{T}}(\phi, t) + \beta_\rho \tilde{\lambda}_\rho^{\mathrm{T}}(\phi, t)\right) C(\phi, t) \left(\beta_T \tilde{\lambda}_T(\phi, t) + \beta_\rho \tilde{\lambda}_\rho(\phi, t)\right) = 0 \tag{6.20}$$

for any β_T and β_ρ by (6.15) and (6.16). It follows from the definition of C, the invariance

condition (6.14), and the stochastic inequalities (5.19-5.20) that

$$C\left(\phi,t\right)=\tilde{X}\left(\phi,t\right)C\left(\phi,0\right)\tilde{X}^{\mathrm{T}}(\phi,t)$$
$$+\tilde{Q}(\phi,t)\tilde{X}(\phi,t)\left(\int_{0}^{t}G\left(\phi,\tau\right)G^{\mathrm{T}}\left(\phi,\tau\right)\mathrm{d}\tau\right)\tilde{X}^{\mathrm{T}}(\phi,t)\tilde{Q}^{\mathrm{T}}(\phi,t). \tag{6.21}$$

By the anticipated convergence towards a stationary probability distribution, it now follows that we seek a solution to this integral equation, such that $C(\phi,\tilde{T})=C(\phi+\rho,0)$, i.e., a solution to the linear algebraic system

$$C\left(\phi+\rho,0\right)=\tilde{X}\left(\phi,\tilde{T}\right)C\left(\phi,0\right)\tilde{X}^{\mathrm{T}}(\phi,\tilde{T})$$
$$+\tilde{Q}(\phi,\tilde{T})\tilde{X}(\phi,\tilde{T})\left(\int_{0}^{\tilde{T}}G\left(\phi,\tau\right)G^{\mathrm{T}}\left(\phi,\tau\right)\mathrm{d}\tau\right)\tilde{X}^{\mathrm{T}}(\phi,\tilde{T})\tilde{Q}^{\mathrm{T}}(\phi,\tilde{T}) \tag{6.22}$$

that also satisfies the condition

$$\left(\beta_{T}\tilde{\lambda}_{T}^{\mathrm{T}}(\phi,0)+\beta_{\rho}\tilde{\lambda}_{\rho}^{\mathrm{T}}(\phi,0)\right)C(\phi,0)\left(\beta_{T}\tilde{\lambda}_{T}(\phi,0)+\beta_{\rho}\tilde{\lambda}_{\rho}(\phi,0)\right)=0 \tag{6.23}$$

for any β_{T} and β_{ρ}.

Indeed, the existence and uniqueness of a solution $C(\cdot,0)$ that also satisfies

$$\left(\beta_{T}\tilde{\lambda}_{T}^{\mathrm{T}}(\phi,t)+\beta_{\rho}\tilde{\lambda}_{\rho}^{\mathrm{T}}(\phi,t)\right)C(\phi,t)\left(\beta_{T}\tilde{\lambda}_{T}(\phi,t)+\beta_{\rho}\tilde{\lambda}_{\rho}(\phi,t)\right)=0 \tag{6.24}$$

for any β_{T} and β_{ρ} may be shown as follows. First, note that by (6.12),

$$\left(\beta_{T}\tilde{\lambda}_{T}^{\mathrm{T}}(\phi,t)+\beta_{\rho}\tilde{\lambda}_{\rho}^{\mathrm{T}}(\phi,t)\right)C(\phi,t)\left(\beta_{T}\tilde{\lambda}_{T}(\phi,t)+\beta_{\rho}\tilde{\lambda}_{\rho}(\phi,t)\right)$$
$$=\left(\beta_{T}\tilde{\lambda}_{T}^{\mathrm{T}}(\phi,0)+\beta_{\rho}\tilde{\lambda}_{\rho}^{\mathrm{T}}(\phi,0)\right)C(\phi,0)\left(\beta_{T}\tilde{\lambda}_{T}(\phi,0)+\beta_{\rho}\tilde{\lambda}_{\rho}(\phi,0)\right) \tag{6.25}$$

i.e., that $\left(\beta_{T}\tilde{\lambda}_{T}^{\mathrm{T}}(\phi,\cdot)+\beta_{\rho}\tilde{\lambda}_{\rho}^{\mathrm{T}}(\phi,\cdot)\right)C(\phi,\cdot)\left(\beta_{T}\tilde{\lambda}_{T}(\phi,\cdot)+\beta_{\rho}\tilde{\lambda}_{\rho}(\phi,\cdot)\right)$ is constant for any β_{T}

and β_ρ. Next, for large k, it follows from the transversal stability of the torus [109] that

$$\tilde{X}(\phi, k\tilde{T}) = \partial_t \tilde{v}\left(\phi + k\rho, 0\right) \tilde{\lambda}_T^{\mathrm{T}}\left(\phi, 0\right) - \partial_\phi \tilde{v}\left(\phi + k\rho, 0\right) \tilde{\lambda}_\rho^{\mathrm{T}}\left(\phi, 0\right) + \mathcal{O}\left(\exp\left(-k/\tau_{\mathrm{tr}}\right)\right) \tag{6.26}$$

where τ_{tr} is a positive constant. Furthermore,

$$\begin{aligned} C(\phi + k\rho, 0) &= \tilde{X}(\phi, k\tilde{T}) C(\phi, 0) \tilde{X}^{\mathrm{T}}(\phi, k\tilde{T}) \\ &\quad + \tilde{Q}(\phi, k\tilde{T}) \tilde{X}(\phi, k\tilde{T}) \left(\int_0^{k\tilde{T}} G(\phi, \tau) G^{\mathrm{T}}(\phi, \tau) \mathrm{d}\tau \right) \tilde{X}^{\mathrm{T}}(\phi, k\tilde{T}) \tilde{Q}^{\mathrm{T}}(\phi, k\tilde{T}) \end{aligned} \tag{6.27}$$

for any k. Here,

$$\begin{aligned} \int_0^{k\tilde{T}} G(\phi, \tau) G^{\mathrm{T}}(\phi, \tau) \mathrm{d}\tau &= \sum_{l=1}^{k} \int_{(l-1)\tilde{T}}^{l\tilde{T}} G(\phi, \tau) G^{\mathrm{T}}(\phi, \tau) \mathrm{d}\tau \\ &= \sum_{l=1}^{k} \tilde{X}^{-1}(\phi, (l-1)\tilde{T}) \Bigg(\int_0^{\tilde{T}} G(\phi + (l-1)\rho, \varrho) \\ &\qquad \cdot G^{\mathrm{T}}(\phi + (l-1)\rho, \varrho) \mathrm{d}\varrho \Bigg) \tilde{X}^{-1,\mathrm{T}}(\phi, (l-1)\tilde{T}) \\ &= \sum_{n=1}^{k} \tilde{X}^{-1}(\phi, (k-n)\tilde{T}) \Bigg(\int_0^{\tilde{T}} G(\phi + (k-n)\rho, \varrho) \\ &\qquad \cdot G^{\mathrm{T}}(\phi + (k-n)\rho, \varrho) \mathrm{d}\varrho \Bigg) \tilde{X}^{-1,\mathrm{T}}(\phi, (k-n)\tilde{T}), \end{aligned} \tag{6.28}$$

since $G\left(\phi, \tau\right) = \tilde{X}^{-1}\left(\phi, \tau\right) F\left(\tilde{v}\left(\phi, \tau\right)\right)$ and

$$\tilde{X}(\phi, (l-1)\tilde{T} + \varrho) = \tilde{X}(\phi + (l-1)\rho, \varrho) \tilde{X}(\phi, (l-1)\tilde{T}). \tag{6.29}$$

For sufficiently large k, the right-hand side of (6.27) is then approximately equal to

$$\sum_{n=1}^{\infty} \tilde{Q}(\phi, k\tilde{T})\tilde{X}(\phi + (k-n)\rho, n\tilde{T})\Bigg(\int_0^{\tilde{T}} G(\phi + (k-n)\rho, \varrho) \cdot G^{\mathrm{T}}(\phi + (k-n)\rho, \varrho)\mathrm{d}\varrho \Bigg)\tilde{X}^{\mathrm{T}}(\phi + (k-n)\rho, n\tilde{T})\tilde{Q}^{\mathrm{T}}(\phi, k\tilde{T}), \tag{6.30}$$

since

$$\tilde{X}(\phi, k\tilde{T})\tilde{X}^{-1}(\phi, (k-n)\tilde{T}) = \tilde{X}(\phi + (k-n)\rho, n\tilde{T}). \tag{6.31}$$

Moreover,

$$\begin{aligned}\tilde{X}(\phi + (k-n)\rho, n\tilde{T}) = {} & \partial_t \tilde{v}\left(\phi + k\rho, 0\right)\tilde{\lambda}_T^{\mathrm{T}}\left(\phi + (k-n)\rho, 0\right) \\ & - \partial_\phi \tilde{v}\left(\phi + k\rho, 0\right)\tilde{\lambda}_\rho^{\mathrm{T}}\left(\phi + (k-n)\rho, 0\right) + \mathcal{O}\left(\exp\left(-k/\tau_{\mathrm{tr}}\right)\right)\end{aligned} \tag{6.32}$$

for large k and $\tilde{Q}(\phi, k\tilde{T}) = \tilde{Q}(\phi + k\rho, 0)$. It follows that (6.30) converges to a finite value since

$$\begin{aligned}&\tilde{Q}(\phi, k\tilde{T})\tilde{X}(\phi + (k-n)\rho, n\tilde{T})\Bigg(\int_0^{\tilde{T}} G(\phi + (k-n)\rho, \varrho) \\ &\qquad \cdot G^{\mathrm{T}}(\phi + (k-n)\rho, \varrho)\mathrm{d}\varrho \Bigg)\tilde{X}^{\mathrm{T}}(\phi + (k-n)\rho, n\tilde{T})\tilde{Q}^{\mathrm{T}}(\phi, k\tilde{T}) \\ &= \mathcal{O}(\exp(-2k/\tau_{\mathrm{tr}})).\end{aligned} \tag{6.33}$$

6.2 Covariance boundary value problem

By differentiation of (6.21), we obtain

$$\frac{\partial C}{\partial t} = \partial_x f(\tilde{v})C + C\partial_x f^{\mathrm{T}}(\tilde{v}) + \tilde{Q}F(\tilde{v})F^{\mathrm{T}}(\tilde{v})\tilde{Q}^{\mathrm{T}} \tag{6.34}$$

The corresponding boundary-value problem obtained by imposing the quasiperiodic boundary condition $C(\phi, \tilde{T}) = C(\phi + \rho, 0)$ and the initial conditions

$$0 = \tilde{\lambda}_T^{\mathrm{T}}(\phi, 0) C(\phi, 0) \tilde{\lambda}_T(\phi, 0), \tag{6.35}$$

$$0 = \tilde{\lambda}_\rho^{\mathrm{T}}(\phi, 0) C(\phi, 0) \tilde{\lambda}_\rho(\phi, 0), \tag{6.36}$$

$$0 = \tilde{\lambda}_T^{\mathrm{T}}(\phi, 0) C(\phi, 0) \tilde{\lambda}_\rho(\phi, 0) \tag{6.37}$$

has a unique solution but appears over-determined as the nominal dimensional deficit equals -3. To resolve this issue, similar to the previous chapter, we introduce three additional auxiliary unknowns into the differential equation by adding the terms $\alpha_1 \partial_t \tilde{v}\, \partial_t \tilde{v}^{\mathrm{T}}$, $\alpha_2 \partial_\phi \tilde{v}\, \partial_\phi \tilde{v}^{\mathrm{T}}$ and $\alpha_3 \left(\partial_t \tilde{v}\, \partial_\phi \tilde{v}^{\mathrm{T}} + \partial_\phi \tilde{v}\, \partial_t \tilde{v}^{\mathrm{T}} \right)$, which we anticipate will lead to a non-degenerate solution with $\alpha_1 = \alpha_2 = \alpha_3 = 0$. Indeed, with these additions,

$$\frac{\partial}{\partial t} \left(\tilde{\lambda}_T^{\mathrm{T}}(\phi, t) C(\phi, t) \tilde{\lambda}_T^{\mathrm{T}}(\phi, t) \right) = \alpha_1, \tag{6.38}$$

$$\frac{\partial}{\partial t} \left(\tilde{\lambda}_\rho^{\mathrm{T}}(\phi, t) C(\phi, t) \tilde{\lambda}_\rho^{\mathrm{T}}(\phi, t) \right) = \alpha_2, \tag{6.39}$$

$$\frac{\partial}{\partial t} \left(\tilde{\lambda}_T^{\mathrm{T}}(\phi, t) C(\phi, t) \tilde{\lambda}_\rho^{\mathrm{T}}(\phi, t) \right) = \alpha_3, \tag{6.40}$$

but since $\tilde{\lambda}_T$, $\tilde{\lambda}_\rho$, and C all satisfy the quasiperiodic boundary condition with irrational ρ, it follows that α_1, α_2 and α_3 must equal 0.

We obtain the covariance matrix for a given point $\tilde{v}(\phi, t)$ on the quasiperiodic torus and relative to a hyperplane perpendicular to the vectors $\tilde{\lambda}_T(\phi, t)$ and $\tilde{\lambda}_\rho(\phi, t)$ from a solution $\left(\tilde{v}(\phi, t), \tilde{T}, \tilde{\lambda}_{\mathrm{T}}(\phi, t), \tilde{\lambda}_\rho(\phi, t), \tilde{C}(\phi, t), \tilde{\alpha}_1, \tilde{\alpha}_2, \tilde{\alpha}_3 \right)$ to the boundary-value problem

$$0 = \frac{\partial v}{\partial t}(\phi, t) - f(v(\phi, t)) \tag{6.41}$$

$$0 = v\left(\phi, T\right) - v\left(\phi + \rho, 0\right), \tag{6.42}$$

$$0 = h\left(v(\cdot, \cdot), p\right), \tag{6.43}$$

$$0 = \partial_t \lambda_T^{\mathrm{T}}(\phi, t) + \lambda_T^{\mathrm{T}}(\phi, t)\partial_x f\left(v(\phi, t)\right) - \lambda_{\mathrm{ps},T}^{\mathrm{T}} \partial_v h\left(v(\cdot, \cdot)\right), \tag{6.44}$$

$$0 = \lambda_T^{\mathrm{T}}\left(\phi, T\right) - \lambda_{\mathrm{bc},T}^{\mathrm{T}}\left(\phi\right), \tag{6.45}$$

$$0 = \lambda_T^{\mathrm{T}}\left(\phi, 0\right) - \lambda_{\mathrm{bc},T}^{\mathrm{T}}\left(\phi - \rho\right), \tag{6.46}$$

$$0 = \eta_{T,T} - \int_{\mathbb{S}} \lambda_{\mathrm{bc},T}^{\mathrm{T}}\left(\phi\right) f\left(v\left(\phi, T\right)\right) \mathrm{d}\phi, \tag{6.47}$$

$$0 = \eta_{\rho,T} + \int_{\mathbb{S}} \lambda_{\mathrm{bc},T}^{\mathrm{T}}(\phi)\partial_\phi v(\phi + \rho, 0)\mathrm{d}\phi, \tag{6.48}$$

$$0 = \partial_t \lambda_\rho^{\mathrm{T}}(\phi, t) + \lambda_\rho^{\mathrm{T}}(\phi, t)\partial_x f\left(v(\phi, t)\right) - \lambda_{\mathrm{ps},\rho}^{\mathrm{T}} \partial_v h\left(v(\cdot, \cdot)\right), \tag{6.49}$$

$$0 = \lambda_\rho^{\mathrm{T}}\left(\phi, T\right) - \lambda_{\mathrm{bc},\rho}^{\mathrm{T}}\left(\phi\right), \tag{6.50}$$

$$0 = \lambda_\rho^{\mathrm{T}}\left(\phi, 0\right) - \lambda_{\mathrm{bc},\rho}^{\mathrm{T}}\left(\phi - \rho\right), \tag{6.51}$$

$$0 = \eta_{T,\rho} - \int_{\mathbb{S}} \lambda_{\mathrm{bc},\rho}^{\mathrm{T}}\left(\phi\right) f\left(v\left(\phi, T\right)\right) \mathrm{d}\phi, \tag{6.52}$$

$$0 = \eta_{\rho,\rho} + \int_{\mathbb{S}} \lambda_{\mathrm{bc},\rho}^{\mathrm{T}}(\phi)\partial_\phi v(\phi + \rho, 0)\mathrm{d}\phi, \tag{6.53}$$

$$\begin{aligned} 0 = \frac{\partial C}{\partial t} &- \partial_x f(v) C + C(\phi, t)\left(\partial_x f(v)\right)^{\mathrm{T}} - Q F(v) F^{\mathrm{T}}(v) Q^{\mathrm{T}} \\ &- \alpha_1 \partial_t v \partial_t v^{\mathrm{T}} - \alpha_2 \partial_\phi v \partial_\phi v^{\mathrm{T}} - \alpha_3\left(\partial_t v \partial_\phi v^{\mathrm{T}} + \partial_\phi v \partial_t v^{\mathrm{T}}\right), \end{aligned} \tag{6.54}$$

$$0 = C(\phi, \tilde{T}) - C(\phi + \rho, 0), \tag{6.55}$$

$$0 = \lambda_T^{\mathrm{T}}(\phi, 0) C(\phi, 0) \lambda_T(\phi, 0), \tag{6.56}$$

$$0 = \lambda_\rho^{\mathrm{T}}(\phi, 0) C(\phi, 0) \lambda_\rho(\phi, 0). \tag{6.57}$$

$$0 = \lambda_T^{\mathrm{T}}(\phi, 0) C(\phi, 0) \lambda_\rho(\phi, 0), \tag{6.58}$$

where $\eta_{T,T} = \eta_{\rho,\rho} = 1$ and $\eta_{T,\rho} = \eta_{\rho,T} = 0$. Here (6.41-6.43) is the quasiperiodic boundary-value problem that yields $\tilde{v}(\phi, t)$ and $\tilde{T}$. Eqs. (6.44-6.53) are the corresponding adjoint

boundary-value problems that must be solved to obtain $\tilde{\lambda}_T$ and $\tilde{\lambda}_\rho$, respectively. The quasiperiodic orbit and the adjoint variables are used in the boundary-value problem (6.54-6.58) to obtain the unique covariance matrix associated with hyperplanes along the surface.

The formulation outlined here is an original formulation using adjoints to capture the effects of noise near transversally stable quasiperiodic invariant tori. Similar to the periodic orbit case in the last chapter, the formulation employs the purposeful introduction of the projection matrix Q in (6.54), the imposition of the non-degeneracy conditions (6.56-6.58), and the introduction of the corresponding "damping" parameters in (6.54). In contrast to previous work [45], we have chosen to use a projection defined by the solution to the adjoint boundary-value problem, and, consequently, associated with planes orthogonal to $\tilde{\lambda}_T(\phi, t)$ and $\tilde{\lambda}_\rho(\phi, t)$, since this is a natural decomposition that respects the spectral properties of the solution $\tilde{X}(t)$ to the variational problem. In the next section, we discuss the implementation of this boundary-value problem in COCO.

6.3 Implementation

As discussed in the previous section, the covariance computation involves solving the torus boundary-value problem (6.41-6.43), the corresponding adjoint problems (6.44-6.53) and the covariance boundary-value problem (6.54-6.58). We implement a discretization of these boundary-value problems in COCO.

6.3.1 Torus boundary-value problem

Following the discretization strategy proposed in [32] and revisited in Chapter 4 for quasiperiodic invariant tori in problems with delay, we approximate the function $\tilde{v}(\phi, t)$ in terms of a Fourier series in ϕ and M individual trajectories along characteristics of the governing PDE

for a discrete, uniform sample of values of ϕ:

$$\phi_j = \frac{j-1}{M}, \tag{6.59}$$

where $j = 1, \ldots, M$. For each trajectory segment, we use the `bvp` toolbox in COCO to construct the corresponding discretized zero problem.

Using the `bvp` toolbox, we first impose a collocation discretization of the differential constraints

$$\frac{\mathrm{d}v}{\mathrm{d}\tau}\left(\phi_j, \tau\right) = T_j f\left(v\left(\phi_j, \tau\right), p_j\right), \tag{6.60}$$

with $j = 1, \ldots, M$. Here p_j and T_j denote the problem parameters and the trajectory length associated with the j-th segment. After construction of all M segments, the problem parameters and the trajectory lengths are glued together per the conditions

$$0 = p_1 - p_j \tag{6.61}$$

$$0 = T_1 - T_j \tag{6.62}$$

$j = 2, \ldots, M$.

Next, the different trajectory segments are coupled through the boundary condition (6.42), whose discretized form is given by

$$(F \otimes I_n) \begin{pmatrix} v\left(\phi_1, 1\right) \\ \vdots \\ v\left(\phi_M, 1\right) \end{pmatrix} = ((R(\rho) \cdot F) \otimes I_n) \cdot \begin{pmatrix} v\left(\phi_1, 0\right) \\ \vdots \\ v\left(\phi_M, 0\right) \end{pmatrix}, \tag{6.63}$$

where F denotes the Fourier discretization matrix [32], $R(\rho)$ is the rotation matrix associated with the rotation number ρ. This condition is imposed as a zero function in COCO during implementation.

Finally we impose the following Poincaré phase conditions (cf. (6.43))

$$0 = \partial_\tau v^* (0,0)^{\mathrm{T}} \left(v(0,0) - v^*(0,0) \right) \tag{6.64}$$

$$0 = \partial_\phi v^* (0,0)^{\mathrm{T}} \left(v(0,0) - v^*(0,0) \right) \tag{6.65}$$

to remove the invariance along the two phase directions.

6.3.2 Adjoint boundary-value problem

The equivalent of the adjoint conditions (6.44-6.48) and (6.49-6.53) used to derive the projection matrix $\tilde{Q}$ are obtained from the vanishing of the variations of the following Lagrangian

$$\begin{aligned} L = \int_{\mathbb{S}} \int_0^1 & \lambda^{\mathrm{T}}(\phi,\tau) \left(\partial_\tau v(\phi,\tau) - T f\left(v(\phi,\tau), p \right) \right) \mathrm{d}\tau \mathrm{d}\phi \\ & + \int_{\mathbb{S}} \lambda_{\mathrm{bc}}^{\mathrm{T}}(\phi) \left(v(\phi+\rho,0) - v(\phi,1) \right) \mathrm{d}\phi + \lambda_{\mathrm{ps}}^{\mathrm{T}} h\left(v(0,0), p \right) \\ & + \eta_\rho (\rho - \mu_\rho) + \eta_T (T - \mu_T) + \eta_p^{\mathrm{T}} (p - \mu_p), \end{aligned} \tag{6.66}$$

with respect to $v(\phi,\tau)$, $v(\phi,0)$, $v(\phi,1)$, T, ρ, and p. For each sampled value of ϕ, these may be obtained directly for the corresponding trajectory segment using the adjoint constructors available in the `bvp` toolbox. This construction is equivalent to deriving the adjoint conditions from the following approximation of the Lagrangian, where integration over $\mathbb{S}$ has been replaced

by an average of the trajectory segments:

$$
\begin{aligned}
L_d = &\sum_{j=1}^{M} \frac{1}{M} \int_0^1 \lambda_j^{\mathrm{T}}(\tau) \left(v'(\phi_j, \tau) - T_j f\left(v(\phi_j, \tau), p_j\right)\right) \mathrm{d}\tau \\
&+ \frac{1}{M} \lambda_{\mathrm{bc}}^{\mathrm{T}} \left(\mathcal{R}(\rho)\, \mathbf{v}(\phi_0) - \mathcal{F}\mathbf{v}(\phi_1)\right) + \sum_{j=2}^{M} \lambda_{p,j} (p_1 - p_j) + \sum_{j=2}^{M} \lambda_{T,j} (T_1 - T_j) \\
&+ \lambda_{\mathrm{ps},1} \left(\partial_\tau v^*(0,0)^{\mathrm{T}} \left(v(0,0) - v^*(0,0)\right)\right) + \lambda_{\mathrm{ps},2} \left(\partial_\phi v^*(0,0)^{\mathrm{T}} \left(v(0,0) - v^*(0,0)\right)\right) \\
&+ \eta_p^{\mathrm{T}}(p - \mu_p) + \eta_T(T_1 - \mu_{T_1}) + \eta_\rho(\rho - \mu_\rho),
\end{aligned} \tag{6.67}
$$

where $\mathcal{F} = F \otimes I_n, \mathcal{R}(\rho) = (R(\rho) \cdot F) \otimes I_n$ and

$$
\begin{aligned}
\mathbf{v}(\phi_0) &= \mathfrak{vec}\left(v(\phi_1, 0), v(\phi_2, 0), \ldots, v(\phi_M, 0)\right), \\
\mathbf{v}(\phi_1) &= \mathfrak{vec}\left(v(\phi_1, 1), v(\phi_2, 1), \ldots, v(\phi_M, 1)\right).
\end{aligned}
$$

The adjoint conditions are then obtained from the vanishing of the variations of L_d with respect to $v(\phi_j, \tau)$, $v(\phi_j, 1)$, $v(\phi_j, 0)$, T_j, and p_j for $j = 1, \ldots, M$, and the rotation number ρ. It follows from the adjoint conditions that the following relations hold

$$
\sum_{j=1}^{M} \int_0^1 \lambda_j^{\mathrm{T}}(\tau)\, f\left(v(\phi_j), p\right) \mathrm{d}\tau = M\eta_T, \tag{6.68}
$$

$$
-\lambda_{\mathrm{bc}}^{\mathrm{T}} \mathcal{R}'(\rho)\, \mathbf{v}(\phi_0) = M\eta_\rho, \tag{6.69}
$$

where $(\eta_T, \eta_\rho) = (1, 0)$ and $(0, 1)$, respectively, when solving for $\tilde{\lambda}_T(\phi, \tau)$ and $\tilde{\lambda}_\rho(\phi, \tau)$.

Notably, the construction using the adjoint constructors in the `bvp` toolbox omits the factor $\frac{1}{M}$ in the first two terms of the Lagrangian L_d. It follows that we must let $(\eta_T, \eta_\rho) = (M, 0)$ and $(0, M)$, respectively, when solving for $\tilde{\lambda}_T(\phi, \tau)$ and $\tilde{\lambda}_\rho(\phi, \tau)$ using the COCO implementation. To construct the two uncoupled sets of adjoint conditions for $\tilde{\lambda}_T$ and $\tilde{\lambda}_\rho$, respectively, using the `bvp` adjoint constructors, we append a second identical instance of the zero problem for $\tilde{v}$ and $\tilde{T}$ with a different function identifier and glue together the problem parameters of the two

instances. These instances are then referred to separately by the `bvp` adjoint constructors.

6.3.3 Covariance boundary-value problem

Finally, the covariance boundary-value problem (6.54-6.58) may also be discretized in terms of a Fourier series in ϕ and solutions along individual characteristics as suggested by the ODEs

$$\begin{aligned}\frac{\mathrm{d}C}{\mathrm{d}\tau}\left(\phi_j,\tau\right) &= T_j\partial_x f(v(\phi_j,\tau),p)C(\phi_j,\tau) + T_jC(\phi_j,\tau)\left(\partial_x f(v(\phi_j,\tau),p)\right)^{\mathrm{T}} \\ &\quad + T_jQ(\phi_j,\tau)F(v(\phi_j,\tau))F^T(v(\phi_j,\tau),p)Q^{\mathrm{T}}(\phi_j,\tau) \\ &\quad + \frac{1}{T_j}\alpha_1\partial_\tau v\left(\phi_j,\tau\right)\frac{1}{T}\partial_\tau v\left(\phi_j,\tau\right)^{\mathrm{T}} + T_j\alpha_2\frac{\partial v}{\partial\phi}\left(\phi_j,\tau\right)\frac{\partial v}{\partial\phi}\left(\phi_j,\tau\right)^{\mathrm{T}} \\ &\quad + \alpha_3\left(\partial_\tau v\left(\phi,\tau\right)\partial_\phi v\left(\phi_j,\tau\right)^{\mathrm{T}} + \partial_\phi v\left(\phi,\tau\right)\partial_\tau v\left(\phi_j,\tau\right)^{\mathrm{T}}\right),\end{aligned} \tag{6.70}$$

the degeneracy conditions

$$0 = \lambda_T\left(\phi_j,0\right)^{\mathrm{T}} C\left(\phi_j,0\right)\lambda_T\left(\phi_j,0\right), \tag{6.71}$$

$$0 = \lambda_T\left(\phi_j,0\right)^{\mathrm{T}} C\left(\phi_j,0\right)\lambda_\rho\left(\phi_j,0\right) \tag{6.72}$$

$$0 = \lambda_\rho\left(\phi_j,0\right)^{\mathrm{T}} C\left(\phi_j,0\right)\lambda_\rho\left(\phi_j,0\right) \tag{6.73}$$

and the quasiperiodic boundary conditions

$$\left(F\otimes I_{n^2}\right)\begin{pmatrix}\mathfrak{vec}\left(C\left(\phi_1,1\right)\right)\\ \vdots \\ \mathfrak{vec}\left(C\left(\phi_M,1\right)\right)\end{pmatrix} = \left(\left(R(\rho)\cdot F\right)\otimes I_{n^2}\right)\begin{pmatrix}\mathfrak{vec}\left(C\left(\phi_1,0\right)\right)\\ \vdots \\ \mathfrak{vec}\left(C\left(\phi_M,0\right)\right)\end{pmatrix} \tag{6.74}$$

Here j varies from $1,\ldots,M$ and T_j denotes the segment durations.

There are two ways through which one can obtain the covariance matrix in this case. The first is to solve the full boundary-value problem for $\tilde{v}(\phi,\tau)$, $\tilde{T}$, $\tilde{\lambda}_T$, $\tilde{\lambda}_\rho$, $\tilde{C}$, $\tilde{\alpha}_1$, $\tilde{\alpha}_2$, and $\tilde{\alpha}_3$. For

such an implementation, the covariance equations need to be appended to the augmented continuation problem using the complementary zero function constructor `coco_add_comp`. This implementation is particularly useful if we want to continue these solutions under variations in problem parameters.

Alternatively, one can implement the covariance boundary-value problem (6.54-6.58) as a stand-alone zero problem using the zero function constructor `coco_add_func`. Such an implementation would require loading already stored solutions $\tilde{v}(\phi, \tau)$, $\tilde{T}$, $\tilde{\lambda}_T$, and $\tilde{\lambda}_\rho$. The advantage of this post-processing implementation is that the covariance computations will be faster than in the former case.

6.4 Coupled Van der Pol Oscillator

To test our formulation, we consider the coupled Van der Pol SDE

$$\begin{pmatrix} \mathrm{d}x_1 \\ \mathrm{d}x_2 \\ \mathrm{d}y_1 \\ \mathrm{d}y_2 \end{pmatrix} = \begin{pmatrix} x_2 \\ -\epsilon\left(x_1^2 - 1\right) x_2 - x_1 \\ y_2 \\ -\epsilon\left(y_1^2 - 1\right) y_2 + (1+\delta)\, y_1 \end{pmatrix} \mathrm{d}t + \begin{pmatrix} 0 \\ \beta\left(y_1 - x_1\right) \\ 0 \\ \beta\left(x_1 - y_1\right) \end{pmatrix} \mathrm{d}t + \sigma \mathrm{d}W_t. \tag{6.75}$$

Here ϵ, δ, β are the problem parameters and $W_t \in \mathbb{R}^4$ is a vector of independent Brownian motions. Quasiperiodic invariant tori of the deterministic drift vector field have been studied in detail by Schilder *et al.* [66] and are used here as a basis for studying the effects of noise. With ϵ fixed to 0.5 and $\sigma = 0$, there exists a family of quasiperiodic invariant tori for varying β and δ with fixed rotation number, approximately equal to $62\sqrt{2}/140$. Indeed, using the initial parameter values $\epsilon = 0.5$, $\beta = 0$, $\delta = 1.503$, and $\rho = 62\sqrt{2}/140$, and the initial solution guess

$$v\left(\phi_j, t\right) = \begin{pmatrix} 2\sin\left(2\pi\phi_j + t\right) & 2\cos\left(2\pi\phi_j + t\right) & 2\sin\left(1.59t\right) & 3.19\cos\left(1.59t\right) \end{pmatrix}^{\mathrm{T}} \tag{6.76}$$

for $t \in [0, 2\pi/1.59]$ and $M = 23$, we obtain the family shown in Fig. 6.1. The invariant torus and the corresponding adjoint variables when $\beta = 0.2$ are shown in Fig. 6.2.

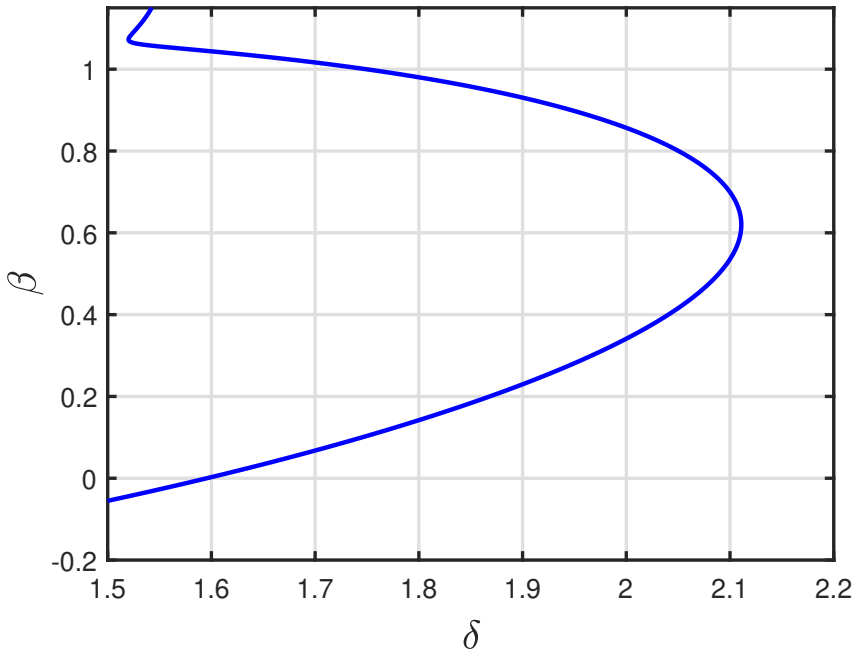

Figure 6.1: Family of quasiperiodic invariant tori for the deterministic coupled Van der Pol oscillator system (6.75). Here, $\epsilon = 0.5$ and the rotation number is fixed at $62\sqrt{2}/140$.

Following the discussion in the previous section, we use the stored data for $\tilde{v}$, $\tilde{T}$, $\tilde{\lambda}_T$, and $\tilde{\lambda}_\rho$ for $\beta = 0.2$ to solve the boundary-value problem for the covariance function. A convergence analysis is first performed to get an estimate of the number of segments (M) and number of discretization intervals (N) that must be used to obtain reliable results. In Table 6.1, we show the maximum of the i-th eigenvalue (ordered by magnitude) of the covariance matrix function over all segments for different numbers of segments and N fixed to 30. We observe that the eigenvalues converge rapidly with increasing M. The two lowest eigenvalues decay to zero, as is expected since the covariance matrix in this case should be positive semi-definite with two zero eigenvalues. Due to memory limitations, we were not able to increase M beyond 31. Table 6.2 shows the maximum of the i-th eigenvalue of the covariance matrix as a function of the number of discretization intervals and M fixed to 31. Here, again, we observe rapid convergence in the eigenvalues with finer discretization.

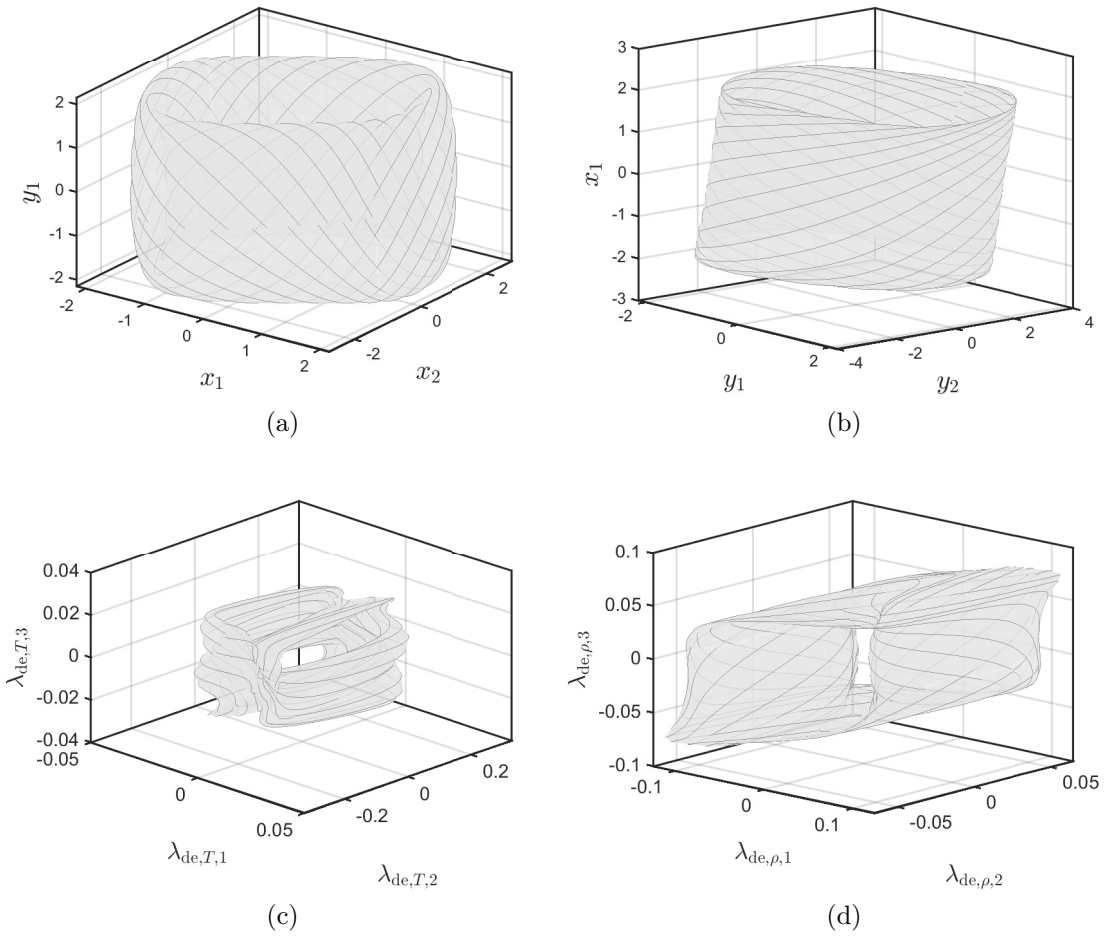

Figure 6.2: (a,b) Projected invariant torus for the coupled Van der Pol oscillator system with $\epsilon = 0.5, \beta = 0.2, \delta = 1.7566$ and rotation number $\rho \approx 62\sqrt{2}/140$. (c,d) Corresponding projected Lagrange multipliers $\tilde{\lambda}_T$ and $\tilde{\lambda}_\rho$. Here M equals 23.

With $M = 31$ and $N = 30$, we consider the section $t = \tilde{T}/2$ on the torus and use the predicted eigenvalues and eigenvectors to graph curves in Fig. 6.3 representing one and two standards deviations of the Gaussian distribution from the invariant torus as a function of ϕ. We compare these predictions to results obtained using numerical simulation. Specifically, we first perform direct numerical simulation of the stochastic trajectories using the Euler-Maruyama integrator in Matlab. The simulation is performed for a duration of 2000 time units, with time-step $\mathrm{d}t = 10^{-4}$, and noise level $\sigma = 0.1$. For each point on the stochastic trajectory, we then compute the values of ϕ and τ that define the corresponding projection $\tilde{Q}(\phi, \tau)$ using the hyperplane definitions (6.15-6.16). For consecutive points along a trajectory

Table 6.1: The eigenvalues of the covariance matrix as a function of the number of segments M. $\gamma_{i,M}$ denotes the maximum of the i^{th} eigenvalue of the covariance matrix over the discretized quasiperiodic torus. Here, $N = 30$.

M	11	15	19	23	27	31
$\gamma_{1,M}$	3.8936	3.9272	3.7621	3.75	3.7617	3.7548
$\gamma_{2,M}$	2.5954	2.5036	2.5991	2.5868	2.5986	2.5826
$\gamma_{3,M}$	0.4137	0.3061	0.0256	9.2×10^{-3}	6.7×10^{-4}	7.7×10^{-4}
$\gamma_{4,M}$	8.2×10^{-3}	2.1×10^{-3}	5.3×10^{-4}	9.5×10^{-5}	2.1×10^{-5}	2.5×10^{-5}

Table 6.2: The eigenvalues of the covariance matrix as a function of the number of discretization intervals N. $\gamma_{i,N}$ denotes the maximum of the i^{th} eigenvalue over the discretized quasiperiodic torus. Here, $M = 31$.

N	10	15	20	25	30
$\gamma_{1,N}$	3.7477	3.7548	3.7476	3.7543	3.7548
$\gamma_{2,N}$	2.567	2.5826	2.5774	2.5835	2.5826
$\gamma_{3,N}$	3.8×10^{-3}	8.9×10^{-4}	7.9×10^{-4}	7.8×10^{-4}	7.7×10^{-4}
$\gamma_{4,N}$	8.73×10^{-4}	4.3×10^{-4}	1.6×10^{-4}	5×10^{-5}	2.5×10^{-5}

on either side of the section $t = \tilde{T}/2$, we use straight-line interpolation to compute a point on the section and the corresponding value of ϕ, by again imposing (6.15-6.16). Finally, we project the deviations x_{tr} onto the predicted normalized eigenvectors $e_1(\phi)$ and $e_2(\phi)$ of the corresponding covariance matrix associated with the nonzero eigenvalues. The results are represented by the red dots in Fig. 6.3 and are consistent with the theoretical bounds.

6.5 Conclusions

In this chapter, we generalized the adjoint-based formulation derived in the previous chapter for limit cycles to the case of transversally stable quasiperiodic invariant two-tori. A further generalization to the case of n-tori with $n > 2$ should be immediate, but inevitably results in a very high-dimensional continuation problem, especially if the `bvp` toolbox constructors are used without taking advantage of the similarity between the various boundary-value problems for $\tilde{\lambda}$.

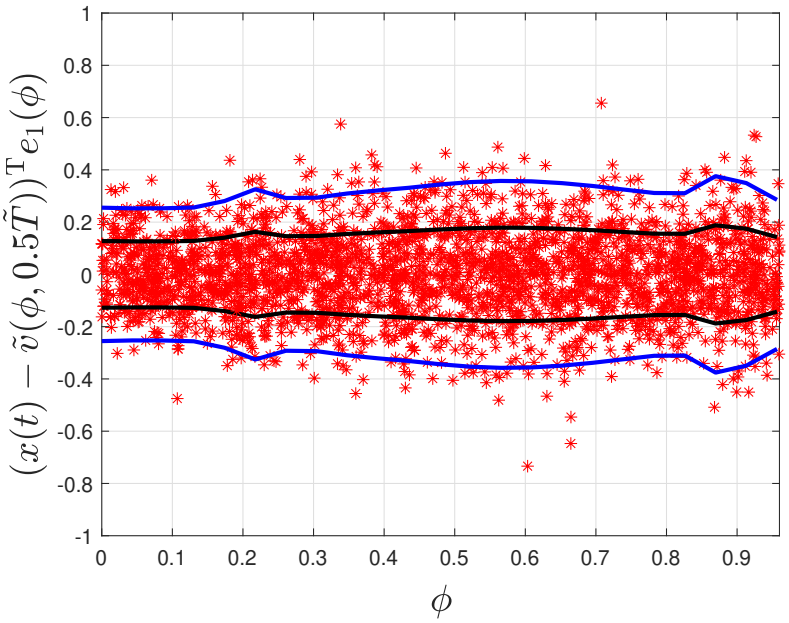

(a)

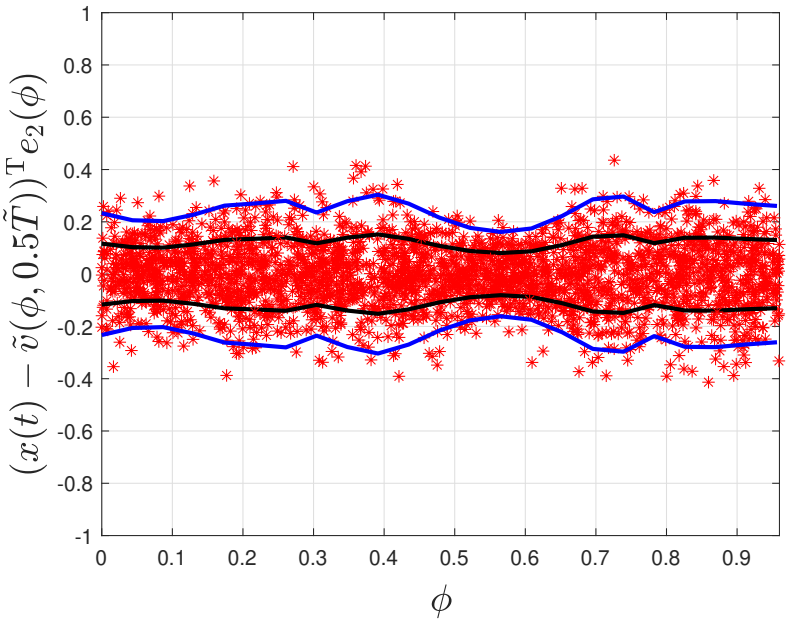

(b)

Figure 6.3: Comparison of predicted bounds in terms of one (black) and two (blue) standard deviations with the results (red dots) of numerical simulation using the Euler-Maruyama integrator for the coupled Van der Pol oscillator system. The results are visualized in terms of projections onto (a) the eigenvector $e_1(\phi)$ corresponding to the largest eigenvalue and (b) the eigenvector $e_2(\phi)$ corresponding to the second-largest eigenvalue of the covariance matrix.

Chapter 7

DISCUSSION AND FUTURE WORK

In this dissertation, we proposed formulations based on adjoints for optimal design of time-delay systems and uncertainty quantification in stochastic systems. The first half of this dissertation focused on generalizing an existing continuation-based optimization strategy to problems involving delay differential constraints. We then proposed a general framework that can handle a wide range of delay-coupled, multi-segment boundary-value problems. In the second half of the dissertation, we proposed a novel covariance-boundary value problem for uncertainty quantification near periodic/quasiperiodic orbits of dynamical systems perturbed with noise. There are a number of different directions in which this work can be extended upon. In the next sections, we provide a chapter-wise summary of the content, followed by opportunities for further research.

7.1 Methods of continuation

The staged approach to problem construction supported by COCO permits the user to build up nonlinear problems gradually by adding new variables and systems of equations and coupling them flexibly to variables defined previously, at each step increasing or decreasing the dimensional deficit (nominally the dimension of the corresponding solution manifold). This is the natural way of thinking about problem construction if algorithms for multi-dimensional continuation are at one's disposal. The initial examples in Chapter 2 showed how bifurcations or function extrema are embedded within higher-dimensional solution manifolds.

Chapter 2 described in detail the abstract staged construction formalism in the full generality currently supported by COCO. A major innovation since its original realization in [32] is that the formalism now supports the simultaneous gradual build-up of adjoint information and also includes a new layer that permits construction of complementarity conditions associated with design optimization in the presence of inequality constraints (as partially described in [35]). The utility of such staged construction with automatic accumulation of adjoints was illustrated using two detailed examples. The first example, a data assimilation problem, was an optimization problem with multiple delay-coupled time segments. The second, a phase response analysis of periodic orbits, was formulated as a linear sensitivity analysis of the orbital duration with respect to perturbations in the boundary conditions. Both examples showed that it is, in principle, possible to perform staged construction of a boundary-value problem associated with multiple segments, coupled to each other by discrete time delays, while automatically accumulating adjoints.

7.2 Design optimization in problems with delay

The various examples in Chapter 3 illustrated the successful application to the case with single time delays of the general methodology to optimization along implicitly defined solutions to integro-differential boundary-value problems first proposed by Kernevéz and Doedel [13] for ordinary differential equations. Here, the partial Lagrangian approach introduced in [14] was used to derive adjoint conditions that were linear and homogeneous in the unknown Lagrange multipliers. This allowed a search for local extrema to proceed along a connected sequence of one-dimensional manifolds of solutions to the necessary conditions for such extrema minus the trivial algebraic adjoint conditions on a subset of the Lagrange multipliers: first, along a branch with vanishing Lagrange multipliers, then switching to a branch with linearly varying Lagrange multipliers, and then along additional branches until all the previously omitted trivial algebraic adjoint conditions were satisfied.

In contrast to the case of ordinary differential equations, the presence of time delays introduces potential discontinuities that must be accounted for in any numerical solution strategy. By the properties of differential equations with time-shifted arguments, such discontinuities propagate across time, gaining an order of continuity for each iteration. Here, we have only accounted for zeroth- or first-order discontinuities in the formulation of the governing boundary-value problems. On each segment along which a function was shown to be continuously differentiable, we have approximated such a function by a continuous piecewise-polynomial function of degree 4 in each mesh interval, ignoring continuity in the first derivative across mesh boundaries or discontinuities of order two or higher within each mesh interval. The piecewise-polynomial approximants were used to impose a discretization of the governing differential equations at a set of collocation nodes within each interval and to evaluate functions with time-shifted arguments on the same or other intervals. Such a collocation strategy is consistent with the approach in [114], and there compared to an alternative mesh strategy that depends on the delay. We have not undertaken a detailed analysis of the sensitivity of the results to the numerical mesh or polynomial degree. Notably, while we rely in this study invariably on uniform meshes, it is common to consider adaptive meshes for which the number of intervals and their relative size may change during continuation.

In all the examples, a Lagrange multiplier associated with a phase condition was found to equal 0 on a local extremum of the corresponding Lagrangian. As stated previously, we nevertheless retained this Lagrange multiplier as an unknown and monitored its value during continuation. Experiments with the number of mesh intervals were used to determine whether this value was effectively 0 also in the computational analysis. An alternative would have been to eliminate this variable from the set of adjoint equations while simultaneously eliminating one of the adjoint conditions. In a single instance, this may indeed be useful, but when relying on a general-purpose implementation as described for the implementation in Chapter 4, it is better to retain the variable and use its numerical value as an indicator of the accuracy of the solution.

7.3 A toolbox for delay-coupled boundary-value problems

Chapter 4 demonstrated that it is possible to perform staged construction of a boundary-value problem associated with multiple segments, coupled to each other by discrete time delays, while automatically accumulating adjoints. The underlying structure is a network of delay-coupled systems of ordinary differential equations, linked by algebraic coupling constraints. A general representation in terms of delay graphs inspired the formulation of an abstract toolbox for delay-coupled problems, where each building block (a differential constraint and a set of algebraic coupling conditions) is sufficiently general but also simple enough to implement its adjoint at the toolbox level. The chapter then went on to formulate the discretized version of this abstract network of equations, first in terms of abstract projections, then with a detailed vectorized description of the resulting algebraic equations. The generality of the toolbox was demonstrated in the context of several numerical examples of coupled systems with delay as they arise for connecting orbits, optimal control problems, and quasiperiodic invariant tori.

7.4 Noise induced behavior near limit cycles

In Chapter 5, we discussed an original boundary-value problem formulation for local covariance analysis near limit cycles perturbed by noise. This was shown to enable efficient computational analysis, including parameter continuation, of the limit cycles and the corresponding covariance matrices describing stationary Gaussian distributions in transversal hyperplanes through points along the limit cycles and with means given by these points. We used examples to demonstrate the utility of the approach and to verify the theoretical predictions using numerical simulations.

A unique feature of the formulation is the construction of the covariance matrix in terms of the original state-space variables rather than a reduced set of coordinates, as is common in the literature when choosing to project onto hyperplanes perpendicular to the vector field.

As a result, the complete boundary-value problem adheres to the construction paradigm of COCO, specifically the possibility of building the complete continuation problem in stages. We have taken advantage of this general structure and implemented a COCO-compatible constructor that appends the covariance boundary-value problem to the periodic-orbit and adjoint boundary-value problems generated using toolbox constructors included with the COCO release. The numerical results reported in this analysis were all obtained using this tool. With the help of this tool, we are now able to investigate the influence of different choices of the dispersion matrix F, including whether particular choices of F may result in covariance bounds that match predefined specifications.

7.5 Noise induced behavior near quasiperiodic orbits

Finally, in Chapter 6, we generalized the covariance formulation discussed in Chapter 5 for stochastically perturbed limit cycles to a formulation capable of characterizing the local effects of noise for stochastically perturbed quasiperiodic invariant two-tori. A major difference in this analysis was that the governing boundary-value problem here depended on two independent variables rather than the single phase variable for the limit cycle. Moreover, since there were two neutral directions of the flow along the torus, multiple adjoint variables were required to construct the appropriate projection matrices.

We implemented a discretized form of the governing boundary-value problem in COCO using a combination of existing toolbox constructors and a new constructor for the linear covariance boundary-value problem. An important contribution was the introduction of "damping" terms that ensured a non-singular continuation problem. An example of a coupled Van der Pol oscillator was used to illustrate the approach.

7.6 Opportunities for future work

7.6.1 More general delay-coupled problems

Several classes of problems involving delay are not covered by the template toolbox developed in this dissertation. These include problems with state- or time-dependent delays, as well as those with distributed delays. Even for discrete delays, we have assumed an explicit form of the differential constraints with similarly explicit algebraic coupling conditions. In contrast, the defining problem in DDE-BIFTOOL admits delay differential equations with a nontrivial (and possibly singular) coefficient matrix on the left-hand side, thereby enabling analysis of problems with nontrivial algebraic coupling conditions. Our general approach to recognizing universality and encoding such universality in the COCO framework, including with attention to the automated construction of adjoints, should inform such further development.

7.6.2 Construction from delay graphs

The collection of differential and algebraic constraints provided in Section 4.2.1 are still one step away from the form in which a user typically formulates a multi-segment boundary-value problem with delay(s). The discussion in Section 4.1.2 provides a template for how to automate this step by encapsulating the data required for a toolbox to construct the associated boundary-value problem and adjoint contributions using a suitable graph representation. In this section, we propose a general theory that is compatible with the abstract toolbox template and apply this to the examples in Section 4.2.2.

As before, associate with each segment

- a duration $T > 0$: we develop all notation for unscaled intervals $[0, T]$ and assume that the involved differential equations are autonomous for simpler notation; the scaling can be performed in a separate final step;
- a delay $\alpha \geq 0$: we only consider a single delay per segment for simpler notation;

- a variable $x : [-\hat{\alpha}, T] \to \mathbb{R}^n$ with $\hat{\alpha} \geq \alpha$ that is involved in the temporal coupling between segments;
- directed links to its *predecessors*; associated to a link from node i to node j is a non-zero coupling matrix B_{ij}, such that

$$\sum_j B_{ij} x_j(T_j + s) = x_i(s) \text{ for all } s \in [-\hat{\alpha}_i, 0], \tag{7.1}$$

  where, in contrast to Section 4.1.2, we sum over all predecessors (allowing for more than one). The graph in Fig. 4.1 in Section 4.1.2 shows that the term predecessor refers to *direct* predecessors (so, a predecessor of a predecessor of segment (node) i is not automatically also a predecessor of node i.)

A node without predecessors can have $\hat{\alpha} = 0$, but in general $\hat{\alpha}$ must be larger than α, even if $\alpha = 0$ for a particular segment. For example, a node i with $\alpha_i = 0$ and duration $T_i = 1$ may be predecessor of a node k with $\alpha_k = 2$. Then $\hat{\alpha}_i$ has to be at least equal to 1. Notably, no information about $\hat{\alpha}$ will be required during construction of the associated coupling conditions. The graph representation immediately implies the *boundary condition*

$$\sum_j B_{ij} x_j(T_j) = x_i(0) \tag{7.2}$$

obtained by letting $s = 0$ in (7.1).

Consider, for example, the single-node graph shown in the left panel of Fig. 7.1. This encapsulates a delay differential equation $\dot{x}(t) = f(x(t), x(t - \alpha))$ for $t \in (0, T)$ and algebraic condition $x(s) = x(T + s)$ for $s \in [-\hat{\alpha}, 0]$ corresponding to the search for a periodic solution of period T. We apply the predecessor coupling as many times as necessary to ensure evaluation

of $x(\tau)$ only for $\tau \in (0,T)$ in the coupling conditions and obtain

$$\dot{x}(t) = f(x(t), y(t)),\ t \in (0,T), \tag{7.3}$$

$$y(t) = \begin{cases} x\left(T + t - \alpha\big|_{\mathrm{mod}[0,T]}\right), & t \in \left(0, \alpha\big|_{\mathrm{mod}[0,T]}\right), \\ x\left(t - \alpha\big|_{\mathrm{mod}[0,T]}\right), & t \in \left(\alpha\big|_{\mathrm{mod}[0,T]}, T\right). \end{cases} \tag{7.4}$$

Finally, (7.2) implies the periodic boundary condition $x(T) = x(0)$.

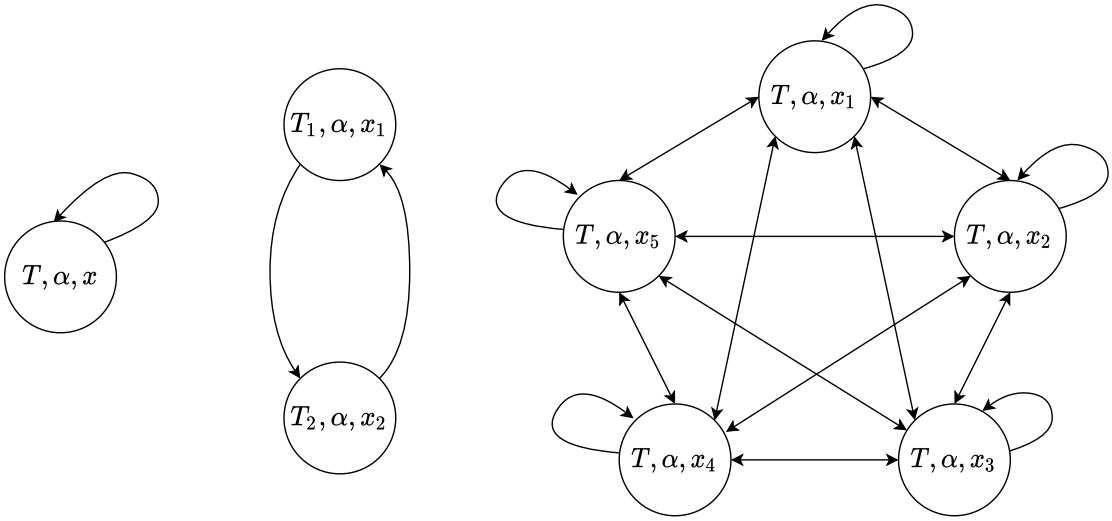

Figure 7.1: Graph representations for delay-coupled boundary-value problems representing (left) a single segment periodic orbit (middle) a two-segment periodic orbit and (right) a quasiperiodic invariant torus approximated with 5 segments.

As a second example, consider the two-node graph shown in the middle panel of Fig. 7.1. This encapsulates the system of delay differential equations

$$\dot{x}_1(t) = f_1(x_1(t), x_1(t-\alpha)),\ t \in (0,T_1), \tag{7.5}$$

$$\dot{x}_2(t) = f_2(x_2(t), x_2(t-\alpha)),\ t \in (0,T_2) \tag{7.6}$$

and algebraic conditions $x_1(s) = x_2(T_2 + s)$ for $s \in [-\hat{\alpha}_1, 0]$ and $x_2(s) = x_1(T_1 + s)$ for $s \in [-\hat{\alpha}_2, 0]$ corresponding to the search for a periodic solution of period $T_1 + T_2$ for a piecewise-defined vector field with delay α. We again apply the predecessor coupling as many

times as necessary to ensure evaluation of $x_1(\tau)$ and $x_2(\tau)$ only for $\tau \in (0, T_1)$ and $\tau \in (0, T_2)$, respectively, in the coupling conditions. For example, if $\alpha < T_1, T_2$, and with $y_1(t) = x_1(t-\alpha)$ and $y_2(t) = x_2(t-\alpha)$, we obtain the coupling conditions

$$y_1(t) = \begin{cases} x_2\left(T_2 + t - \alpha\right), & t \in (0, \alpha)\,, \\ x_1\left(t - \alpha\right), & t \in (\alpha, T_1)\,, \end{cases} \tag{7.7}$$

$$y_2(t) = \begin{cases} x_1\left(T_1 + t - \alpha\right), & t \in (0, \alpha)\,, \\ x_2\left(t - \alpha\right), & t \in (\alpha, T_2)\,. \end{cases} \tag{7.8}$$

If, instead, $T_1 < \alpha < T_2$, we obtain

$$y_1(t) = x_2\left(T_2 + t - \alpha\right),\ t \in (0, T_1)\,, \tag{7.9}$$

$$y_2(t) = \begin{cases} x_2\left(T_1 + T_2 + t - \alpha\right), & t \in (0, \alpha - T_1)\,, \\ x_1\left(T_1 + t - \alpha\right), & t \in (\alpha - T_1, \alpha)\,, \\ x_2(t - \alpha), & t \in (\alpha, T_2)\,. \end{cases} \tag{7.10}$$

In either case, (7.2) implies the boundary conditions $x_1(T) = x_2(0)$ and $x_2(T) = x_1(0)$.

For a general construction, we associate with each node one or several finite paths through our graph consisting of predecessors to this node and their predecessors. Specifically, a sequence $\kappa = (\kappa_1, \ldots, \kappa_\ell)$ with $\kappa_1 = i$ is a *history* for the i-th segment if κ_{k+1} is a predecessor to κ_k for $k = 1, \ldots, \ell - 1$ and

$$\sum_{j=2}^{\ell-1} T_{\kappa_j} < \alpha_i \leq \sum_{j=2}^{\ell} T_{\kappa_j}. \tag{7.11}$$

In the second example above, the sequence $(1, 2)$ is a history for segment 1 when $\alpha < T_2$ and the sequence $(2, 1)$ is a history for segment 2 when $\alpha < T_1$. In contrast, when $T_1 < \alpha < T_1 + T_2$, the sequence $(2, 1, 2)$ is a history for segment 2.

For a given history, there exists a smallest index ι such that

$$\alpha_i < T_i + \sum_{j=2}^{\iota} T_{\kappa_j}. \tag{7.12}$$

In particular, when $\alpha_i < T_i$, $\iota = 1$. In contrast, for the history $(2, 1, 2)$ in the second example above with $T_1 < \alpha < T_1 + T_2$, $\iota = 2$ and $\kappa_\iota = 1$. All indices between ι and ℓ result in $\ell - \iota$ internal boundaries at

$$\alpha_i - \sum_{j=2}^{\ell-k} T_{\kappa_j},\ k = 1, \ldots, \ell - \iota \tag{7.13}$$

and a partition of $[0, T_i]$ into $\ell - \iota + 1$ subintervals separated by these boundaries. For example, if $\ell - \iota = 1$, then $[0, T_i]$ is decomposed into the subintervals $[0, \alpha_i]$ and $[\alpha_i, T_i]$. Given these definitions, the k-th coupling condition for the i-th segment associated with the history κ is given by

$$\begin{aligned} y_i(t) = A_k(\kappa) x_{\kappa_{\ell-k+1}} \left(t - \alpha_i + \sum_{j=2}^{\ell-k+1} T_{\kappa_j} \right), \\ t \in \left[\max\left(0, \alpha_i - \sum_{j=2}^{\ell-k+1} T_{\kappa_j}\right), \min\left(T_i, \alpha_i - \sum_{j=2}^{\ell-k} T_{\kappa_j}\right) \right], \end{aligned} \tag{7.14}$$

where

$$A_k(\kappa) = B_{\kappa_1\kappa_2} \cdots B_{\kappa_{\ell-k}\kappa_{\ell-k+1}} \tag{7.15}$$

and an empty matrix product is interpreted as an identity matrix. From the boundary condition

$$B_{\kappa_{l-k}\kappa_{l-k+1}} x_{\kappa_{l-k+1}}(T_{\kappa_{l-k+1}}) = x_{\kappa_{l-k}}(0), \tag{7.16}$$

we obtain

$$A_k(\kappa) x_{\kappa_{\ell-k+1}} \left(T_{\kappa_{\ell-k+1}}\right) = A_{k+1}(\kappa) x_{\kappa_{\ell-k}}\left(0\right), \tag{7.17}$$

which, in turn implies continuity of $y_i(t)$ at the k-th internal boundary.

In a general graph, a segment may be associated with two or more distinct histories. In the

simplest case, any two such histories κ and κ' of a segment i correspond to identical sequences of durations $(T_{i,1}, \ldots, T_{i,\ell})$. In this special case, the partition of $[0, T_i]$ into subintervals is a property of the segment. We sum over the set of all histories, K_i, of the i-th segment to obtain a composite coupling condition

$$y_i(t) = \sum_{\kappa \in K_i} A_k(\kappa) x_{\kappa_{\ell-k+1}} \left(t - \alpha_i + \sum_{j=2}^{\ell-k+1} T_{\kappa_j} \right) \tag{7.18}$$

on the k-th subinterval. After appropriate time rescaling, this form matches the general coupling condition in Section 4.2.1 and ensures that continuity of the algebraic state variables follows from the boundary conditions on the differential state variables. It is straightforward to show that the graph in the right-most panel of Fig. 7.1 is an example of the special case for which (7.18) applies and that the corresponding coupling conditions match the third example in Section 4.2.2.

In problems where α_i and/or T_i vary during continuation, the indices ℓ and ι may change discretely at critical junctures necessitating a switch between different sets of coupling conditions. The constructive methodology introduced in this section may be deployed to yield a set of equations that remain valid on both sides of such junctures. For example, in the case of the single segment in the left panel of Fig. 7.1, the predecessor coupling relationship $x(s) = x(T + s)$ yields

$$x(t-\alpha) = \begin{cases} x(t-\alpha), & t \in (\alpha, T) \\ x(T+t-\alpha), & t \in (\alpha - T, \alpha) \\ x(2T+t-\alpha), & t \in (\alpha - 2T, \alpha - T) \\ \quad \vdots & \end{cases} \tag{7.19}$$

For $\alpha < T$, the third condition could be omitted, since the left-hand side is never evaluated outside $[0, T]$. If we, nevertheless, retain this condition in our formulation, we need to omit

the redundant imposition of continuity across $t = \alpha - T$, since this implies that $x(0) = x(1)$, something that already follows from continuity at $t = \alpha$. Similarly, for $\alpha > T$, the first condition could be omitted, since an inverted interval is assumed to be empty. Again nothing prevents us from retaining this condition also for this case provided that we omit imposing continuity across $t = \alpha$. With proper treatment of continuity, retaining all three conditions allows for variations of α/T across 1. By adding the next condition in the sequence, we include the possibility of variations of α/T across 2, and so on.

Future work should implement some version of this graph representation with the COCO toolbox described in this dissertation to support automated problem construction with a minimum of input data.

7.6.3 Adaptive discretization

When a(n augmented) continuation problem is defined on an infinite-dimensional Banach space $\mathcal{U}_\Phi$, it may be appropriate to change discretization (or *remesh* the problem) during continuation, e.g., in order to stay within pre-imposed bounds on the discretization errors (see Part V of [32] for an extensive discussion of such adaptive meshing). In COCO, a continuation problem is said to be *adaptive* if

- it is accompanied by instructions for switching between different discretizations without changing the dimensional deficit, and
- all monitor functions are defined independently of the problem discretization and then discretized accordingly.

During continuation, COCO will remesh an adaptive continuation problem at some frequency defined by the corresponding atlas algorithm and according to an algorithm particular to the discretization scheme. Since the monitor functions must be defined independently of the discretization, they span the coordinate axes of an invariant, finite-dimensional projection of $\mathcal{U}_\Phi$ which may serve to visualize an arbitrary solution manifold. Indeed, as long as a sufficient number of independent monitor functions are included with the continuation

problem, continuation may proceed along such a solution manifold in terms of a geometry defined in the projected space, independently of any adaptive changes to the mesh. This is the solution implemented in the `atlas_kd` atlas algorithm [115].

For the abstract toolbox template presented in Section 4.2.1, the corresponding discretization in Section 4.2.7 is uniquely determined by the order N and polynomial degree m, since the mesh points $\tau_{\mathrm{pt},j} = (j-1)/N$ were assumed to be evenly distributed over the interval $[0,1]$ (even though this was not required by the abstract form of problem discretization discussed in Section 4.2.6). A simple form of adaptation would allow discrete changes to N and/or m during continuation, in order to accommodate variations of an estimated discretization error. Since such changes would inevitably change the relationship between individual base points and the corresponding time instants, it would be inappropriate to define a monitor function that evaluated, e.g., to $x_{\mathrm{bp},j}$ for $j \in \{2,\ldots,N(m+1)-1\}$. In contrast, a monitor function that evaluated to the value of $x(\cdot)$ at a particular fixed time or the integral of $x(\cdot)$ over the interval $[0,1]$ would be defined (if not computed) independently of the particular mesh, since the piecewise polynomial $\tilde{x}(\cdot)$ is a continuous function at every point of the solution manifold.

In a more sophisticated form of adaptation, not only could the number N of mesh intervals (or, less commonly, the polynomial degree m) vary during continuation, but one would also allow for non-uniform mesh intervals with unevenly spaced time meshes $\{\tau_{\mathrm{pt},j}\}_{j=1}^{N+1}$. The COCO toolbox `coll` implements a mesh-selection strategy that chooses the order N and the mesh points $\tau_{\mathrm{pt},j}$ such that they equidistribute an estimated (positive) density $e(\tau)$ of a given error measure according to

$$N = \frac{\langle e \rangle^{(m+1)/m}}{\mathtt{tol}^{1/m}}, \int_0^{\tau_{\mathrm{pt},j}} e(\tau)\mathrm{d}\tau = \frac{j-1}{N}\langle e \rangle,\ j = 2,\ldots,N \tag{7.20}$$

where

$$\langle e \rangle = \int_0^1 e(\tau)\mathrm{d}\tau \tag{7.21}$$

and `tol` is a user-defined tolerance. For a delay-coupled system of differential constraints, a

similar strategy would need to be concerned about possible loss of orders of differentiability of the exact solution at certain breakpoints even in the presence of smooth problem coefficients. Such breakpoints occur, for example, in initial-value problems with delay, including the data assimilation problem from Section 2.3.3 or the optimal control problem in Section 4.3.4. Similar breakpoints would be expected in the adjoint variables for periodic delay-coupled boundary-value problems when the corresponding objective functional is not invariant with respect to time shifts. The reduced regularity of the solution at these breakpoints may lead to poles in the estimates for the error measure density $e(\tau)$ and, consequently, to inefficient placement of mesh points or reduced accuracy. For initial-value problems, the interaction of mesh selection and breakpoints has been discussed extensively [116], [117].

We leave an implementation of such an adaptive mesh strategy to future work.

7.6.4 Application of uncertainty quantification

As mentioned at the conclusion of Chapter 6, it is straightforward to generalize the theory for two-tori to one for n-tori. Since this requires the computation of n adjoint variables in the construction of the projection matrix, it appears important to consider a construction approach in COCO that avoids the need to duplicate the boundary-value problem governing the function $v(\phi, t)$ in order to derive additional sets of adjoint boundary-value problems. This could be accomplished by developing an alternative toolbox constructor that provides a more flexible placement of the adjoint contributions than the existing toolbox constructors. Similarly, there are opportunities to generalize the constructor for the covariance problem to handle adaptive meshes.

While this dissertation only considered underlying deterministic systems that were smooth and without delay, it may be interesting to consider generalizations to limit cycle and transversally stable quasiperiodic invariant tori for hybrid dynamical systems or problems with delay. Additionally, even in the smooth case, one might wish to perform optimization of the covariance matrix along families of limit cycles or transversally stable quasiperiodic

invariant tori. For this purpose, rather than deriving yet another set of adjoint conditions, it might be worthwhile to consider approximate approaches that trap stationary points between solutions to the original covariance problem. These are relatively challenging but mathematically rewarding directions.

Appendix A

OPTIMAL DELAY THROUGH MULTIPLE SCALES

We review the application of the method of multiple scales to the optimal selection of a time delay that results in a minimal peak displacement amplitude in the harmonically-forced response of a Duffing oscillator under delayed displacement and velocity feedback, as discussed in Section 3.2.1.

Consider the delay-differential equation

$$\ddot{z}(t) + 2\epsilon\zeta\dot{z}(t) + z(t) + \epsilon\mu z^3(t) = 2\epsilon a z(t-\alpha) + 2\epsilon b\dot{z}(t-\alpha) + \epsilon\gamma\cos((1+\epsilon\sigma)t) \quad \text{(A.1)}$$

for $0 < \epsilon \ll 1$. We seek an approximate solution of the form

$$z(t) = z_0(T_0, T_1, \ldots) + \epsilon z_1(T_0, T_1, \ldots) + \cdots, \quad \text{(A.2)}$$

where $T_i = \epsilon^i t$. To leading order in ϵ,

$$z_0(T_0, T_1, \ldots) = A(T_1, \ldots) e^{iT_0} + cc, \quad \text{(A.3)}$$

where cc denotes complex conjugate terms. Elimination of secular terms at higher orders in ϵ then yields a set of conditions on the derivatives of the complex amplitude A with respect to

its arguments. In particular, if we let

$$A\left(T_1,\ldots\right)=\frac{1}{2}\rho(T_1,\ldots)e^{i\sigma T_1-\varphi(T_1,\ldots)}, \tag{A.4}$$

it follows from the first-order analysis that steady-state oscillations with angular frequency $1+\epsilon\sigma$ result provided that

$$\frac{1}{2}\gamma\sin\varphi=\zeta\rho+a\rho\sin\alpha-b\rho\cos\alpha, \tag{A.5}$$

$$\frac{1}{2}\gamma\cos\varphi=\rho\left(\sigma+a\cos\alpha+b\sin\alpha-\frac{3\mu\rho^2}{8}\right). \tag{A.6}$$

Elimination of φ yields the desired, implicit, frequency-amplitude relationship

$$\rho^2\left(\sigma+a\cos\alpha+b\sin\alpha-\frac{3\mu\rho^2}{8}\right)^2+\rho^2\left(\zeta+a\sin\alpha-b\cos\alpha\right)^2-\frac{\gamma^2}{4}=0, \tag{A.7}$$

from which we deduce the maximum value of ρ given by

$$\rho_{\max}\doteq\frac{\gamma}{2|\zeta+a\sin\alpha-b\cos\alpha|} \tag{A.8}$$

obtained when

$$\sigma=\frac{3\mu\rho_{\max}^2}{8}-a\cos\alpha-b\sin\alpha. \tag{A.9}$$

In the special case that $b=-a$, the maximum value of ρ achieves the local minimum $\gamma/2(\zeta+\sqrt{2}a)^2$ for $\alpha=\pi/4$, while for $b=0$, the local minimum $\gamma/2(\zeta+a)^2$ is obtained when $\alpha=\pi/2$.

Appendix B

CODE OVERVIEW FOR DDE TOOLBOX

The purpose of this additional material is to give an overview of the implementation related to the toolbox template discussed in Chapter 4. As discussed in Section 4.2, the toolbox template consists of M differential constraints (4.11) coupled to each other through the algebraic coupling conditions (4.14). Here we discuss the COCO compatible implementation of these equations and the corresponding adjoint contributions.

B.1 Implementation of the differential constraints

The code for implementation of the differential constraints (4.11) for a trajectory segment is shown below

```
function [data,y] = ddaecoll_F(prob, data, u)
x  = u(data.xbp_idx);
y  = u(data.ybp_idx);
T0 = u(data.T0_idx);
T  = u(data.T_idx);
p  = u(data.p_idx);
NTST  = data.ddaecoll.NTST;
xx  = reshape(data.W*x, data.x_shp);
yy  = reshape(data.W*y, data.y_shp);
tcn = T*data.taucn+T0;
fcn = data.fhan(tcn',xx, yy, pp);
ode = 2*NTST*data.Wp*x-T*fcn(:);   % Collocation conditions
cnt = data.Q*x;                    % Continuity conditions
y = [ode; cnt];
end
```

The input `prob` refers to the COCO problem structure, the field `data` contains the pre-stored interpolation matrices as well as the indices to extract the different variables from the array

u. This array contains the base points corresponding to $x_{\text{bp}}, y_{\text{bp}}$, the initial time T_0, segment length T and the problem parameters p. After extracting the variables, we calculate the function values f_{cn} at the collocation nodes in line 11 and impose the discretization of the differential constraint (4.11) in line 12. This imposition corresponds to the vectorized algebraic constraints (4.101). In addition to these conditions, the code also appends the condition corresponding to the continuity of x_{bp} across different intervals in line 14. This corresponds to the vectorized implementation of (4.89).

B.2 Implementation of the adjoints of the differential constraints

In COCO, the adjoint contributions from each stage of construction are added as

$$\lambda_{\text{bp}}^{\text{T}} J, \tag{B.1}$$

where J is the matrix from each stage of construction. With this in mind, the code for the vectrorized implementation of the adjoints of the differential constraints (4.11) is shown below

```
1  function [data, J] = adj(prob, data, u) %#ok<INUSL>
2  seg  = data.ddaecoll_seg;
3  opt  = data.ddaecoll_opt;
4  NTST = seg.ddaecoll.NTST;
5
6  x  = u(seg.xbp_idx);
7  y  = u(seg.ybp_idx);
8  T0 = u(seg.T0_idx);
9  T  = u(seg.T_idx);
10
11 p  = u(seg.p_idx);
12 pcn = repmat(p, seg.p_rep);
13 pbp  = repmat(p, seg.pbp_rep);
14
15 xcn = reshape(seg.W*x, seg.x_shp); % Values at collocation nodes
16 ycn = reshape(seg.Wy*y, seg.y_shp);
17 tcn = seg.taucn*T+T0;
18
19 xbp  = reshape(x,seg.xbp_shp);
20 ybp  = reshape(y,seg.ybp_shp);
21 tbp  = seg.tbp*T+T0;
22 fcn   = seg.fhan(tcn', xcn, ycn, pcn);
23 fdtcn = seg.dfdthan(tcn', xcn, ycn, pcn);
24 fdxcn = seg.dfdxhan(tcn', xcn, ycn, pcn);
```

```
25 fdpcn = seg.dfdphan(tcn', xcn, ycn, pcn);
26 fdybp = seg.dfdyhan(tbp', xbp, ybp, pbp);
27
28 % adjoint with respect to delta_x
29 dxode = sparse(seg.dxrows, seg.dxcols, fdxcn(:));
30 J = -2*NTST*seg.Wp'-T*seg.W'*dxode;
31
32 % adjoint with respect to delta_x^(j+1)(-1), delta_x^(1)(-1), and delta_x^(N)(1)
33 J = [ J, seg.Q', -opt.id0, opt.id1 ];
34
35 % adjoint with respect to delta_ybp
36 dyode = sparse(opt.dybprows, opt.dybpcols, fdybp(:));
37 J = [ J, -T*dyode ];
38
39 % adjoint with respect to T0 and T
40 dT0ode = T*fdtcn;
41 dTode  = fcn + T*fdtcn.*opt.dTtcn;
42 J = [ J, -(0.5/NTST)*seg.W'*seg.wts2*[dT0ode(:) dTode(:)] ];
43
44 % adjoint with respect to p
45 dpode = fdpcn;
46 dpode = sparse(seg.dprows, seg.dpcols, dpode(:));
47 J = [ J, -(0.5*T/NTST)*seg.W'*seg.wts2*dpode ];
48
49 end
```

The adjoint contribution from the differential constraints depend on the original variables u introduced in the imposition of the differential constraints (B.1). The input u to the above function therefore corresponds to these variables from the previous stage of construction corresponding to the segment whose adjoint contributions we are interested to construct. The variable `data` is a pre-defined data structure containing the necessary indices and matrices to impose the adjoint conditions.

To impose the adjoint contributions, here we first extract the variables and then evaluate the necessary Jacobian matrices for the adjoint implementation. Line 30 contains the adjoint contribution associated with the variations $\delta x(\tau)$ in (4.102) evaluated at the collocation nodes. To this matrix, we append the adjoint contributions from the continuity condition as well as with the variations $\delta x(0)$ and $\delta x(1)$. This has been done using the pre-defined matrices on line 33. Next we add the adjoint contribution associated with variations $\delta y(\tau)$ in (4.103) on line 37. Note that these adjoint contributions for y are added at the base points and not the collocation nodes. Next the adjoint contributions associated with the

variations δT_0 (4.104), δT (4.105) are added on line 42. Finally, the adjoint contribution from the differential constraint associated with the variations δp are shown on line 47. This contribution corresponds to the first term in (4.106).

B.3 Implementation of the coupling constraints

We now discuss the imposition of the algebraic coupling constraints (4.14) for the k-th coupling condition. For brevity, we only discuss the main aspects of the implementation. The algebraic coupling conditions (4.14) depend on the the state variables from the different trajectory segments, segment durations, coupling delays, interval boundaries and the coupling matrices. The input u to the coupling function therefore contains these variables which are extracted using pre-defined indices.

Let `tbp_k` denote the base points that lie in the k-th coupling condition. Then for the imposition of the coupling condition (4.110) we use the following code

```
1  %% Equations corresponding to the k-th coupling condition
2
3  taubp_lshift = (Ti/Tj_k)*(tbp_k(:)-kron(ones(Nbp_k,1),Delta_k));
4  mesh = 0:1/NTST:1;
5  jbp_lshift = floor(interp1(mesh,1:NTST+1,taubp_lshift(:),'linear','extrap'));
6  jbp_lshift(jbp_lshift>NTST) = NTST;
7  jbp_lshift(jbp_lshift<=0) = 1;
8  rows = repmat((jbp_lshift(:)-1)'*(NCOL+1), [(NCOL+1),1]) +...
9         repmat((1:(NCOL+1))',[1, Nbp_k]);
10 cols = repmat(1:Nbp_k,[NCOL+1,1]);
11 tc = 2*NTST*taubp_lshift(:,1)+1-2*jbp_lshift(:,1);
12 Lc = coll_L(seg.tm, tc);
13 Lbp_lshift = sparse(rows,cols,Lc',(NCOL+1)*NTST,Nbp_k);
14 Sx = 0;     %==temporary variable to add contributions from different s
15 for s=1:Sk
16     Aks = Ak(:,1+(s-1)*dim:s*dim);
17     x_jks_bp = Xibp(1+(Xj_k(s)-1)*xbpdim:Xj_k(s)*xbpdim);
18     Sx = Sx + kron(Lbp_lshift',Aks)*x_jks_bp(:);
19 end
20 temp = reshape(1:xbpdim,seg.xbp_shp); %===for y variable to get (Nm+1)n index
21 idx = temp(:,idx_k);
22 ybp_k = ybp(idx(:));
23 f_coupling(bp+1:bp+Nbp_k*dim,1) = ybp_k-Sx;
```

In line 3, we first calculate the shifted base points which correspond to (4.107). Then on lines 4-8, we calculate the interval in which the shifted points lie. With the help of the shifted base

points and the corresponding intervals, we construct the interpolation matrix $\mathcal{L}^k_{\text{bp}\downarrow\text{sh}}$ (4.109) in line 13. Then we iterate S_k times to compute the summation term in (4.110). Finally we impose the algebraic constraint (4.110) in line 23. The above code is repeated C_i times to impose the algebraic constraint for all the coupling conditions.

B.4 Implementation of the adjoints of the coupling constraints

In this section, we discuss the adjoint contributions from the coupling constraints. Here again the adjoint contributions depend on the variables used to impose the discretized algebraic coupling constraints in (B.3). These variables are therefore passed to the adjoint constructor.

To impose the adjoint contribution associated with the variations of $\delta x_{j_{k,s}}(\cdot)$ discretized at the collocation nodes, we first obtain the set of collocation nodes taucn_ks lying in the interval $(\xi_{b,k}, \xi_{e,k})$. Then we use the following code to impose the adjoint contributions

```
1  taucn_ushift = (Tj_k/Ti)*taucn_ks(:)+Delta_k;
2  mesh = 0:1/NTST:1;
3  jcn_ushift = floor(interp1(mesh,1:NTST+1,taucn_ushift(:),'linear','extrap'));
4  jcn_ushift(jcn_ushift>NTST) = NTST;
5  jcn_ushift(jcn_ushift<=0)   = 1;
6  rows = repmat((jcn_ushift(:)-1)'*(NCOL+1), [(NCOL+1),1]) +...
7         repmat((1:(NCOL+1))',[1, length(taucn_ushift(:))]);
8  cols = repmat(1:length(taucn_ushift(:)),[NCOL+1,1]);
9  tc = 2*NTST*taucn_ushift(:,1)+1-2*jcn_ushift(:,1);
10 Lc = coll_L(seg.tm, tc);
11 Lcn_ushift = sparse(rows,cols,Lc',(NCOL+1)*NTST,length(taucn_ushift(:)));
12
13 for s=1:Sk
14     Aks = Ak(:,1+(s-1)*dim:s*dim);
15     idx = 1+(idx_ks(1)-1)*dim+(Xj_k(s)-1)*xcndim:idx_ks(end)*dim+...
16                                                  (Xj_k(s)-1)*xcndim;
17     J_x(:,idx) = -(Tj_k/Ti)*kron(Lcn_ushift,Aks);
18 end
```

In the first line, we compute the shifted collocation nodes in (4.111). Then we compute the interval in which these nodes lie in lines 2-5. Using the computed intervals, we compute the corresponding mapping in the interval $[-1, 1]$ in line 9, and compute the corresponding polynomial interpolation matrix. The command on line 11 then computes the matrix $\mathcal{L}^k_{\text{cn}\uparrow\text{sh}}$ in (4.111). Then we iterate over s to impose the adjoint contribution with respect to $\delta x_{j_{k,s}}(\cdot)$.

Next we impose the adjoint contributions with respect to δp, $\delta T, \delta T_{jk}$ and $\delta \Delta_k$. For this we first compute the set of collocation nodes taucn_k that lie in the $k-$th coupling interval. Then we use the following code to implement the adjoint contributions corresponding to conditions (4.113-4.118) in Chapter 4.

```
1
2  taucn_lshift = (Ti/Tj_k)*(taucn_k(:)-kron(ones(Ncn_k,1),Delta_k));
3  mesh = 0:1/NTST:1;
4  jcn_lshift = floor(interp1(mesh,1:NTST+1,taucn_lshift(:),'linear','extrap'));
5  jcn_lshift(jcn_lshift>NTST) = NTST;
6  jcn_lshift(jcn_lshift<=0)   = 1;
7  rows = repmat((jcn_lshift(:)-1)'*(NCOL+1), [(NCOL+1),1]) +...
8         repmat((1:(NCOL+1))',[1, length(taucn_lshift(:))]);
9  cols = repmat(1:length(taucn_lshift(:)),[NCOL+1,1]);
10 tc = 2*NTST*taucn_lshift(:,1)+1-2*jcn_lshift(:,1);
11 Lc = coll_L(seg.tm, tc); Lcp = coll_Lp(seg.tm, tc);
12 Lcn_lshift  = sparse(rows,cols,Lc',(NCOL+1)*NTST,length(taucn_lshift(:)));
13 Lcn_lshiftp = sparse(rows,cols,Lcp',(NCOL+1)*NTST,length(taucn_lshift(:)));
14
15 for s=1:Sk
16     Aks  = Ak(:,1+(s-1)*dim:s*dim);
17     Aksp = Akp(:,1+(s-1)*dim:s*dim,1:pdim);
18     x_jks_bp = reshape(Xibp(1+(Xj_k(s)-1)*xbpdim:Xj_k(s)*xbpdim),...
19                                                  [dim,NTST*(NCOL+1)]);
20
21     J_p(:,1:pdim) = J_p(:,1:pdim)-Wmu_k'*Omega_k*...
22         kron(x_jks_bp*Lcn_lshift,eye(dim))'*...
23         reshape(Aksp(:),[dim^2,pdim]);
24
25     J_T(:,Ti_id) = J_T(:,Ti_id) -  (1/Ti)*Wmu_k'*Omega_k*...
26         kron(diag(taucn_lshift(:)),eye(dim))*...
27         kron(Lcn_lshiftp',Aks)*x_jks_bp(:);
28
29     J_T(:,Tj_id{k}) = J_T(:,Tj_id{k}) + (1/Tj_k)*Wmu_k'*Omega_k*...
30         kron(diag(taucn_lshift(:)),eye(dim))*...
31         kron(Lcn_lshiftp',Aks)*x_jks_bp(:);
32
33     J_Delta(:, Delta_id{k}) = J_Delta(:, Delta_id{k})+(Ti/Tj_k)*Wmu_k'*...
34         Omega_k*kron(Lcn_lshiftp',Aks)*x_jks_bp(:);
35
36 end
```

Appendix C

CODE OVERVIEW FOR UNCERTAINTY QUANITFICATION NEAR PERIODIC ORBITS

In this section, we provide the COCO compatible implementation of the boundary value problem (5.37-5.39) to compute the covariance matrix. As discussed in Section 5.4, we use the complementary zero function constructor to impose these conditions. In this implementation, the array u contains the base points corresponding to the periodic orbit, trajectory length T and the problem parameters p. l is the array of adjoint variables. The array v contains the unknown base points corresponding to the covariance matrix and the auxiliary variable α.

```
1  function [data,y] = periodic_covar(prob, data, u, l, v)
2  maps = data.maps;
3  NTST = maps.NTST;
4  NCOL = maps.NCOL;
5  xdim = maps.xdim;
6
7  xbp       = u(maps.xbp_idx);
8  lambda_bp = l;                                  %====Lagrange Multiplier
9  covar_bp  = v(data.covar_vidx);                 %===Covariance base points
10 Cbp       = reshape(covar_bp, data.covar_shp);  %===Covariance matrix form
11
12 T        = u(maps.T_idx);
13 p        = u(maps.p_idx);
14 alpha    = v(data.covar_alpha_vidx);
15
16
17 xcn = reshape(maps.W*xbp,maps.x_shp);
18 lambda_cn = reshape(maps.W*lambda_bp,maps.x_shp);
19 Cperp_cn  = maps.W*Cbp;
20
21 fcn   = data.fhan(xcn,repmat(p,maps.p_rep));
22 dfdx  = data.dfdxhan(xcn,repmat(p,maps.p_rep));
23 dxode = full(sparse(maps.fdxrows, maps.fdxcols, dfdx(:)));
24
```

```
%====Storing DFDX' in a vertical rectangular matrix
A1 = dxode';
rows = reshape(1:xdim*NTST*NCOL,[xdim,NTST*NCOL]);
rows = repmat(rows,[xdim,1]);
cols = repmat(1:NTST*NCOL*xdim,[xdim,1]);
idx  = sub2ind(size(dxode),rows(:),cols(:));
A2 = A1(idx);

rows = reshape(1:xdim*NTST*NCOL,[xdim,NTST*NCOL]);
rows = repmat(rows,[xdim,1]);
cols = repmat(1:xdim,[xdim,1]);
cols = repmat(cols,1,NTST*NCOL);
dxodetransp = sparse(rows(:), cols(:), A2);


% Storing covariance matrix at nodes in a diagonal form

% Step 1: Extracting the indices of the appropriate elements from the
%         rectangular matrix
rows = reshape(1:xdim*NTST*NCOL,[xdim,NTST*NCOL]);
rows = repmat(rows,[xdim,1]);
cols = repmat(1:xdim,[xdim,1]);
cols = repmat(cols,[1,NTST*NCOL]);
idx  = sub2ind(size(Cperp_cn),rows(:),cols(:));
C1   = Cperp_cn(idx);

% Step 2: Storing the elements in a diagonal matrix form
rows = reshape(1:xdim*NTST*NCOL,[xdim,NTST*NCOL]);
rows = repmat(rows,[xdim,1]);
cols = repmat(1:xdim*NTST*NCOL,[xdim,1]);
Cdiag  = sparse(rows(:),cols(:),C1(:));

%====Generating the projection matrix: Q
rows = 1:NTST*NCOL*xdim;
cols = repmat(1:NTST*NCOL,xdim,1);
FODE = sparse(rows(:),cols(:),fcn(:));

rows = repmat(1:NTST*NCOL,xdim,1);
cols = 1:NTST*NCOL*xdim;
LAMBDA = sparse(rows(:),cols(:),lambda_cn(:));

Q = kron(eye(NTST*NCOL),eye(xdim)) - FODE*LAMBDA;

Fnoise = data.Fnoisehan(xcn,repmat(p,maps.p_rep));
Fnoise = sparse(maps.fdxrows, maps.fdxcols, Fnoise(:));
Bcn    = Q*(Fnoise*Fnoise')*Q';


%==Storing Bcn in a rectangular matrix form

% Step 1: Extracting the indices of the diagonal elements
rows = reshape(1:xdim*NTST*NCOL,[xdim,NTST*NCOL]);
rows = repmat(rows,[xdim,1]);
cols = repmat(1:NTST*NCOL*xdim,[xdim,1]);
idx  = sub2ind(size(Bcn),rows(:),cols(:));
B1   = Bcn(idx);
```

```
81
82  % Step 2: Storing the elements in a rectangular matrix form
83  rows = reshape(1:xdim*NTST*NCOL,[xdim,NTST*NCOL]);
84  rows = repmat(rows,[xdim,1]);
85  cols = repmat(1:xdim,[xdim,1]);
86  cols = repmat(cols,1,NTST*NCOL);
87  Bcntilde = full(sparse(rows(:), cols(:), B1(:)));
88
89
90  %============= Storing f*f' in a rectangular matrix form
91
92  % Calculating the product
93  Fprod = FODE*FODE';
94
95  % Extracting the indices
96  rows = reshape(1:xdim*NTST*NCOL,[xdim,NTST*NCOL]);
97  rows = repmat(rows,[xdim,1]);
98  cols = repmat(1:NTST*NCOL*xdim,[xdim,1]);
99  idx  = sub2ind(size(Fprod),rows(:),cols(:));
100 Fprod1   = Fprod(idx);
101
102 % Storing the extracted elements in rectangular form
103 rows = reshape(1:xdim*NTST*NCOL,[xdim,NTST*NCOL]);
104 rows = repmat(rows,[xdim,1]);
105 cols = repmat(1:xdim,[xdim,1]);
106 cols = repmat(cols,1,NTST*NCOL);
107 fftransp = full(sparse(rows(:), cols(:), Fprod1(:)));
108
109 y1 = -W*Cbp + (T/2/NTST)*dxode*(W*Cbp)+...
110      (T/2/NTST)*Cdiag*dxodetransp + (T/2/NTST)*Bcntilde-...
111      alpha*(T/2/NTST)*fftransp;
112 y2 = Q*Cbp;
113 y3 = Cbp(data.covar_v0_rowidx,:)-Cbp(data.covar_v1_rowidx,:);
114 y4 = lambda_bp(1:xdim,1)'*Cbp(data.covar_v0_rowidx,:)*lambda_bp(1:xdim,1);
115
116 y = [y1(:); y2(:); y3(:); y4(:)];
117
118 end
```

Here, we follow the discretization methodology discussed in [32] for a variational problem to implement the discretization corresponding to (5.37-5.39). After constructing the appropriate matrices we impose the discretized problem in line 109-114. Specifically, line 113 contains the discretization corresponding to (5.37), where, W and W' are the interpolation matrices introduced in Chapter 4. The continuity condition corresponding to the covariance matrix elements has been imposed in line 112. Then in line 113, we impose the periodicity condition and finally, the initial condition (5.39) in line 114.

References

[1] Z. Ahsan, H. Dankowicz, and J. Sieber, "Optimization along families of periodic and quasiperiodic orbits in dynamical systems with delay," *Nonlinear Dynamics*, vol. 99, no. 1, pp. 837–854, 2020.

[2] Z. Ahsan, H. Dankowicz, M. Li, and J. Sieber, "Methods of continuation and their implementation in the coco software platform with application to delay differential equations," *Nonlinear Dynamics*, pp. 1–63, 2022.

[3] J. Sieber and B. Krauskopf, "Tracking oscillations in the presence of delay-Induced essential instability," *Journal of Sound and Vibration*, vol. 315, no. 3, pp. 781–795, 2008.

[4] G. Orosz, B. Krauskopf, and R. E. Wilson, "Bifurcations and multiple traffic jams in a car-following model with reaction-time delay," *Physica D: Nonlinear Phenomena*, vol. 211, no. 3-4, pp. 277–293, 2005.

[5] J. Tlusty and M. Polacek, "The stability of machine tools against self-excited vibrations in machining," *International Research in Production Engineering, ASME*, vol. 1, pp. 465–474, 1963.

[6] L. Göllmann, D. Kern, and H. Maurer, "Optimal control problems with delays in state and control variables subject to mixed control–state constraints," *Optimal Control Applications and Methods*, vol. 30, no. 4, pp. 341–365, 2009.

[7] A. Yusoff and N. Sims, "Optimisation of variable helix tool geometry for regenerative chatter mitigation," *International Journal of Machine Tools and Manufacture*, vol. 51, no. 2, pp. 133–141, 2011.

[8] T. Insperger and G. Stépán, "Semi-discretization method for delayed systems," *International Journal for Numerical Methods in Engineering*, vol. 55, no. 5, pp. 503–518, 2002.

[9] A. Iglesias, Z. Dombovari, G. Gonzalez, J. Munoa, and G. Stepan, "Optimum selection of variable pitch for chatter suppression in face milling operations," *Materials*, vol. 12, no. 1, p. 112, 2019.

[10] A. Iglesias, J. Munoa, and J. Ciurana, "Optimisation of face milling operations with structural chatter using a stability model based process planning methodology," *International Journal of Advanced Manufacturing Technology*, vol. 70, no. 1-4, pp. 559–571, 2014.

[11] S. Wojciechowski, R. Maruda, S. Barrans, P. Nieslony, and G. Krolczyk, "Optimisation of machining parameters during ball end milling of hardened steel with various surface inclinations," *Measurement: Journal of the International Measurement Confederation*, vol. 111, pp. 18–28, 2017.

[12] H. Liao, "Nonlinear dynamics of duffing oscillator with time delayed Term," *Computer Modeling in Engineering and Sciences*, vol. 103, no. 3, pp. 155–187, 2014.

[13] J. Kernévez and E. Doedel, "Optimization in bifurcation problems using a continuation method," in *Bifurcation: Analysis, Algorithms, Applications*, Springer, 1987, pp. 153–160.

[14] M. Li and H. Dankowicz, "Staged construction of adjoints for constrained optimization of integro-differential boundary-value problems," *SIAM Journal on Applied Dynamical Systems*, vol. 17, no. 2, pp. 1117–1151, 2018.

[15] A. Rubino, M. Pini, P. Colonna, *et al.*, "Adjoint-based fluid dynamic design optimization in quasi-periodic unsteady flow problems using a harmonic balance method," *Journal of Computational Physics*, vol. 372, pp. 220–235, 2018.

[16] J. Calver and W. Enright, "Numerical methods for computing sensitivities for ODEs and DDEs," *Numerical Algorithms*, vol. 74, no. 4, pp. 1101–1117, 2017.

[17] E. J. Doedel, A. R. Champneys, F. Dercole, *et al.*, *AUTO-07p: Continuation and bifurcation software for ordinary differential equations*, https://github.com/auto-07p/auto-07p, Accessed: 2021-04-22.

[18] B. Ermentrout, *Simulating, analyzing, and animating dynamical systems: a guide to XPPAUT for researchers and students*. SIAM, 2002.

[19] A. Dhooge, W. Govaerts, and Y. A. Kuznetsov, "MATCONT: A MATLAB package for numerical bifurcation analysis of ODEs," *ACM Transactions on Mathematical Software (TOMS)*, vol. 29, no. 2, pp. 141–164, 2003.

[20] K. Engelborghs, T. Luzyanina, and D. Roose, "Numerical bifurcation analysis of delay differential equations using DDE-BIFTOOL," *ACM Transactions on Mathematical Software (TOMS)*, vol. 28, no. 1, pp. 1–21, 2002.

[21] J. Sieber, K. Engelborghs, T. Luzyanina, G. Samaey, and D. Roose, *DDE-BIFTOOL Manual — Bifurcation analysis of delay differential equations*, sourceforge.net/projects/ddebiftool and sourceforge.net/p/ddebiftool/git/ci/master/tree/ddebiftool_coco.

[22] R. Szalai, *Knut: A continuation and bifurcation software for delay-differential equations*, https://rs1909.github.io/knut/, Accessed: 2021-03-26.

[23] C. Kuehn, "Efficient gluing of numerical continuation and a multiple solution method for elliptic PDEs," *Applied Mathematics and Computation*, vol. 266, pp. 656–674, 2015.

[24] H. Uecker, D. Wetzel, and J. D. Rademacher, "Pde2path-A Matlab package for continuation and bifurcation in 2D elliptic systems," *Numerical Mathematics: Theory, Methods and Applications*, vol. 7, no. 1, pp. 58–106, 2014.

[25] L. T. Watson, S. C. Billups, and A. P. Morgan, "Algorithm 652: HOMPACK: A suite of codes for globally convergent homotopy algorithms," *ACM Transactions on Mathematical Software (TOMS)*, vol. 13, no. 3, pp. 281–310, 1987.

[26] J. P. England, B. Krauskopf, and H. M. Osinga, "Computing one-dimensional global manifolds of poincaré maps by continuation," *SIAM Journal on Applied Dynamical Systems*, vol. 4, no. 4, pp. 1008–1041, 2005.

[27] F. Dercole and Y. A. Kuznetsov, "SlideCont: An Auto97 driver for bifurcation analysis of filippov systems," *ACM Transactions on Mathematical Software (TOMS)*, vol. 31, no. 1, pp. 95–119, 2005.

[28] P. Thota and H. Dankowicz, "TC-HAT: A novel toolbox for the continuation of periodic trajectories in hybrid dynamical systems," *SIAM Journal on Applied Dynamical Systems*, vol. 7, no. 4, pp. 1283–1322, 2008.

[29] H. M. Osinga and J. Moehlis, "Continuation-based computation of global isochrons," *SIAM Journal on Applied Dynamical Systems*, vol. 9, no. 4, pp. 1201–1228, 2010.

[30] M. Otter, H. Elmqvist, and F. E. Cellier, "Modeling of multibody systems with the object-oriented modeling language Dymola," *Nonlinear Dynamics*, vol. 9, no. 1, pp. 91–112, 1996.

[31] W. Schiehlen, *Advanced multibody system dynamics: simulation and software tools*. Springer Science & Business Media, 2013, vol. 20.

[32] H. Dankowicz and F. Schilder, *Recipes for continuation*. SIAM, 2013.

[33] H. Dankowicz, F. Schilder, and M. Saghafi, "Continuation of connecting orbits with Lin's method using COCO," in *Proceedings of the 7th European Nonlinear Dynamics Conference (ENOC 2011)*, 2011.

[34] B. Krauskopf and T. Rieß, "A Lin's method approach to finding and continuing heteroclinic connections involving periodic orbits," *Nonlinearity*, vol. 21, no. 8, p. 1655, 2008.

[35] M. Li and H. Dankowicz, "Optimization with equality and inequality constraints using parameter continuation," *Applied Mathematics and Computation*, vol. 375, p. 125 058, 2020.

[36] M. Scheutzow, "Stabilization and destabilization by noise in the plane," *Stochastic Analysis and Applications*, vol. 11, no. 1, pp. 97–113, 1993.

[37] J. Gao, C. Chen, S. Hwang, and J. Liu, "Noise-induced chaos," *International Journal of Modern Physics B*, vol. 13, no. 28, pp. 3283–3305, 1999.

[38] C. Kuehn, "Deterministic continuation of stochastic metastable equilibria via Lyapunov equations and ellipsoids," *SIAM Journal on Scientific Computing*, vol. 34, no. 3, A1635–A1658, 2012.

[39] R. Kozma, "On the constructive role of noise in stabilizing itinerant trajectories in chaotic dynamical systems," *Chaos: An Interdisciplinary Journal of Nonlinear Science*, vol. 13, no. 3, pp. 1078–1089, 2003.

[40] B. Andò, S. Baglio, C. Trigona, N. Dumas, L. Latorre, and P. Nouet, "Nonlinear mechanism in mems devices for energy harvesting applications," *Journal of Micromechanics and Microengineering*, vol. 20, no. 12, p. 125 020, 2010.

[41] H. Kim, W. C. Tai, J. Parker, and L. Zuo, "Self-tuning stochastic resonance energy harvesting for rotating systems under modulated noise and its application to smart tires," *Mechanical Systems and Signal Processing*, vol. 122, pp. 769–785, 2019.

[42] D. H. Zanette, "Effects of noise on the internal resonance of a nonlinear oscillator," *Scientific reports*, vol. 8, no. 1, pp. 1–9, 2018.

[43] B. Øksendal, "Stochastic differential equations," in *Stochastic differential equations*, Springer, 2003.

[44] S. Biswas, A. Rounak, P. Perlikowski, and S. Gupta, "Characterising stochastic fixed points and limit cycles for dynamical systems with additive noise," *Communications in Nonlinear Science and Numerical Simulation*, vol. 101, p. 105 870, 2021.

[45] I. A. Bashkirtseva and L. B. Ryashko, "Stochastic sensitivity of 3d-cycles," *Mathematics and Computers in Simulation*, vol. 66, no. 1, pp. 55–67, 2004.

[46] N. Berglund and B. Gentz, *Noise-induced phenomena in slow-fast dynamical systems: a sample-paths approach*. Springer Science & Business Media, 2006.

[47] S. Louca, "Stable limit cycles perturbed by noise," *arXiv preprint arXiv:1506.00756*, 2015.

[48] I. Bashkirtseva and L. Ryashko, "Sensitivity analysis of stochastically forced quasiperiodic self-oscillations," *Electronic Journal of Differential Equations*, vol. 2016, no. 240, pp. 1–12, 2016.

[49] I. Bashkirtseva, V. Nasyrova, and L. Ryashko, "Analysis of noise effects in a map-based neuron model with canard-type quasiperiodic oscillations," *Communications in Nonlinear Science and Numerical Simulation*, vol. 63, pp. 261–270, 2018.

[50] I. Bashkirtseva, L. Ryashko, and S. Zaitseva, "Analysis of nonlinear stochastic oscillations in the biochemical goldbeter model," *Communications in Nonlinear Science and Numerical Simulation*, vol. 73, pp. 165–176, 2019.

[51] Z. Ahsan, C. Kuehn, and H. Dankowicz, "A covariance boundary value problem for stochastically perturbed limit cycles," in *ASME International Design Engineering Technical Conferences Computers and Information in Engineering Conference*, American Society of Mechanical Engineers, 2022.

[52] E. J. Doedel, B. Krauskopf, and H. M. Osinga, "Global bifurcations of the Lorenz manifold," *Nonlinearity*, vol. 19, no. 12, p. 2947, 2006.

[53] J. Guckenheimer, B. Krauskopf, H. M. Osinga, and B. Sandstede, "Invariant manifolds and global bifurcations," *Chaos: An Interdisciplinary Journal of Nonlinear Science*, vol. 25, no. 9, p. 097 604, 2015.

[54] L. K. Abbas, X. Rui, P. Marzocca, M. Abdalla, and R. De Breuker, "A parametric study on supersonic/hypersonic flutter behavior of aero-thermo-elastic geometrically imperfect curved skin panel," *Acta Mechanica*, vol. 222, no. 1, pp. 41–57, 2011.

[55] G. Kewlani, J. Crawford, and K. Iagnemma, "A polynomial chaos approach to the analysis of vehicle dynamics under uncertainty," *Vehicle System Dynamics*, vol. 50, no. 5, pp. 749–774, 2012.

[56] L. Amandio, A. Marta, F. Afonso, J. Vale, A. Suleman, and A. Araujo, "Stochastic optimization in aircraft design," in *Engineering Optimization*, CRC Press, 2014, pp. 267–272.

[57] M. H. Koh and R. Sipahi, "Optimizing agent coupling strengths in a network dynamics with inter-agent delays for achieving fast consensus," in *2016 American Control Conference (ACC)*, IEEE, 2016, pp. 5358–5363.

[58] G. Haller and S. Ponsioen, "Nonlinear normal modes and spectral submanifolds: Existence, uniqueness and use in model reduction," *Nonlinear Dynamics*, vol. 86, no. 3, pp. 1493–1534, 2016.

[59] R. Szalai, "Model reduction of non-densely defined piecewise-smooth systems in banach spaces," *Journal of Nonlinear Science*, vol. 29, no. 3, pp. 897–960, 2019.

[60] ——, "Invariant spectral foliations with applications to model order reduction and synthesis," *Nonlinear Dynamics*, vol. 101, no. 4, pp. 2645–2669, 2020.

[61] C. Touzé and M. Amabili, "Nonlinear normal modes for damped geometrically nonlinear systems: Application to reduced-order modelling of harmonically forced structures," *Journal of Sound and Vibration*, vol. 298, no. 4-5, pp. 958–981, 2006.

[62] B. Krauskopf, H. M. Osinga, and J. Galán-Vioque, *Numerical continuation methods for dynamical systems*. Springer, 2007, vol. 2.

[63] W. Govaerts, "Numerical bifurcation analysis for ODEs," *Journal of Computational and Applied Mathematics*, vol. 125, no. 1-2, pp. 57–68, 2000.

[64] F. J. Munoz-Almaraz, E. Freire, J. Galán, E. Doedel, and A. Vanderbauwhede, "Continuation of periodic orbits in conservative and Hamiltonian systems," *Physica D: Nonlinear Phenomena*, vol. 181, no. 1-2, pp. 1–38, 2003.

[65] W.-J. Beyn, "The numerical computation of connecting orbits in dynamical systems," *IMA Journal of Numerical Analysis*, vol. 10, no. 3, pp. 379–405, 1990.

[66] F. Schilder, H. M. Osinga, and W. Vogt, "Continuation of quasi-periodic invariant tori," *SIAM Journal on Applied Dynamical Systems*, vol. 4, no. 3, pp. 459–488, 2005.

[67] M. Dellnitz and A. Hohmann, "The computation of unstable manifolds using subdivision and continuation," in *Nonlinear dynamical systems and chaos*, Springer, 1996, pp. 449–459.

[68] D. A. Barton, "Stability calculations for piecewise-smooth delay equations," *International Journal of Bifurcation and Chaos*, vol. 19, no. 02, pp. 639–650, 2009.

[69] J. P. Chávez, Z. Zhang, and Y. Liu, "A numerical approach for the bifurcation analysis of nonsmooth delay equations," *Communications in Nonlinear Science and Numerical Simulation*, vol. 83, p. 105 095, 2020.

[70] T. Luzyanina, K. Engelborghs, K. Lust, and D. Roose, "Computation, continuation and bifurcation analysis of periodic solutions of delay differential equations," *International Journal of Bifurcation and Chaos*, vol. 7, no. 11, pp. 2547–2560, 1997.

[71] D. Roose and R. Szalai, "Continuation and bifurcation analysis of delay differential equations," in *Numerical continuation methods for dynamical systems*, Springer, 2007, pp. 359–399.

[72] E. L. Allgower and K. Georg, *Introduction to numerical continuation methods*. SIAM, 2003.

[73] Y. A. Kuznetsov, *Elements of applied bifurcation theory*. Springer Science & Business Media, 2013, vol. 112.

[74] F. Schilder, H. Dankowicz, and M. Li, *Continuation Core and Toolboxes (COCO)*, https://sourceforge.net/projects/cocotools, Accessed: 2021-03-26.

[75] E. J. Doedel, "Lecture notes on numerical analysis of nonlinear equations," in *Numerical continuation methods for dynamical systems*, Springer, 2007, pp. 1–49.

[76] G. D'Avino, S. Crescitelli, P. Maffettone, and M. Grosso, "On the choice of the optimal periodic operation for a continuous fermentation process," *Biotechnology Progress*, vol. 26, no. 6, pp. 1580–1589, 2010.

[77] J. O. Toilliez and A. J. Szeri, "Optimized translation of microbubbles driven by acoustic fields," *The Journal of the Acoustical Society of America*, vol. 123, no. 4, pp. 1916–1930, 2008.

[78] M. Wyczalkowski and A. J. Szeri, "Optimization of acoustic scattering from dual-frequency driven microbubbles at the difference frequency," *The Journal of the Acoustical Society of America*, vol. 113, no. 6, pp. 3073–3079, 2003.

[79] V. Acharya and T. Lieuwen, "Non-monotonic flame response behaviors in harmonically forced flames," *Proceedings of the Combustion Institute*, 2020.

[80] I. M. Gelfand, R. A. Silverman, *et al.*, *Calculus of variations*. Courier Corporation, 2000.

[81] D. Liberzon, *Calculus of variations and optimal control theory: a concise introduction*. Princeton university press, 2011.

[82] S. G. Krantz and H. R. Parks, *The implicit function theorem: history, theory, and applications*. Springer Science & Business Media, 2012.

[83] C. T. Kelley, *Iterative methods for linear and nonlinear equations*. SIAM, 1995.

[84] M. Crisfield, "An arc-length method including line searches and accelerations," *International Journal for Numerical Methods in Engineering*, vol. 19, no. 9, pp. 1269–1289, 1983.

[85] M. E. Henderson, "Multiple parameter continuation: Computing implicitly defined k-manifolds," *International Journal of Bifurcation and Chaos*, vol. 12, no. 03, pp. 451–476, 2002.

[86] R. Seydel, *Practical bifurcation and stability analysis*. Springer Science & Business Media, 2009, vol. 5.

[87] J. Guddat, F. G. Vazquez, and H. T. Jongen, *Parametric optimization: singularities, pathfollowing and jumps*. Springer, 1990.

[88] H. Dankowicz and F. Schilder, "An extended continuation problem for bifurcation analysis in the presence of constraints," *Journal of Computational and Nonlinear Dynamics*, vol. 6, no. 3, 2011.

[89] A. Ben-Tal and J. Zowe, "A unified theory of first and second order conditions for extremum problems in topological vector spaces," in *Optimality and stability in mathematical programming*, Springer, 1982, pp. 39–76.

[90] T. Traverso and L. Magri, "Data assimilation in a nonlinear time-delayed dynamical system with Lagrangian optimization," *Lecture Notes in Computer Science (including subseries Lecture Notes in Artificial Intelligence and Lecture Notes in Bioinformatics)*, vol. 11539, pp. 156–168, 2019.

[91] B. Ermentrout, "Type I membranes, phase resetting curves, and synchrony," *Neural Computation*, vol. 8, no. 5, pp. 979–1001, 1996.

[92] W. Govaerts and B. Sautois, "Computation of the phase response curve: A direct numerical approach," *Neural Computation*, vol. 18, no. 4, pp. 817–847, 2006.

[93] E. M. Izhikevich, *Dynamical systems in neuroscience*. MIT press, 2007.

[94] P. Langfield, B. Krauskopf, and H. M. Osinga, "A continuation approach to computing phase resetting curves," in *Advances in Dynamics, Optimization and Computation*, Springer, 2020, pp. 3–30.

[95] C. Chicone and W. Liu, "Asymptotic phase revisited," *Journal of Differential Equations*, vol. 204, no. 1, pp. 227–246, 2004.

[96] V. Novičenko and K. Pyragas, "Phase reduction of weakly perturbed limit cycle oscillations in time-delay systems," *Physica D: Nonlinear Phenomena*, vol. 241, no. 12, pp. 1090–1098, 2012.

[97] M. Heinkenschloss, *PDE Constrained Optimization*, https://archive.siam.org/meetings/op08/Heinkenschloss.pdf, Accessed: 2018-12-25.

[98] M. Hinze, R. Pinnau, M. Ulbrich, and S. Ulbrich, *Optimization with PDE constraints*. Springer Science & Business Media, 2008.

[99] Z. P. Olikara, "Computation of quasi-periodic tori and heteroclinic connections in astrodynamics using collocation techniques," Ph.D. dissertation, University of Colorado at Boulder, 2016.

[100] H. Hu, E. H. Dowell, and L. N. Virgin, "Resonances of a Harmonically Forced Duffing Oscillator with Time Delay State Feedback," *Nonlinear Dynamics*, vol. 15, no. 4, pp. 311–327, 1998.

[101] R. Rusinek, A. Weremczuk, K. Kecik, and J. Warminski, "Dynamics of a Time Delayed Duffing Oscillator," *International Journal of Non-Linear Mechanics*, vol. 65, pp. 98–106, 2014.

[102] C. A. Paul, "Designing efficient software for solving delay differential equations," *Journal of Computational and Applied Mathematics*, vol. 125, no. 1-2, pp. 287–295, 2000.

[103] A. Andò and D. Breda, "Convergence analysis of collocation methods for computing periodic solutions of retarded functional differential equations," *SIAM Journal on Numerical Analysis*, vol. 58, no. 5, pp. 3010–3039, 2020.

[104] G. Samaey, K. Engelborghs, and D. Roose, "Numerical computation of connecting orbits in delay differential equations," *Numerical Algorithms*, vol. 30, no. 3, pp. 335–352, 2002.

[105] L. Glass and M. Mackey, "Mackey-Glass equation," *Scholarpedia*, vol. 5, no. 3, p. 6908, 2010.

[106] L. Berezansky, E. Braverman, and L. Idels, "The Mackey–Glass model of respiratory dynamics: Review and new results," *Nonlinear Analysis: Theory, Methods & Applications*, vol. 75, no. 16, pp. 6034–6052, 2012.

[107] L. Berezansky and E. Braverman, "Mackey-Glass equation with variable coefficients," *Computers & Mathematics with Applications*, vol. 51, no. 1, pp. 1–16, 2006.

[108] S. Smith, "Optimal control of delay differential equations using evolutionary algorithms," *Complexity International*, vol. 12, pp. 1–10, 2005.

[109] H. Dankowicz and J. Sieber, "Sensitivity analysis for periodic orbits and quasiperiodic invariant tori using the adjoint method," *arXiv preprint arXiv:2111.02122*, 2021.

[110] D. J. Higham and P. E. Kloeden, *An Introduction to the Numerical Simulation of Stochastic Differential Equations*. SIAM, 2021, vol. 169.

[111] J. Galan-Vioque, F. Almaraz, and E. Macıas, "Continuation of periodic orbits in symmetric hamiltonian and conservative systems," *The European Physical Journal Special Topics*, vol. 223, no. 13, pp. 2705–2722, 2014.

[112] D. J. Higham, "An algorithmic introduction to numerical simulation of stochastic differential equations," *SIAM review*, vol. 43, no. 3, pp. 525–546, 2001.

[113] Y. Mao and H. Dankowicz, *Design of active network filters as hysteretic sensors (arxiv)*, 2021. arXiv: 2103.13963 [math.DS].

[114] K. Engelborghs and E. J. Doedel, "Stability of piecewise polynomial collocation for computing periodic solutions of delay differential equations," *Numerische Mathematik*, vol. 91, no. 4, pp. 627–648, 2002.

[115] H. Dankowicz, Y. Wang, F. Schilder, and M. E. Henderson, "Multidimensional manifold continuation for adaptive boundary-value problems," *Journal of Computational and Nonlinear Dynamics*, vol. 15, no. 5, 2020.

[116] N. Guglielmi and E. Hairer, "Implementing Radau IIA methods for stiff delay differential equations," *Computing*, vol. 67, no. 1, pp. 1–12, 2001.

[117] L. F. Shampine and S. Thompson, "Numerical solution of delay differential equations," in *Delay Differential Equations*, Springer, 2009, pp. 1–27.